**9th International Symposium on
Capillary Electrophoresis
Budapest, 5–7 October 1994**

JOURNAL OF

CHROMATOGRAPHY A

INCLUDING ELECTROPHORESIS AND OTHER SEPARATION METHODS

ELSEVIER

JOURNAL OF
CHROMATOGRAPHY A
INCLUDING ELECTROPHORESIS AND OTHER SEPARATION METHODS

ELSEVIER

Amsterdam – Lausanne – New York – Oxford – Shannon – Tokyo

9TH INTERNATIONAL SYMPOSIUM ON CAPILLARY ELECTROPHORESIS

Budapest (Hungary), 5–7 October 1994

Guest Editor

F. KILÁR

(Budapest, Hungary)

CONTENTS

PROTEINS

DRUGS

OTHER APPLICATIONS

Preface

The 9th International Symposium on Capillary Electrophoresis (ITP'94) was held in Budapest, Hungary, from 3–7 October 1994.

The successful series of the European capillary electrophoresis ITP symposia continued with this meeting in Budapest. In 1979 specialists in isotachophoresis met for the first time in Baconfy. Belgium (1st International Symposium on Isotachophoresis), and later in Eindhoven, The Netherlands (ITP'80), in Goslar, Germany (ITP'82), in Hradec Kralové, Czech Republic (ITP'84) and in Maastricht, The Netherlands (ITP'86). The rising number of laboratories in Europe which are working with other capillary electrophoretic techniques have led to the effect that the symposia in Vienna, Austria (ITP'88), in Tatranska Lomnica, Czech Republic (ITP'90) and in Rome, Italy (ITP'92) also covered broader topics of capillary electrophoresis.

ITP'94 was started with a Two-Day Short Course on Capillary Electrophoresis held at the same location on 3 and 4 October. Lectures on fundamental and practical aspects of capillary zone electrophoresis, isoelectric focusing, capillary gel electrophoresis and micellar electrokinetic chromatography were given by invited speakers in the morning sessions. Demonstrations of practical applications carried out on seven different types of capillary electrophoresis equipment from leading companies were presented in the afternoon sessions.

The scientific programme of the symposium started on 5 October. The keynote lectures in the opening sessions given by Professor Barry Karger (Capillary electrophoresis: Quo vadit?),

halfway through the scientific programme given by Professor Stellan Hjertén (Attempts to improve performance and to increase applicability of capillary electrophoresis) and in the closing session given by Professor Csaba Horváth (The place of capillary electrophoresis in analytical separations) provided a strong frame for the symposium. The lecture sessions with 39 oral presentations were devoted to Micellar electrokinetic chromatography, Isotachophoresis, Chiral separation, Isoelectric focusing, Separation of biopolymers, Theoretical and methodological aspects of capillary electrophoresis and Applications. The posters (as many as 50) were on view during the entire meeting, which, together with the two poster sessions organized in the late afternoon, provided space and time for direct discussions for the participants in small groups.

There were over 140 registered participants (not including the company representatives) from 19 European countries —from Russia to England and from Sweden to Turkey— and from USA, Japan, Israel and Canada making the symposium a highly international and friendly scientific event.

The main purpose of this symposium was to review the different separation principles of capillary electrophoresis available today, thereby helping the advanced scientists to generate new ideas for new principles and providing the application chemists, pharmacologists, biochemists, and many others with an overview of the various techniques in order to facilitate selection of the most appropriate one for the problems at hand.

The exhibition of commercial instrumentation confirmed that both the modular and fully automated types of equipment have future prospects to fulfill the requirements of variable detection techniques or unattended overnight analyses by capillary electrophoresis.

It is my pleasant duty to thank all the participants —professors and students, seniors and young researchers— for ensuring a very special atmosphere of the meeting during all the scientific as well as the social programmes. I would like to thank the Hungarian Biochemical Society and the University Medical School of Pécs for the support, and everyone concerned who contributed to this successful symposium from the very beginning until the very end. The contribution of the leading companies made the participation possible for researchers from countries where the scientific needs and the economic background are still not in the best harmony.

Last but not least, I would like to thank the participants for the high scientific activity which made it possible to publish this special issue and the guest editors Dr. Petr Boček and Dr. Zdenek Deyl for their effort and care in producing it.

Pécs, Hungary   Ferenc Kilár
                                             Chairman of ITP'94

Micellar electrokinetic chromatography using high-molecular-mass surfactants: comparison between anionic and cationic surfactants and effects of modifiers

Hiroto Ozaki[a],[*], Akinobu Ichihara[b], Shigeru Terabe[a]

[a]*Faculty of Science, Himeji Institute of Technology, Kamigori, Hyogo 678-12, Japan*
[b]*Dai-ichi Kogyo Seiyaku Co. Ltd., 55, Nishi-shichijo, Shimogyo-ku, Kyoto 600, Japan*

Abstract

Two high-molecular-mass surfactants, butyl acrylate–butyl methacrylate–methacrylic acid copolymer sodium salt (BBMA) and butyl methacrylate–methacryloyloxyethyltrimethylammonium chloride copolymer (BMAC), were utilized as new pseudo-stationary phases in micellar electrokinetic chromatography (MEKC). As with BBMA, BMAC was successfully employed as a pseudo-stationary phase, but reversal of the electroosmotic flow was observed. The capacity factors were proportional to the concentration of BMAC, and the critical micelle concentration was effectively zero. The effect of the addition of methanol and a non-ionic surfactant were studied in MEKC with BBMA. Chiral separation was studied by cyclodextrin (CD) modified MEKC with BBMA: enantiomers of dansylated-DL-amino acids were separated with 2% BBMA and 10 mM β-CD, giving larger separation factors than those obtained with 100 mM sodium dodecyl sulfate and 60 mM β-CD.

1. Introduction

Micellar electrokinetic chromatography (MEKC) [1–5], is a mode of capillary electrophoresis, where ionic micelles are used as pseudo-stationary phases. The separation by MEKC is based on the differential partitioning of analytes between the micelle and the surrounding aqueous phase. Therefore, it is important for manipulating resolution and selectivity in MEKC to select suitable surfactants and modifiers [6]. Different surfactants generally show different selectivity. Bile salts [7–9] and a double-chain surfactant [10], which have significantly different

molecular structures compared to sodium dodecyl sulfate (SDS), have shown remarkably different selectivity in comparison with SDS.

In MEKC, the capacity factor, k', which is defined as the ratio of the number of the analyte molecules incorporated into the micelle to that in the aqueous phase, is related to the volume of the micelle, V_{mc}, through

$$k' = K(V_{mc}/V_{aq}) \tag{1}$$

where K is the distribution coefficient and V_{aq} is the volume of the aqueous phase. The volume of the micelle is given as

$$V_{mc} = \bar{v}(C_{srf} - CMC) \tag{2}$$

where $\bar{v}$ is the partial specific volume of the surfactant forming the micelle, C_{srf} is the con-

---

* Corresponding author. Permanent address: Kaneka Techno Research Co. Ltd., 1-2-80, Yoshida-cho, Hyogo-ku, Kobe 652, Japan.

centration of the surfactant, and CMC is the critical micelle concentration. CMC depends on temperature, salt concentration, and additives.

High-molecular-mass surfactants are oligomers of monomeric surfactants or the polymers which show surface active properties as a whole. Palmer et al. [11,12] reported on MEKC with an oligomer synthesized from undecylenate. We reported on MEKC with butyl acrylate–butyl methacrylate–methacrylic acid copolymer sodium salt (BBMA), whose structure is shown in Fig. 1A [13,14]. BBMA is not an oligomer of the surfactant but a polymer which shows surface active properties. BBMA showed significantly different selectivity for naphthalene derivatives in comparison with SDS [14]. The CMC of BBMA was found to be effectively zero [14]. It was suggested that the stability of the micelle concentration of BBMA was superior to other surfactants.

Cyclodextrin (CD) is a chiral compound and capable of recognizing the molecular chirality. Therefore, CD modified MEKC (CD–MEKC) is useful for separating enantiomers [15–18]. Chiral separation of dansylated-DL-amino acids (Dns-DL-AAs) by CD–MEKC with SDS has been described previously [19]. SDS or low-molecular-mass surfactant molecules are considered to be co-included into the cavity of CD with the analyte enantiomers. BBMA is expected to be too large to be included into the cavity of CD.

In this paper, we describe the use of a cationic high-molecular-mass surfactant, the effects of modifiers in MEKC with BBMA, and the chiral

separation by CD–MEKC with BBMA. Butyl methacrylate–methacryloyloxyethyltrimethylammonium chloride (BMAC), as shown in Fig. 1B, is a cationic high-molecular-mass surfactant whose main chain is similar to that of BBMA. In MEKC with BBMA, methanol was used as a modifier of the aqueous phase and octaoxyethylene dodecanol [$(EO)_8R_{12}$], which is expected to form a mixed micelle, as a modifier of the micelle. CD–MEKC with BBMA was applied to separation of enantiomers of Dns-DL-AAs. Results of CD–MEKC with BBMA were compared with those using SDS.

2. Experimental

2.1. Reagents

BBMA and BMAC were supplied by Dai-ichi Kogyo Seiyaku (Kyoto, Japan). BBMA was provided as a 23% aqueous solution having a viscocity of 170 cP at 25°C. Since BBMA contains a minor amount of low-molecular-mass components, it was purified by the reprecipitation method with acetone [13,14]. BMAC was obtained as a 50% solution in water containing 40% 2-propanol and 10% methanol, and used without further purification. SDS, $(EO)_8R_{12}$, α-CD, β-CD and γ-CD were purchased from Nacalai Tesque (Kyoto, Japan). All other reagents were of analytical grade and water was purified with a Milli-Q system. All sample compounds, naphthalene derivatives and Dns-DL-AAs, were of analytical grade and used as received. Sample solutes were dissolved in about 25% aqueous methanol, which also served as a marker of the electroosmotic flow. Phenanthrene was used as a tracer of the micelle.

2.2. Apparatus

MEKC was performed with a Bio-Rad BioFocus 3000 CE System (Hercules, CA, USA) using a fused-silica capillary of 50 μm I.D. obtained from Polymicro Technologies (Phoenix, AZ, USA). The length of the capillary used in
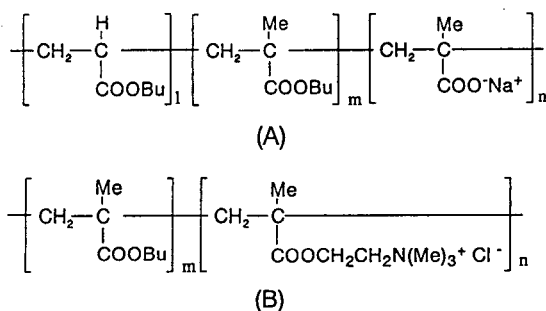
Fig. 1. Molecular structure of BBMA (A) and BMAC (B). Me = methyl; Bu = butyl.

MEKC was 36.5 cm (32 cm to the detector) or 54.5 cm (50 cm to the detector). The capillary was thermostated at 30°C and sample vials were at 15°C. Samples were injected by the pressurization method [2–5 s at 1 p.s.i. (6894.76 Pa)]. Separated zones were detected at 210, 250 and 280 nm simultaneously under the multi-wavelength mode and the electropherograms shown in this paper were recorded at 210 nm.

3. Results and discussion

3.1. Separation by MEKC with BMAC

A mixture of naphthalene derivatives was separated by MEKC with 2% BMAC and 20% 2-propanol in 100 mM borate–50 mM phosphate buffer (pH 7.0). BMAC was not soluble in an aqueous buffer without 2-propanol. Since the direction of electroosmotic flow was reversed, all solutes were injected at the negative end and migrated toward the positive electrode. Fig. 2 shows separations of naphthalene derivatives by MEKC with three different surfactants, BBMA, BMAC, and SDS. The migration order with BMAC was similar to that with BBMA, except for 1-naphthylamine and 1-naphthaleneethanol. However, it was significantly different from that with SDS. In Fig. 2A and B, the peaks with BMAC were just as sharp as with BBMA,
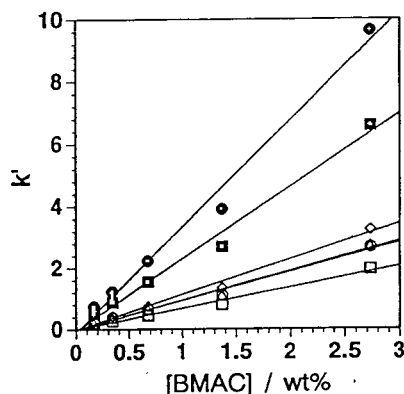
Fig. 3. Dependence of the capacity factor (k') on the concentration of BMAC. Solutes: $\square$ = 1-naphthalenemethanol; $\bigcirc$ = 1,6-dihydroxynaphthalene; $\triangle$ = 1-naphthylamine; $\diamond$ = 1-naphthaleneethanol; $\blacksquare$ = 2-naphthol; $\bullet$ = 1-naphthol. The conditions were the same as in Fig. 2B except for the concentration of BMAC.

suggesting that the adsorption of BMAC onto the capillary wall did not cause a serious loss of efficiency.

Fig. 3 shows the dependence of the capacity factors of the naphthalene derivatives on the concentration of BMAC. The capacity factors were proportional to the BMAC concentration and all the plotted lines passed through or nearly through the origin. The CMC of BMAC was nearly zero as deduced from Eq. 2, therefore the
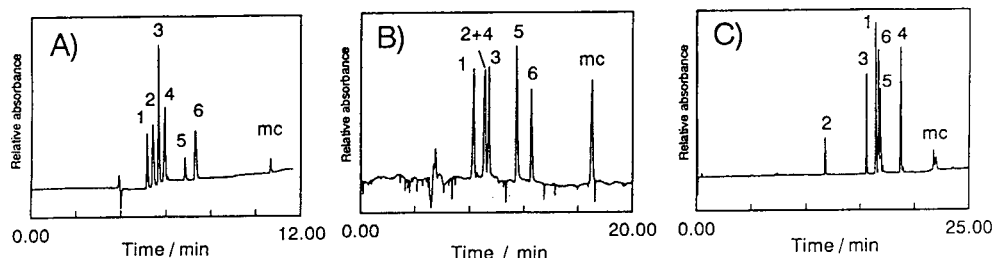
Fig. 2. MEKC separations of naphthalene derivatives with BBMA (A), BMAC (B), and SDS (C). Peaks: 1 = 1-naphthalenemethanol; 2 = 1,6-dihydroxynaphthalene; 3 = 1-naphthylamine; 4 = 1-naphthaleneethanol; 5 = 2-naphthol; 6 = 1-naphthol; mc = phenanthrene. Conditions: capillary, 36.5 cm (32 cm to the detector) × 50 μm I.D.; separation solution, (A) 2% BBMA in 50 mM phosphate–100 mM borate buffer (pH 8.0), (B) 2% BMAC and 20% 2-propanol in 50 mM phosphate–100 mM borate buffer (pH 7.0), (C) 50 mM SDS in 50 mM phosphate–100 mM borate buffer (pH 7.0); applied voltage (A) 15 kV, (B) 20 kV, (C) 20 kV; detection 210 nm.

micelle of BMAC was formed from one mole-
cule.

3.2. Effects of additions of methanol and a non-ionic surfactant on the MEKC separation with BBMA

The effect of the pH, the compositon, and the molecular mass of BBMA on the MEKC sepa-
ration have been reported previously [13,14]. The effect of modifiers of the aqueous phase on separation were investigated in this study. Fig. 4 shows the dependence of capacity factors of the naphthalene derivatives on the concentration of methanol. The capacity factors decreased with an increase in the methanol concentration. Fig. 5 shows the effect of methanol on the separation of the naphthalene derivatives using BBMA and SDS. The migration order of 1,6-dihydroxynaph-
thalene was altered by the methanol addition to the BBMA system as shown in Fig. 5B and that of 1-naphthol changed in the SDS system as in Fig. 5D. The capacity factors decreased by the methanol addition both to the BBMA and SDS systems.

Fig. 6 shows the dependence of the capacity factors on the concentration of $(EO)_8R_{12}$ added to the BBMA solution. The capacity factors

Fig. 5. Separation of the naphthalene derivatives with BBMA (A), BBMA and methanol (B), SDS (C), and SDS and methanol (D). The solutes are the same as in Fig. 2. Separation solution, (A) 2% BBMA in 50 mM phosphate–100 mM borate buffer (pH 8.0), (B) 40% methanol in the same BBMA solution as used in (A), (C) 50 mM SDS in 50 mM phosphate–100 mM borate buffer (pH 7.0), (D) 40% methanol in the same SDS solution as used in (C); applied voltage, 10 kV. The other conditions are the same as in Fig. 2.

increased with an increase in the amount of $(EO)_8R_{12}$ probably because of the increase in the micellar volume by the formation of a mixed

Fig. 4. Dependence of the capacity factors (k') of the naphthalene derivatives on the concentration of methanol. The solutes are the same as in Fig. 3. Separation solution, 2% BBMA and methanol in 50 mM phosphate–100 mM borate buffer (pH 8.0); applied voltage, 10 kV. The other conditions are the same as in Fig. 2.
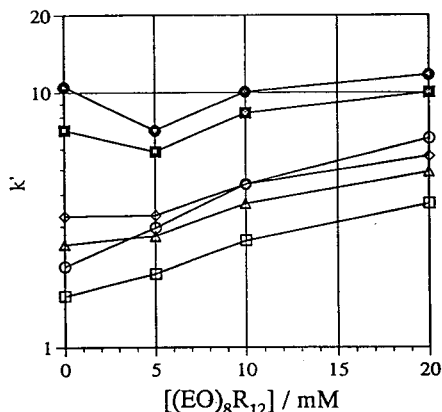
Fig. 6. Dependence of the capacity factors (k') of the naphthalene derivatives on the concentration of $(EO)_8R_{12}$. The solutes are the same as in Fig. 3. Separation solution, 2% BBMA and $(EO)_8R_{12}$ in 50 mM phosphate–100 mM borate buffer (pH 8.0); applied voltage, 10 kV. The other conditions are the same as in Fig. 2.

micelle [6,21]. In the case that mixed micelle is not formed and two kinds of micelles are formed, the capacity factors should decrease with an increase in the ammount of the non-ionic surfactant. Therefore, the results strongly suggest that $(EO)_8R_{12}$ formed a mixed micelle with BBMA. The migration order of 1,6-dihydroxynaphthalene was changed more significantly than the others with an increase in the concentration of $(EO)_8R_{12}$. The migration-time window became narrower with increasing non-ionic surfactant concentration because of the decrease in the surface charge density.

Fig. 7 shows the separation of the naphthalene derivatives by MEKC with three different mixed micelles containing $(EO)_8R_{12}$. It should be noted that the mixed micelle with BBMA shows a different selectivity compared to either the mixed micelles with SDS or with sodium laurate, which also have a carboxylate group as the polar group. The addition of a non-ionic surfactant to

SDS solutions resulted on the alteration of selectivity [5,21,22] as shown in Fig. 5C and Fig. 7B.

3.3. Chiral separation of Dns-DL-AAs by CD–MEKC with BBMA

Table 1 lists the results of the separation of enantiomers of ten Dns-DL-AAs by CD–MEKC with 10 mM β-CD and 2% BBMA. The results with 60 mM β-CD and 100 mM SDS [19] are also given in Table 1. The migration time of the BBMA micelle in the CD–BBMA system was assumed to be equal to that of phenanthrene observed with 2% BBMA in the absence of β-CD. BBMA was used without purification in these experiments. The separation solution used was clear at first, but a white precipitate was observed after a few hours. In Table 1, nine pairs of the ten enantiomeric pairs were successfully separated with the BBMA system and the separation factors of eight pairs of these were larger than those with the SDS system.

The migration times of different DNS-AAs were close each other in the BBMA system; from 10 to 11 min, except for those of Dns-DL-Asp with the SDS system, where the migration times of DNS-AAs were widely spread [19]. The migration order with the BBMA system was significantly different from that with the SDS system. It should be noted that Dns-DL-Phe migrated fastest of all and Dns-DL-Nle migrated faster than Dns-DL-Nva. This order is not consistent with the hydrophobicity of the analyte. The results suggest that Dns-DL-AAs are mainly solubilized by the BBMA micelle with the incorporation of the Dns-group into the hydrophobic core of the micelle.

Table 2 summarizes the results obtained with 2% unpurified or purified BBMA with 10 mM β-CD and 20% methanol, and the results from Ref. [19] with 60 mM β-CD, 100 mM SDS and 20% methanol. The separation solution prepared with unpurified BBMA generated a white precipitate after a day, but that with purified BBMA did not show any changes. In Table 2, all enantiomers were separated with both the BBMA systems and all separation factors were

Fig. 7. Separations of the naphthalene derivatives using $(EO)_8R_{12}$ with sodium laurate (A), SDS (B), and BBMA (C). The solutes are the same as in Fig. 2. Separation solution, (A) 50 mM sodium laurate and 20 mM $(EO)_8R_{12}$ in 50 mM phosphate–100 mM borate buffer (pH 7.0), (B) 50 mM SDS and 20 mM $(EO)_8R_{12}$ in the same buffer as used in (A), (C) 2% BBMA and 20 mM $(EO)_8R_{12}$ in the same buffer as used in (A); applied voltage, 20 kV. Other conditions are the same as in Fig. 2.

Table 1
Separation of Dns-DL-AAs by CD–MEKC

Dns-DL-AAs	2% BBMA–10 mM β-CD			100 mM SDS–60 mM β-CD
	t_1/min	t_2/min	α[a]	α[b]
Phe	10.00	10.00	1.00	1.04
Leu	10.61	10.73	1.05	1.03
Nle	10.67	10.78	1.04	1.02
Trp	10.54	10.60	1.02	1.04
Met	10.67	10.76	1.03	1.00
Nva	10.70	10.87	1.07	1.02
Val	10.61	10.75	1.05	1.03
Ser	10.92	11.01	1.03	1.00
Thr	10.76	10.91	1.05	1.00
Asp	15.47	15.97	1.10	1.03

Conditions: capillary, 54.5 cm (50 cm to the detector) × 50 μm I.D.; separation solution, 2% unpurified BBMA and 10 mM β-CD in 50 mM phosphate–100 mM borate buffer (pH 8.0); applied voltage, 20 kV; detection wavelength, 210 nm.
[a] The migration time of the micelle was assumed to be equal to that of phenanthrene observed with 2% BBMA solution without β-CD.
[b] From Ref. 19.

larger than those with the SDS system. The purified BBMA clearly showed better resolution than the unpurified BBMA.

BBMA forms a molecular micelle which consists of one molecule, whereas SDS forms a micelle in the presence of the monomeric molecule whose concentration is equal to the CMC.

The white precipitate mentioned above was probably a complex formed from β-CD and a minor component of BBMA which was removed by the purification, because the BBMA molecule should not form a complex with β-CD. The results of Table 1 show that BBMA was superior to SDS for the separation of enantiomeric Dns-

Table 2
Separation of Dns-DL-AAs by CD–MEKC with methanol

Dns-DL-AAs	2% unpurified BBMA –10 mM β-CD			2% purified BBMA –10 mM β-CD			100 mM SDS –60 mM β-CD
	t_1/min	t_2/min	α[a]	t_1/min	t_2/min	α[b]	α[c]
Phe	13.03	13.25	1.05	10.46	10.61	1.06	1.03
Leu	13.52	13.80	1.07	10.87	11.08	1.08	1.03
Nle	13.57	13.80	1.05	10.84	11.01	1.06	1.02
Trp	13.77	13.84	1.02	11.31	11.36	1.02	1.01
Met	13.91	14.08	1.04	11.15	11.31	1.06	1.02
Nva	13.93	14.12	1.04	11.15	11.31	1.06	1.02
Val	14.09	14.35	1.06	11.59	11.79	1.07	1.03
Ser	14.35	14.53	1.04	11.73	11.89	1.24	1.02
Thr	14.68	14.98	1.07	11.90	12.14	1.08	1.04
Asp	25.67	27.08	1.30	21.49	22.50	2.15	1.05

Conditions are same as shown in Table 1 except for the addition of 20% methanol to the separation solution.
[a,b] See the footnote a and b in Table 1.
[c] From Ref. [19].

DL-AAs owing to the absence of the monomeric surfactant molecules which might be co-included with the enantiomer into the cavity of β-CD. Furthermore, the results of Table 2 show that the purified BBMA was superior to the un-purified BBMA because of the absence of the minor components which gave the precipitate. From Tables 1 and 2, the addition of methanol to the BBMA system increased the resolution except for Dns-DL-Nva in comparison with the results with SDS system [19]. Fig. 8 shows the example of the separation of enantiomers by CD–MEKC with purified BBMA. Enantiomers of timepidium bromide were successfully resolved under the same condition as in Fig. 8.

The other CDs were also employed together with purified BBMA. No enantiomer of the ten Ds-DL-AAs were separated with 10 mM α-CD and 2% BBMA. The separation solution did not generate any precipitate. Seven of the ten Dns-DL-AAs (Leu, Nle, Met, Nva, Val, Thr and Asp) were successfully separated with 10 mM γ-CD and 2% BBMA. The separation factors of three of the seven (Val, Thr and Asp) were larger, but those of the other four were less than those obtained with 60 mM γ-CD and 100 mM SDS [19]. The separation solution gave a white precipitate after few hours. It should be noted that γ-CD tends to generate the precipitate more than β-CD. These results suggest that in the

BBMA system β-CD is most suitable for CD–MEKC separation of Dns-DL-AAs. In the SDS system γ-CD is more suitable than β-CD except for Trp, Ser and Asp [19]. With the purified BBMA, which will not generate precipitate with γ-CD, Dns-DL-AAs will be better separated with the BBMA and γ-CD system than with the SDS and γ-CD system.

4. Conclusions

BMAC, as BBMA, is found to be a useful high-molecular-mass surfactant for MEKC. BMAC gave a zero CMC, reversed direction of electroosmotic flow, and different selectivity. Additions of methanol or $(EO)_8R_{12}$ changed separation and selectivity in MEKC with BBMA. For the chiral separation of Dns-DL-AAs by CD–MEKC, BBMA was superior to SDS because of the absence of monomeric surfactant.

Acknowledgements
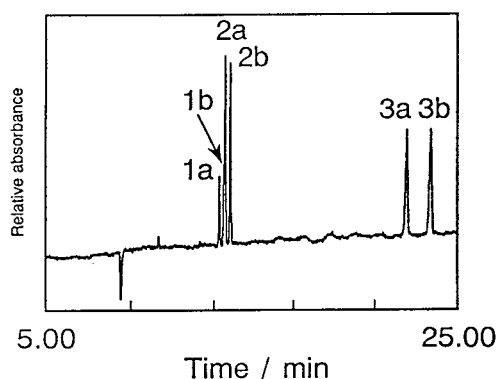
Fig. 8. Separations of Dns-DL-AAs by CD–MEKC with BBMA: 1a, 1b = Dns-DL-Phe; 2a, 2b = Dns-DL-Thr; 3a, 3b = Dns-DL-Asp. Separation solution, 10 mM β-CD, 2% BBMA and 20% methanol. Other conditions are the same as in Table 1.

References

[1] S. Terabe, K. Otsuka, K. Ichikawa, A. Tsuchiya and T. Ando, Anal. Chem., 56 (1984) 111–113.
[2] S. Terabe, K. Otsuka and T. Ando, Anal. Chem., 57 (1985) 834–841.
[3] J. Vindevogel and P. Sandra, Introduction to Micellar Electrokinetic Chromatography, Huthig, Heidelberg, 1992.
[4] S. Terabe, in N. Guzman (Editor), Capillary Electrophoresis Technology, Marcel Dekker, New York, 1993, pp. 65–87.
[5] S. Terabe, N. Chen and K. Otsuka, Adv. Electrophoresis, 7 (1994) 87–153.

[6] S. Terabe, J. Pharm. Biomed. Anal., 10 (1992) 705–715.

[7] H. Nishi, T. Fukuyama, M. Matsuo and S. Terabe, J. Chromatogr., 513 (1990) 279–295.

[8] R.O. Cole, M.J. Sepaniak, W.L. Hinze, J. Gorse and K. Oldiges, *J. Chromatogr.*, 557 (1991) 113–123.

[9] R.D. Holland and M.J. Sepaniak, Anal. Chem., 65 (1993) 1140–1146.

[10] M. Tanaka, T. Ishida, T. Araki, A. Masuyama, Y. Nakatsuji, M. Okahara and S. Terabe, J. Chromatogr., 648 (1993) 468–473.

[11] C.P. Palmer, M.Y. Khaled and H.M. McNair, J. High Resolut. Chromatogr., 15 (1992) 756–762.

[12] C.P. Palmer and H.M. McNair, J. Microcol. Sep., 4 (1992) 509–514.

[13] S. Terabe, H. Ozaki and Y. Tanaka, J. Chin. Chem. Soc., 41 (1994) 251–257.

[14] H. Ozaki, S. Terabe and A. Ichihara, J. Chromatogr. A, 680 (1994) 117–123.

[15] H. Nishi, T. Fukuyama and S. Terabe, J. Chromatogr., 553 (1991) 503.

[16] T. Ueda, F. Kitamura, R. Mitchel, T. Metcalf, T. Kuwana and A. Nakamoto, Anal. Chem., 63 (1991) 2979–2981.

[17] K. Otsuka and S. Terabe, J. Liq. Chromatogr., 16 (1993) 945–953.

[18] K. Otsuka and S. Terabe, in N. Guzman (Editor), Capillary Electrophoresis Technology, Marcel Dekker, New York, 1993, pp. 617–629.

[19] S. Terabe, Y. Miyashita, Y. Ishihama and O. Shibata, J. Chromatogr., 636 (1993) 47–55.

[20] K. Otsuka, S. Terabe and T. Ando, J. Chromatogr., 332 (1985) 219–226.

[21] S. Terabe, H. Ozaki and Y. Ishihama, Bunseki Kagaku, 42 (1993) 859–866.

[22] E.L. Little and J.P. Foley, J. Microcol, Sep., 4 (1992) 145–154.

Microemulsion electrokinetic chromatography with different organic modifiers: separation of water- and lipid-soluble vitamins

R.L. Boso[a], M.S. Bellini[a], I. Mikšík[b], Z. Deyl[b],*

[a]Glaxo Research Laboratories, Via A. Fleming 4, 37100 Verona, Italy
[b]Institute of Physiology, Academy of Sciences of the Czech Republic, Videňská 1083, CZ-14220 Prague 4, Czech Republic

Abstract

Microemulsions prepared by using either sodium dodecyl sulfate (SDS) or trimethyltetradecylammonium bromide (TTAB) were tested with regard to the migration time, selectivity and number of theoretical plates using a set of both water-soluble and lipid-soluble vitamins. While in the separations where SDS was used as the surface-active agent for microemulsion preparation, better resolutions were obtained with both hydrophilic and lipophilic vitamins, with TTAB the best separations were obtained with the micelle-forming reagent only or with diethyl ether as the microemulsion-forming component. In the SDS-based separations nicotinic acid was moving with the same velocity (relative to the endoosmotic flow) regardless of the emulsion or micellar phase used. It is proposed that owing to its behaviour it can serve as an ideal internal standard in further studies on microemulsion separations.

1. Introduction

Microemulsion capillary electrophoresis (electrokinetic chromatography, MEEKC) represents a variation of micellar electrokinetic chromatography commonly applied today. Whereas in the latter the partition process occurs between the surrounding background electrolyte and the micelle, in microemulsion separations the partitioning takes place between the background electrolyte and the microemulsion droplets.

Microemulsions are microheterogeneous liquids which have characteristic properties as solvents such as optical transparency, thermodynamic stability and high solubilization power. The first attempt to apply these microemulsions for electrokinetic separations was published by Watarai [1] in 1991. In this case an oil-in-water emulsion was applied, consisting of water–sodium dodecyl sulfate (SDS)–1-butanol–heptane (89.28:3.31:6.61:0.81, w/w); 0.01 M phosphoric acid or 0.01 M hydrogen-carbonate buffer served for controlling the pH of the electrolyte. In separating a test mixture of fluorescent aromatic compounds at pH 3.0, it was observed that all of the solutes, including neutral and anionic species, migrated to the anodic end. It was concluded that the migration of the anionic microemulsion droplets is faster than the electroosmotic flow, which is in the opposite direction to the migration of the droplets. The migration order could be related to hydrophobicity, indicating that the better partitioning solutes migrate faster. Under alkaline conditions the endo-

---

* Corresponding author.

osmotic flow becomes faster than the electro-phoretic mobility of the microemulsion and con-sequently the solutes migrated to the cathodic end.

More recently, fundamental characteristics of MEEKC were described by Terabe et al. [2]. A microemulsion consisting of heptane–SDS–butanol–buffer (0.81 : 1.66 : 6.61 : 90.92, w/w) was mainly employed.

The separation selectivity of MEEKC was compared with that of MEKC by using three different test mixtures. In microemulsion sepa-rations stronger affinity to the droplets compared with SDS micelles was observed with non-polar compounds. The migration time window could be extended by increasing the proportion of SDS in the microemulsion. It was also observed that the plate heights were higher in MEEKC.

Microemulsions prepared by mixing the or-ganic solvent, water (buffer), surfactant and cosurfactant (such as a medium-chain alcohol) are transparent and thermodynamically stable. According to Terabe et al. [2], they consist of an organic solvent-containing core surrounded by the surfactant and cosurfactant. Their role is to stabilize the droplet.

The higher solubilization power of microemul-sions has been claimed also as an advantage offering a wider dynamic range in sample con-centration [3].

Despite the great potential of this technique, there have been only a few reports on the use of microemulsion systems so far.

In order to obtain some information about both lipid- and water-soluble solutes, a mixture of lipid- and water-soluble vitamins was selected as the test mixture. A mixture of similar compo-sition has been fully separated by Ong et al. [4] using 30 mM SDS in 0.1 M borate–0.05 M phosphate (pH 7.6); however, addition of β-cyclodextrin (3 mM) was needed, in particular to obtain an adequate separation of the vitamin B-group members. More recently, micellar elec-trokinetic chromatography was applied to the separation of water-soluble vitamins by Dinelli and Bonetti [5]. The analytical procedure used the same Beckman system as in this work, but with a 70 cm × 100 μm I.D. capillary at 25°C

operated with 50 mM sodium borate–22.5 mM SDS–10% (v/v) methanol (pH 8.0) at 16 kV.

In this work, we attempted to compare the efficiency of microemulsions containing different solvents as the organic phase core. The efficiency of different solvents was tested using water- and organic solvent-soluble vitamins.

2. Experimental

Electrokinetic chromatography was performed on a P/ACE System 2100 (Beckman, Palo Alto, CA, USA) with a 47 cm (40 cm to the detector) × 50 μm I.D. fused-silica capillary (un-treated) (Polymicro Technologies, Tucson, AZ, USA). The device was run routinely at 10 kV (about 17.5 μA) at 25°C. UV detection at 214 nm was applied. The instrument was computer oper-ated using the System Gold software.

All the reagents and standards (samples) were of analytical-reagent grade. The set of vitamins used for testing the different emulsions was obtained from Merck (Darmstadt, Germany) and solvents were purchased from Carlo Erba (Milan, Italy).

Both an anionic (SDS; Sigma, St. Louis, MO, USA) and a cationic surfactant [trimethyltet-radecylammonium bromide (TTAB); Sigma] were used to prepare the microemulsions.

Microemulsions were prepared by mixing the organic solvent (0.81%, w/w), SDS (or TTAB) (6.62 or 3.31%, w/w, respectively) and butanol (6.61%, w/w) with 20 mM phosphate buffer (pH 7.0) (85.96 or 89.28%, w/w) according to the method of Watarai [1]. Alternatively, 500 mM SDS or TTAB (in water) were mixed 2:1 with the solvent in question, vortex mixed and ti-trated with 1-butanol until the mixture cleared (no addition of 1-butanol was needed in the case of 2-methyl-2-propanol). The resulting solution was diluted with 20 mM phosphate buffer (pH 7.0) to yield a 20 mM solution with respect to the surfactant. With SDS-containing background electrolytes, a high voltage was applied to the anodic end of the capillary, whereas with TTAB the polarity was reversed.

Samples were routinely prepared as solutions
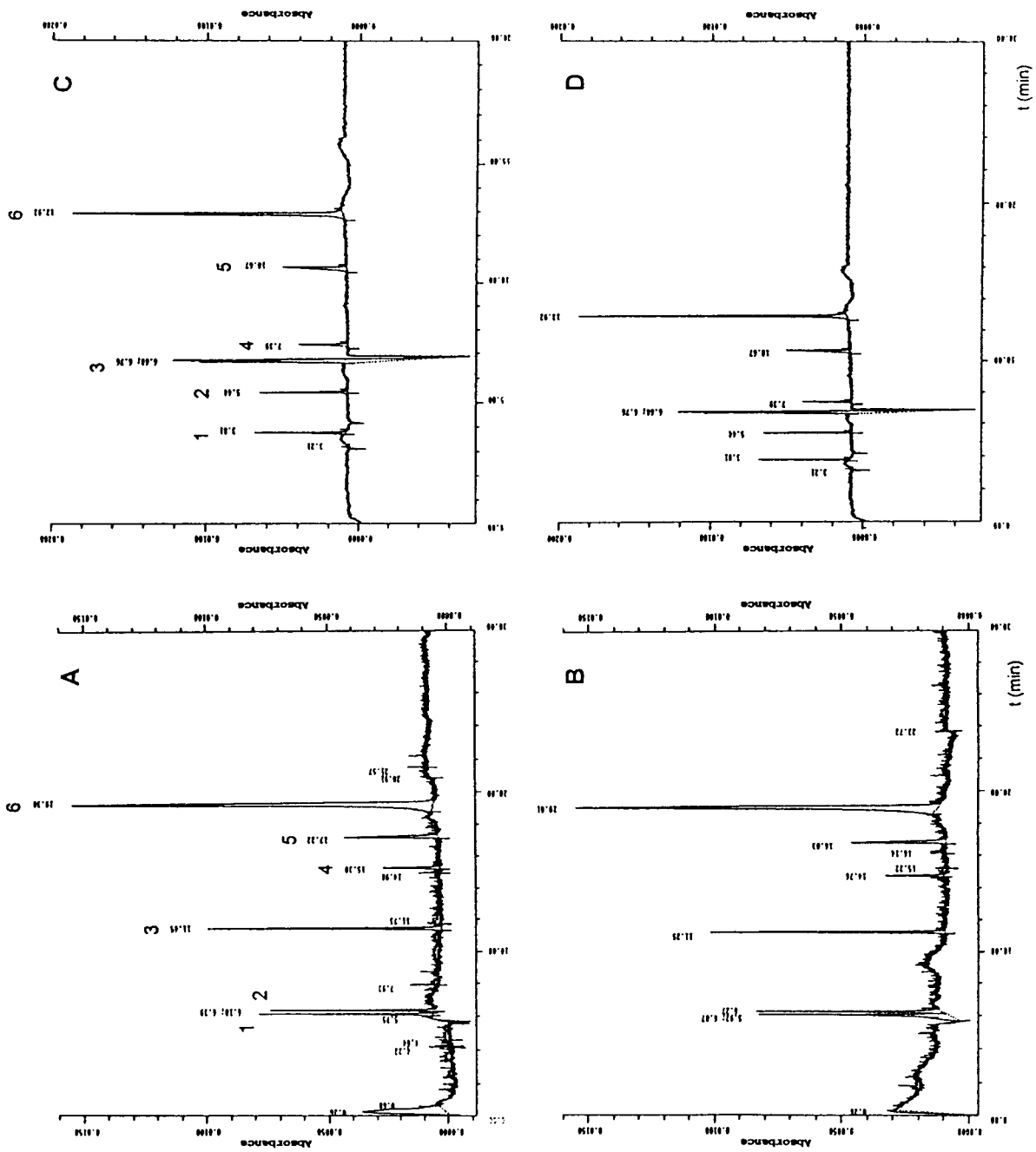
Fig. 1. Comparison of results obtained with two different methods of micellar phase preparation: (A) SDS-*n*-hexane (0.81% *n*-hexane, 6.62% SDS, 6.61% *n*-butanol, 85.96% phosphate buffer); (B) 500 mM SDS-n-hexane ($2:1$), *n*-butanol added until the solution cleared. Peaks: $1 =$ nicotinamide; $2 =$ pyridoxol; $3 =$ nicotinic acid; $4 =$ thiamine; $5 =$ vitamin E; $6 =$ vitamin A. (C) TTAB-*n*-amyl alcohol (0.81% *n*-amyl alcohol, 3.31% TTAB, 6.61% *n*-butanol, 89.28% phosphate buffer); (D) 500 mM TTAB-*n*-amyl alcohol ($2:1$), *n*-butanol added until the solution cleared. Peaks: $1 =$ thiamine; $2 =$ nicotinic acid; $3 =$ pyridoxol; $4 =$ nicotinamide; $5 =$ vitamin E; $6 =$ vitamin A.

of 100 μg/ml in methanol–water (1:1, v/v) and were applied by an overpressure of $3.45 \cdot 10^7$ Pa for 3 s.

3. Results and discussion

As shown in Fig. 1, there was a very small difference, if any, between the two methods of microemulsion preparation. Therefore, the method using dilution of concentrated surfactant was preferred in subsequent experiments. In order to visualize the effect of different microemulsions most clearly, suboptimum conditions for the separation in the background electrolyte were selected. Figs. 2 and 3 summarize the retention time changes with different organic phases in the microemulsion core with SDS and TTAB surfactants respectively. In both cases pyridoxol (vitamin B_6) and nicotinamide represented the critical combination that was difficult to separate. With TTAB-containing mobile phases the situation was further complicated by

the fact that both of these vitamins were running near the endoosmotic flow peak.

3.1. SDS

Whereas no separation of pyridoxol (B_6), thiamine (B_1) and nicotinamide occurred with the background electrolyte containing SDS at 20 mM concentration only, on changing the micellar phase to an n-hexane-, n-heptane- or cyclohexane-containing emulsion resulted in a resolution of 1.0 or higher (in the case of cyclohexane) (Table 1). Another change observed was the reversed elution of vitamin E relative to vitamin A. In the absence of the microemulsion-forming agent vitamin A is eluted before vitamin E; this observation confirms the previously published results of Ong et al. [4]. However, in any of the organic solvents tested (including those capable of separating pyridoxol and nicotinamide), vitamin A moves more swiftly to the anode, which results in a later appearance of its peak on the electropherogram (Fig. 1) as compared with
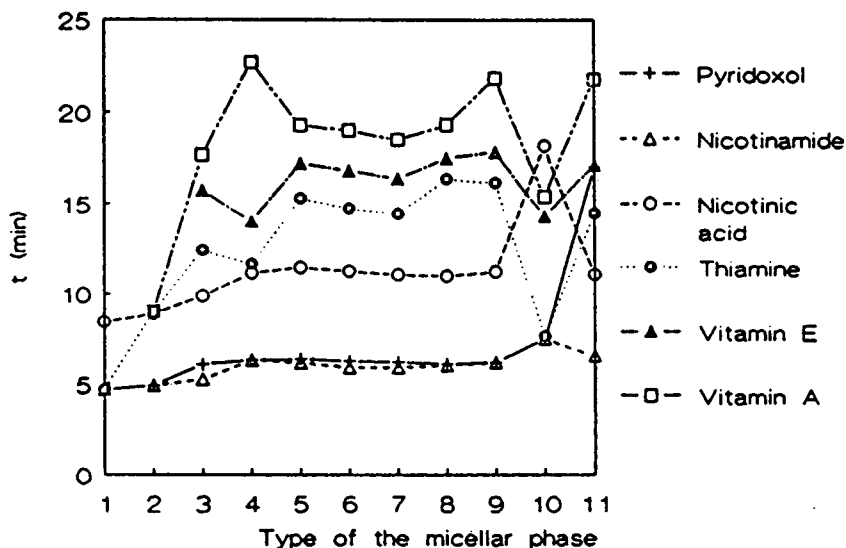
Fig. 2. Changes in electrophoretic mobility in different microemulsion phases with SDS as surfactant. (1) 20 mM phosphate buffer (pH 7.0); (2) 20 mM SDS (vitamin E did not elute within a 28-min running time; (3) 20 mM phosphate buffer (pH 7.0)–50 mM SDS, microemulsion phase prepared by mixing SDS and diethyl ether (4:1) (see Experimental); (4) 20 mM phosphate buffer (pH 7.0)–50 mM SDS, microemulsion phase prepared by mixing SDS and diethyl ether (2:1); (5) as (4), but with n-hexane; (6) as (4), but with n-heptane; (7) as (4), but with cyclohexane; (8) as (4), but with chloroform; (9) as (4), but with methylene chloride; (10) as (4), but with 2-methyl-2-propanol; (11) as (4), but SDS and octanol were mixed 10:2.
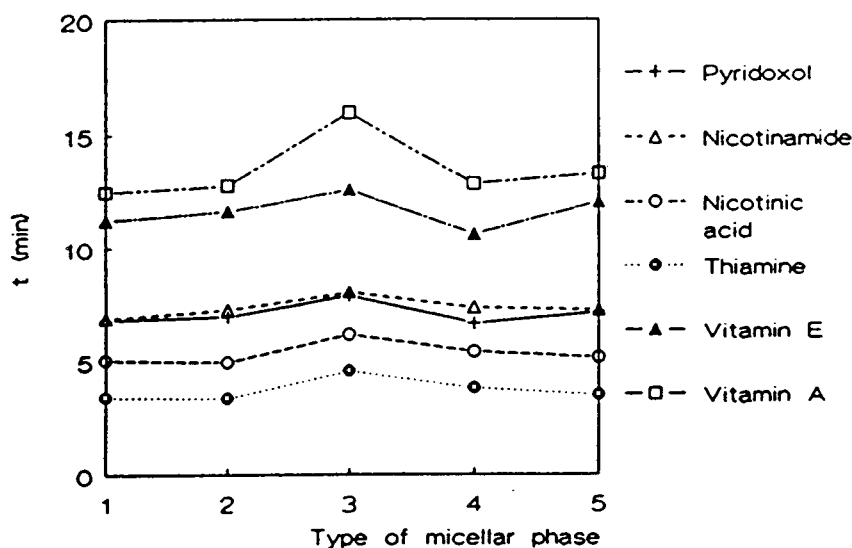
Fig. 3. Changes in electrophoretic mobility in different microemulsion phases with TTAB as surfactant. (1) 20 mM phosphate buffer (pH 7.0)–10 mM TTAB; (2) as (1), but with diethyl ether added to concentrated (500 mM) TTAB in a ratio 1:2; (3) as (2), but with 2-methyl-2-propanol; (4) as (2), but with n-amyl alcohol; (5) as (2) but with 2-methyl-2-propanol, prepared by mixing the solvent with TTAB in a ratio 1:4.

vitamin E (the sequence of these two peaks is interchanged).

The time after which the vitamin A peak passes the detector can be efficiently influenced by the proportion of the organic solvents in the

Table 1
Resolution of the critical pair pyridoxol–nicotinamide

Surfactant used	Organic component of the emulsion	Resolution[a]
SDS	SDS only	No separation
	Diethyl ether	0.90
	n-Hexane	1.00
	n-Heptane	1.00
	Cyclohexane	1.50
	Chloroform	0.70
	Octanol	No separation
TTAB	TTAB only	0.87
	Diethyl ether	0.85
	2-Methyl-2-propanol	0.75 (divided by EOF in two peaks)
	n-Amyl alcohol	0.50

[a] $R = \Delta t / 4\sigma_t$, where Δt is the difference in time of elution between two consecutive peaks and σ_t is the standard width of a single peak.

microemulsion. If the proportion of, e.g., diethyl ether in the microemulsion is increased, the time delay to the detector of vitamin A is increased in spite of the fact that all the other vitamins (including vitamin E) exhibit a shorter running time. Concomitantly, with a higher proportion of the organic solvent in the microemulsion, the resolution of the water-soluble pyridoxol–nicotinamide pair is lost.

Comparing these results with the migration times in cyclohexane-loaded micelles, one there is a much longer migration time of vitamin E compared with the diethyl ether-containing emulsion. In contrast, the running time of vitamin A is shorter, indicating that this vitamin interacts with the cyclohexane microemulsion less readily than with the emulsion prepared with diethyl ether.

Table 2 gives the numbers of theoretical plates achieved with different organic components of the microemulsion and different components of the test mixture. Generally, low plate counts were observed with the solutes moving in front of the electropherogram. However, selection of a proper organic component of the microemulsion can increase the plate count of these (water-

Table 2
Number of theoretical plates for the test mixture in microemulsions containing different organic solvents with SDS as surfactant

Vitamin	Diethyl ether	n-Hexane	n-Heptane	Cyclo-hexane	Chloroform	Octanol
Nicotinamide	17 978	82 495	77 400	215 001	180 821	} 234 327
Pyridoxol	79 847	244 992	87 117	237 383	230 552	
Nicotinic acid	585 680	283 181	280 462	271 559	266 674	272 050
Thiamine	13 500	505 634	478 356	463 988	148 640	116 478
Vitamin E	536 495	444 792	435 888	149 185	162 374	72 651
Vitamin A	100 125	196 997	200 099	190 016	91 905	65 730

No. of theoretical plates (N) calculated according to the equation $N = 5.54 \, (t_r/\sigma)^2$, where t_r is the migration time and σ is the peak width at half-height [5,6]. Data obtained represent averages of three measurements; S.D. lies within 5–10% relative limits.

soluble) vitamins by a factor of more than ten (compare nicotinamide counts in diethyl ether- and cyclohexane-containing microemulsions). The highest plate counts in the mixture tested were always seen with nicotine acid. This is perhaps due to the very clear separation mechanism, based on its charge only. Indeed, the retention of nicotonic acid in our experiments varied in parallel with the endoosmotic flow and no influence was observed regarding the changing organic core of the microemulsion droplets (Table 3). This makes nicotonic acid a very suitable internal standard in future investigations on microemulsion separations. Typical runs showing the separations obtained with n-hexane-, n-heptane- and cyclohexane containing microemulsions are shown in Fig. 4.

The partition mechanism of vitamin A is the other extreme, as it is preferentially influenced by the nature of the organic component of the microemulsion. It always virtually coincides with the peak of Sudan III, whatever organic modifier is used in the emulsion. Consequently, the position of vitamin A in the electrophoregrams shown indicates the end of the separation window. In the absence of the organic component of the microemulsion (in micellar separations) this is not true, as the last-eluting component is always vitamin E, which elutes within the separation window, elution of the Sudan III peak being delayed after the vitamin E peak.

3.2. TTAB

An overview of migration differences using TTAB as surfactant for microemulsion preparation is shown in Fig. 3. Table 4 summarizes the N values for individual components of the test mixture. Data regarding resolution of the critical pair pyridoxol–nicotinamides are presented in Table 1.

In general, the effect of the organic microemulsion phase in the presence of a cationic surfactant is much less pronounced than that with an anionic surfactant. As can be be predicted, the sequence of the water-soluble vitamins (vitamin B_1, nicotinic acid, pyridoxol, nicotinamide) is reversed compared with the SDS-based separations, where nicotinamide is the first peak from the mixture to be seen in the detector. On the other hand, the lipophilic species, vitamin E and A emerge in the same sequence in

Table 3
Relative retention of the nicotinic acid peak with respect to the endoosmotic flow

Organic solvent added to SDS	Relative migration
None	1.90
Diethyl ether	1.91
n-Hexane	1.88
n-Heptane	1.92
Cyclohexane	1.90
Chloroform	1.86
Octanol	1.80
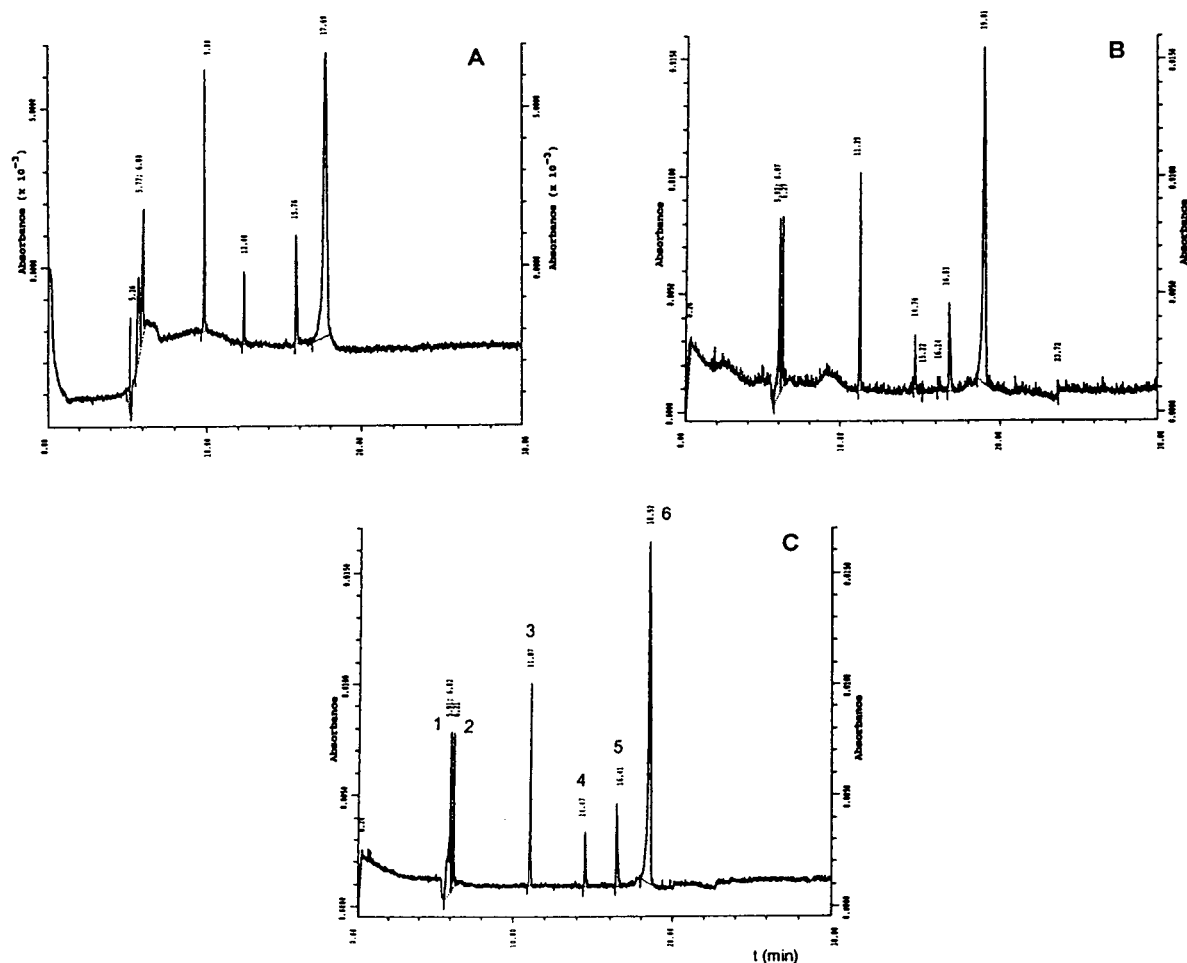
Fig. 4. Typical profiles obtained with (A) SDS–diethyl ether, (B) SDS–*n*-hexane and (C) SDS–cyclohexane. Peaks: 1 = nicotinamide; 2 = pyridoxol; 3 = nicotinic acid; 4 = thiamine; 5 = vitamin E; 6 = vitamin A. Microemulsion phase was prepared by mixing two parts of 500 m*M* SDS with 1 part of the solvent (see Experimental), except with diethyl ether, where the ratio was 4:1. No separation of nicotinamide and pyridoxol was obtained with micelles containing a lower proportion of SDS.

Table 4
Number of theoretical plates for the test mixture components in microemulsions containing different organic solvents with TTAB as surfactant

Vitamin	No organic solvent	Diethyl ether	2-Methyl-2-propanol	*n*-Amyl alcohol
Thiamine	17 685	24 869	31 495	32 167
Nicotinic acid	55 824	54 078	131 386	178 873
Pyridoxol	102 166	298 184	383 196	98 883
Nicotinamide	104 435	116 799	399 787	120 365
Vitamin E	57 689	75 190	179 738	128 694
Vitamin A	21 640	22 691	289 364	114 164

Definition of *N* and data representation as in Table 2.

both instances, indicating that the main parti-
tioning occurs between the organic phase core in
the emulsion droplet and the aqueous phase, the
surfactant yielding to this system the charge and
mobility towards cathode. No complete resolu-
tion of the critical pair pyridoxol–nicotinamide
was obtained and in fact the best resolution was
obtained either without any organic solvent
added to the surfactant or addition of diethyl
ether. Typical separations are shown in Fig. 5.
At least, however, addition of the organic sol-
vent to the cationic surfactant can result in a
better peak shape, as indicated in Table 4.

4. Conclusions

Microemulsion separations, as tested with a
set of lipid- and water-soluble vitamins, with
both anionic and cationic surfactants can offer
better resolution than micellar electrokinetic
chromatography alone. However, in this case,
SDS-based microemulsions are superior to the
TTAB systems. Whereas in the former the sepa-
ration can be influenced not only by the lipo-
philic vitamins but also by the hydrophilic vita-
mins, with TTAB the best separations obtained
were either in the micellar mode only or in the
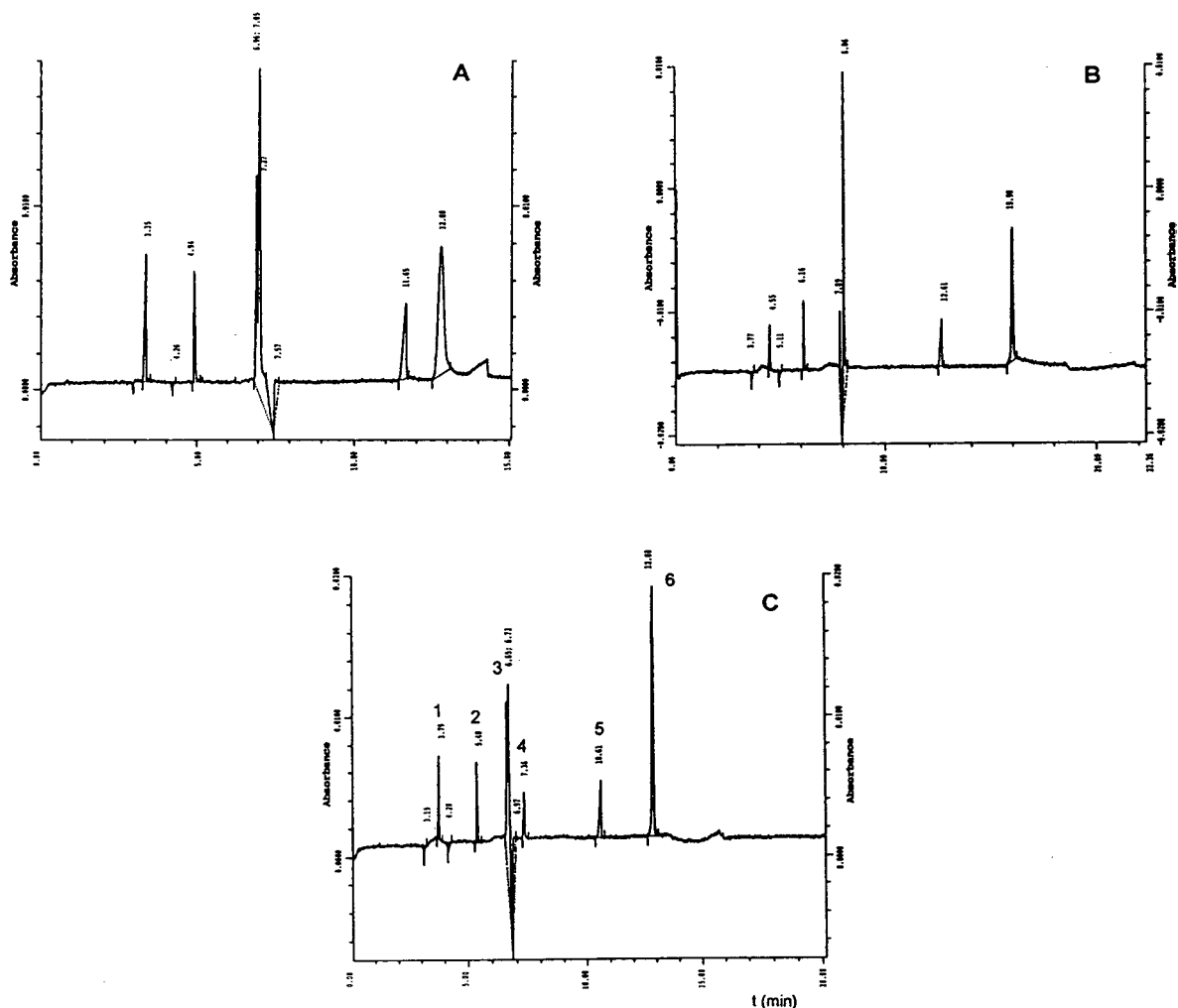
Fig. 5. Typical profiles obtained with (A) TTAB–diethyl ether, (B) TTAB–2-methyl-2-propanol and (C) TTAB–n-amyl alcohol.
Peaks: 1 = thiamine; 2 = nicotinic acid; 3 = pyridoxol; 4 = nicotinamide; 5 = vitamin E; 6 = vitamin A.

presence of diethyl ether as the microemulsion component. In the SDS-based separations nicotinic acid can serve as an internal standard as its behaviour does not depend on the composition of the micellar phase. In fact, its relative position (with respect to the endoosmotic flow) is the same with different microemulsions or micelles or even without any surfactant present in the system. On the other hand, vitamin A interacts readily with all the microemulsion phases used and indicates the end of the separation window. Along with Sudan III, it can be used to determine the size of the separation window.

Acknowledgement

References

[1] H. Watarai, Chem. Lett., (1991) 391.
[2] S. Terabe, N. Matsubara, Y. Ishihama and Y. Okada, J. Chromatogr., 608 (1992) 23.
[3] S.F.Y. Li, Capillary Electrophoresis (Journal of Chromatography Library, Vol. 52), Elsevier, Amsterdam, 1992.
[4] C.P. Ong, C.L. Ng, H.K. Lee and S.F.Y. Li, J. Chromatogr., 547 (1991) 419.
[5] G. Dinelli and A. Bonetti, Electrophoresis, 15 (1994) 1147.

MECCSIM, training software for micellar electrokinetic capillary chromatography

Jetse C. Reijenga[a],[*], Milan Hutta[b]

[a]*Department of Chemical Engineering, Eindhoven University of Technology, P.O. Box 513, 5600 MB Eindhoven, Netherlands*
[b]*Institute of Chemistry, Faculty of Science, Comenius University, 84215 Bratislava, Slovak Republic*

Abstract

A training simulation program for micellar electrokinetic capillary chromatography was developed. The software provides a high speed of calculation, visual detail and model accuracy with a user-friendly interface. The instrument parameters that can be varied include capillary material, length, internal diameter and wall thickness, thermostating temperature, voltage and polarity. Hydrostatic injection is simulated using time and pressure as variables. The following properties of the buffer can be varied: pH, ionic strength, and sodium dodecylsulfate (SDS) concentration. The retention model is based on experimental values for $\delta H°$ and $\delta S°$, obtained from the literature. In addition, the temperature and ionic strength dependence of the critical micelle concentration and the partial specific volume of the SDS micelle is taken into account. This allows the calculation of the temperature dependence of the partition coefficients and capacity factors and thus of the retention and migration behaviour. In addition, a number of dispersion factors are included in the model.

1. Introduction

Computerized simulations of analytical separation techniques can be used in different contexts: fundamental research, method development, training and demonstration. For most analytical techniques, the fundamentals no longer have secrets from the specialists in the field. For relatively new techniques, simulation from basic principles, such as the equation of continuity and other differential equations and charge and mass balances, can provide more insight. These programs do an exact calculation, without any assumptions or approximations. The

system has to be defined very precisely, all data (constants, variables) and their mutual dependence must be available. As a result, they require calculation times in the range of at least minutes to hours, depending on the time and place resolution required. These are not suitable for training purposes.

At the other end of the spectrum we have the demonstration software, illustrating and visualizing in a qualitative way what the result of a separation will look like. A requirement for such training software is a high speed of calculation and a user-friendly interface. The price that is paid for such convenience is that a lesser degree of accuracy can be obtained. The kind of simulations that we have developed in recent years [1–3] have provided a high speed of calculation, visual detail and model accuracy with a user-

* Corresponding author.

friendly interface. The principle goal has been to simulate the results of the separation (such as a chromatogram or electropherogram) rather than the dynamics of it. Several assumptions as to the mutual independent behaviour, especially in the initial stages of separation, have consequently been necessary. The simulated results, however, do not deviate too much from the experimental results [3] and are certainly sufficient for training purposes.

Micellar electrokinetic chromatography is a relatively new technique, introduced in 1985 [4,5]. Within a relatively short time, a considerable body of literature has become available and the first textbook on the subject gives an impressive overview [6]. One of the more illustrative features of this book is the large number of illustrations of simulated electropherograms, used to illustrate the different aspects of migration and dispersion.

2. Description of the program

2.1. User interface

The basic structure of the program consists of the user interface of previously published training software for gas chromatography [1] and free capillary zone electrophoresis [2,3]. The program runs on any IBM-compatible PC under DOS, with a graphics monitor (CGA/EGA/VGA) and optionally a mouse. A numeric coprocessor is advisable to keep calculation times within 1 s. Several shortcut keys were added for fine tuning of selectivity parameters. Full-screen graphics alternates with current instrument settings along with the pull-down menus. Details on the availability of the program can be obtained from the first author on request.

2.2. Database

The data stored were thermodynamic properties $\delta H°$ and $\delta S°$ taken from the literature [6,7]. A supplementary program was written to edit the database (change values, add components). An additional possibility is to include also

synthetic components with imaginary, "ideal" properties, e.g., a $\delta H°$ value of -100 kJ mol^{-1} for an electroosmotic flow (EOF) marker.

2.3. Retention model

For the retention model, first the temperature rise due to heat dissipation in the capillary is calculated with an iteration [2]. The conductivity of the buffer has contributions from the buffer anion, the buffer cation, sodium, dodecyl sulfate, micelles and hydrogen and hydroxide ions. The ionic strength I is also calculated. A complication is that the mobilities of all ions will depend on the ionic strength of the buffer and also on the temperature. Then the micellar specific volume V (mg l^{-1}) and critical micelle concentration c_{cmc} are corrected for this temperature T and ionic strength I using a (mutually independent) linear fit to experimental data from different publications (e.g., [7,8]):

$$V = V_0 + \frac{\delta V}{\delta T}(T - 298) + \frac{\delta V}{\delta I} \cdot I \qquad (1)$$

$$c_{cmc} = c_{cmc,0} + \frac{\delta c_{cmc}}{\delta T}(T - 298) + \frac{\delta c_{cmc}}{\delta I} \cdot I \qquad (2)$$

Both the micellar specific volume V_0 and the critical micelle concentration $c_{cmc,0}$ under reference conditions of zero ionic strength and 25°C and all four differential coefficients can be changed by the user of the program. Further details are given in Table 1.

From the analytical concentration of SDS, c_{sds}, and its molar mass, M_{sds}, the phase ratio β is now calculated:

$$\beta = \frac{10^{-3} M_{sds} V(c_{sds} - c_{cmc})}{1 - 10^{-3} M_{sds} V(c_{sds} - c_{cmc})} \qquad (3)$$

For those cases where $c_{sds} < c_{cmc}$ and thus $\beta < 0$, there are no micelles and β is taken as zero.

The electroosmotic mobility, u_{eof}, in SDS solutions depends on pH. It is fitted from experimental data [9], with the following relationship:

$$\mu_{eof} = [80 - 0.0015(12 - pH)^5] \cdot 10^{-9} \qquad (4)$$

where it is presumed that under these conditions

Table 1
Relevant "constants" in the migration and dispersion model

Symbol	Dimensions		Default
	Units	Range	
c_{cmc}	$mmol\,l^{-1}$	1–8	3
$\dfrac{1}{c_{cmc}}\cdot\dfrac{\delta c_{cmc}}{\delta T}$	K^{-1}	−0.05 to +0.05	+0.033
V	$ml\,g^{-1}$	0.1–3	0.81
$\dfrac{1}{V}\cdot\dfrac{\delta V}{\delta T}$	K^{-1}	−0.05 to +0.05	+0.001
$\dfrac{1}{c_{cmc}}\cdot\dfrac{\delta c_{cmc}}{\delta I}$	$l\,mol^{-1}$	−9 to +9	+6.25
$\dfrac{1}{V}\cdot\dfrac{\delta V}{\delta I}$	$l\,mol^{-1}$	−9 to +9	+0.2
d_i	m	10^{-9}–10^{-7}	10^{-8}
D_{aq}	$m^2\,s^{-1}$	$5\cdot10^{-11}$–$2\cdot10^{-9}$	10^{-9}
D_{mc}	$m^2\,s^{-1}$	$5\cdot10^{-11}$–$2\cdot10^{-9}$	10^{-9}
k_d	s^{-1}	10–10 000	10 000
σ_{ep}	–	0–0.01	0.01

μ_{eof} does not depend on ionic strength or c_{sds}. The temperature dependence of electroosmosis works mainly through the viscosity of the liquid near the capillary wall, η, as can be seen from the equation for the zeta potential, ζ. This value can now also be calculated, using the dielectric constant ε:

$$\zeta = -\frac{\mu_{eof}}{\eta\varepsilon} \tag{5}$$

In contrast to the previously developed simulator for HPCE, here the ζ potential is not an independent variable.

Then, the net electroosmotic velocity v_{eof} is calculated from the electroosmotic mobility and the field strength E:

$$v_{eof} = \mu_{eof}E \tag{6}$$

Positive velocities are directed towards the detector. The same can be done for the net micellar velocity, v_{mic}, where it is assumed that the micellar mobility, μ_{mic}, has a constant value of $-61.9\cdot10^{-9}$ m^2 V^{-1} s^{-1}:

$$v_{mic} = (\mu_{mic} + \mu_{eof})E \tag{7}$$

For each of the separands, the Gibbs free energy change $\delta G°$ is calculated from T, $\delta H°$ and $\delta S°$ values in the database:

$$\delta G° = \delta H° - T\delta S° \tag{8}$$

which in turn is converted into the temperature-dependent distribution coefficient K:

$$K = \exp\left(-\frac{\delta G°}{RT}\right) \tag{9}$$

With the phase ratio β, this yields the capacity factor, k', for each separand:

$$k' = \beta K \tag{10}$$

The field of application of micellar electrokinetic capillary chromatography (MECC) is mainly the analysis of non-ionic compounds, but in order to extend the possibilities of the simulation program to the more general case, ionic compounds can also be simulated. Here data on the pH dependence of the distribution coefficient as a function of pH are usually not available. A recent publication [10] reported on computer-assisted modelling of MECC of ionizable compounds. Distribution coefficients of ionized and non-ionized forms were determined. Their ratio ranged between 2 and 34. In the model we assume that the distribution coefficient refers mostly to the uncharged compound and that the distribution coefficient of the charged form is ten times smaller. Now the effective charge of the ion z is calculated from pK and pH, as described previously [2]. For ionizable monovalent separands, Eq. 10 is modified to

$$k' = (1 - 0.9|z|)\beta K \tag{11}$$

For each separand, the net velocity v_{net} is determined by its distribution between aqueous and micellar phase:

$$v_{net} = \frac{k'}{1 + k'}\cdot v_{mic} + \frac{1}{1 + k'}\cdot v_{eof} \tag{12}$$

Only if this net velocity is positive will the separand reach the detector and the retention time, t_R, can be calculated using the capillary length to the detector, L_d:

$$t_R = L_d/v_{net} \tag{13}$$

Also calculated in this way are the retention times of the marker, $t_{R,eof}$ (where $v_{net} = v_{eof}$), and of the micelle, $t_{R,mc}$ (where $v_{net} = v_{mic}$).

2.4. Dispersion model

A number of dispersion factors in MECC are similar to those in HPCE. The off-column dispersion factors used in this study are therefore identical with those given previously [2,3]. An overview of dispersion factors on-column in MECC has been given [5,6]. The following contributions can be distinguished: longitudinal diffusion (with diffusion coefficients D_{aq} and D_{mc}), sorption and desorption kinetics (with rate constant k_d), intermicelle diffusion (with D_{aq}), electrophoretic dispersion (with σ_{ep}) and thermal gradient effects. A number of interesting publications have been especially devoted to these effects [11,12]. In spite of the fact that under practical working conditions some of the effects mentioned are negligible, all are included in the present model. The purpose was to illustrate which parameters determine efficiency and to what extent. For an overview of the dispersion model incorporated into the present simulator, we refer to the relevant literature (Table 5.6 in Ref. [6]).

Table 1 lists the most important parameters included in the dispersion terms. The values of the constants in the dispersion terms show a considerable degree of uncertainty when consulting the different literature sources. Therefore, these "constants" can be changed, upon which they are automatically saved, so that subsequent simulation sessions start with the parameters so updated. This makes it possible to see in detail what would happen if a different detergent with other properties were to be used. The only limitation is that the thermodynamic properties $\delta H°$ and $\delta S°$ remain the same for that particular separand. On the other hand, $\delta H°$ and $\delta S°$ values can be temporarily changed to see the result of a change in separand properties, independent of the buffer system chosen.

3. Results and discussion

3.1. Temperature effects

As in MECC the temperature in the capillary is important, even more so than in CE, several workers have investigated this aspect. A linear relationship between the temperature rise and the power dissipation (W m^{-1}) was theoretically predicted [2,3] and was experimentally verified using thermochromic solutions [13]. Experiments for determining this temperature rise from MECC [7] did not yield the same result, although insufficient details of the capillary dimensions were provided in both publications. We assume that in both cases the O.D. was 375 μm and I.D. 75 μm. A temperature rise of 0.33°C m W^{-1} is then simulated for a quartz capillary, compared with 0.3°C m W^{-1} in Ref. [13] and 3°C m W^{-1} in Ref. [7].

3.2. Homologous series

The separation of a series of alkylbenzenes was simulated using data from Ref. [8] (see Fig. 1). In actual practice the migration time of the micelle can be determined by an iteration procedure, applied to such a homologous series [14]. When using different homologous series, a different value of t_{mc} was found [8], indicating that the micelle marker used (Sudan 3) was not fully micellarized. When calculating the capacity factor for Sudan 3, using the t_{mc} thus obtained, values in the range 100–200 were found [8]. In the simulation, a synthetic, temperature-independent marker for the micelle migration time was introduced, having $\delta H° = 0$ and $\delta S° = 100$ J mol^{-1} K^{-1}. The resulting capacity factor for this component was 1100, but it can still be distinguished from t_{mc}, where naturally k' approaches infinity.

3.3. Method development

Provided that sufficiently reliable data are available, the MECCSIM program can be used for method development. A typical application is shown in Fig. 2 for the separation of a mixture of
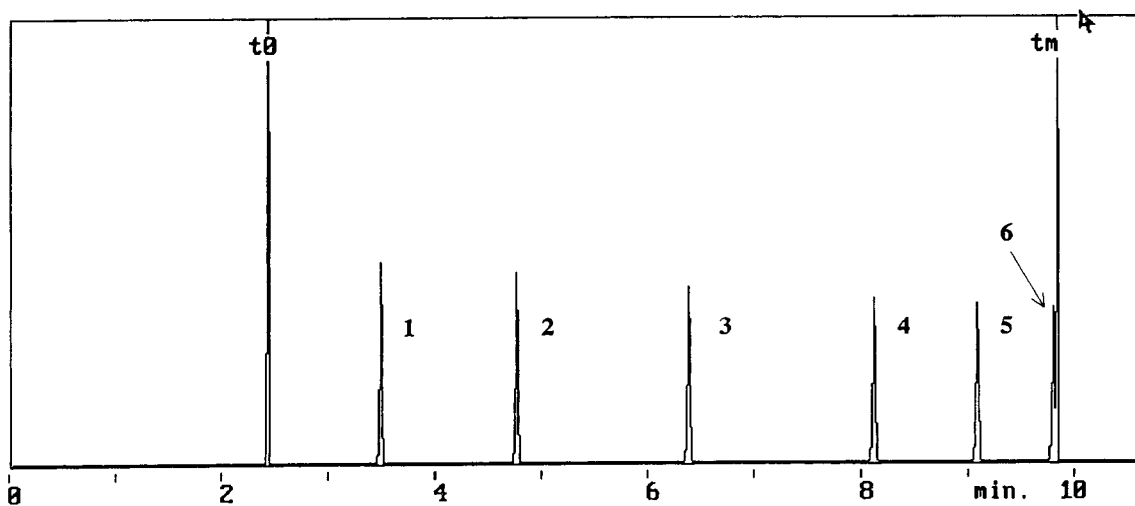
Fig. 1. Simulated chromatogram of a homologous series of alkylbenzenes [8] at 25°C, 20 kV, pH 8.5, 50 mmol l^{-1} SDS in a 50 μm I.D./375 μm O.D. quartz capillary with a length to the detector of 455 mm and 501 mm total length. Peaks: 1 = benzene; 2 = toluene; 3 = ethylbenzene; 4 = propylbenzene; 5 = butylbenzene; 6 = a synthetic component, with $\delta H° = 0$ and $\delta S° = 100$ J mol^{-1} K^{-1}.

six cold medicines [7]. As can be seen, the distribution coefficients result in a very broad range of capacity factors (0.16–124 in this case), so that almost the full retention window has to be used for simultaneous determination. This puts obvious constraints on the buffering system.

3.4. Comparison of input data

Literature values for thermodynamic properties of $\delta H°$ and $\delta S°$ in the water–SDS system under buffered MECC conditions are scarce. Influences of buffer type, ionic strength and pH
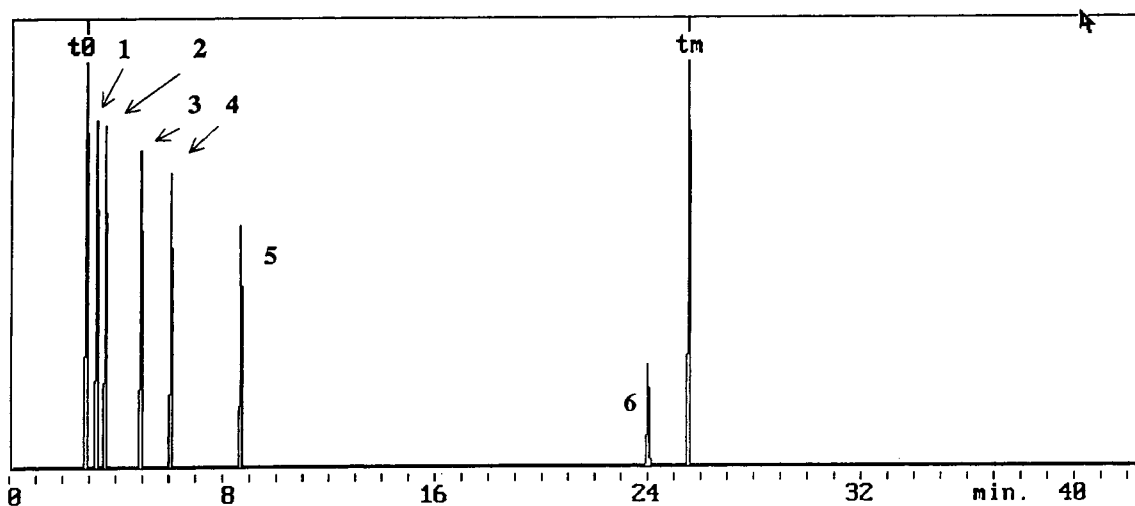
Fig. 2. Simulated chromatogram of a standard mixture of cold medicines [7] at 30°C, 20 kV, pH 7.0, 50 mmol l^{-1} SDS in a 75 μm I.D./375 μm O.D. quartz capillary of length 500 mm Peaks: 1 = acetaminophen; 2 = caffeine; 3 = guaifenisin; 4 = ethenzamide; 5 = isopropylantipyrine; 6 = trimethoquinol.

on the partition coefficient and thus on these thermodynamic properties can never be excluded. Two databases were made, based on results from two sources [7,8]. In the first publication [7], several buffers were used, in some cases leading to significantly but not extremely different values for $\delta H°$ and $\delta S°$. The c_{cmc} was also different in three different pH 7.0 buffers.

In the second publication, only one pH 8.5 buffer was used. The following solutes were measured by both: resorcinol, phenol, nitrobenzene and toluene. The results for $\delta H°$ and $\delta S°$ for these four solutes from the two publications differed considerably (see Table 2). Some values determined by micellar liquid chromatography (MLC) [15] were also included for comparison.

The $\delta G°$ and K values were also different, although the electropherograms based on the data from the first two sources were similar (see Fig. 3a and b). There can be two explanations. One might stress that values in different buffers may not be compared, but that does not explain the similarity between the two simulated chromatograms from entirely different $\delta H°$ and $\delta S°$ values. In the second publication [8], small relative standard deviations for $\delta H°$ and $\delta S°$ are claimed (3–5%); the systematic difference with [7] could be caused by the buffer.

Another conclusion might be that MECC is not a very reliable way of determining $\delta H°$ and

$\delta S°$, where we must not overlook the fact that in order to obtain $\delta H°$ and $\delta S°$ from t_R one needs equally reliable values of t_{eof}, t_{mc}, V, c_{cmc} and c_{sds} under the experimental conditions concerned. Also, the temperature in these measurements is changed over a relatively small interval on the kelvin scale.

3.5. Kinetic limitations

Using the MECC simulator, separations can be highly optimized in terms of analysis time, using all the variables available. In this way one can go far beyond present limitations of equipment design. For example, the dispersive effect of heat production can be kept to a minimum when using a 5-μm capillary. If the wall of the capillary is also very thin, there will be only a small temperature increase at the high power dissipations usually encountered in MECC. Under these circumstances (analysis times in seconds, not minutes), kinetic limitations are seen to play a key role in dispersion, provided that the detector has a time constant <0.1 s, also unlikely at present. The effect of changing k_d on this kinetic limitation can now easily be visualized.

In practice, heat development will be an important limitation in speeding up analyses. With respect to thermostating, two limiting cases

Table 2
Experimental results from different sources [7,8,15] for thermodynamic properties $\delta H°$ (kJ mol^{-1}), $\delta S°$ (J mol^{-1} K^{-1}) and $\delta G°$ (kJ mol^{-1}) at 40°C for some solutes in SDS

Parameter	Ref.	Resorcinol	Phenol	Nitrobenzene	Toluene
$\delta H°$	[7]	−12.5	−11.1	−9.7	−7.6
	[8]	−6.1	−5.8	−5.0	−3.8
	[15]		−9.3		−2.2
$\delta S°$	[7]	−17.4	−5.4	+7.4	+21.1
	[8]	+7.5	+13.6	+23.8	+34.2
	[15]		−12.5		+25.9
$\delta G°$	[7]	−7.05	−9.41	−12.0	−14.2
	[8]	−8.45	−10.1	−12.4	−14.5
	[15]		−5.4		−10.3
K	[7]	15.0	37.2	101	234
	[8]	25.7	48.5	117	263
	[15]		8.0		52
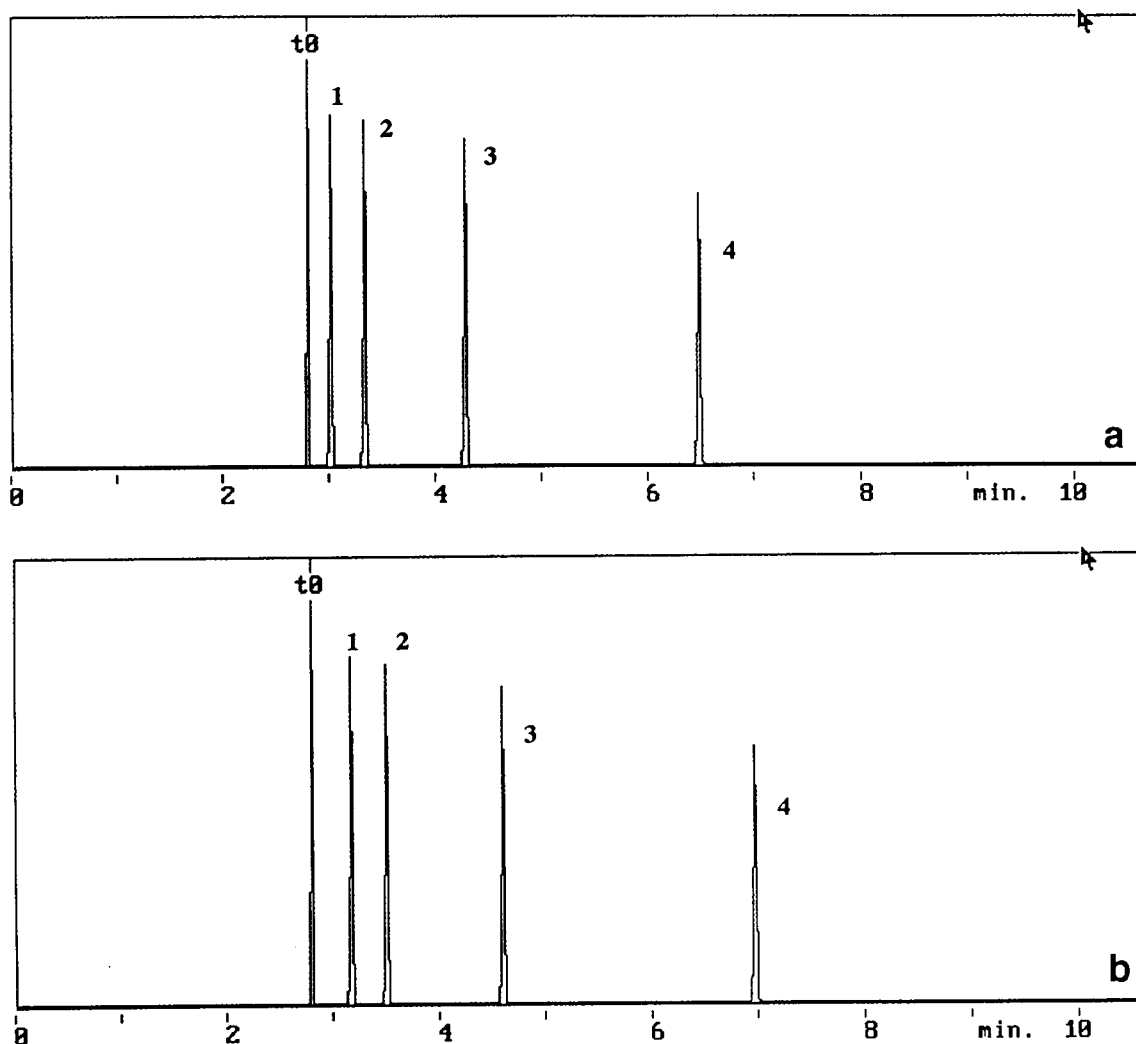
Fig. 3. Simulated chromatogram at 40°C, 20 kV, pH 7.0, 50 mmol l⁻¹ SDS in a 75 μm I.D./375 μm O.D. quartz capillary of length 500 mm. Peaks: 1 = resorcinol; 2 = phenol; 3 = nitrobenzene; 4 = toluene. Based on data from (a) Ref. [7] and (b) Ref. [8].

are distinguished in the simulation program: in one, perfect liquid cooling (no temperature gradient outside the capillary) is assumed; in the other, the capillary is hanging in still air (large temperature gradient outside capillary), given by Knox's equation [16]. The cooling situation in practice will often be ill-defined but certainly between these limiting cases.

The former, idealized case is illustrated in Fig. 4 for the separation of xylenols. Under these conditions of high power dissipation (61 W m⁻¹),

the temperature in the 300 mm × 75 μm I.D. capillary is increased from 30 to 62°C. This is about as far as one can go in speeding up the analysis with perfect liquid cooling. For the other limiting case where the capillary is hanging in still air, only 1.4 W m⁻¹ would result in the same 32°C temperature rise. As the power dissipation is proportional to E^2, the voltage should be 6.6 times lower for air cooling in order to obtain the same temperature rise, thus illustrating the need for a good cooling mechanism.
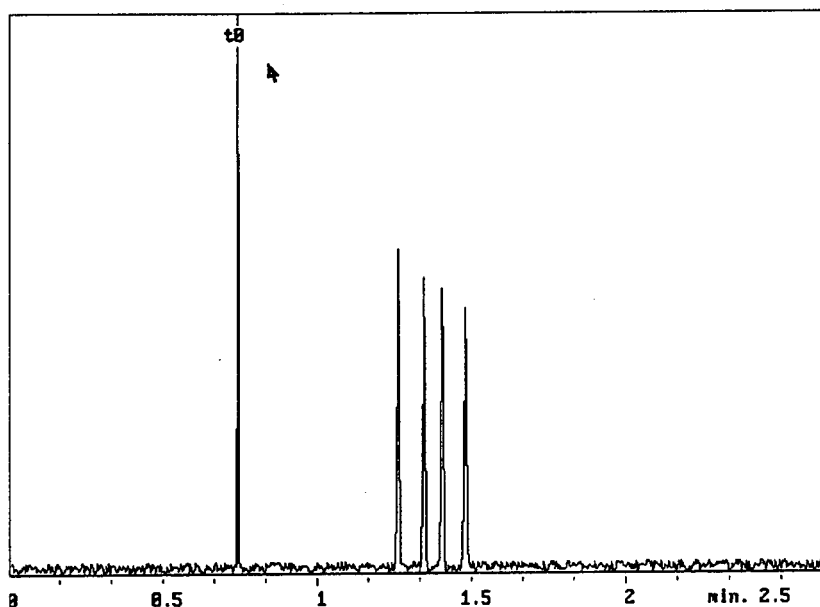
Fig. 4. Simulated chromatogram at 30°C, 30 kV, pH 6.0, 50 mmol l^{-1} SDS in a 75 μm I.D./375 μm O.D. quartz capillary of length 300 mm. Peaks from left to right: 2,6-xylenol, 2,3-xylenol, 3,4-xylenol and 2,4-xylenol.

4. Conclusions

The simulation model makes it possible to illustrate the influence of a large number of sample, buffer and equipment parameters on chromatograms obtained by MECC. The possibility of changing the "constants" in the migration and dispersion model makes it possible for the simulation program to learn from the input of new experimental data and thus to refine the theoretical model. Synthetic mixture can be used to visualize the many factors involved in retention and dispersion so that the examples given in the Vindevogel and Sandra's book [6] can be generated by the user in a very flexible manner.

The use of MECCSIM in method development, however, is still limited by the lack of sufficiently reliable data of $\delta H°$ and $\delta S°$, or alternatively k', values under different but well defined conditions.

Symbols and abbreviations

c_{mic} critical micelle concentration (mol l^{-1})

c_{sds} analytical concentration of SDS (mol l^{-1})
d_i intermicelle distance (m)
D_{aq} diffusion coefficient in the aqueous phase (m^2 s^{-1})
D_{mc} diffusion coefficient in the micelle phase (m^2 s^{-1})
E field strength (V m^{-1})
I ionic strength of the buffer (mol l^{-1})
k' capacity factor
k_d (de)sorption rate constant (s^{-1})
K distribution coefficient
L_d capillary length to the detector (m)
M_{sds} molar mass of SDS (g mol^{-1})
R gas constant (8.314 J mol^{-1} K^{-1})
T average temperature in the capillary (K)
t_R retention time (s)
$t_{R,eof}$ retention time of EOF marker (s)
$t_{R,mc}$ retention time of the micelles (s)
v_{eof} net electroosmotic velocity (m s^{-1})
v_{mic} net micellar velocity (m s^{-1})
V specific volume of micelle (ml g^{-1})
z effective charge of ion
β phase ratio
$\delta G°$ change in Gibbs free energy (J mol^{-1})
$\delta H°$ change in Free energy (J mol^{-1})

$\delta S°$ change in entropy ($J\ mol^{-1}\ K^{-1}$)

ε dielectric constant of the buffer ($0.708 \cdot 10^{-9}\ F\ m^{-1}$)

η buffer viscosity near capillary wall ($10^{-2}\ N\ s\ m^{-2}$)

μ_{eof} electroosmotic mobility ($m^2\ V^{-1}\ s^{-1}$)

μ_{mc} micellar mobility ($m^2\ V^{-1}\ s^{-1}$)

σ_{ep} relative standard deviation of μ_{mc}

ζ zeta potential of the capillary wall (V)

References

[1] J.C. Reijenga, J. Chromatogr., 588 (1991) 217.

[2] J.C. Reijenga and E. Kenndler, J. Chromatogr. A, 659 (1994) 403.

[3] J.C. Reijenga and E. Kenndler, J. Chromatogr. A., 659 (1994) 417.

[4] S. Terabe, K. Otsuka and T. Ando, Anal. Chem., 57 (1985) 834.

[5] S.F.Y. Li, Capillary Electrophoresis (Journal of Chromatography Library, Vol. 52), Elsevier, Amsterdam, 1992.

[6] J. Vindevogel and P. Sandra, Introduction to Micellar Electrokinetic Chromatography, Hüthig, Heidelberg, 1992.

[7] S. Terabe, T. Katsura, Y. Okada, Y. Ishihama and K. Otsuka, J. Microcol. Sep., 5 (1993) 23.

[8] P.G.H.M. Muijselaar, H.A. Claessens and C.A. Cramers, Anal. Chem. 66 (1994) 635.

[9] K. Otsuka and S. Terabe, J. Microcol. Sep., 1 (1989) 150.

[10] C. Quang, J.K. Strasters and M.G. Khaledi, Anal. Chem., 66 (1994) 1646.

[11] M.J. Sepaniak and R.O. Cole, Anal. Chem., 59 (1987) 472.

[12] S. Terabe, K. Otsuka and T. Ando, Anal. Chem., 61 (1989) 251.

[13] H. Wätzig, Chromatographia, 33 (1992) 445.

[14] M.M. Bushey and J.W. Jorgenson, Anal. Chem., 61 (1989) 491.

[15] F.P. Tomasella and L.J. Cline Love, Anal. Chem., 62 (1990) 1315.

[16] J.H. Knox, Chromatographia, 26 (1988) 329.

Capillary electrophoresis device with double UV detection and its application to the determination of effective mobilities of peptides

Václav Kašička*, Zdeněk Prusík, Petr Mudra, Jiří Štěpánek

Institute of Organic Chemistry and Biochemistry, Academy of Sciences of the Czech Republic, Flemingovo 2, 166 10 Prague 6, Czech Republic

Abstract

A new experimental device for high-performance capillary electrophoresis (HPCE) with a double UV detection system and with thermostating of the whole separation compartment was developed. UV detection is doubled by producing two apertures placed symmetrically close to the axis of the optical path of the single-beam UV detector and by the adjustment of the capillary loop on these two apertures. The double-detection system allows exact measurements of electrophoretic and electroosmotic flow velocities. A procedure for the determination of effective mobilities from the data obtained by the double UV detection system was developed and applied to determine the effective mobilities of synthetic peptides (diglycine, triglycine, growth hormone releasing peptide and its derivatives and fragments). The measurements are performed at constant temperature (25°C) and low input power at which temperature increase in the capillary can be neglected and temperature corrections of temperature-dependent magnitudes need not be included in the calculations.

1. Introduction

In the field of peptide chemistry capillary zone electrophoresis (CZE) is mostly used as a high-performance, high-sensitive technique for picoanalysis of both synthetic peptides and peptides isolated from natural material [1–3]. However, the application potential of CZE in this field is much broader. It can be used not only for purity determination of analyzed peptides but also for their more complex physico-chemical characterization. Important characteristics, e.g., effective charges, effective electrophoretic mobilities, dissociation constants, relative molecular masses and diffusion coefficients can be obtained

from CZE data. Up to now only a few studies have been performed in which the effective electrophoretic mobilities of peptides have been measured by CZE and the correlation between the effective mobility, effective charge and relative molecular mass has been investigated [4–7].

All these measurements were performed with systems using single-beam UV detectors. This means the migration velocity was measured as an average velocity, with which the particle is moving from the injection end of the capillary to the detection position. It is obvious that not all such measurements are quite accurate, since the conditions are not always stable for the whole time of experiment.

In the beginning of the experiment the applied voltage, current and temperature are changing.

---

* Corresponding author.

Furthermore, depending on the sample solution and the background electrolyte (BGE) composition in the beginning of the experiment, different transient processes such as moving boundary electrophoresis or isotachophoresis can occur. Only after some time, which can be a significant part of the total time of an experiment, a real zone electrophoretic regimen is achieved and the separation conditions are stable and correct for mobility measurement.

Consequently, the electrophoretic mobilities obtained from such measurements represent average values, which are dependent on the given experimental device and conditions, which cannot be considered as qualitative characteristics of the analytes related to given background electrolyte and temperature only.

The aim of this work was to overcome these shortcomings of effective mobility determination in a single detector CZE device by a new design of the CZE device with a double UV detection system. In this device the migration velocity is measured on a well-defined part of the capillary between two UV detection positions, the distance of which is exactly known, where the sample components migrate under stable and equilibrated conditions [8].

This double-detection or multi-detection approach is suitable not only for effective mobility determination but also for monitoring the dynamics of electromigration separation processes. Recently some devices of such a type have been described in the literature. The system developed by Beckers et al. [9] uses two a.c. conductivity detectors, Terabe and Isemura [10] and Towns and Regnier [11] use two or several UV detectors placed along the capillary. The advantage of our system is that it uses, similarly as the system of Srichaiyo and Hjertén [12], only one UV detector and the capillary goes twice through it. In our device the whole separation compartment is thermostated to constant temperature (25°C). During the electrophoretic and electroosmotic flow velocities measurement the input power is lowered so that the temperature increase inside the capillary can be neglected and temperature corrections of temperature-dependent magnitudes need not be included in the calculation of electrophoretic mobilities.

2. Experimental

2.1. Chemicals

All chemicals were of analytical-reagent grade. Diglycine and triglycine were obtained from Reanal (Budapest, Hungary), phenol and acetic acid were from Lachema (Brno, Czech Republic).

Growth hormone releasing peptide and its derivatives and fragments were synthesized at our institute [13]. The list of analyzed peptides and their sequences are given in Table 1.

2.2. Capillary zone electrophoresis (CZE)

Separations were performed with the newly developed double UV detection CZE device, which is described in Section 3.

Acetic acid (0.5 mol/l, pH 2.5) was used as BGE. Sample was applied by at an overpressure of 0.006 bar for 5–15 s. Separations were performed at constant temperature 25°C.

Table 1
List of analyzed peptides and their sequences

Peptide	Sequence
His[1]-GHRP:	H–His–D-Trp–Ala–Trp–D-Phe–Lys.NH$_2$
Tyr[1]-GHRP:	H–Tyr–D-Trp–Ala–Trp–D-Phe–Lys.NH$_2$
Digly-GHRP:	H–Gly–Gly–His–D-Trp–Ala–Trp–D-Phe–Lys.NH$_2$
GHRP-frag.:	H–Ala–Trp–D-Phe–Lys.NH$_2$

GHRP = growth hormone releasing peptide.

3. Results and discussion

3.1. HPCE device with double UV detection

The scheme of the constructed double UV detection device for HPCE is shown in Fig. 1. The core of the device is a fused-silica capillary, C, with outer polyimide coating and with no modification of the inner surface (supplied by the Institute of Glass and Ceramics Materials of Czech Academy of Sciences, Prague, Czech Republic) with the following dimensions: I.D. 0.055 mm, O.D. 0.107 mm, total length 297 mm, effective length 1 (from the injection end to the first detector) 160 mm, effective length 2 (from the injection end to the second detector) 205 mm, distance of two detection positions 45 mm.

Polypropylene Eppendorf tubes (1.5 ml) serve as electrode vessels, EV. A high-voltage power supply, HV, (0.1–20 kV, 1–500 μA), developed earlier in our Institute was used in a constant-voltage mode.

Pneumatically formed overpressure, p, at the injection end of the capillary is used for filling and washing the capillary with BGE or other solutions ($\Delta p = 0.1$ bar) and for sample introduction ($\Delta p = 0.006$ bar).

The whole separation compartment (capillary, electrode vessels and detector) is thermostated by flowing air at 25°C. Combination of water cooling of the case of the separation compart-

ment and heating wire inside the separation unit is used to quickly achieve the temperature equilibrium.
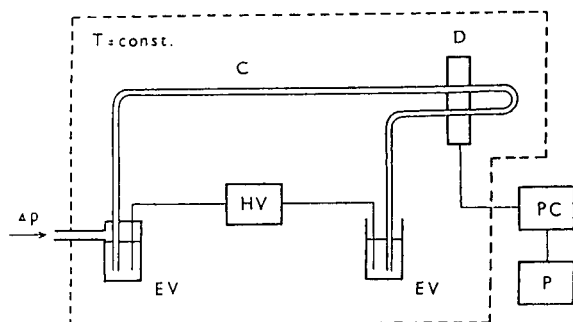
3.2. Double UV detection system

The device is equipped with a newly designed double UV detection system which allows measurement of UV absorption at two positions in the capillary. The schematic diagram of the total set-up of the detector is shown in Fig. 2a, the detail of the double passage of the capillary through the detector is shown in Fig. 2b. The detector uses some components of the previously developed device [14].

The UV light source is an iodine low-pressure electrodeless discharge lamp, I_2DL, (UV lamp type 1, LKB, Bromma, Sweden). The discharge lamp is excited by a high-frequency oscillator, HFO, with 100 MHz frequency and 6 W input
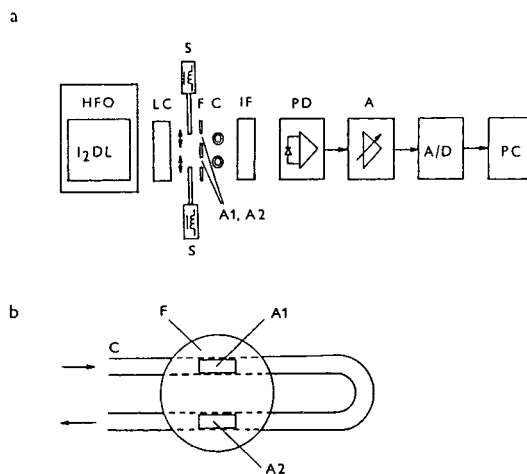
Fig. 2. Schematic diagram of the double UV detection system. (a) Total set-up: I_2DL = iodine discharge lamp; HFO = high-frequency oscilator; LC = light condensor; S = solenoids with needle cores; F = copper foil with two apertures A1, A2; C = cross-section of double passage of the capillary through the detector; IF = interference filter; PD = photodiode with built-in preamplifier; A = amplifier; A/D = analog–digital converter; PC = personal computer. (b) Detailed view of the double capillary passage through the detector: C = capillary loop; F = copper foil; A1, A2 = apertures to which capillary loop with two windows is fixed. Arrows indicate migration direction of an analyte through the double UV detection system.

Fig. 1. Scheme of the HPCE device with double UV detection system. C = Fused-silica capillary; D = double UV detection system; HV = high-voltage power supply; EV = electrode vessels; PC = personal computer; P = printer; Δp = pneumatically formed overpressure, T = const. = thermostated space with constant temperature.

power. The thermostating of the lamp at constant temperature (25°C) ensures the high stability of the light intensity and the detection system can work in a single-beam mode. The light condensor, LC, concentrates the light on two apertures with the dimensions 0.05×0.300 mm which are electrochemically produced on the copper foil, F, and which are placed symmetrically close to the optical axis of the detector. The capillary loop is attached to the foil in such a way that two windows of the capillary (short parts of capillary with removed polyimide coating) are placed exactly behind the two apertures. The adjustment and sealing of the capillary to the foil is performed under a microscope. The apertures can be alternatively opened or closed by the needle cores of two solenoids, S, situated between the light condensor and the foil.

After going through the capillary the light passes the interference filter, IF, (LKB, Bromma, Sweden) by which the detection wavelength 206 nm is selected. The light is detected by a silicone photodiode, PD, with a built-in pre-amplifier (type OP-AMP-Photodiode HUV 1000B, EG and G, Salem, MA, USA). The signal is further amplified by an operational amplifier, A, filtered and digitized by a 14-bit analog-digital converter, A/D. The data are collected during 100-ms sampling periods by a personal computer, PC (Xerius, 286/16, Elko, Prague, Czech Republic). Home-made software [15] is used for data acquisition, evaluation and presentation.

3.3. Determination of effective mobilities from the data of the double UV detection CZE device

A procedure has been developed for determination of effective electrophoretic mobilities of analytes separated by CZE with the double UV detection system. The procedure is based on exact measurement of migration velocity on a part of the capillary between the two detectors. Consider a mixture of a charged component, A, and a non-charged component (electroosmotic flow marker), M. The schematic electropherogram of CZE separation of this mixture in the device with double UV detection is shown in Fig.
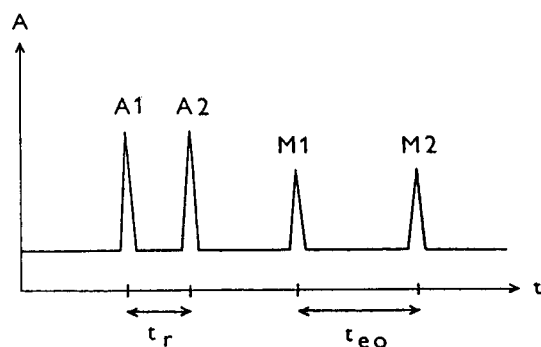
Fig. 3. Schematic electropherogram of the CZE separation of charged component A and non-charged component M obtained with the double UV detection system. A1 (A2) = peak of component A at the first (second) detection position; M1 (M2) = peak of component M at the first (second) detection position. A = absorbance; t = time, t_r (t_{eo}) = migration time of component A (component M) between two detection positions.

3. Peak A1 represents the passage of component A through the first detection position, peak A2 represents the passage of A through the second detection position. Similarly M1 and M2 represent the first and the second passage of M through the detector. From the time intervals t_r and t_{eo} and from the known distance of the detectors, d, the resulting migration velocity of charged component, v_r, and electroosmotic flow velocity, v_{eo}, are calculated.

$$v_r = d/t_r \tag{1}$$

$$v_{eo} = d/t_{eo} \tag{2}$$

Since the resulting migration velocity, v_r, is a sum of electrophoretic velocity, v_{ep}, and electroosmotic flow velocity, v_{eo}, the electrophoretic velocity, v_{ep}, can be obtained as a difference between v_r and v_{eo}:

$$v_{ep} = v_r - v_{eo} = d(t_{eo} - t_r)/t_r \cdot t_{eo} \tag{3}$$

The effective electrophoretic mobility, m_{ef}, is defined as electrophoretic velocity related to unit intensity of electric field, i.e.

$$m_{ef} = v_{ep}/E = v_{ep} \cdot l/U \tag{4}$$

where E is the intensity of electric field, U is the

voltage on the capillary and l is the total length of the capillary.

Combining Eqs. 3 and 4 we can obtain for m_{ef}

$$m_{ef} = \frac{l \cdot d \cdot (t_{eo} - t_r)}{U \cdot t_{eo} \cdot t_r} \qquad (5)$$

i.e. effective electrophoretic mobility can be calculated from the capillary parameters l and d, from the voltage, U, applied on the capillary and from experimentally measured migration times t_{eo} and t_r.

The electrophoretic mobilities are relatively strongly dependent on temperature (ca. 2.5% change of mobility per 1°C). Therefore, the obtained values of effective mobilities have to be related to a defined temperature (mostly 25°C). This problem is solved in our procedure in the following way. The whole separation compartment, i.e., capillary and electrode vessels, is thermostated at a constant temperature of 25°C and the measurement of migration velocities is performed at such a low input power that the temperature increase inside the capillary due to Joule heat can be neglected. Consequently, the measured data are directly related to 25°C and no corrections of temperature-dependent magnitudes have to be included in the calculations of the electrophoretic mobilities.

In order to find out the level of input power up to which the temperature increase inside the capillary due to Joule heat can be neglected the dependence of driving current on the applied voltage was measured (see Fig. 4). In the linear part of this dependence the Ohm's law is valid, i.e., the resistance of BGE inside the capillary is constant. The deflection from linearity starts at voltages (input power), at which the Joule heat causes temperature increase inside the capillary and lowers the BGE resistance.

Consequently, the working conditions for CZE measurement of electrophoretic mobilities were chosen in the linear part of the current–voltage dependence. Most of separations were performed at 7.0 kV, 6.3 μA (0.15 W/m input power) which is sufficiently lower than the values at which the deflection of linearity starts (11 kV, 0.5 W/m). Obviously, using the double UV
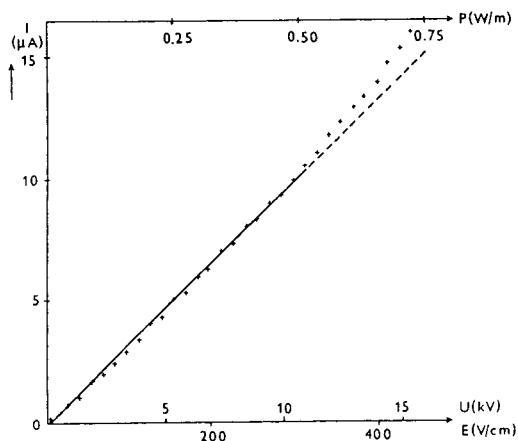
Fig. 4. Dependence of current, I, on the voltage, U, applied to the capillary in the flowing-air-thermostated separation compartment. E = intensity of electric field corresponding to applied voltage; P = input power corresponding to applied voltage and driving current in the capillary.

detection device it is not necessary to perform the whole experiment at such low input power. In order to speed up the measurements at the beginning of the experiment the higher voltage can be applied and only when the first analyte is nearing the first detection position the voltage is decreased to a lower value.

3.4. CZE analysis of peptides and determination of their effective mobilities.

The developed double UV detection CZE device was used for analysis of several synthetic peptides and for measurement of their effective electrophoretic mobilities.

The CZE separation of a test mixture containing synthetic peptides diglycine and triglycine and an electroosmotic flow marker, phenol, is shown in Fig. 5. As expected, separation of this three-component mixture by the double UV detection CZE device provides an electropherogram with six peaks. Generally, n-component mixtures will generate electropherogram with $2n$ peaks.

The higher peak heights of the same sample components at the first detection position (aperture A1, peaks 1, 2, 3 in Fig. 5) than at the second one (aperture A2, peaks 1', 2', 3' in Fig.
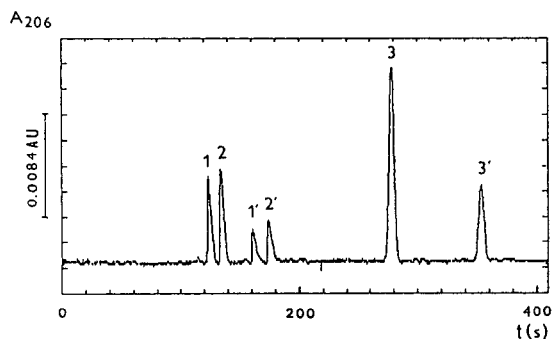
Fig. 5. Separation of a test mixture of diglycine, triglycine and phenol by the double UV detection CZE device. 1 (1') = diglycine (1 mg/ml) in the first (second) detection position; 2 (2') = triglycine (1 mg/ml) in the first (second) detection position; 3 (3') = phenol (0.3 mg/ml) in the first (second) detection position. A = absorbance at 206 nm; t = migration time. Sample components dissolved in BGE (0.5 mol/l acetic acid, pH 2.5). Sample introduction overpressure 0.006 bar applied for 5 s. Voltage 7.0 kV, current 7.3 μA. The other separation conditions are given in the text.
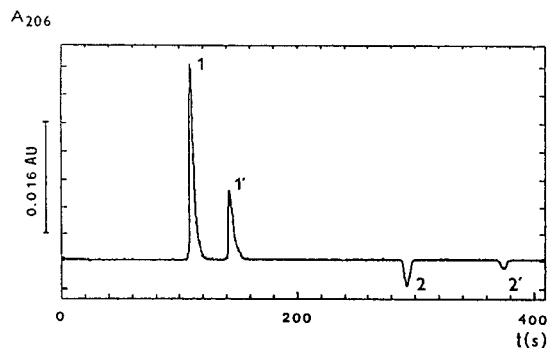
Fig. 6. Analysis of diglycyl growth hormone releasing peptide by the double UV detection CZE device. 1 (1') = peptide peak in the first (second) detection position; 2 (2') = peak of electroosmotic flow marker in the first (second) detection position. A = absorbance at 206 nm; t = migration time. Sample (1 mg/ml) dissolved in BGE. The other experimental conditions are given in the text and in Fig. 5.

5) reflect better adjustment of the capillary window on the aperture A1 than on the aperture A2. The signal of the detector is very sensitive on this adjustment. A small change in the relative position between the capillary and the aperture causes that some light is not going through the core of the capillary but through its walls which results in a signal decrease of the detector. However, the sensitivity of both detection positions of the developed system is sufficient for our measurements (noise at the level $4 \cdot 10^{-4}$ AU).

The double UV detection system was mostly used in a mode with simultaneous measurement of UV absorption at both detection positions, i.e., both apertures are opened and the sum of the light coming in the two light beams is measured by the photodiode. With respect to the relatively low light amount going through the miniature apertures, this mode is more suitable than the mode with alternatively opened and closed apertures, since the photodiode noise is relatively lower, i.e., the signal-to-noise ratio is higher at higher light intensities. If linearity of detection is preferred over its sensitivity, then the mode with alternatively opened apertures should be used.

CZE analysis of diglycyl growth hormone releasing peptide is shown in Fig. 6. From the differences of migration times of the peptides at the second and at the first detection position the resulting migration time of their movement between the two detectors is obtained and using the other experimental data (see Eq. 5) the effective electrophoretic mobilities of peptides were calculated. The results are summarized in Table 2.

The better reproducibility of effective mobilities obtained from shorter series (five experiments performed in series during few hours, RSD = 0.4–0.8%) than from the longer series (twenty experiments during few days, RSD = 1.2–1.3%) can be explain by the fact that local micro changes of the double-layer composition (electrokinetic potential) at the inner surface of the capillary, resulting in electroosmotic flow velocity variation, are smaller during shorter periods of time. Also the other sources of variance, such as e.g. slight changes of pH and ionic strength of BGE, can be expected to be smaller during the shorter time period than during the longer one. The uncertainty caused by a sampling period of 0.1 s for migration time, e.g. $t = 40$ s, $(0.1/40) \times 100 = 0.25\%$ should be also taken into account as a source of variance of the measured data.

Table 2
Calculated effective electrophoretic mobilities of peptides analyzed by the double UV detection CZE device

Peptide	$m_{ef} \cdot 10^9$ $(m^2V^{-1}s^{-1})$	z_{ef}	RSD (%)	n
Diglycine	25.6 ± 0.3	0.78	1.2	20
Triglycine	22.3 ± 0.3	0.84	1.3	20
Diglycine	25.1 ± 0.2	0.78	0.8	5
Triglycine	21.9 ± 0.1	0.84	0.4	5
His[1]-GHRP	35.6 ± 0.3	3.0	0.8	5
Tyr[1]-GHRP	23.5 ± 0.2	2.0	0.6	5
Diglycyl-GHRP	34.0 ± 0.2	3.0	0.6	5
GHRP-frag.	30.0 ± 0.2	2.0	0.7	5

m_{ef} = Effective electrophoretic mobility at 25°C (in 0.5 mol/l acetic acid, pH 2.5), RSD = relative standard deviation, n = number of measurements.

Effective mobility, m_{ef}, of the peptide is a function of its effective charge and size (relative molecular mass, M_r). Several relations have been suggested to describe this dependence [7]. Among them the Offord equation [16] is the most frequently used:

$$m_{ef} = k \cdot z_{ef} \cdot (M_r)^{-2/3} \qquad (6)$$

where k is constant of proportionality and z_{ef} is the effective charge of peptide. From this relation it follows that the ratio m_{ef}/z_{ef} should be directly proportional to $(M_r)^{-2/3}$.

In Fig. 7 the ratio of determined effective mobilities (see Table 2) and their calculated effective charges is plotted against relative molecular mass of peptides, $(M_r)^{-2/3}$. For calculation of the effective charges our previously developed program was used [17]. The very good agreement of our data with the Offord equation is evident.

4. Conclusions

The developed HPCE device with the double UV detection system was shown to be a suitable tool for the fast and accurate measurement of electrophoretic mobilities and potentially of other physico-chemical characteristics of the peptides analyzed or other substances.

Acknowledgements

Fig. 7. Dependence of the ratio of effective mobility and effective charge, m_{ef}/z_{ef}, on the relative molecular mass, $(M_r)^{-2/3}$, of analyzed peptides.

References

[1] M.V. Novotny, K.A. Cobb and J. Liu, Electrophoresis, 11 (1990) 735.

[2] J.C. Colburn, in P.D. Grossman and J.C. Colburn (Editors), Capillary Electrophoresis: Theory and Practice, Academic Press, San Diego, CA, 1992, p. 237.

[3] C.A. Monnig and R.T. Kennedy, Anal. Chem., 66 (1994) 280R.

[4] P.D. Grossman, J.C. Colburn and H.H. Lauer, Anal. Biochem., 179 (1989) 28.

[5] E.C. Rickard, M.M. Strohl and R.G. Nielsen, Anal. Biochem., 197 (1991) 197.

[6] M.A. Survay, D.M. Goodall, S.A.C. Wren and R.C. Rowe, J. Chromatogr., 636 (1993) 81.

[7] V.J. Hilser, G.D. Worosila and S.E. Rudnick, J. Chromatogr., 630 (1993) 329.

[8] V. Kašička, Z. Prusík, J. Štěpánek and P. Mudra, presented at 8th Int. Symp. on Capillary Electrophoresis and Isotachophoresis, Rome, October 6–10, 1992, Abstracts, p. 29.

[9] J.L. Beckers, Th.P.E.M. Verheggen and F.M. Everaerts, J. Chromatogr., 452 (1988) 591.

[10] S. Terabe and T. Isemura, J. High Resolut. Chromatogr., 14 (1991) 52.

[11] J.K. Towns and F.E. Regnier, Anal. Chem., 64 (1992) 2473.

[12] T. Srichaiyo and S. Hjertén, J. Chromatogr., 604 (1992) 85.

[13] J. Hlaváček, O. Smékal, J. Pospíšek and T. Barth, Collect. Czech. Chem. Commun., 59 (1994) 707.

[14] Z. Prusík, V. Kašička, S. Staněk, G. Kuncová, M. Hayer and J. Vrkoč, J. Chromatogr., 390 (1987) 87.

[15] K. Danihelka and P. Mudra, unpublished results.

[16] R.E. Offord, Nature, 211 (1966) 591.

[17] V. Kašička and Z. Prusík, J. Chromatogr., 470 (1989) 209.

ELSEVIER

Continuous micropreparative trapping in carrier ampholyte-free isoelectric focusing

Mirko Deml*, Jan Pospíchal, Josef Chmelík

Institute of Analytical Chemistry, Academy of Sciences of the Czech Republic, Veveří 97, CZ-611 42 Brno, Czech Republic

Abstract

The micro-isolation of a minor ampholyte from a mixture of four ampholytes using carrier ampholyte-free isoelectric focusing (IEF) is described. The separation is achieved in two consecutive steps. In the first step, a concentrated mixed zone of minor ampholyte-containing major ampholytes is formed when the original mixture is loaded into the column by electromigration. During this loading, a flux of solvolytic ions from both ends of the column is set up in such a way that one end of the zone formed is immobilized in the column. It is achieved by selection of the pH range, which includes the pI value of the minor ampholyte but not the pI values of the major ampholytes. The minor ampholyte is captured in this zone completely, whereas the major ampholytes migrate through this zone to the outlet reservoir. After the zone has acquired a reasonable volume, the loading step is interrupted. In the second step, either the complete contents of the column are separated by conventional carrier ampholyte-free IEF in a pH range that includes the pI values of all the ampholytes, or using a smaller pH range the minor ampholyte can be separated and isolated completely. Zone formation was modelled by computer simulation for a two-ampholyte mixture and verified experimentally for a four-ampholyte mixture in an instrument for electrically controlled IEF by using coloured low-molecular-mass ampholytes.

1. Introduction

Modern capillary electrophoretic techniques, such as capillary zone electrophoresis (CZE), isotachophoresis (ITP) or capillary isoelectric focusing (CIEF), have outstanding separation abilities in terms of selectivity, resolution and speed of analysis [1]. The sophisticated detection techniques developed recently have decreased the detection limits to the level of single molecules [2].

Usually these techniques work in a one-dimen-

sional mode only, which is frequently insufficient when complex biological mixtures are to be analysed. The presence of the large amounts of salts, the great complexity of biological samples and the high concentration ratio of the substances of interest adversely affect the analytical results. Therefore, the analysis of biological samples requires either an enhanced separation power of the method or sample pretreatment prior to analysis.

The use of two-dimensional analysis by coupling an electrophoretic technique with another separation technique, e.g., MS or HPLC [3,4], helps to resolve substances that cannot be resolved in one run. Surprisingly, the combination of two electrophoretic techniques can also sig-

---

* Corresponding author.

nificantly increase the resolution and this approach is frequently used. Combined ITP and CZE [5–8] is used mainly for the preseparation and preconcentration of samples. Moreover, the major bulk waste component can be easily eliminated from a CZE run using more sophisticated equipment, which results in simplification of the complex separated sample prior to proper analysis. The load used does not exceed the volume of the capillary [9], which does not need to be sufficient for the detection or preparation of minor components.

Such a simplification of the sample components with higher volumes of the load is used in non-capillary free-solution focusing techniques [10–12], where a range of the substances of close pI and/or pure substance themselves is the result of the separation run. These techniques are used for the preparation of purified samples. Bier et al. [10] used zwitterionic buffer mixtures in recycling IEF, where the sample was divided into three parts, anodic, cathodic and middle, where substances of interest were focused. Using buffers of higher concentration enhanced the solubility of proteins. Righetti et al. [11] introduced isoelectric membranes tailored for particular separations. The sample is introduced between two membranes, where substances with pI values different from the pI range of the membranes are flushed out by electromigration.

This paper describes another method of collecting an amphoteric compound A of interest from a sample containing higher concentrations of ampholytes B, C and D and KCl (electrolyte).

If a sample is placed in a load reservoir connected with a waste reservoir by a tube and electric current is passed through such a column, the minor ampholyte can be trapped in the tube as a stopped zone. Almost all major ampholytes leave the tube to the waste reservoir, passing through the created trapped zone of minor ampholyte.

In the trapped zone, under suitable conditions, the concentration of the originally minor ampholyte A is higher than those of the originally major ampholytes. In this way selective enrichment can be achieved.
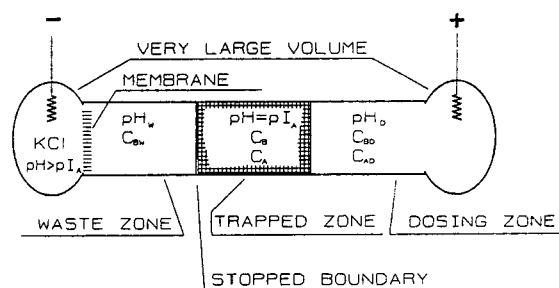
Fig. 1. Schematic diagram of the experimental arrangement. The loaded sample mixture is on the anodic and the waste zone on the cathodic side of the column.

2. Theory

A schematic diagram of the basic arrangement is shown in Fig. 1. The waste zone is at the cathodic side and the loading zone at the anodic side. If the waste zone has a pH value pH_W higher than the pI value of the minor ampholyte, pI_A, no minor ampholyte can enter the waste zone. On the opposite side, the slowly moving boundary between the trapped and loading zones must have a pH value from the side of the loading zone, pH_D, that is lower than pI_A.

The properties of the waste and loading zones determine the conditions for immobilization of the trapped zone. For the specific composition of the loaded sample mixture, there is only one proper composition of the waste zone.

To calculate the compositions of the waste and the trapped zones, a program developed and described earlier was used [13]. The program was upgraded for the calculation of two biprotic ampholytes in a loaded sample mixture containing also salts of strong and weak bases and acids as a background electrolyte. This program is based on: (1) equality of flows of the background electrolyte in all zones; (2) electroneutrality; (3) dependence of degree of dissociation of substances on pH; (4) constant omega function in all zones; (5) constant driving current in all zones; and (6) mass balance.

Let us first discuss the simplest part of the system, the neutralization boundary. It is created in the background electrolyte by partial replace-

ment (modification) of the cations and anions at the anodic and cathodic sides of the column with H^+ and OH^- ions, respectively. Flows of solvolytic ions H^+ and OH^- (J_H, J_{OH}) enter the neutralization boundary created in the background electrolyte from opposite sides. If these fluxes are equal, i.e.,

$$J_{H^+} = J_{OH^-} \tag{1}$$

the neutralization boundary stops and does not move. Then the sum of the flows of ions of the background electrolyte ($J_{B,H}$, $J_{B,OH}$) are also equal on both sides:

$$\sum J_{B,H^+} = \sum J_{B,OH^-} \tag{2}$$

Further, let us discuss the properties of the ampholyte zone. If the zone of the trapped ampholyte is created between two such modified zones which were stopped, it cannot move. The ampholyte is in its isoelectric state, and if the mobilities of its cationic and anionic forms are equal, it is also in the isoionic state. The amount of the dissociated fraction for the biprotic ampholyte is given by [14]

$$\alpha = \frac{2}{2 + 10^{pI - pK_1}} \tag{3}$$

where α is the degree of dissociation of both cationic and anionic forms of the ampholyte and pK_1 is the dissociation constant. Only the dissociated fraction can transfer electric charge (protons).

At the boundaries of the trapped zone with background electrolyte, a dynamic equilibrium exists, and the flows of the solvolytic ions are divided into two parts. The first part of the solvolytic flow neutralizes the oppositely charged ampholyte and solvolytic ions to the neutral form, creating water by neutralization. The second part of this flow enters the zone, ionizes the ampholyte and carries the charge to the other side of the zone, where the same effect with ions of opposite sign occurs. Assuming that the ampholyte is in the isoelectric state, only half of the solvolytic flow reaching the boundary enters the

zone and is carried by the ampholyte to the opposite side of the zone.

In the trapped zone of the ampholyte, the flows of the solvolytic ions are also divided into two parts. They are partially carried by the ampholyte ($J_{A,A}$) and partially they continue as flows of free solvolytic ions ($J_{H,A}$, $J_{OH,A}$). The sum of these flows is equal to the flow of solvolytic ions entering from the background electrolyte, i.e.,

$$J_{H^+} = J_{OH^-} = J_{H,A} + J_{A,A} \tag{4}$$

Of course, the sum of flows ions of background electrolyte in the zone of ampholyte ($J_{B,A}$) must be equal to the flows of these ions in the modified background electrolyte ($J_{B,H}$; $J_{B,OH}$):

$$\sum J_{B,H^+} = \sum J_{B,OH^-} = \sum J_{B,A} \tag{5}$$

In other words, Eqs. 4 and 5 indicate that the amount of electricity carried by solvolytic and/or non-solvolytic ions is constant in each part of the whole system.

The flow of the ampholyte in the trapped zone ($J_{A,A}$) is given by

$$J_{A,A} = C_A U_A \alpha I / \kappa_A \tag{6}$$

where C_A is the analytical (total) concentration of the ampholyte is its zone, I is the current, U_A is the ionic mobility of the ionized form A and κ_A is the conductivity of the zone. Since in the isoelectric state the fraction of the ionized ampholyte α is constant (neglecting the influence of the ionic strength on the pK value), the flow of solvolytic ions from surroundings is balanced by setting its total concentration. Any change of the solvolytic flows from the surroundings results in a change in concentration of the ampholyte, i.e.,

$$\Delta J_H = J_{H,A} + J_{OH,A} + \Delta C_A U_A \alpha I / \kappa_A \tag{7}$$

From Eq. 7, it follows that the concentration of the ampholyte in the zone is proportional to the flow of the solvolytic ions and to its physicochemical properties, which also determine the amount of free solvolytic ions in the zone. The computer program is based on this idea.

Mobilities, pK values of all substances, con-

centration of the background electrolyte, concentrations of the ampholytes in the load and the chosen pH value of the waste zone are the input data for the program. From these data, the program calculates the compositions and the pH values of all zones that fulfil the conditions of the stopped boundary between the loading and trapped zones.

The procedure for computation is as follows. The compositions of the loading and waste zones are calculated first. The concentrations of both loaded ampholytes in the trapped zone are then obtained by iteration, until equal flows of background electrolyte in all zones are reached.

It should be stressed that the diffusion and depletion of the primary background electrolyte due to the presence of the neutralization reaction on the boundaries is neglected. This is acceptable at a small difference in pH between the waste zones and the loading zone. By comparison with simulation data obtained from the program by Thormann and co-workers [15,16], only a minor difference in the concentrations of ampholytes was found, not exceeding 5%. In that program the mentioned effects were not neglected.

Calculated data for ampholyte A ($pI_A = 7.4$, $pK_1 = 6.9$, $pK_2 = 7.9$; $\mu_1 = \mu_2 = 30 \cdot 10^{-9}$ m^2 V^{-1} s^{-1}) and for ampholyte B ($pI_B = 7.9$, $pK_1 = 7.4$, $pK_2 = 8.4$; $\mu_1 = \mu_2 = 30 \cdot 10^{-9}$ m^2 V^{-1} s^{-1}) are given in Table 1. In all calculations, 10 mM KCl was used as the primary electrolyte. The concentration of the loaded major ampholyte was always 10^{-3} M and the concentration of the minor ampholyte A varied from 10^{-5} to 10^{-3} M.

The transfer number of the trapped ampholyte in the loaded mixture varied from $2.1 \cdot 10^{-4}$ to $2.43 \cdot 10^{-2}$ and represents the amount of trapped ampholyte per unit of electric charge passed through the column.

The value of C_A^* represents the concentration of the trapped ampholyte in the case when no major ampholyte is loaded. The most important fact is shown in the middle column. The widely varying ratio of the concentration of the minor to major ampholyte in the loading zone (from 1:1 to 1:100) results in a nearly constant concentration of minor ampholyte in the trapped zone. The ratio C_A/C_B here varies from 1:0.81 to 1:0.55. If the concentration of minor ampholyte in the loading mixture is decreased by two orders of magnitude, its concentration in the trapped zone decreases by about 9%. In this way, a mixture enriched in the minor ampholyte is obtained.

For verification of the accuracy of the calculated data, a computer simulation was performed. A simulated column was filled with a mixture of previously calculated composition (see Table 2). The initial conditions are that the continuously loading (source) zone is placed at the anodic side and the continuously depleting waste zone on the cathodic side. Development of the concentration, pH and conductivity profiles along the column with time is shown in Fig. 2. The concentrations in the simulated trapped zone ($c_A = 2.23$ mM, $c_B = 1.24$ mM) are in good agreement with the calculated values ($c_A = 2.45$ mM, $c_B = 1.37$ mM), and their ratios are 1.798 and 1.788, respectively.

Table 1
Calculated data for model mixture containing two ampholytes, A and B, in 10 mM KCl

Loaded mixture			Trapped zone (pH = pI_A)			Non-trapped zone		Transfer number, $10^3 T_A$
c_A (mmol)	c_B (mmol)	pH	c_A (mmol)	c_B (mmol)	c_A^* (mmol)	c_B (mmol)	pH	
0.01	1	3.81	2.45	1.37	4.012	4.0	7.74	0.21
0.1	1	3.83	2.48	1.38	4.087	4.0	7.74	2.11
0.5	1	4.02	2.26	1.53	4.043	3.9	7.72	11.2
1	1	4.38	2.09	1.71	4.088	4.0	7.70	24.3

Table 2
Compositions of electrolytes used for simulation

Parameter	Loading zone	Waste zone
pH	3.83	7.74
Ampholyte A	1 mM	0 mM
Ampholyte B	10 mM	40 mM
K^+	7.952 mM	4.539 mM
Cl^-	9.199 mM	5.107 mM

3. Experimental

3.1. Chemicals

Low-molecular-mass p*I* markers of p*I* 5.3, 6.2, 8.6 and 10.1 were obtained from Dr. K. Šlais (Institute of Analytical Chemistry, Brno, Czech Republic), their chemical compositions and properties have been published elsewhere [17]. They are readily soluble in water and are coloured.

The apparatus used for the focusing is a modification of the previously used laboratory-made four-pole column [13] and will be described more precisely in a subsequent paper. The apparatus has four electrode chambers connected with a separation channel and one pair of electrode chambers on each side of the separation capillary. In each pair of equal polarity, one chamber is filled with the primary (background) electrolyte (here 0.01 *M* KCl) and the other with a modification electrolyte or loaded mixture. A solution of a strong base serves as a cathodic modification electrolyte and the loaded mixture contains the ampholytes dissolved in primary electrolyte with a properly adjusted pH value.

The flows of ions from the electrode chambers pass through the washed membranes into the separation channel, which is a quartz capillary (120 mm × 0.35 mm I.D.). The capillary is efficiently cooled by a stream of air from a flat nozzle, mounted on the supporting rack.
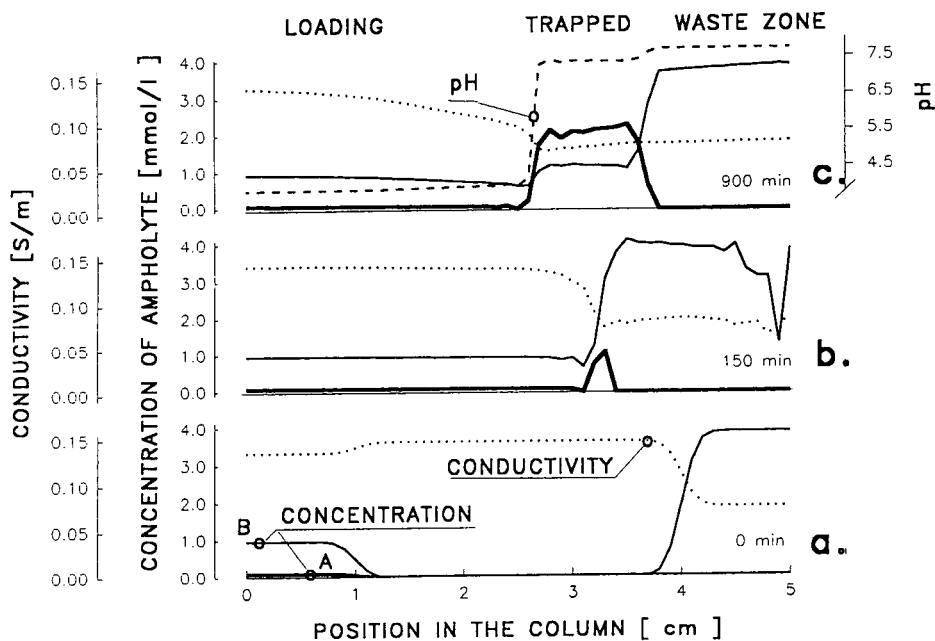
Fig. 2. Simulated time course of trapping. (a) Concentration profiles of the minor and major ampholytes (full thick and thin lines, respectively) and conductivity profile (dotted line) at the start of trapping; (b) developed profiles after 150 min; (c) profiles after 900 min; dashed line pH profile. Current density, 20 A m^{-2}.

3.2. Trapping procedure

After filling the appropriate electrode chambers with solutions of the loaded mixture and basic modification and neutral primary electrolytes, the membrane washing is started to keep the composition of the electrolytes constant during the run. The capillary is filled with the loaded mixture. The separation is started by setting the ratio of the driving currents on both regulators and switching on the main driving current. Solvolytic ions and the loaded mixture ions continuously penetrate the capillary, where the trapped ampholyte creates a zone. When the creation of the trapped zone starts, some fine readjustment of the driving current, depending on the position and velocity of the zone in the column, is obviously necessary. Non-trapped ampholytes migrate via the trapped zone to a waste zone and subsequently through a membrane of the primary electrolyte out of the column and into the electrode drain solution. After some time, the whole capillary is filled with the trapped zone, which contains substantially enriched trapped ampholyte. Subsequent interruption of the continuous loading and decreasing the pH range cause the major ampholytes to leave the trapped zone. In the capillary only the pure trapped ampholyte remains.

3.3. Micropreparation

The driving current is switched off and a thin needle (quartz capillary) is inserted into the column through the opened filling valve on one side of the column. The contents of the column between the membrane and the trapped zone are removed by suction and replaced with air. A small bubble of air on the other side of the trapped zone is inserted, to prevent remixing with other possible zones. After repositioning the needle to the centre of the zone, the zone is drawn into the needle using an attached microsyringe. The needle is removed from the column and the microprepared zone (ca. 5 μl) is transferred into a microvial, where it is stored at 0°C.

Analytical control was effected by capillary isoelectric focusing with electroosmotic displacement of zones (CIEF). CIEF was performed by using a laboratory-made capillary electrophoretic device. It features a 70 cm effective length, 90 cm total length × 75 μm I.D. fused-silica capillary (Polymicro Technologies, Phoenix, AZ, USA), a CZE 1000R electric power supply (Spellmann, New York, USA) and a Spectra Focus fast-scanning UV–Vis spectrophotometric detector (Thermo Separation Products). Results were recorded in the wavelength range 370–600 nm and the spectra of the individual peaks were used for identification of the coloured ampholytes.

All experiments were performed with 10 mM phosphoric acid as anolyte and 20 mM sodium hydroxide containing 0.1% hydroxypropylmethylcellulose (Sigma, St. Louis, MO, USA) as catholyte at 20 kV constant voltage. The sample ampholytes were dissolved in a 2% solution of the carrier ampholyte Servalyt 3–10 (Serva, Heidelberg, Germany) and were injected gravitationally into the anodic end of capillary (raising it to 70 cm for 5 min). The experimental procedure has been described in detail elsewhere [18,19].

4. Results

To demonstrate the performance of the method for more complicated loaded mixtures, a model mixture of four ampholytes (low-molecular-mass pI markers) of pI 5.3, 6.2, 8.6 and 10.1 was chosen at concentrations of 10^{-3}, 10^{-4}, 10^{-3} and 10^{-3} M, respectively. The minor ampholyte of pI 6.4 is red and the others are yellow. This model mixture, dissolved in 0.01 M KCl (primary electrolyte) with pH adjusted to 5.5, served as the loading mixture in subsequent experiments.

The time course of the experiment is shown in Figs. 3a, b and c, where the trapped zone (pI 6.2, the darker zone) was photographed after times of 10, 25 and 120 min, respectively. The zone grows, and by 120 min it is 20 mm long. The non-trapped ampholyte (pI 10.1 and 8.6,
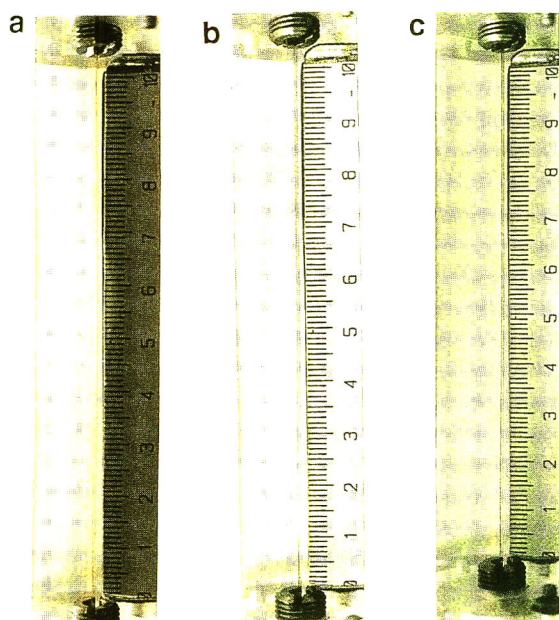
Fig. 3. Time course of trapping. Zones after (a) 10, (b) 25 and (c) 120 min. The zones of trapped ampholyte are in positions 39–40, 31–34, and 55–75, respectively. The driving current was 200 μA during the first 10 min, then decreased to 100 μA.

lighter zone) pass through the column to the waste electrode chamber and from it they are rinsed out by a continuous flow of fresh electrolyte. The equivalent length of the non-trapped zone without rinsing (under these conditions) should be ca. 400 mm.

The CIEF analysis of this mixture (wavelength 410 nm, maximum absorbance of major ampholytes) is shown in Fig. 4. The ampholytes migrate in order of their decreasing pI values, the first peak being ampholyte of pI 10.1 and the last peak ampholyte of pI 5.3. Fig. 5 shows the CIEF analysis of the trapped zone when continuous loading was not stopped. As can be seen, the ratio of the minor to major ampholyte concentration is dramatically changed. The minor ampholyte is more concentrated in the mixed trapped zone than in the original loading mixture, and originally major ampholytes are at lower concentration. Only a small amount of ampholyte of pI 5.3 is present in the trapped zone.

Fig. 6 shows the CIEF analysis of the isolated zone, refocused in the column, after the loading was stopped. It can be seen that the zone
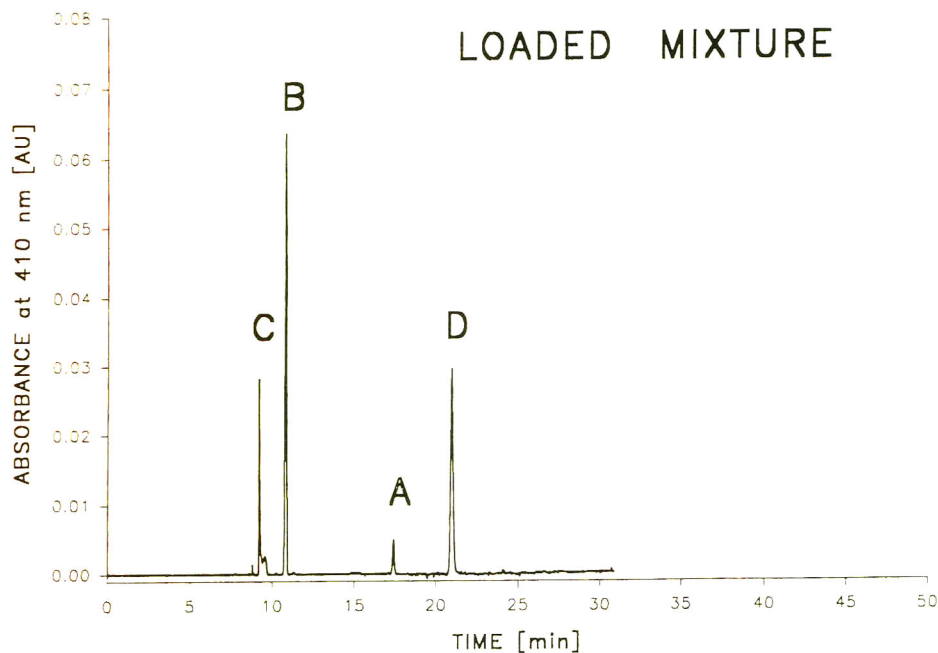
Fig. 4. CIEF analysis of the loaded mixture of four pI markers of pI (A) 6.2, (B) 8.6, (C) 10.1 and (D) 5.3.
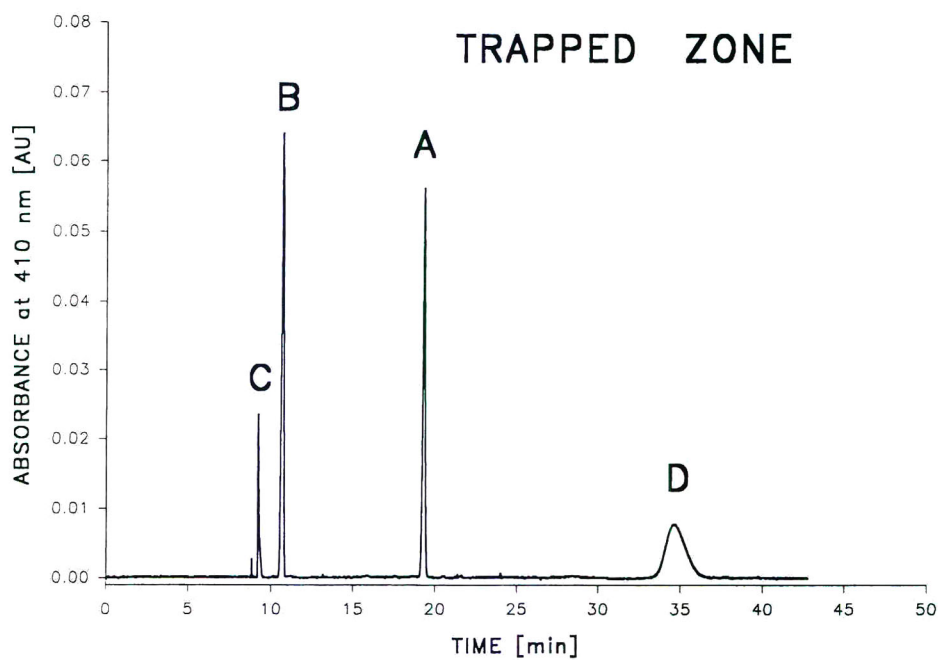
Fig. 5. CIEF analysis of the trapped zone. Details as in Fig. 4.
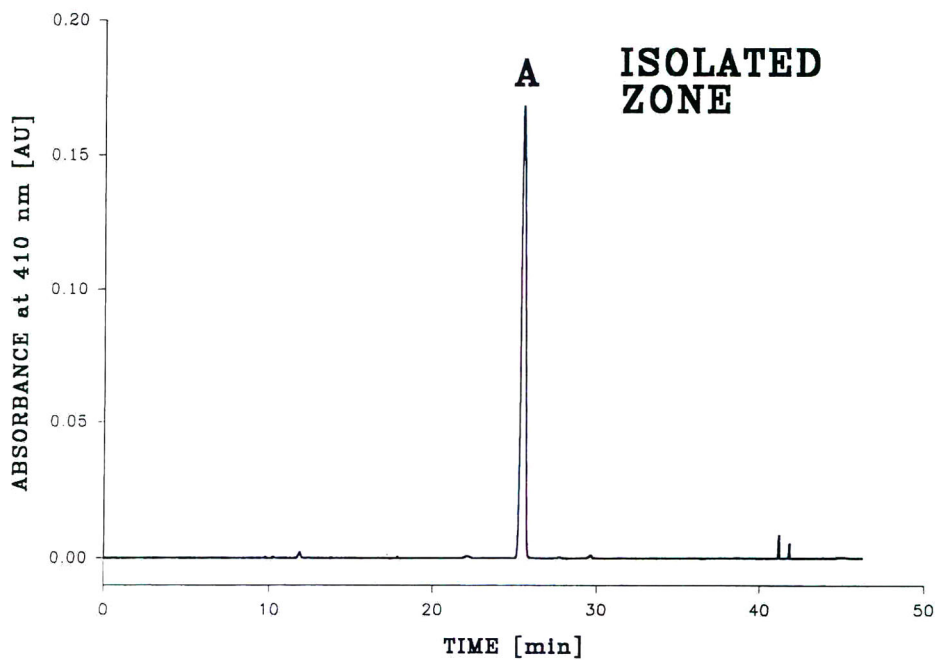
Fig. 6. CIEF analysis of the isolated zone. Details as in Fig. 4.

contains mainly minor ampholyte, the major ampholytes having left the zone. Ampholytes leaving the isolated zone to the cathodic side are shown in Fig. 7. Here, small amounts of ampholytes B and C were detected together with some impurities X of original product of ampholyte A. These impurities were also found in the original product of ampholyte A (Fig. 8). On the anodic side, no impurities were detected after refocusing of the isolated zone. CIEF analysis of the cathodic drain electrolyte shows only the presence of ampholytes B and C (Fig. 9), which confirms the theoretical considerations.

5. Conclusion

The developed continuous trapping method showed good results in simulations and experiments. The method allows trapping of a minor ampholyte component from a large-volume load. The concentration of the trapped substance is favourably high. The relative enrichment of the minor ampholyte in the trapped zone is sufficiently high.

The volume of the load from which the trapped ampholyte originates is more than one order of magnitude higher than the volume of the separation capillary. The method is based on carrier ampholyte-free IEF and the microprepared substance contains only ions of the background electrolyte.

Acknowledgement
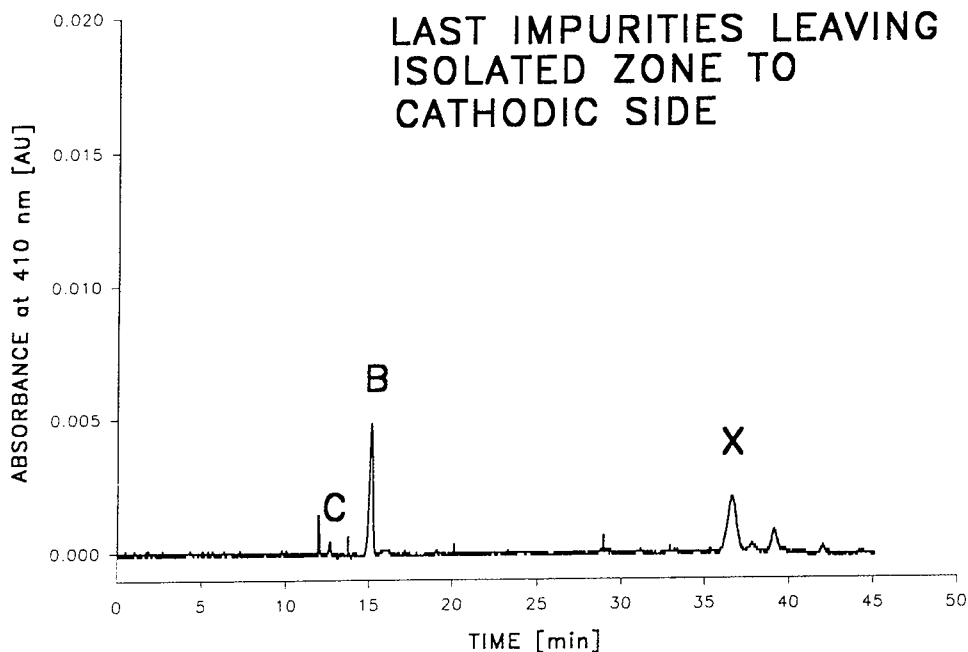
Fig. 7. CIEF analysis of the impurities leaving the isolated zone to the cathodic side. X denotes impurities of the original product A. Details as in Fig. 4.
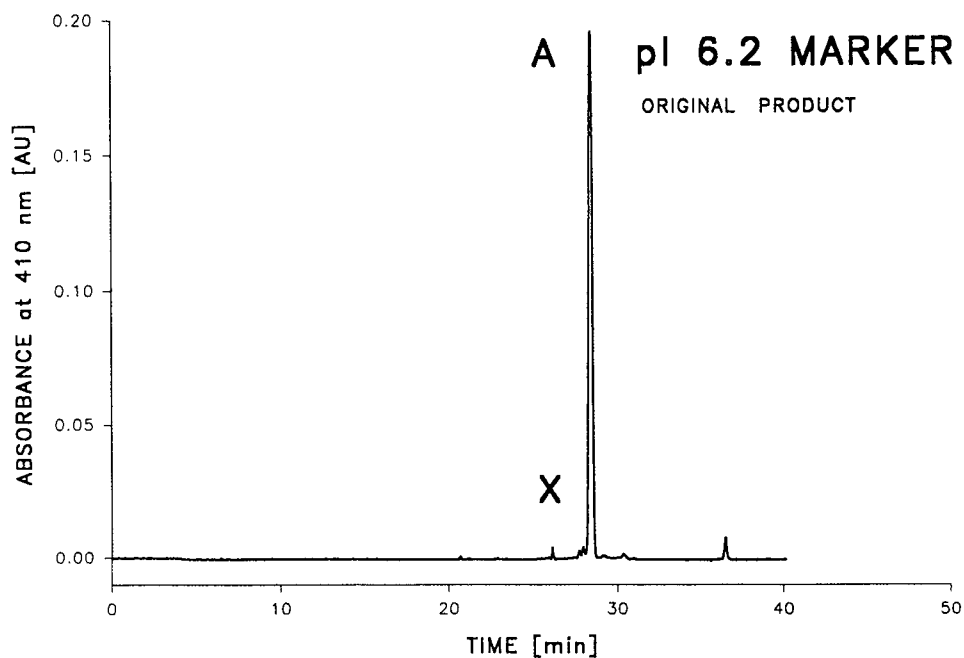
Fig. 8. CIEF analysis of the original product A. Details as in Fig. 4.
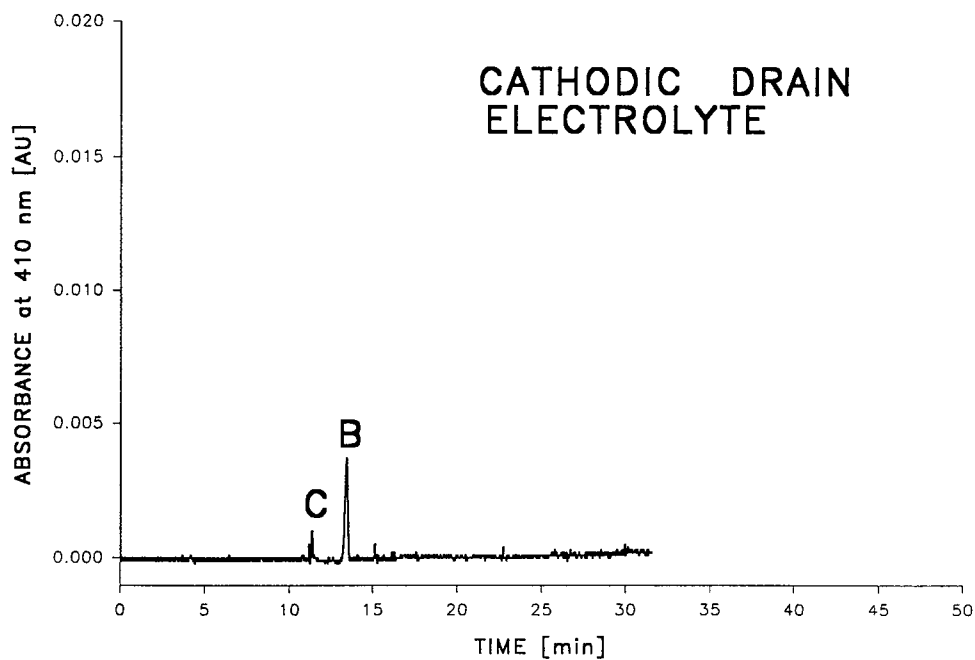
Fig. 9. CIEF analysis of cathodic drain electrolyte. Details as in Fig. 4.

References

[1] C.A. Monning and R.T. Kennedy, Anal. Chem., 66 (1994) R280.

[2] D.Y. Chen, K. Adelhem, X.L. Cheng and N.J. Dovichi, Analyst, 119 (1994) 349.

[3] M.A. Moseley, L.J. Deterding, K.B. Tomer and J.W. Jorgenson, J. Chromatogr., 480 (1989) 1989.

[4] M.M. Bushey and J.W. Jorgenson, Anal. Chem., 62 (1990) 978.

[5] M. Deml, F. Foret and P. Boček, J. Chromatogr., 320 (1985) 159.

[6] V. Dolník, K.A. Cobb and M. Novotny, J. Microcol. Sep., 2 (1990) 127.

[7] D. Kaniansky and J. Marák, J. Chromatogr., 498 (1990) 191.

[8] F. Foret, V. Šustáček and P. Boček, J. Microcol. Sep., 2 (1990) 229.

[9] S. Hjertén, J. Liao and R. Zhang, J. Chromatogr. A, 676 (1994) 409.

[10] M. Bier, J. Ostrem and R.B. Marguez, Electrophoresis, 14 (1993) 1011.

[11] P.G. Righetti, E. Wenisch, A. Jungbauer, H. Katinger and M. Faupel, J. Chromatogr., 500 (1990) 681.

[12] E. Wenish, K. Vorauer, A. Jungbauer, H. Katinger and P.G. Righetti, Electrophoresis, 15 (1994) 647.

[13] J. Pospíchal, M. Deml and P. Boček, J. Chromatogr., 638 (1993) 179.

[14] H. Svensson, Acta Chem. Scand., 15 (1961) 325.

[15] R.A. Mosher, D.A. Saville and W. Thormann, The Dynamics of Electrophoresis, VCH, Weinheim, 1992.

[16] R.A. Mosher, P. Gebauer, J. Caslavska and W. Thormann, Anal. Chem., 64 (1991) 2991.

[17] K. Šlais and Z. Friedl, J. Chromatogr. A, 661 (1994) 249.

[18] J. Chmelík and W. Thormann, J. Chromatogr., 632 (1993) 229.

[19] J. Caslavska, S. Molteni, K. Šlais, F. Matulík and W. Thormann, J. Chromatogr. A, 680 (1994) 549.

ELSEVIER

Electroosmosis in capillary zone electrophoresis with non-uniform zeta potential

Blahoslav Potoček[a], Bohuslav Gaš[a,*], Ernst Kenndler[b], Milan Štědrý[a]

[a]*Faculty of Science, Charles University, Albertov 2030, 128 40 Prague 2, Czech Republic*
[b]*Department of Analytical Chemistry, University of Vienna, Währinger Strasse 38, A1090 Vienna, Austria*

Abstract

The influence of the longitudinally non-uniform zeta potential on processes in capillary zone electrophoresis was studied. The velocity field of the electroosmotic flow in capillary tubes is modelled by the Navier–Stokes equations. Their stationary solution represents convective transport of a solute which is taken into account in the continuity equation for the concentration distribution. All equations are studied numerically. The results represent the time evolution of initial forms of sample peaks. These are presented in graphical form for several cases of zeta potentials which are either instructive or closely related to situations encountered in practice. It is shown that plug-like flow in the capillary cannot be expected and that a non-uniform zeta potential generally leads to significant dispersion of peaks.

1. Introduction

One of the most important phenomena accompanying the separation process in capillary zone electrophoresis (CZE) is the electroosmotic flow (EOF). This flow can be easily explained by invoking the electric double layer. Of all the possible reasons for its formation, the following two are worth mentioning: the specific adsorption of charged ionic species and protolysis of dissociable groups on the inner surface of the separation column. Since the net charge density ρ in the diffusion part of the double layer differs significantly from zero, an applied longitudinal electric field of strength E exerts the volume force $E\rho$ on the diffusion layer. As a consequence, the diffusion layer moves and owing to

viscosity forces this movement is propagated to the rest of the liquid in the column.

In the description of the process, the electric potential Φ can be substituted for the net charge density ρ. The Poisson and Boltzmann equations provide relationships among ρ and Φ [1]. In this paper, it is the value of the potential Φ on the wall–liquid interface which will be used to characterize the process. This function is called the zeta potential and is usually denoted by ζ.

Many papers have dealt with the problem of EOF under the assumption that ζ does not depend on the coordinate running along the longitudinal axis of the capillary [2–7]. A conclusion drawn from above-mentioned papers is that EOF generally has little influence on the efficiency in CZE when the driving electroosmotic force is uniform along the column.

Cases in which any of the quantities involved, e.g., the zeta potential ζ or the longitudinal field

---

* Corresponding author.

E, are supposed to vary along the axis of the capillary are treated only occasionally. However, there are various reasons for the assumption of an axially non-uniform zeta potential. These can be both intentional ones caused by a chemical treatment of the inner surface of the capillary and casual ones caused by a reaction and/or an adsorption of a solute [8] at the interface.

Anderson and Idol [9] have studied the stationary flow pattern in a capillary under the influence of a zeta potential, which is a periodic non-uniform function of the axial variable. As governing equations of the flow they have taken the Stokes equations, i.e., the Navier–Stokes equations in which convective terms are neglected. Relations for fluid velocity have been derived by means of Fourier series expansion and, moreover, an equation for the mean fluid velocity has been presented.

Chien and Helmer [10] have proposed a model to calculate the average electroosmotic velocity and the variance of sample peaks in field-amplified capillary electrophoresis, using a capillary column filled with two different concentrations of the same buffer. Thus, in their analysis, it is the field strength that appears to have a non-uniform distribution along the column. They realized that the radial velocity profile in parts with different concentrations has a parabolic shape and showed that the difference between the local electroosmotic velocities in both parts of the column and the mean velocity contributes to the dispersion of a solute in accordance with the Golay equation.

Towns and Regnier [11] have described how partial coverage of the inner surface of the column by adsorption of a protein leads to the mismatch between local and bulk electroosmotic velocity and consequently to a decrease in efficiency of separation.

Nowadays, attempts are made to use a radial electric potential across a capillary wall for a direct control of the zeta potential [12,13]. In the experimental equipment the radial electric potential is applied over a part but not the entire length of the column. Although experimental observations have been reported [14,15] indicating that the dispersion of peaks in this case does

not satisfy the conclusions of Chien and Helmer, probably owing to surface conductivity, at least a gradual change in the axial distribution of the zeta potential [15] should be expected.

In this work, our aim was to study the migration of a solute in electrophoretic columns under the joint influence of the electrophoretic flux and convective transport through the electroosmotic flow caused by a longitudinally inhomogeneous zeta potential. A model is adopted in which the flow pattern in the column is found as a stationary solution of the Navier–Stokes equations with boundary conditions which depend on a given zeta potential. This stationary solution of the Navier–Stokes equations is found numerically. Another numerical procedure provides the concentration distribution of the solute as a function of two spatial variables and time. Results of simulations are given and commented on for three different distributions of zeta potential. It is concluded that the axially non-uniform zeta potential generally leads to dispersion of sample peaks and, sometimes, a noticeable radial distortion of the peak should be expected. In particular, the classical plug-like electroosmotic flow cannot be expected in cases where axial homogeneity of some quantities no longer holds.

2. Theory

We shall deal with a capillary column of radius a and finite length L. It will be assumed that $L \gg a$ and that all flows and fluxes and also the concentration distribution will be rotationally symmetrical.

2.1. Velocity field in the column

The velocity vector, $\vec{v}$, is equal to a two-dimensional vector (v_x, v_r), which consists of v_x, the axial, and v_r, the radial velocity component. Each component of the velocity vector depends on the axial coordinate x, the radial coordinate r and time t. The governing equations for the velocity $\vec{v}$ are the Navier–Stokes equations in which, with a view to rotational symmetry of the process, cylindrical variables will be used.

As the fluid is viscous, the boundary condition on the wall–liquid interface should be that the velocity is equal to zero and the volume force $E\rho$, from which the EOF stems, should occur in the Navier–Stokes equations. In this paper, for simplicity the fluid velocity on the column wall will be set to equal the electroosmotic plug velocity determined by the Helmholtz–Smoluchowski equation and, consequently, the volume force $E\rho$ does not appear in the equations governing the flow. This approximation was also used by other workers [9–11,16] and can be well accepted in most real instances when the thickness of the diffusion layer is much less then the inner diameter of the capillary column. Thus, the apparent electroosmotic velocity $v(x)$ at a point at the column wall with longitudinal coordinate x will be

$$v(x) = \frac{-\varepsilon E}{\eta} \zeta(x) \qquad (1)$$

where ε is the permitivity of the liquid, E is the driving electric field strength, $\zeta(x)$ is the zeta potential, dependent on the axial x coordinate, and η is the dynamic viscosity of the liquid. In this paper it is further assumed for simplicity that the driving electric field is a constant vector parallel to the axis of the capillary.

The acceptance of the approximation used, Eq. 1, is well supported by Tikhomolova [6], who analytically calculated the time development of the electroosmotic velocity profile in the cylindrical column. Her results show that the velocity at the inner edge of the diffusion layer acquires the Helmholtz–Smoluchowski value $-\varepsilon E\zeta/\eta$ in a very short time even when the rest of the liquid is still not moving.

As the double layer is neglected, it is possible to express the boundary condition on the capillary wall for the axial velocity component in the form

$$v_x(x, a, t) = v(x) \qquad (2)$$

where $v(x)$ is given by Eq. 1.

The velocity field and the function $p = p(x, r, t)$, describing pressure, satisfy the Navier–Stokes equations for incompressible fluid, which are considered in the domain $x \in \langle 0, L \rangle$, $r \in \langle 0, a \rangle$,

$t \in \langle 0, \infty)$ and can be be given in the following form [17]:

$$\frac{\partial v_x}{\partial t} + v_x \frac{\partial v_x}{\partial x} + v_r \cdot \frac{\partial v_x}{\partial r}$$
$$= \nu \left[\frac{\partial^2 v_x}{\partial x^2} + \frac{1}{r} \cdot \frac{\partial}{\partial r} \left(r \cdot \frac{\partial v_x}{\partial r} \right) \right] - \frac{1}{\rho_M} \cdot \frac{\partial p}{\partial x} \qquad (3)$$

$$\frac{\partial v_r}{\partial t} + v_x \frac{\partial v_r}{\partial x} + v_r \frac{\partial v_r}{\partial r}$$
$$= \nu \left[\frac{\partial^2 v_r}{\partial x^2} + \frac{1}{r} \cdot \frac{\partial}{\partial r} \left(r \frac{\partial v_r}{\partial r} \right) - \frac{v_r}{r^2} \right] - \frac{1}{\rho_M} \cdot \frac{\partial p}{\partial r}$$
$$(4)$$

$$\frac{\partial v_x}{\partial x} + \frac{1}{r} \cdot \frac{\partial}{\partial r} (r v_r) = 0 \qquad (5)$$

where $\nu \equiv \eta/\rho_M$ is the kinematic viscosity and ρ_M is the mass density of the liquid. It will be assumed that the fluid is at rest at time $t = 0$, and therefore

$$v_x(x, r, 0) = 0 , \quad v_r(x, r, 0) = 0 \qquad (6)$$

On the capillary wall, the axial velocity is prescribed and the radial velocity must be equal to zero, i.e.

$$v_x(x, a, t) = v(x) , \quad v_r(x, a, t) = 0 \qquad (7)$$

On the axis of the capillary, the components of the velocity satisfy these geometrical conditions:

$$\frac{\partial v_x}{\partial r}(x, 0, t) = 0 , \quad v_r(x, 0, t) = 0 \qquad (8)$$

It is assumed that both ends of the capillary are under constant pressure and, moreover, there is no difference between these pressures, i.e.,

$$p(0, r, t) = p_L , \quad p(L, r, t) = p_R \qquad (9)$$

where p_L and p_R are constants for which $p_L = p_R$. If all significant changes occur in the area far from both ends of the capillary, it is acceptable to formulate the boundary conditions at the ends in the form

$$\frac{\partial v_x}{\partial x}(0, r, t) = 0 , \quad v_r(0, r, t) = 0 \qquad (10)$$

$$\frac{\partial v_x}{\partial x}(L, r, t) = 0 , \quad v_r(L, r, t) = 0 \qquad (11)$$

The second and third terms in Eqs. 3 and 4 are

convective terms which bring non-linearity into the Navier–Stokes equations. The Reynolds number Re, used to assess the significance of the convective terms, is defined for the case of flow in a cylindrical tube as $Re = av_0\rho_M/\eta$, where v_0 is a characteristic velocity. The convective terms could be neglected if $Re \ll 1$. Under the conditions that are typical of EOF in CZE, $v_0 = 1$ mm s^{-1}, $a \approx 100$ μm, $\rho_M = 1000$ kg m^{-3} and $\eta = 0.001$ Pa s, so $Re \approx 0.1$. This means that the convective terms might play a certain role in the capillary flow in CZE and were taken into account by using the Navier–Stokes equations.

It is obvious that the solution of the described system of equations depends on the function $v(x)$. With time increasing, this solution converges to a time-independent solution. A numerical procedure will be used to obtain an approximation to this stationary velocity field.

2.2. Concentration distribution

Once the velocity field is known, the concentration distribution of a solute, $c(x, r, t)$, can be calculated by solving the continuity equation

$$\frac{\partial c}{\partial t} = D\left[\frac{\partial^2 c}{\partial x^2} + \frac{1}{r} \cdot \frac{\partial}{\partial r}\left(r \cdot \frac{\partial c}{\partial r}\right)\right]$$
$$- v_x \cdot \frac{\partial c}{\partial x} - v_r \cdot \frac{\partial c}{\partial r} - \text{sgn}(z)\frac{\partial(cuE)}{\partial x} \quad (12)$$

with the initial condition

$$c(x, r, 0) = c_0(x, r) \quad (13)$$

and the boundary conditions consisting of a condition on the capillary wall given by

$$\frac{\partial c}{\partial r}(x, a, t) = 0 \quad (14)$$

a geometrical condition on the capillary axis given by

$$\frac{\partial c}{\partial r}(x, 0, t) = 0 \quad (15)$$

and the following conditions in the ends of the capillary:

$$c(0, r, t) = c_L, \quad c(L, r, t) = c_R \quad (16)$$

Here, D is the diffusion coefficient, u is the

electrophoretic mobility of the solute and z is its charge number. It is seen that the continuity Eq. 12 takes several fluxes into account, namely the diffusional flux (the first term on the right-hand side), the flow in the electroosmotic velocity field (the second and third terms) and the electrophoretic flux (the fourth term). The electrophoretic flux is the movement of a solute with the velocity $v_{ep} = \text{sgn}(z)uE$ only in the axial direction due to the Coulombic force acting on possibly charged particles of the solute.

It will be assumed that

$$c_L = c_R = 0 \quad (17)$$

The initial concentration distribution described by function $c_0(x, r)$ must satisfy all boundary conditions. Since in this paper the function $c_0(x, r)$ will have the form $c_0(x)$, i.e., it does not depend on the radial variable r, we shall assume that

$$c_0(0) = c_0(L) = 0 \quad (18)$$

In problems of movement of a solute along a tube, the mean radial concentration c_m is a useful quantity:

$$c_m(x, t) = \frac{2}{a^2}\int_0^a c(x, r, t)r \, dr \quad (19)$$

The dispersion $\sigma^2(t)$ will be defined in analogy with the dispersion of c_m in the unbounded capillary by

$$\sigma^2(t) = \frac{1}{c_{tot}(t)}\int_0^L c_m(x, t)[x - \mu(t)]^2 \, dx \quad (20)$$

where $\mu(t)$, the mean x-coordinate of the solute, is

$$\mu(t) = \frac{1}{c_{tot}(t)}\int_0^L c_m(x, t)x \, dx \quad (21)$$

and

$$c_{tot}(t) = \int_0^L c_m(x, t) \, dx \quad (22)$$

The mean velocity of the convective flow in the capillary tube, v_m, is defined by

$$v_m(t) = \frac{2}{a^2} \int_0^a v_x(x, r, t) r \, dr \qquad (23)$$

This value, due to the condition of incompressibility, does not depend on the variable x. With the time increasing, $v_m(t)$ converges to a stationary value. This value will be referred to as the stationary mean velocity. In cases when both convective flow and electrophoretic flux act together, the solute moves at the velocity $v_m + v_{ep}$.

There have been several studies of the time development of a solute concentration (or, at least, dispersion of a solute) under the influence of various types of flows in tubes. A stationary velocity field with parabolic profile has been considered [18–22] and the electroosmotic velocity profile encountered in stationary EOF with zeta potential uniform along the capillary tube has been investigated [3,4,7].

Using the Stokes equations, Anderson and Idol [9] derived that the stationary mean velocity, v_m, attains the value given by

$$v_m = \frac{1}{L} \int_0^L v(x) \, dx \qquad (24)$$

For the sake of completeness, it is shown in the Appendix how Eq. 24 can be obtained through a simple computation with the Stokes equations. If the Navier–Stokes equations are used, Eq. 24 is not exactly valid. However, only a small deviation of the stationary mean velocity from the value given by Eq. 24 can be expected. This is what has been confirmed by numerical simulations.

3. Methods of solution

The Navier–Stokes Eqs. 3–5 were transformed into a system of partial differential equations for a pair of functions, ψ and ξ [23]. The stream function ψ, provides the velocity components through the equations

$$v_x = \frac{1}{r} \cdot \frac{\partial \psi}{\partial r}, \quad v_r = -\frac{1}{r} \cdot \frac{\partial \psi}{\partial x} \qquad (25)$$

The vorticity of the velocity field, ξ, is given by

$$\xi = \frac{\partial v_r}{\partial x} - \frac{\partial v_x}{\partial r} \qquad (26)$$

The functions ξ and ψ satisfy the following system:

$$\frac{\partial \xi}{\partial t} + v_x \cdot \frac{\partial \xi}{\partial x} + v_r \cdot \frac{\partial \xi}{\partial r} - \frac{v_r \xi}{r}$$
$$= \nu \left[\frac{\partial^2 \xi}{\partial x^2} + \frac{1}{r} \cdot \frac{\partial}{\partial r} \left(r \cdot \frac{\partial \xi}{\partial r} \right) - \frac{\xi}{r^2} \right] \qquad (27)$$

$$\frac{\partial^2 \psi}{\partial x^2} + r \cdot \frac{\partial}{\partial r} \left(\frac{1}{r} \cdot \frac{\partial \psi}{\partial r} \right) = -r\xi \qquad (28)$$

The conditions to which the function ξ is subject consist of an initial condition

$$\xi(x, r, 0) = 0 \qquad (29)$$

and the boundary conditions

$$\xi(x, a, t) = -\frac{\partial}{\partial r} \left(\frac{1}{r} \cdot \frac{\partial \psi}{\partial r} \right)(x, a, t) ,$$
$$\xi(x, 0, t) = 0 \qquad (30)$$

$$\frac{\partial \xi}{\partial x}(0, r, t) = 0 , \quad \frac{\partial \xi}{\partial x}(L, r, t) = 0 \qquad (31)$$

The boundary conditions for ψ are

$$\psi(x, a, t) = \chi(t) , \quad \psi(x, 0, t) = 0 \qquad (32)$$

$$\frac{\partial \psi}{\partial x}(0, r, t) = 0 , \quad \frac{\partial \psi}{\partial x}(L, r, t) = 0 \qquad (33)$$

where the function $\chi(t)$ is a function which depends on only one variable, t, and satisfies the relationship

$$L \cdot \frac{d\chi}{dt}(t) = -\nu a \int_0^L \xi(x, a, t) \, dt$$
$$- \int_0^L \int_0^a \left(v_x \cdot \frac{\partial v_x}{\partial x} + v_r \cdot \frac{\partial v_x}{\partial r} \right) r \, dr \, dx \qquad (34)$$

Finite difference methods were used to solve the Navier–Stokes equations and the parabolic equation for the concentration of a solute. With a Reynolds number of moderate value, we were able to apply all methods [17,23,24] in a straightforward and standard manner.

4. Results and discussion

The mathematical model described above enables one to calculate a velocity field and peak shapes of a solute for arbitrary axial distributions of the zeta potential. We shall discuss several instances of such forms of the zeta potential which are either instructive or closely related to situations encountered in practice. In all simulations, the liquid is meant to be water with dynamic viscosity $\eta = 0.001$ Pa s and mass density density $\rho_M = 1000$ kg m^{-3}.

4.1. Half-covered capillary column

A capillary column is considered in which the right half is covered by a deactivation layer. The consequence is that, except for a transition region around the centre of the capillary, the zeta potential is constant and equals zero in the right part of the capillary and a non-zero value in the left-hand side of the capillary.

Various widths of the transition region between the covered and uncovered parts of the capillary are modelled by taking three functions $\zeta(x)$ with various steepness in the transient region. These functions, playing the role of the input boundary conditions, are depicted in Fig. 1a as curves 1, 2 and 3. All these functions are such that the local electroosmotic velocity generated by the value of the zeta potential at the left end of the capillary is 1 mm s^{-1} and that at the right end is zero.

The corresponding stationary velocity fields obtained by solving Eqs. 3–11 for a capillary with an inner diameter of 100 μm ($a = 50 \cdot 10^{-6}$ m) are shown in Fig. 1b for all three cases of $v(x)$. In this and all analogous figures the radial size of the capillary is considerably enlarged and so the radial velocity component has also been magnified in the same ratio. The vectors of the velocity are depicted as "weathercocks" streaming in the flow. The lengths of lines attached to the depicted points are proportional to the magnitude of the velocity. It is seen that a radial component of the velocity appears mainly in the transient region. At a distance a few diameters from the transient region the radial flows are

negligible and the axial component of the velocity field has an almost parabolic profile. In the left part of the column the axial component of the velocity is maximum at the column wall and nearly zero on the axis whereas in the right part of the column the situation is the opposite, i.e. the maximum velocity is on the axis and zero at the wall.

We shall investigate the time development of a Gaussian peak of a solute with a diffusion coefficient $1 \cdot 10^{-10}$ m^2 s^{-1}, the centre of which is at a position $x = 8$ mm in the capillary tube, its initial variance is $\sigma_i^2 = 2.5 \cdot 10^{-7}$ m^2 and its concentration in the maximum is 4 mol m^{-3} (4 mM). The initial axial distribution of the solute is depicted in Fig. 1a. The initial condition, Eq. 13, is

$$c_0(x, r) = 4 \exp\left[-\frac{(x - 0.008)^2}{2 \cdot 2.5 \cdot 10^{-7}} \right] \qquad (35)$$

In fact, this function satisfies the boundary conditions given by Eqs. 18 only approximately, but the small difference can be neglected. It will be assumed for simplicity that the solute has no electric charge, i.e., $u = 0$ and consequently $v_{ep} = 0$ in this case.

Numerically solving Eqs. 12–18 gives the concentration distribution $c(x, r, t)$. The mean velocity v_m calculated with the aid of Eq. 24 is 0.5 mm s^{-1}, whereas v_m obtained from the movement of the simulated peak of the solute is about 0.49 mm s^{-1} for all three cases. This indicates a slight influence of convective terms in the Navier–Stokes equations.

The time-dependent variance of the solute calculated by Eq. 20 is depicted in Fig. 1c for all three cases of v. The mean velocity v_m is almost the same in all three cases but the corresponding dispersion of a passing solute peak depends considerably on the course of the function v. The less steep the function $v(x)$ in the transient region, the smaller is the resulting value of the solute variance. In the situation described, the main cause of the peak dispersion is due to the parabolic profile of the axial velocity component, which dominates over the radial component. In accordance with Chien and Helmer's considera-

Fig. 1. Simulation of the stationary velocity field in a half-covered capillary column. Diffusion coefficient D, $1 \cdot 10^{-10}$ m^2 s^{-1}; radius of column a, $50 \cdot 10^{-6}$ m; length of column L, 0.05 m; electrophoretic velocity v_{ep}, 0. c_0 = Initial condition, Eq. 35. 1–3 = Three different cases corresponding to three profiles of the electroosmotic velocity $v(x)$ at the column wall. Dashed line = time-dependent variance of convective diffusion in a laminar parabolic flow with the velocity of 0.5 mm s^{-1}. (a) Initial condition and boundary conditions; (b) velocity fields; (c) and (d) simulated time-dependent variance.

tions [10], it is the difference between the "local" and mean velocity which contributes mainly to the peak broadening. The term "local" velocity means the velocity v at the site of the peak, but it should be realized that the peak has a certain axial width, so there is no uniqueness in the determination of the local velocity.

In the parts of the column outside the transient region, the difference between the velocity v and the mean velocity given by Eq. 24 is $v_{\text{dif}} = \pm 0.5$ mm s^{-1}. For comparison, a dashed line with the slope $v_{\text{dif}}^2 a^2 / 24D$ is drawn in Fig. 1c and d, which corresponds to a laminar parabolic flow with a velocity of 0.5 mm s^{-1}.

Additionally, it is worth noting that the simulated curves start with almost zero slope at time $t = 0$, but after a few seconds the slope stabilizes to a value which is near to that predicted by

$v_{\mathrm{dif}}^2 a^2 / 24D$. The part of Fig. 1c around $t = 0$ is enlarged and shown in Fig. 1d. This result can be viewed in the context of the conclusions in the paper by Gill and Sankarasubramanian [22]. For the case of unsteady convective diffusion in the laminar flow, they calculated that the slope of variance stabilizes at time $t \approx 0.2 a^2 / D$. In our case this value is 5 s, which corresponds well with the simulated case.

A solute peak exhibits interesting changes in its radial and axial profiles when passing through the transient region. These changes are especially profound when, roughly, the velocity of the axial movement of the solute is comparable to the speed of the radial diffusion flux. In typical CZE conditions this can happen in rather thick columns or in the case of a low diffusion coefficient of the solute. Fig. 2a shows both the axial and radial profiles of an analyte with diffusion coefficient $5 \cdot 10^{-11}$ m^2 s^{-1} (this would correspond, e.g., to the diffusion coefficient of conalbumin) in a column of 150 μm I.D. passing through the transient region depicted as curve 1 in Fig. 1a. The curves in Fig. 2a come from the solutions to the Eqs. 12–18. The mean radial concentration profile c_{m} at various times is given by the thick line. In Fig. 2b a time record is depicted which would be recorded by a detector located at a position just behind the transient region. In spite of peculiar changes in the axial and radical peak profiles, the time record is only a simple tailing profile.

4.2. Partly-covered capillary column

In this example, a segment of the capillary column a part of which, say one third or two thirds is covered by a layer hindering the formation of a non-zero zeta potential. Fig. 3a illustrates the corresponding functions $v(x)$, i.e., the distribution of the electroosmotic velocity along the column. Although this case is a slight generalization of the previous half-and-half case, the flow pattern of the velocity field is different because significant vortices in the flow may appear. Fig. 3b shows a plot of the calculated velocity fields in both cases. The "weathercocks" directing to the left indicate the appearance of

vortices. Nevertheless, it should be realized that the mean flow of the liquid directs to the right in both cases with a mean velocity of about 1/3 or 2/3 mm s^{-1}, respectively.

4.3. Partly uncovered capillary column at the detector position

Capillary columns with an inner coating suppressing the EOF are often used. The columns are also always coated from the outer side by a polymer coating. As the outer polymer coating is UV absorbing, it is necessary to remove it at the site of the UV absorption detector. This is often done by means of a flame which burns off the polymer coating in the region of the capillary where the detector will be located. However, the inner coating will also be destroyed by this procedure. Such a situation can cause severe problems from the point of dispersion of the passing solute due to the EOF occurring in the uncovered region. This situation is stimulated in a 5-cm segment of a covered capillary column, 1 cm of which is uncovered. The detector is situated in the middle of the uncovered part. Fig. 4a shows the function $v(x)$ and Fig. 4b the calculated velocity field in the capillary of 100 μm I.D. The closed vortices in the velocity field are evident.

An initial Gaussian peak of a solute with a diffusion coefficient of $2 \cdot 10^{-10}$ m^2 s^{-1} will be assumed to move in the column. The centre of its initial position will again be at $x = 8$ mm and its initial variance will be $\sigma_i = 2.5 \cdot 10^{-7}$ m^2. The mean velocity v_{m} of the flow in the capillary according to Eq. 24 is 0.2 mm s^{-1}. Now it is assumed that the solute has an electric charge causing its migration in the electric field with an electrophoretic velocity $v_{\mathrm{ep}} = 0.5$ mm s^{-1}. The total velocity of the movement of the solute in the column will therefore be $v_{\mathrm{m}} + v_{\mathrm{ep}} = 0.7$ mm s^{-1}. Fig. 4c shows a plot of σ^2 against time. There is apparently a significant total increase in the solute dispersion while the peak is passing through the uncovered region of the capillary. However, rather than knowing the dispersion changing with time, one may be interested in the
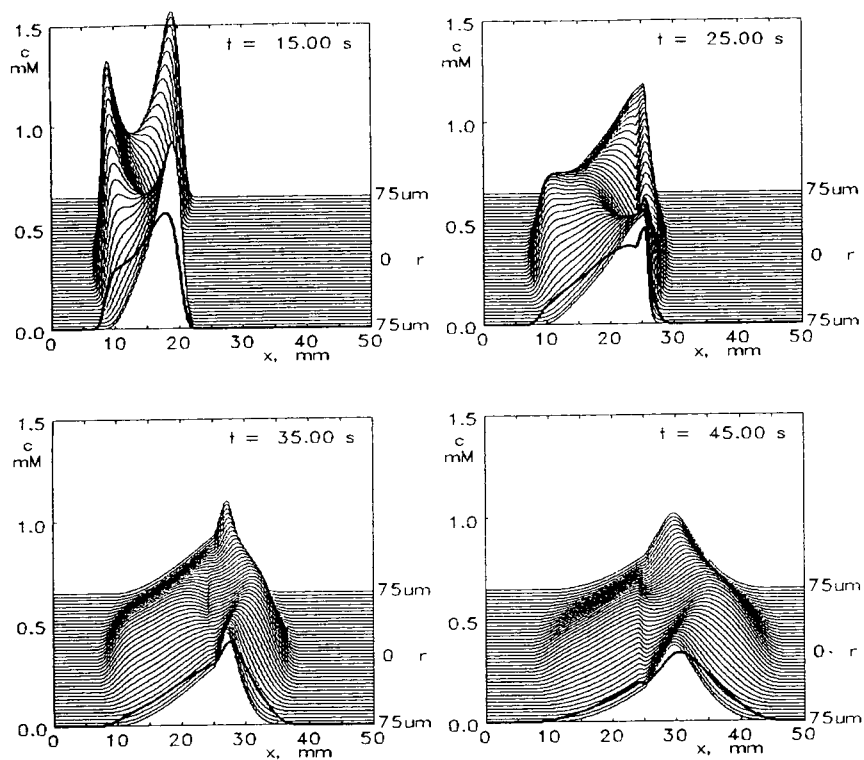
(a)
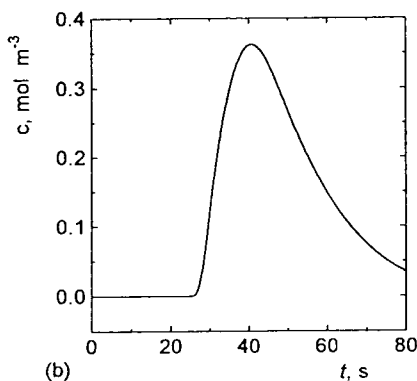
(b)

Fig. 2. Simulation of the peak profiles at various times t in a half-covered capillary column. Diffusion coefficient D, $5 \cdot 10^{-11}$ m^2 s^{-1}; radius of column a, $75 \cdot 10^{-6}$ m; length of column L, 0.05 m; electrophoretic velocity v_{ep}, 0. Thick line = mean axial concentration, c_m. (a) Axial and radial profiles of the peak; (b) time record of a detector located at $x = 0.03$ m.

signal of a detector at a given position. Hence, in Fig. 4d a time record of the mean concentration of the solute is presented for a time range large enough to enable the peak to pass the detector.

The graph exhibits an asymmetric shape due to severe dispersion during its passage through the detector.

Finally, it should be realized that the widths of

(a)

(b)
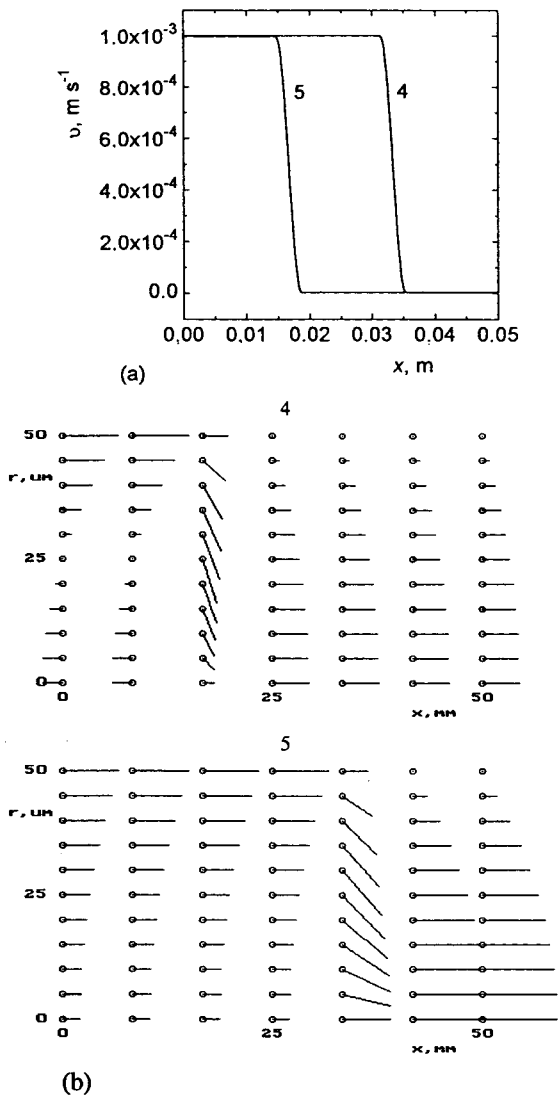
Fig. 3. Simulation of the stationary velocity field in a partly covered capillary column. Radius of column a, $50 \cdot 10^{-6}$ m; length of column L, 0.05 m; 4 and 5 = two different cases corresponding to two profiles of the electroosmotic velocity $v(x)$ at the column wall. (a) Boundary conditions; (b) velocity fields.

peaks in CZE are mostly much greater than the radius of the columns and, in the considered cases of a non-uniformly distributed zeta po-

tential, the radial profile of the axial velocity is approximately parabolic. This brings the main contribution to the overall peak shape and its dispersion and, consequently, the well established theory of convective diffusion in laminar flow can be employed with good precision.

The contribution of the radial flow in transient regions and the convective terms are comparatively less significant. Nevertheless, many more extreme situations can be found where the use of the present model will be necessary.

5. Appendix

Here we derive Eq. 24, as we believe, in a simpler and more straightforward manner than in Ref. [9]. If non-linear terms in the Navier–Stokes equations are left out, the Stokes equations are obtained. Hence, by Eq. 3 the equation for the component v_x of the stationary solution $\vec{v}(x, r)$ of the Stokes equations is

$$0 = \nu \cdot \frac{\partial^2 v_x}{\partial x^2} + \nu \cdot \frac{1}{r} \cdot \frac{\partial}{\partial r}\left(r \cdot \frac{\partial v_x}{\partial r}\right) - \frac{1}{\rho} \cdot \frac{\partial p}{\partial x}$$

This equation is multiplied by r and integrated over any domain $x \in \langle 0, L \rangle$, $r \in \langle 0, \sigma \rangle$, $\sigma \in (0, a)$. By applying integration by parts and taking the boundary conditions into account, the first and third terms on the right-hand side are shown to be zero. Hence the relationship reduces to

$$\int_0^L \int_0^\sigma \frac{\partial}{\partial r}\left(r \cdot \frac{\partial v_x}{\partial r}\right) dr \, dx = 0$$

This provides

$$\sigma \int_0^L \frac{\partial v_x}{\partial r}(x, \sigma) \, dx = 0$$

from which it is obtained immediately that the function $r \rightarrow \int_0^L v_x(x, r) \, dx$ is constant in the interval $\langle 0, a \rangle$. Hence, according to the boundary condition Eq. 2, for every $r \in (0, a)$ it holds that

$$\int_0^L v_x(x, r) \, dx = \int_0^L v(x) \, dx$$

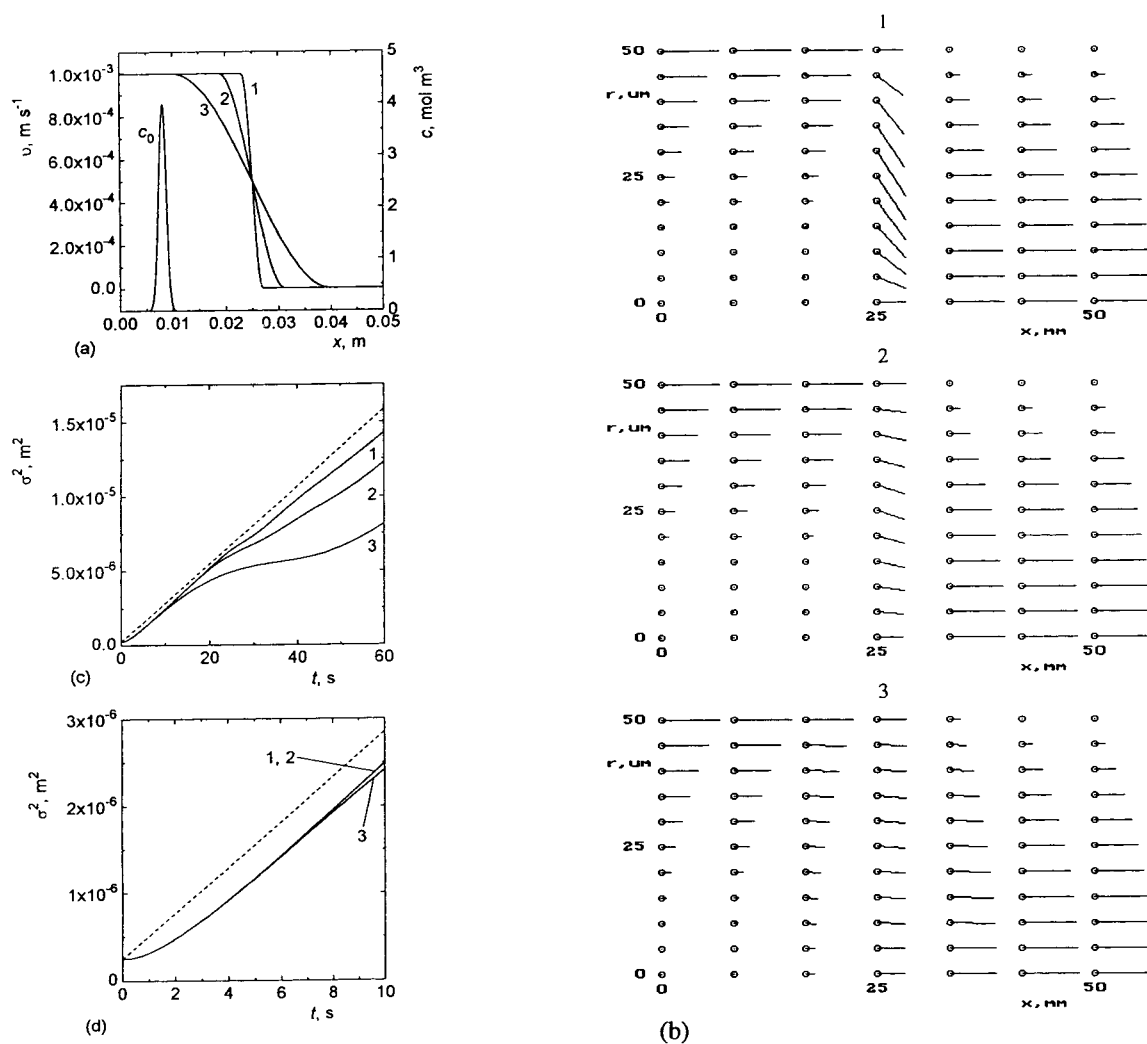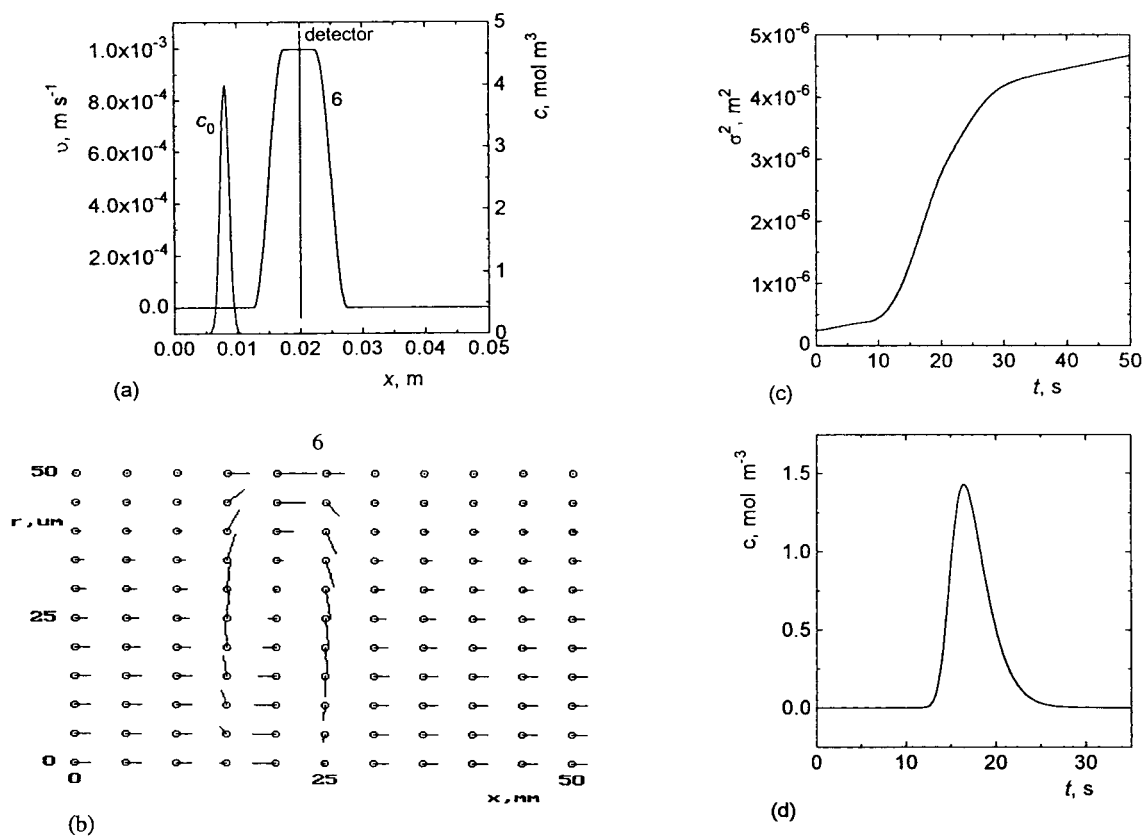Fig. 4. Simulation of the stationary velocity field in a partly uncovered capillary column. Diffusion coefficient D, $2 \cdot 10^{-10}$ m^2 s^{-1}; radius of column a, $50 \cdot 10^{-6}$ m; length of column L, 0.05 m; electrophoretic velocity v_{ep}, 0.5 mm s^{-1}. c_0 = Initial condition, Eq. 35. 6 = Profile of the electroosmotic velocity $v(x)$ at the column wall. (a) Initial condition and boundary conditions; (b) velocity field; (c) simulated time-dependent variance; (d) time record of a detector located at $x = 0.02$ m.

From Eq. 5, it follows that the function $x \to \int_0^a v_x(x, r)r \, dr$ is constant on $(0, L)$. Hence,

$$
\begin{aligned}
v_m &= \frac{2}{a^2} \int_0^a v_x(x, r)r \, dr \\
&= \frac{2}{La^2} \int_0^L \int_0^a v_x(x, r)r \, dr \, dx \\
&= \frac{2}{La^2} \int_0^L v(x) \, dx \int_0^a r \, dr \\
&= \frac{1}{L} \int_0^L v(x) \, dx
\end{aligned}
$$

The first and last terms form Eq. 24.

Acknowledgement

References

[1] R.S. Berry, J.A. Rice and J. Rosse, Physical Chemistry, Wiley, New York, 1979.
[2] C.L. Rice and R.J. Whitehead, Phys. Chem., 69 (1965) 4017.
[3] M. Martin and G. Guiochon, Anal. Chem., 56 (1984) 614.

[4] M. Martin, G. Guiochon, Y. Walbroehl and J.V. Jorgenson, Anal. Chem., 57 (1985) 559.

[5] V.P. Andreev and E.E. Lisin, Electrophoresis, 13 (1992) 832.

[6] K.P. Tikhomolova, Electroosmosis, Ellis Horwood, New York, 1993.

[7] B. Gaš, M. Štědrý and E. Kenndler, J. Chromatogr., 709 (1995) 63.

[8] P. Chowdiah, D.T. Wasan and D. Didaspow, AICHE J., 27 (1981) 975.

[9] J.L. Anderson and W.K. Idol, Chem. Eng. Commun., 38 (1985) 93.

[10] R.L. Chien and J.C. Helmer, Anal. Chem., 63 (1991) 1354.

[11] J.T. Towns and F.E. Regnier, Anal. Chem., 64 (1992) 2473.

[12] C.L. Lee, W.C. Blanchard and C.T. Wu, Anal. Chem., 62 (1990) 1550.

[13] K. Ghowsi and R.J. Gale, J. Chromatogr., 559 (1991) 95.

[14] C.T. Wu, T.L. Huang, C.S. Lee and C.J. Miller, Anal. Chem., 65 (1993) 568.

[15] M.A. Hayes, I. Kheterpal and A.G. Ewing, Anal. Chem., 65 (1993) 2010.

[16] E.V. Dose and G.J. Guiochon, J. Chromatogr., 625 (1993) 263.

[17] T.J. Mueller, in H.J. Wirz and J.J. Smolderen (Editors), Numerical Methods in Fluid Dynamics, Hemisphere, 1978, Ch. 2.

[18] G. Taylor, Proc. R. Soc. London, Ser. A, 219 (1953) 186.

[19] G. Taylor, Proc. R. Soc. London, Ser. A, 225 (1954) 473.

[20] R. Aris, Proc. R. Soc. London, Ser. A, 235 (1956) 67.

[21] W.N. Gill, Proc. R. Soc. London, Ser. A, 298 (1967) 335.

[22] W.N. Gill and S. Sankarasubramanian, Proc. R. Soc. London, Ser. A, 316 (1970) 341.

[23] P.J. Roache, Computational Fluid Dynamics, Hermosa, Albuquerque, 1976.

[24] R. Peyret and T.D. Taylor, Computational Methods for Fluid Flow, Springer, New York, 1983.

Contribution of the electroosmotic flow to peak broadening in capillary zone electrophoresis with uniform zeta potential

Bohuslav Gaš[a,*], Milan Štědrý[a], Ernst Kenndler[b]

[a]*Faculty of Science, Charles University, Albertov 2030, CZ-128 40 Prague 2, Czech Republic*
[b]*University of Vienna, Institute of Analytical Chemistry, Währinger Strasse 38, A-1090 Vienna, Austria*

Abstract

An expression is derived which gives the plate height contribution caused by an electroosmotic flow (EOF) in a cylindrical capillary with longitudinally uniform zeta potential. The derivation is made in terms of effective thickness of the electric double layer (an analogue to the Debye length). Typical values of the effective thickness calculated for common situations are given. The resulting expression for the plate height, $H_{eo} = \beta^2 v_{eo}/D$, enables one to calculate the plate height simply as a function of the diffusion coefficient, D, of the solute, the electroosmotic velocity, v_{eo}, and the thickness of the electric double layer, β. The impact of peak broadening by the EOF is compared with that from longitudinal diffusion and extra-column effects for solutes with widely varying diffusion coefficients.

1. Introduction

On the border between a liquid and a solid phase, the intensity of the electric field is not necessarily zero owing to the presence of an electric double layer. The structure of this double-layer is described by various models, of which the Stern–Gouy–Chapman model [1] is generally accepted. According to this model, it consists of a compact or Stern layer that adheres on the solid surface and the diffuse layer in the liquid, where the volume charge density is significantly greater than in the rest of liquid. For an aqueous solution of small ions in contact with, e.g., fused silica, glass or even an organic polymer such as PTFE, the Stern layer mostly possesses an excess

of negative charge. This is a result of adsorption of negative ionic species and/or protolysis of dissociable groups on the surface.

The excess of negative charge on the surface must be compensated for by an excess of positive ions in the diffuse layer. Consequently, the electroneutrality condition in the diffuse layer is no longer valid.

The plane formed by the centres of the ions from the diffuse layer, which are in closest proximity to the compact layer, is named the outer Helmholtz plane. The diffuse layer in principle ranges from the outer Helmholtz plane to infinite distance and it is of primary importance for electrokinetic effects. The excess of net charge in the diffuse layer is responsible for the electroosmotic flow (EOF) that can occur in electrophoretic separation columns. In this case, the longitudinal driving electric field acting in the

---

* Corresponding author.

direction of the column axis generates the driving electroosmotic force in the diffuse layer. The net charge in the layer, however, drops to zero very quickly when the distance from the wall exceeds several nanometers under circumstances usual in capillary zone electrophoresis (CZE).

The potential profile in the diffuse layer for a double layer with planar geometry can be attained by solving the Poisson–Boltzmann equation [2,3]. Rice and Whitehead [4] calculated stationary velocity profiles of the EOF in cylindrical capillaries employing a linear approximation of the exponential terms in the Poisson–Boltzmann equation. They pointed out, however, that this approximation fails when the potential in the diffuse layer becomes higher than ca. 50 mV.

Martin and co-workers [5,6] determined the contribution of the radial electroosmotic velocity profile in a capillary tube to the sample peak dispersion. They approximated the original velocity profile either by a power function or by a partly flat and a partly quadratic profile. It should be noted that they also employed the linear approximation of the Poisson–Boltzmann equation [5,6].

Andreev and Lisin [7] made a detailed study of potential and velocity radial profiles in a capillary tube numerically without any linearization. The temperature effects acting significantly in CZE were also taken into account.

It is the main aim of this paper to give a derivation of the contribution of the EOF to the peak dispersion in open CZE columns assuming a longitudinally uniform driving electroosmotic force along the capillary column. This is assessed in terms of the fraction of the solute in the diffuse layer which lags behind the travelling peak. The profiles of the electric potential in the diffuse layer are calculated for cylindrical symmetry based on the Poisson–Boltzmann equation without any approximation in accordance with Andreev and Lisin [7]. This approach is not limited to either the magnitude of the potential or any linearization. This approach enables us to express the peak dispersion contribution of the EOF by a simple closed equation.

2. Assumptions of the model

An open cylindrical capillary tube of radius a with homogeneous properties across the length is assumed to be filled with a homogeneous liquid solution of a background electrolyte consisting of n species of ions, the ith of which has a concentration c_i^0 and charge number z_i. As a consequence of the longitudinal homogeneity, the properties of the electric double layer are also homogeneous across the length. Further, the setting of the problem exhibits cylindrical symmetry. As the studied process is homogeneous with respect to the coordinate which can be identified with the axis of the capillary, there is only one spatial coordinate, the radial coordinate r, on which all quantities depend. If the net charge density at a distance r from the axis of the capillary is denoted by $\rho(r)$, the outer driving electric field of constant strength E exerts a driving force $E\rho(r)$ on a unit volume of the electrolyte.

The radial distribution of the electric potential ϕ is given by the Poisson–Boltzmann equation in the cylindrically symmetrical setting

$$\frac{1}{r} \cdot \frac{d}{dr}\left(r \cdot \frac{d\phi}{dr}(r)\right)$$
$$= -\frac{1}{\varepsilon} \sum_{i=1}^{n} c_i^0 z_i F \exp\left[-\frac{z_i F \phi(r)}{RT}\right] \qquad (1)$$

where ε is the permitivity of the electrolyte solution, R is the gas constant, T is the absolute temperature and F is the Faraday constant. With the two boundary conditions

$$\frac{d\phi}{dr}(0) = 0, \quad \phi(a) = \zeta \qquad (2)$$

Eq. 1 determines the potential ϕ on $r \in \langle 0, a \rangle$. The value of the potential ϕ on the outer Helmholtz plane, for simplicity identified here with the wall of the capillary, is denoted by ζ and is called the electrokinetic or zeta potential.

Only the axial component, v_x, of the velocity of the EOF depends on the r coordinate, i.e., $v_x = v_x(r)$. It can be derived that the stationary radial velocity profile of v_x is

$$v_x(r) = \frac{\varepsilon E}{\eta} [\phi(r) - \zeta] \tag{3}$$

where η is the dynamic viscosity of the liquid. Since $\phi(0)$ is nearly zero in electrophoretic columns with diameters above 10 μm, the stationary velocity of the flow at the centre of the capillary is

$$v_x(0) \equiv v_{eo} = -\varepsilon E \zeta / \eta \tag{4}$$

This is identical with the well known Helmholtz–Smoluchowski relationship.

3. Derivation and discussion

3.1. Effective thickness of the electric double layer

The total axial flux J_x of an analyte with concentration c_a moving in a capillary tube is given by

$$J_x = c_a 2\pi \int_0^a r v_x(r) \, dr \tag{5}$$

In the derivation of the lagged part, it is assumed that the same flux J_x is transported by the velocity v_{eo} but in a cylinder with radius $a - \beta$, so

$$J_x = c_a \pi (a - \beta)^2 v_{eo} \tag{6}$$

where β is the effective thickness of the diffuse layer and can be interpreted as the thickness of the cylindric sheath of liquid sticking on the column wall without being moved. Equating Eqs. 5 and 6, β is then

$$\beta = a - \sqrt{\frac{2}{v_{eo}} \int_0^a r v_x(r) \, dr} \tag{7}$$

The effective thickness β is an analogue of the Debye length (or thickness) κ^{-1}, which is the effective thickness of the ionic atmosphere but obtained from the linearized Poisson–Boltzmann equation and is defined for, e.g., uni–univalent electrolytes as

$$\kappa^{-1} = \frac{1}{F} \sqrt{\frac{\varepsilon RT}{2c}} \tag{8}$$

For the calculation of β, the following two steps are to be followed:

(i) Calculation of the potential $\phi(r)$ by solving the differential Eqs. 1 and 2. The equations were solved numerically by the Hamming predictor–corrector method [8] after substituting $d\phi/dr$. This enables one to solve the set of two differential equations of the first order. Integration starts from the point $r = a$ with $\phi(a) = \zeta$. The boundary condition in $r = 0$, $d\phi/dr(0) = 0$, is attained by iterative shooting.

(ii) Determining β by numerical integration of Eq. 7 using Eq. 3. The numerical integration was performed using the Simpson formula.

Table 1 shows the effective thickness β calculated for various ζ potentials (or corresponding electroosmotic mobilities u_{eo}, defined as $u_{eo} = v_{eo}/E$) and various concentrations c^0 of an aqueous solution of a uni–univalent electrolyte ($i = 1, 2$; $c_1^0 = c_2^0 \equiv c^0$; $z_1 = 1$; $z_2 = -1$) acting as the background electrolyte. For comparison, the corresponding Debye lengths are also given in Table 1. The difference between β and κ^{-1} is caused by linearization of the exponential terms when deriving the Debye length κ^{-1}. Although the linearization may be well founded in deriving the ionic atmosphere of a single ion [9], it fails in the case of an electric double layer when the zeta potential exceeds about 50 mV [4] (see also Table 1), which corresponds to an electroosmotic mobility of about $35 \cdot 10^{-9}$ m^2 V^{-1} s^{-1}. However, such a situation is commonly reached in CZE when using untreated silica capillaries. It can be seen that the deviation is significant for high zeta potentials where β is found to be nearly a factor of two smaller than κ^{-1}.

3.2. Peak dispersion due to longitudinally uniform EOF

The total peak dispersion is the result of the individual contributions. For a linear case the

Table 1
Dependence of the effective thickness β on concentration of a uni–univalent electrolyte and zeta potential ζ

ζ (V)	u_{eo} (10^{-8} m^2 V^{-1} s^{-1})	Concentration c^0 (mmol l^{-1})				
		0.01	0.1	1	10	100
		β (nm)				
0.02	1.38	95.1	30.1	9.51	3.01	0.951
0.05	3.45	91.1	28.8	9.11	2.88	0.911
0.1	6.91	79.8	25.2	7.98	2.52	0.798
0.2	13.81	55.8	17.7	5.58	1.77	0.558
		κ^{-1} (nm)				
		95.9	30.3	9.59	3.03	0.959

u_{eo} = Electroosmotic mobility; κ^{-1} = Debye length.

final variance of the peak is the sum of the individual peak variances. In the case of EOF the lagging sheath of liquid in the diffuse layer near the column wall causes a radial diffusion flux of the lagged part of the analyte from the wall to the centre. Consequently, the axial profile of the sample moving in a capillary column will be dispersed. This will be the contribution of the uniform EOF to the total peak dispersion.

From the effective thickness β, the fraction F of liquid sticking on the column wall and virtually not moving can be found. Assuming $\beta \ll a$ in common electrophoretic columns, this fraction is given by

$$F = \frac{2\pi a \beta}{\pi a^2} = \frac{2\beta}{a} \qquad (9)$$

Knowing the fraction F, an approximate derivation of the influence of the radial velocity profile $v_x(r)$ on peak dispersion in CZE can be performed. Aris [10] and Giddings [11] derived that the variance σ^2 of a solute peak caused by a non-movable fraction F at the capillary wall but undergoing radial diffusional transport in the case of plug-like flow with velocity $\bar{v}$ is

$$\sigma^2 = \frac{F^2(1-F)a^2}{4D} \cdot \bar{v}^2 t \qquad (10)$$

where D is the diffusion coefficient of the ana-

lyte. This model can be adopted for derivation of the peak dispersion due to a uniform EOF when assuming that $\beta \ll a$. In the case under discussion, the fraction F is very small compared with 1 and the assumptions that $\bar{v} \approx v_{eo}$ and $1 - F \approx 1$ are acceptable. Eq. 10 can further be simplified by substituting F and introducing β, leading to

$$\sigma_{eo}^2 = \frac{\beta^2}{D} \cdot v_{eo}^2 t \qquad (11)$$

where σ_{eo}^2 is the variance caused by the uniform EOF. Transformation of this expression using the relationship between the length-based variance and the theoretical plate height H_{eo} leads to the simple equation

$$H_{eo} = \frac{\beta^2}{D} \cdot v_{eo} \qquad (12)$$

This expression enables one to determine easily the dispersion caused by the EOF for a given electroosmotic velocity. Naturally, the validity of Eq. 12 is restricted to cases where the dimension of molecules or particles of the analyte is considerably smaller than the effective thickness β.

It should be realized that the described derivation is in fact a simplification of the approach introduced by Martin and co-workers [5,6] for conditions that are typical in CZE. Further, it is worth noting that the plate height is not depen-

dent on the radius of the column, at least if $\beta \ll a$.

It is useful to compare the contribution of the uniform EOF to the plate height with that originating from the inevitable longitudinal diffusion, H_{dif}, which is expressed by $H_{dif} = 2D/v_{eo}$. The relationship between these two contributions can clearly be seen from the ratio H_{eo}/H_{dif}, which reflects the impact of the EOF on the efficiency relative to diffusion and is expressed by

$$\frac{H_{eo}}{H_{dif}} = \frac{\beta^2 v_{eo}^2}{2D^2} \qquad (13)$$

For given experimental conditions, this ratio depends strongly on the nature of the solute because the diffusion coefficient of the particular compound is squared in the denominator. In Fig. 1, the ratio H_{eo}/H_{dif} is depicted as a function of the diffusion coefficient for various velocities. For the usual conditions, e.g., a concentration of

0.01 mol l^{-1} of a uni–univalent background electrolyte (β is about 3 nm, see Table 1), the effect of peak broadening due to the EOF is in fact negligible for small solutes for all realistic velocities. It increases with decreasing diffusion coefficient (and increasing mass). For a velocity of 1–2 mm s^{-1} (which is common in CZE) it reaches the same value as the longitudinal diffusional dispersion for compounds with a diffusion coefficient in the range $2 \cdot 10^{-12}$–$5 \cdot 10^{-12}$ m^2 s^{-1}; here the ratio is unity.

It is obvious that even under these conditions both diffusional and electroosmotic contributions will probably not play a significant role in peak broadening because other effects not taken into account here, such as extra-column or adsorption effects, will dominate. Therefore, not only the relationship between diffusional and electroosmotic dispersion must be considered, but also the magnitude of the individual peak broadening contributions. For the above-mentioned usual conditions in CZE (background concentration 0.01 mol l^{-1}, $\beta \approx 3$ nm, electroosmotic velocity 1–2 mm s^{-1}), the contribution of the EOF will be negligible for almost all solutes.

The situation can change when the concentration of the background electrolyte is decreased. Some examples of these contributions are given in Table 2 for a concentration of 1 mmol l^{-1} and not too large ζ potentials ($\beta \approx 10$ nm) for six compounds with various diffusion coefficients. For a small molecule such as an aromatic acid, H_{dif} is about 10^{-6} m, in contrast to the minute value of $6 \cdot 10^{-11}$ m for H_{eo}. For large solutes, however, both plate height contributions are in the same range of 10^{-8}–10^{-7} m.

Such a plate eight may be of the same order of magnitude as that caused by extra-column peak broadening, e.g., due to the finite length of the injection zone. Taking a length of 1 mm in a capillary with a 250-mm distance between the injector and detector, the corresponding contribution of the initial sample plug length to peak broadening (expressed again by the plate height) is $3.3 \cdot 10^{-7}$ m.

For lower concentrations of the background electrolyte, e.g. 10^{-4} mol l^{-1} (leading to $\beta \approx 25$ nm), the electroosmotic dispersion might in fact

Fig. 1. Contribution of the EOF to the plate height, H_{eo}, related to that caused by longitudinal diffusion, H_{dif}, as a function of the diffusion coefficient, D, of the solute. Curves for electroosmotic velocities of 1, 2.5 and 5 mm s^{-1} are shown. The effective thickness, β, is 3 nm, which corresponds to a concentration of the background electrolyte of about 10 mmol l^{-1}.

Table 2
Contributions of EOF and longitudinal diffusion to peak broadening for five compounds with different diffusion coefficients

Compound	Molecular mass[a]	Diffusion coefficient $(m^2 s^{-1})$[a]	H_{eo} (m)	H_{dif} (m)
Naphthalenesulphonic acid	200	$5 \cdot 10^{-9}$	$6 \cdot 10^{-11}$	$3.3 \cdot 10^{-6}$
Myoglobin	18 000	$1 \cdot 10^{-10}$	$3 \cdot 10^{-9}$	$6.6 \cdot 10^{-8}$
Albumin	69 000	$6 \cdot 10^{-11}$	$5 \cdot 10^{-9}$	$4 \cdot 10^{-8}$
Glutamate dehydrogenase	313 000	$4 \cdot 10^{-11}$	$7.5 \cdot 10^{-9}$	$2.7 \cdot 10^{-8}$
α_2-Macroglobulin	820 000	$2.4 \cdot 10^{-11}$	$1.3 \cdot 10^{-8}$	$1.6 \cdot 10^{-8}$

Conditions: electroosmotic velocity $v_{eo} = 3$ mm s^{-1}; concentration of the background electrolyte $c^0 = 1$ mmol l^{-1} ($\beta = 10$ nm).
[a] Molecular masses and diffusion coefficients of proteins were taken from Ref. [12].

dominate both of the other effects (diffusion and extra-column) for large solutes.

Hence one can conclude that a significant contribution to peak dispersion due to the EOF can arise in such rare, but not unrealistic, cases.

Acknowledgement

References

[1] P. Delahay, Double Layer and Electrode Kinetics, Interscience, New York, 1965.
[2] W.J. Moore, Physical Chemistry, Prentice-Hall, Englewood Cliffs, NJ, 1972.
[3] O.F. Devereux and P.L. De Bruyn, Interaction of Plane Parallel Double Layers, MIT Press, Cambridge, MA, 1963.
[4] C.L. Rice and R. Whitehead, J. Phys. Chem., 69 (1965) 4017–4024.
[5] M. Martin and G. Guiochon, Anal. Chem., 56 (1984) 614–620.
[6] M. Martin, G. Guiochon, Y. Walbroehl and J.V. Jorgenson, Anal. Chem., 57 (1985) 559–561.
[7] V.P. Andreev and E.E. Lisin, Electrophoresis, 13 (1992) 832–837.
[8] A. Ralston, A First Course in Numerical Methods, McGraw-Hill, New York, 1965.
[9] J.C. Poirier, in B.G. Conway and R.G. Barradas (Editors), Chemical Physics of Ionic Solutions, Wiley, New York, 1934.
[10] R. Aris, Proc. R. Soc. London, Ser. A, 252 (1959) 538.
[11] J.C. Giddings, Dynamics of Chromatography, Marcel Dekker, New York, 1965.
[12] H. Ch. Curtius and M. Roth (Editors), Clinical Biochemistry, Principles and Methods, Vol. I, Walter de Gruyter, Berlin, 1974.

ELSEVIER

Galvanic decoupling of a postcolumn amperometric detector in capillary electrophoresis

D. Kaniansky*, P. Havaši, F. Iványi, J. Marák

*Department of Analytical Chemistry, Faculty of Natural Sciences, Comenius University, Mlynská Dolina CH-2,
842 15 Bratislava, Slovak Republic*

Abstract

A postcolumn amperometric detector for capillary electrophoresis techniques with galvanic decoupling of the detection electrodes and the detection circuit from the power unit of the detector (via a laboratory constructed d.c.–d.c. converter) and from the recording devices (via an opto-coupling device) was developed. The high insulating resistance achieved in this way (ca. 10^{11}–10^{12} Ω) reduced leak currents from the electrophoretic equipment through the detector to the low pA level. It was also effective in eliminating problems due to changes in the potential at the column outlet as found when current detection devices were used. The decoupling protected the detector in situations when the column outlet was at a potential of 4–5 kV. The detector was tested by isotachophoretic experiments carried out in a hydrodynamically closed separation compartment. Dispersions of the analyte zones in the detector were reduced about tenfold in comparison with a previous design of the detector. Experiments with a urine sample, however, revealed that the resolving power of the detector is limited in the isotachophoretic separations of complex mixtures of electrochemically active constituents. The use of a copper electrode was tested in the separation of triethylenetetramine and impurities present in its technical-grade preparation. This detection approach was shown to provide a high sensitivity for this amine and for impurities forming strong complexes with Cu(II) cations.

1. Introduction

Electrochemical methods combined with high-efficiency separation techniques offer remarkable selectivities and sensitivities for electrochemically active analytes (for a review see, e.g., Refs. [1–6]). Many of these analytes can be advantageously separated by capillary electrophoresis (CE), and capillary zone electrophoresis (CZE), capillary isotachophoresis (ITP) and micellar electrokinetic chromatography (MEKC) are CE techniques that can be mentioned in this respect. Since the first paper dealing with amperometric

detection in CE appeared [7] increasing interest in this subject has been apparent [8–29].

In coupling amperometric detection with CE, three main problems were recognized [7]: (1) bipolar behaviour of the materials of which the working electrodes are made in the driving electric field accompanied by electrochemical phenomena as found in research on conductivity detection in ITP (Ref. [30], p. 176); (2) leaks of the driving current through the detection electrodes to the ground of the amperometric detector; and (3) transport of the separated constituents into the detection cell to achieve favourable hydrodynamic conditions for detection.

* Corresponding author.

The solution to the last of these problems is closely related to the concept of the separation compartment. While a hydrodynamically closed separation compartment requires the use of a suitable pump (see [7] and below), hydrodynamically opened separation systems use electroosmotically generated flow [14,17,18,20,22–24,26] or laminar flow induced by the electroosmotic pumping [8–13,15–17,19,21,25,27,28].

Leaks of the driving current through the detection cell are minimized by separating the detection cell from the end of the column by a capillary tube (detection capillary) filled with the electrolyte solution while the end of the column is coupled to the earth potential of the high-voltage power supply. Various types of the coupling devices have been proposed for this purpose [7,8,16,21,25]. These precautions need not be used for columns of 25 μm I.D. or less [28] working with low driving currents.

From the descriptions of the amperometric detectors used in CE [7–29], it is apparent that current electroanalytical measuring systems are preferred. These measuring systems were not designed for amperometric measurements under the conditions typical for electrophoretic separations. Therefore, their insulating resistances may not be sufficient to eliminate leak currents through the detection cell, e.g., when the working electrode is placed in the electrophoresis column or very close to the column outlet [29] or when the potential at the column outlet changes [7]. The column outlet can acquire a very high potential, e.g., when a bubble is formed at the end of the column. Although such a situation rarely occurs when the CE equipment is handled properly, a high potential on the input of the measuring system can cause damage to the detector when it is not designed with these facts in mind.

Recently, electrochemical phenomena occurring at the working electrode inserted into the solution in the column through which the driving current was flowing were demonstrated [28]. Associated with the bipolar behavior of the working electrodes, they give some implications concerning the proper construction of the working electrode for CE and implicitly stress a need

to reconsider the design of the measuring electronics of the amperometric detector for CE.

The aim of this work was to develop an amperometric detector for CE meeting the following requirements: (i) minimum leak currents through the detection cell from the electrophoretic equipment; (ii) protection of the detector circuits and recording devices in situations when the column outlet acquires a very high potential; (iii) following our previous concept of the detection cell [7], to construct a cell with a reduced dead volume; and (iv) compatibility of the detector with both hydrodynamically closed and opened separation compartments.

This paper describes the construction of an amperometric detector in which the electrophoretic column and the measuring circuitry of the detector are galvanically decoupled from the recording devices and from the power unit of the detector. An improved detection cell of the detector is described. The detector was tested in a combination with a hydrodynamically closed CE separation unit. ITP separations were chosen for these tests because they have some advantages for these purposes: (1) well defined changes of the potential at the column outlet can be created easily as they are inherently linked with the ITP separation principles (see, e.g., Ref. [30]); (2) the dispersion in the postcolumn detector can be evaluated using appropriate spacing constituents in the samples; and (3) the dispersion due to the postcolumn detection can be related in a straightforward way to that due to the ITP separation itself which is available from the response of the on-column conductivity detector.

2. Experimental

2.1. Instrumentation

A schematic diagram of the CE separation unit used in this work is given in Fig. 1. The unit was assembled from modules developed in this laboratory following our modular concept of the CE equipment [31]. An on-column conductivity detection cell [32] was used to monitor the
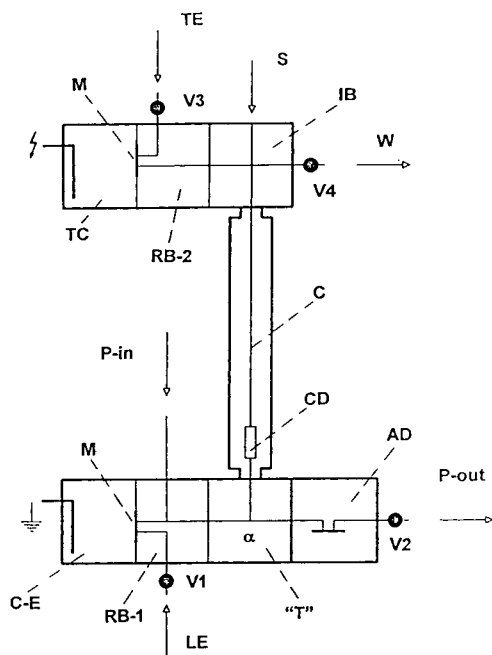
Fig. 1. Schematic diagram of the hydrodynamically closed CE separation unit with a postcolumn amperometric detector. IB = injection block for a microsyringe sample injection; C = capillary tube; CD = on-column conductivity detection cell; "T" = elution T-piece; α = bifurcation point; AD = amperometric detection cell; RB-1 = refilling block for the capillary tube (C); C-E = counter-electrode compartment; M = Cellophane membranes; LE = inlet for the leading electrolyte solution; P-in, P-out = inlet and outlet for the elution solution, respectively; RB-2 = refilling block for the terminating compartment (TC) and the injection block (IB); TE = inlet for the terminating electrolyte solution; W = waste; S = position for the injection of the sample; V1–V4 = valves.

separation in a 200 mm × 0.30 mm I.D. capillary tube made of a copolymer of fluorinated ethylene and propylene (FEP). The separation unit was used with the electronic units of a CS isotachophoretic analyser (Villa-Labeco, Spišská Nová Ves, Slovak Republic).

A laboratory-made syringe pump with a pumping head made of plastic material was used to deliver the electrolyte solution and the separated constituents to the detection cell. The pumping rate was 3.0 μl/min throughout this work.

A measuring unit of a PA-3 polarographic analyser (Laboratorní Přístroje, Prague, Czech Republic) was used in comparative experiments. Its mechanical earthing was disconnected and the insulating resistance of its power transformer determined the leak currents. This measuring unit was used in a combination with the detection cell described elsewhere [7]. All amperometric measurements were performed against a laboratory-made Ag–AgCl (1 M KCl) reference electrode.

A 3 mm diameter glassy carbon (Tokay Electrode, Nagoya, Japan) was glued by epoxy into a hole drilled into an epoxy rod serving as the body of the working electrode (see Fig. 5). The surface of the electrode was ground with sandpapers of fine grades and finally polished with a very fine grade of polishing powder. The copper electrode was constructed in the same way using a transformer copper wire of 3 mm diameter. Its surface was finally electrolytically coated with a layer of copper from a 1% aqueous solution of copper(II) sulphate at 20 μA for 2 h.

2.2. Operation of the CE equipment with the postcolumn amperometric detection

The separation unit used in this work (Fig. 1) is hydrodynamically closed by valves (V1–V4) and cellophane membranes (M). During the separation only the valve at the outlet from the detection cell (V2) is opened to collect the pumped (elution) solution into a waste vessel made of PTFE. The separated constituents, after detection in the conductivity detector (CD), are transported by the driving current into the stream of the pumped solution in a T-piece ("T"). The solution containing the transferred constituents from the column is transported into the detection cell (AD) attached to the T-piece.

2.3. Chemicals and sample handling

Chemicals used for the preparation of the solutions of the leading and terminating electrolyte solutions were brought from Serva (Heidelberg, Germany), Sigma (St. Louis, MO, USA), Reanal (Budapest, Hungary) and La-

chema (Brno, Czech Republic). Other chemicals were obtained from the same sources, except for triethylenetetramine (technical grade), which was from Spolchemie (Ústí nad Labem, Czech Republic).

The leading electrolyte solutions were prepared without anticonvective additives. To eliminate negative effects of electroosmosis [30] the walls of the capillary tube were coated with methylhydroxyethylcellulose 30 000 (Serva) by pushing a 0.5% aqueous solution of this cellulose derivative through the capillary tube [33].

Some of the analytes studied are easily oxidized by oxygen. Therefore, their stock standard solutions (2–10 mM) in water were thoroughly deoxygenated with nitrogen. The solutions used for the analyses prepared daily by dilution with deoxygenated water. Solutions at 10^{-6} mol/l or lower concentrations were prepared immediately before injection into the equipment.

A Model 701N microsyringe (Hamilton, Bonaduz Switzerland) was used to inject sample solutions into the CE instrument. To minimize losses of the analytes by their interactions with metallic parts of the syringe, ethylenediaminetetraacetic acid (EDTA) was added at 10^{-5} mol/l to the sample solution. When this was not effective, a new syringe was used. Syringes were washed daily with demineralized water and with methanol and finally dried with nitrogen.

3. Results and discussion

3.1. Galvanic decoupling of the amperometric detector

The CE instrument with postcolumn amperometric detector (Fig. 1) can be represented by a simplified electrical equivalent as shown in Fig. 2. General requirements concerning the design of the detection circuit of the instrument are apparent from this scheme and they can be summarized as follows: (1) the value of R_{CE} should be minimized so that the bifurcation point in the connecting T-piece (end of the column) is close to the earth potential of the high-voltage power supply (connected to the counter elec-
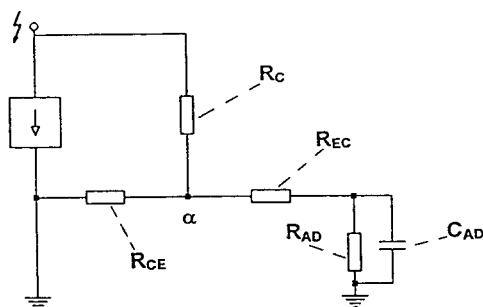
Fig. 2. Electrical equivalent scheme of the CE separation unit with a postcolumn amperometric detector. R_C = resistance of the column; R_{CE} = resistance of the channel to the counter electrode; R_{EC} = resistance of the elution channel (detection capillary); R_{AD} = resistance of the amperometric detection system relative to the earth potential; C_{AD} = capacitance of the detection system; α = bifurcation point.

trode; see Fig. 1); (2) the resistance in the direction to the ground of the measuring electronics of the amperometric detector should be maximized so that the leak currents from the column are reduced to a minimum; and (3) the working electrode is placed in such a position that negative effects due to the bipolar behaviour of the working electrode (see below) are negligible.

An ideal solution to the first of these requirements ($R_{CE} \approx 0$) is to place the counter electrode at the column outlet. Although this is possible [21], such a solution introduces the risk of disturbances in the separation compartment due to migrating products of the electrode reactions. In this work, the value of R_{CE} was reduced by using a connecting channel between the bifurcation point and the counter electrode of 3.5 mm I.D. This gave an electric resistance of 40–50 kΩ for the leading electrolytes used in this work (Table 1) and, consequently, potentials of 1–3 V (against the earth potential of the power supply) at the bifurcation point for 30–50-μA driving currents. When used in ITP separation, this potential increased to 5–15 V on the entrance of the terminating zone when the solution in the direction to the detection cell was not pumped (these values were calculated using a published computer program [30]).

To meet the second requirement, we designed

Table 1
Electrolyte solutions

Parameter	System No.		
	1	2	3
Solvent	H_2O	H_2O	H_2O
Leading anion	Cl^-	Cl^-	Na^+
Concentration (mM)	10	10	10
Counter constituent	HIS	BALA	Borate
pH of the leading electrolyte	6.0	3.9	9.3
Terminating anion	MES	Acetate	$Tris^+$
Concentration (mM)	5	5	5

HIS = histidine; BALA = β-alanine; MES = 2-(N-morphol-ino)ethane sulphonate; Tris = tris(hydroxymethyl)amino-methane. The leading electrolyte solutions were used without anticonvective additives (electroosmosis was suppressed as described under Experimental).

the measuring electronics of the amperometric detector as shown in Fig. 3. The potentiostat itself (I in Fig. 3) is based on a current two-electrode arrangement for amperometric mea-surements [34]. Placed on a high-quality insulat-ing plate (PTFE), it is powered by a perfectly insulated d.c.–d.c. converter (IV in Fig. 3) having leak currents of less than 10 pA when its secondary coil is kept at a 10 kV potential. This d.c.–d.c. converter was tested to withstand po-tentials as high as 20 kV at the column outlet without any damage to the other measuring and recording circuits operating at ground potential. The signal from the the potentiostat to the registration devices (line recorder, computer) is transferred via an interface (II in Fig. 3) based on the use of a photo-coupling device. The insulating resistance of this device is considerable higher than 10 GΩ and its operation was found to be reliable also when the potential at the column outlet was 4 kV.

3.2. Amperometric detection cell and its use with galvanically decoupled detection circuit

In CE with postcolumn amperometric detec-tors, mainly fibre and disc types of working electrodes are used (see, e.g., [7,8,28,29]). From the point of view of the bipolar properties of electrically conductive materials placed in the

electric field in the column (Ref. [30], 176), it can be deduced that these electrodes will exhibit different behaviour under such experimental conditions. These differences are clear from the schematic illustrations in Fig. 4. Here, the fibre electrode inserted into the solution in the column will be polarized on application of the driving current and a potential difference between the two sides of the fibre exposed to the solution will be the result. When this potential difference is sufficient to drive an oxidation reaction at the anodic side and at the same time a reduction reaction at the cathodic side, the driving current will flow through the electrode as shown schematically in Fig. 4A. For example, in this way water can be electrolysed with the pro-duction of oxygen and hydrogen on the anodic and cathodic sides of the electrode, respectively. This process cannot be eliminated even when the electrode is disconnected from the measuring circuitry ($R_D \approx \infty$).

The disc electrode inserted into the solution in the column makes direct contact with it only through a front plane (Fig. 4B). On application of the driving current only one end of the electrode is available for the electrode reaction in the solution and the electrode reaction loop cannot be closed via the electrode itself. This indicates that the disc electrodes offer a more convenient alternative as far as the bipolar effects are concerned. However, this assumes in some respects an idealized situation (the contact plane of the disc electrode is placed in an equipotential of the driving field, no local po-tential gradients on the surface of the electrode, e.g., due to its roughness) and in practice some negative effects probably cannot be eliminated to a certain extent.

A schematic view of the detection cell used in this work is given in Fig. 5. The cell was mechanically fixed to the T-piece (2 in Fig. 5) and the distance of the surface of the working electrode from the outlet of the elution channel (4 in Fig. 5) was defined by PTFE spacers (5 in Fig. 5). Although the cell was designed to accommodate various types of working elec-trodes (simple fibres, strand of fibers [35], disc), we preferred in this work the disc type as shown
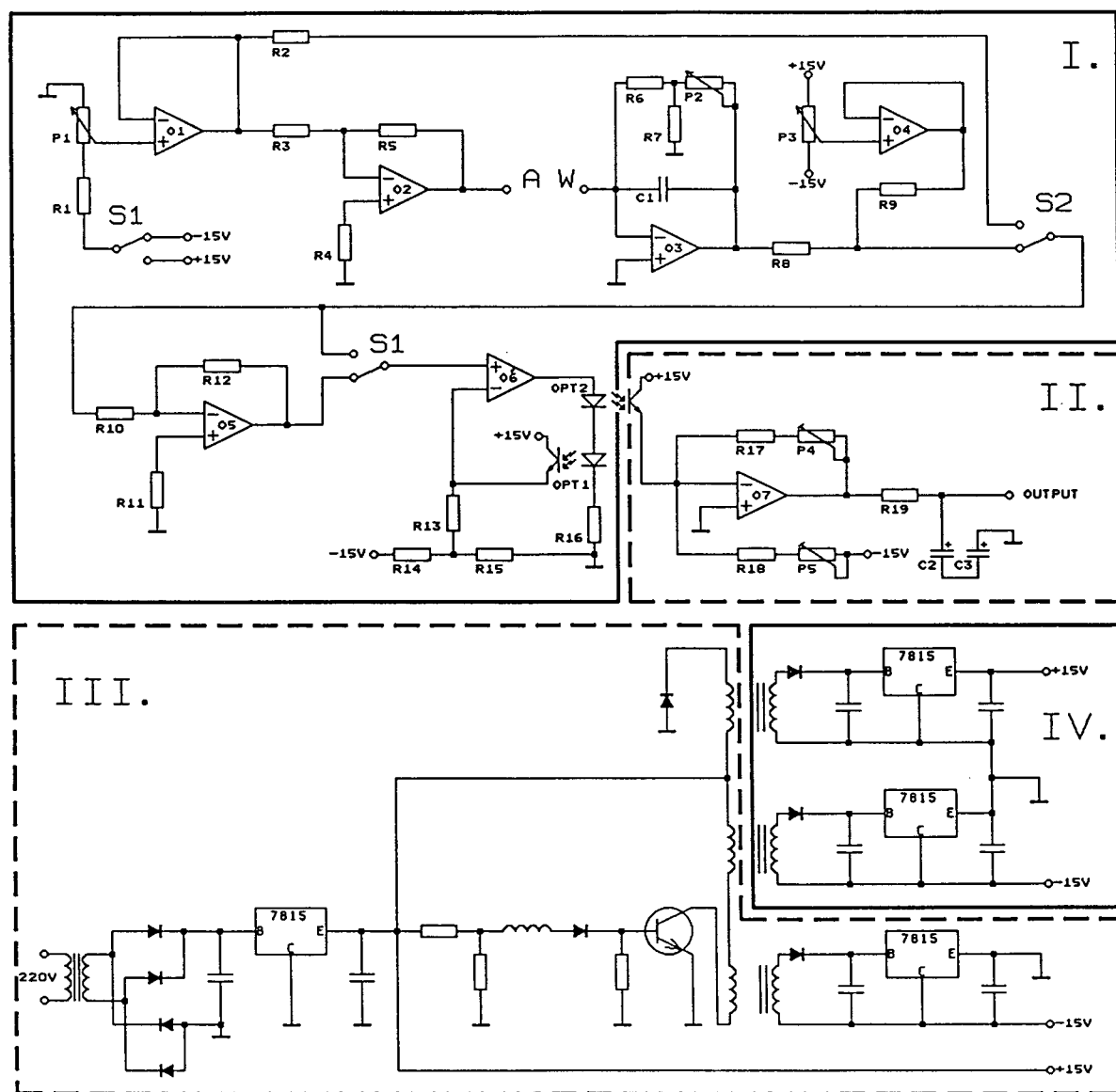
Fig. 3. Electronic circuit of the amperometric detector. I = potentiostat in a two-electrode arrangement; II = interface between the potentiostat and the registration devices; III = power unit of the detector; IV = d.c.–d.c. converter. Semiconductor components: OA_1, OA_2, OA_4–OA_7 = MAA 741 (AD 741); OA_3 = MAC 155 (LF 155); OPT1, OPT2 = WF MB 101. Resistors: R_1, R_4, R_{11}, R_{14} = 47 kΩ; R_2, R_3, R_8, R_9, R_{10}, R_{12}–R_{14} = 10 kΩ; 5 kΩ; R_6 = 3 MΩ; R_7 = 1 kΩ; R_{15} = 510 Ω; R_{16} = 22 Ω; R_{17} = 180 kΩ; R_{18} = 15 kΩ. Potentiometers: P_1, P_3 = 100 kΩ; P_2 = 5 MΩ. Capacitors: C_1 = 150 pF; C_2, C_3 = 50 μF. S_1 = polarity switch; S_2 = switch for the measurements of potential on the working electrode or the detection current. Full-line frames contain the circuits operating on the high-voltage side (I and IV) and which are galvanically decoupled from the power unit (III) and from the interface (II).
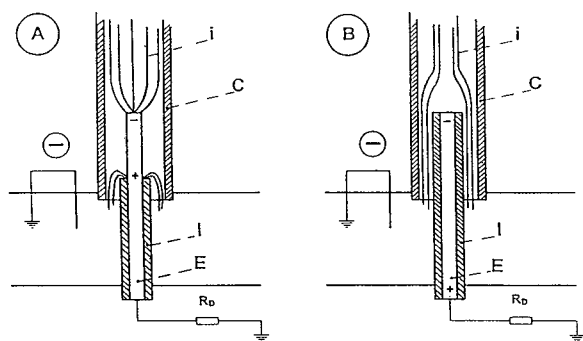
Fig. 4. Bipolar behaviour of (A) fibre and (B) disc electrodes inserted into the capillary tube (C) through which the driving current flows. Current lines (i) indicate the paths of the driving current. E = electrode; I = insulating layer; R_D = insulating resistance of the detector to the ground.

in Fig. 5 for the following reasons: (i) inherently better properties in terms of the bipolar effects as discussed above; (ii) we could compare the present detection system with that developed in our previous work [7]; and (iii) the working electrode could be aligned easily without using micropositioners.

The optimum solution in this respect requires that the choice considers mainly the signal-to-

nose ratio [36]. A detailed investigation of various types of working electrodes along this line is the subject of our current research.

3.3. Evaluation of the performance of the detector

The change in the potential at the column outlet was found to be a source of undesirable disturbances in the amperometric detector coupled to the ITP separation [7]. The isotachopherograms in Fig. 6 illustrate this problem. When the measuring unit of the current amperometric system (see Experimental) was used in conjunction with the CE equipment, a 5 V change in the potential at the column outlet due to the entry of the terminating zone into the elution channel (see Fig. 5) caused a response of

Fig. 5. Amperometric detection cell attached to the T-piece. 1 = T-piece; 2 = channel to the counter electrode; 3 = connection for the column; 4 = elution channel (detection capillary) of 4 mm × 0.2 mm I.D.; 5 = PTFE spacer (0.05 mm); 6 = O-ring for a leak-proof connection; 7 = amperometric cell; 8 = working electrode; 9 = connecting cable to the electronics of the detector; 10 = epoxy body of the electrode; 11 = connecting channel for the reference electrode.

Fig. 6. Responses of the amperometric detectors on the entrance of the terminating zone into the elution channel in the bifurcation point. A = modified PA-3 detector (see Experimental); B = present detector (Figs. 3 and 5); I and II = without and with pumping of the elution solution, respectively. C = isotachopherogram from the conductivity detector. Electrolyte system No. 1 (Table 1) was used for the separations and the leading electrolyte served also as the elution solution. A glassy carbon electrode was set at +400 mV vs. an Ag–AgCl (1 M KCl) reference electrode. The driving current was 45 μA. L and T = leading and terminating zones, respectively; R, i and t = increasing resistance, detection current and time, respectively.

the detector equal to ca. 100 nA (I-A in Fig. 6). It must be stressed that in this instance the elution solution was not pumped and the detection cell had a conductive connection with the column outlet via the elution channel (capillary tube of 100 mm × 0.25 mm I.D.). The electric resistance of this connection was ca. 16 MΩ. This false response did not occur when the composition of the solution at the column outlet and in the elution channel was kept constant by pumping the elution solution (II-A in Fig. 6). From these experiments, it is apparent that even small fluctuations in the potential at the column outlet can contribute significantly to the overall noise of the detector. Isotachopherograms I-B and II-B (Fig. 6) were obtained, under conditions otherwise identical with those for their counterparts (I-A and II-A), with the present detector. These experiments show that the galvanic decoupling of the electrophoretic equipment and the potentiostat from the rest of the detector circuits (Fig. 3) eliminated the problems with the false response of the detector. In the experiments illustrated by the isotachopherogram I-B in Fig. 6 this false response could not be resolved from the noise of the detector (ca. 90 pA). This is, at least, a 10^3-fold improvement when related to the response of the detector without such a strict decoupling (I-A in Fig. 6).

Leak currents through the detection cell were very significantly reduced using the present detector. While in runs I-A and II-A in Fig. 6 the background current increase due to the driving current was 30–35 nA, it could not be resolved from the detector noise (ca. 90 pA) with the galvanic decoupling as developed in this work.

These improvements in the performance of the measuring electronics of the detector enables us to decrease significantly the dead volume of the detection cell {a 100-nl volume of the elution channel with the present detection cell (Fig. 5) vs. 4900 nl with the previous detector [7]}. The overall dispersion of the analyte zones in the detection cell was evaluated in the ITP separation of nitrite and ascorbate in the spike mode of analysis [7] using succinate as a spacing constituent. Isotachopherograms from these experiments are given in Fig. 7. Here, the analytes
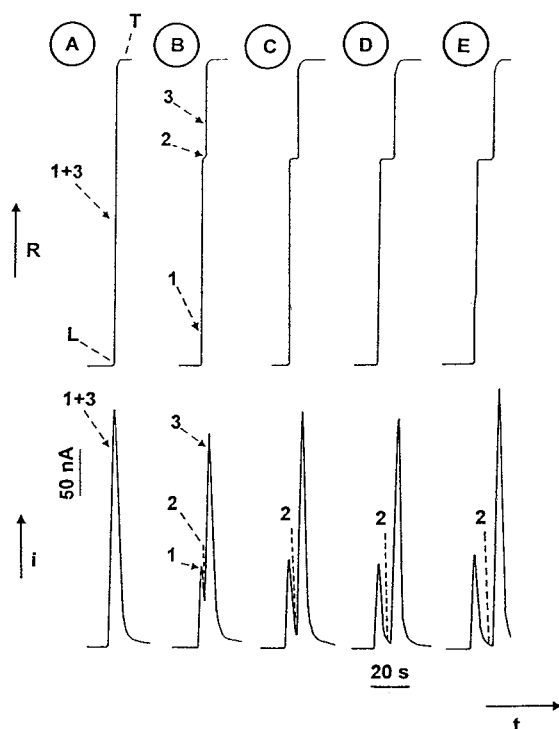
Fig. 7. Resolution of nitrite (1) and ascorbate (3) by the present amperometric detector. Succinate (2) was used as a spacing constituent and its zone lengths in the column were (A) 0, (B) 1, (C) 2, (D) 3.5 and (E) 4.5 mm. The amounts of nitrite and ascorbate injected were always 80 and 8 pmol, respectively. The sample volume was 1 μl. A glassy carbon electrode was set at +800 mV vs. an Ag–AgCl (1 M KCl) reference electrode. The separations were carried out in electrolyte system No. 2 (Table 1) and the leading electrolyte was used also for elution. The driving current was 50 μA. Other symbols as in Fig. 6.

were injected in amounts not sufficient for the formation of their own zones detectable by the conductivity detector. They migrated focused in the interzonal boundary layer between the leading and terminating zones (Fig. 7A) or spaced by the succinate zone in the corresponding interzonal boundary layers (Fig. 7B–E). Under our working conditions the boundary layer can be estimated to have a 0.1–0.2 mm thickness [30]. With a migration velocity of ca. 0.5 mm/s the analytes were transferred into the elution solutions at the column outlet within 0.2–0.4 s. This corresponded to their transfers into 10–20nl

volumes of the elution solution. From the iso-tachopherograms obtained from the amperometric detector we can see that they passed through the detection cell in ca. 500-nl volumes. This dispersion can be conveniently expressed via the length of the spacing zone giving a baseline resolution of the analytes by the amperometric detector [7]. The isotachopherogram in Fig. 7 show that this was achieved for a 2-mm length of the succinate zone. This is almost one order of magnitude improvement in the dispersion compared with what was possible with out previous detector [7]. However, a comparison with conductivity detection (see Fig. 7) shows that the present detection cell is not exploiting fully the resolving power of the ITP separation and a further improvement of its construction is desirable.

The noise of the detector (peak-to-peak) was typically in the range 70–100 pA, depending on the electrolyte system, pumping rate and state of the surface of the working electrode. Considering the signal-to-noise ratio of 3 and the working conditions as used in experiments in Fig. 7, this gives an estimate of the limit of detection of 5–7 fmol for ascorbate or a 5×10^{-9}–$7 \cdot 10^{-9}$ mol/l concentration of this analyte for a 1-μl sample injection volume. However, in experiments aimed at confirming this estimated value we could not detect ascorbate when its concentration in the sample was lower than $5 \cdot 10^{-8}$–$8 \cdot 10^{-8}$ mol/l. This is probably due to the fact that the injection of the sample with the aid of a microsyringe having both needle and plunger made of stainless steel can be accompanied by an oxidation reaction of the labile analytes due to traces of Fe(III) ions [37] and the precautions taken to minimize this effect (see Experimental) may not be sufficient for such low concentrations. Experiments carried out with ITP with UV detection (254 nm) and with proportionally higher sample injection volumes using a PTFE-lined injection valve gave identical conclusions.

Human urine containing hundreds of acidic constituents [38], many of which can be expected to be oxidizable electrochemically, was briefly studied to show the possibilities of the present detector in the analysis of complex mixtures of electrochemically active constituents. Isotacho-pherograms obtained in these experiments are given in Fig. 8, from which it is apparent that the resolution of the separands was the main problem for both detectors. On the other hand, from the response of the conductivity detector we can estimate that the concentrations of the oxidizable analytes in the sample were 10^{-4} mol/l or less while the amperometric detector indicated a high sensitivity. Solving the resolution problems, e.g., by using a mixture of appropriately chosen
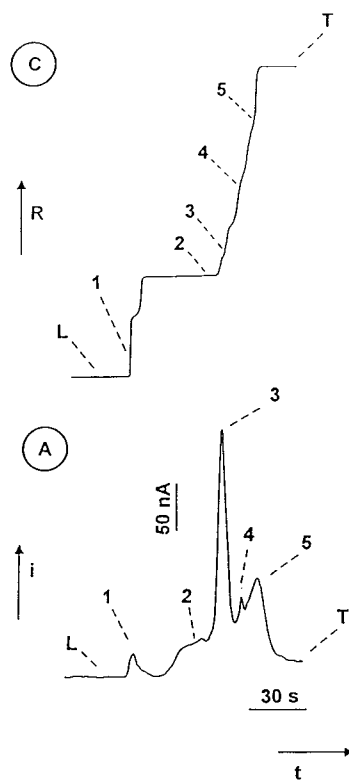
Fig. 8. ITP separation and postcolumn amperometric detection of anionic human urine constituents at pH 3.9. A 2-μl volume of the sample [a mid-stream fraction diluted 1:10 (v/v) with water] was injected. (C and A) = isotachopherograms from the conductivity and amperometric detectors, respectively. The numbers (1–5) indicate identical regions on the isotachopherograms. The separations were carried out in electrolyte system No. 2 (Table 1) using the leading electrolyte also for elution. The driving current was 50 μA. The working electrode (glassy carbon) was set at 800 mV vs. an Ag–AgCl (1 *M* KCl) reference electrode. Other symbols as in Fig. 6.

spacing constituents or via a combination of ITP with CZE [39], we can expect very sensitive analytical procedures for the oxidizable analytes present in urine.

CE techniques are convenient alternatives to the separation of cationogenic amines. At present, their selective detection (not considering chemical derivatization reactions), especially for trace analysis applications, is not available. The use of a copper electrode polarized anodically as proposed for HPLC and flow analysis systems [1–3] and for CZE of amino acids, peptides [15] and sugars [17] was tested in conjunction with

the present amperometric detector. Triethylenetetramine of a technical grade served as an analyte in these tests. From the isotachopherograms obtained (Fig. 9), we can see that the polyamine contained seven impurities, four of which gave a response to the amperometric detector. The staircase-like appearance of the response for the main constituent is unexpected as a straight plateau should ideally be achieved. A possible explanation for this reproducible response may lie in the kinetics of the chelate formation at the electrode [3, 15] and in the presence of borate in the electrolyte solution (Table 1), which is reported to have a negative influence on the response of the copper electrode [3]. Nevertheless, considering the noise of the detector (50–80 pA), our results clearly indicate that this detection approach could be very sensitive, e.g., for polyamines. A detailed study focused on the use of an amperometric detector with a copper electrode for the trace determination of amines by CE techniques will be a subject of our future research.
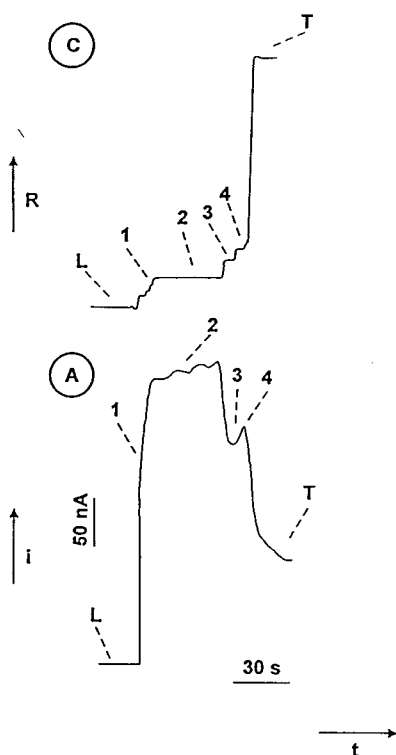
Fig. 9. ITP separation of cationic constituents present in triethylenetetramine of technical grade with amperometric detection at a copper electrode. A 2 μl volume of the polyamine (10^{-3} mol/l concentration) was injected. The numbers (1–4) indicate identical regions on the isotachopherograms. The separations were carried out in electrolyte system No. 3 (Table 1) using the leading electrolyte also for elution. The driving current was 40 μA. The copper electrode was polarized at 200 mV vs. an Ag–AgCl (1 M KCl) reference electrode. Other symbols as in Fig. 6.

4. Conclusions

The described postcolumn amperometric detector for CE with galvanic decoupling of the detection electrodes and the detection circuit from the power unit of the detector and from the recording devices alleviates problems due to leak currents flowing from the electrophoretic equipment through the detector. This solution also eliminated false responses of the detector caused by potential changes at the column outlet.

Components used for the decoupling (d.c.–d.c. converter and opto-coupler) serve as devices that protect the detector in situations when a high voltage occurs at the column outlet (e.g., bubble formation in the column). In the detector described here, parameters of the opto-coupler restricted this function to 4–5 kV. Nevertheless, this protective function can be improved by using a more appropriate opto-coupling device and a detector withstanding the full voltage of the high-voltage power supply can be constructed.

In this work the detector was used with a

detection cell with a dead volume ca. 50 times smaller than that described previously [7]. Although a tenfold improvement in the dispersion of the analyte zones could be achieved, the ITP experiments with practical samples indicate that a further decrease is desirable. This, however, requires that the optimum construction of the cell will consider also the signal-to-noise performance of the detector [36].

Although the detector was tested in ITP experiments carried out in a hydrodynamically closed separation compartment, it is apparent that it can be used in CZE and MEKC. It is obvious that the hydrodynamic concept of the separation compartment plays only a minor role in this respect.

References

[1] D.C. Johnson, S.G. Weber, A.M. Bond, R.M. Wightman, R.E. Shoup and I.S. Krull, Anal. Chim. Acta, 180 (1986) 187.

[2] K. Štulík and V. Pacáková, Electroanalytical Measurements in Flowing Liquids, Ellis Horwood, Chichester, 1987.

[3] K. Štulík, Analyst, 114 (1989) 1519.

[4] P.T. Kissinger, J. Chromatogr., 488 (1989) 31.

[5] M.D. Ryan and J.Q. Chambers, Anal. Chem., 64 (1992) 79R.

[6] M.D. Ryan, E.F. Bowden and J.Q. Chambers, Anal. Chem., 66 (1994) 360R.

[7] D. Kaniansky, P. Havaši, J. Marák and R. Sokolík, J. Chromatogr., 366 (1986) 153.

[8] R.A. Wallingford and A.G. Ewing, Anal. Chem., 59 (1987) 1762.

[9] R.A. Wallingford and A.G. Ewing, Anal. Chem., 60 (1988) 258.

[10] R.A. Wallingford and A.G. Ewing, Anal. Chem., 60 (1988) 1972.

[11] R.A. Wallingford and A.G. Ewing, Anal. Chem., 61 (1988) 98.

[12] T.A. Olefirowicz and A.G. Ewing, Anal. Chem., 62 (1990) 1872.

[13] T.A. Olefirowicz and A.G. Ewing, J. Chromatogr., 499 (1990) 713.

[14] X. Huang, R.N. Zare, S. Sloss and A.G. Ewing, Anal. Chem., 63 (1991) 189.

[15] C.E. Engstrom-Silverman and A.G. Ewing, J. Microcol. Sep., 3 (1991) 141.

[16] T.J. O'Shea, R.D. Greenhagen, S.M. Lunte, M.R. Smyth, D. Radzik and N. Watanabe, J. Chromatogr., 593 (1992) 305.

[17] L.A. Colon, R. Dadoo and R.N. Zare, Anal. Chem., 65 (1993) 476.

[18] S. Sloss and A.G. Ewing, Anal. Chem., 65 (1993) 577.

[19] T.J. O'Shea, S.M. Lunte and W.R. LaCourse, Anal. Chem., 65 (1993) 948.

[20] W. Lu and R.M. Cassidy, Anal. Chem., 65 (1993) 1649.

[21] W.Th. Kok and Y. Sahin, Anal. Chem., 65 (1993) 2497.

[22] W. Lu and R.M. Cassidy, Anal. Chem., 65 (1993) 2878.

[23] W. Lu, R.M. Cassidy and A.S. Baranski, J. Chromatogr., 640 (1993) 433.

[24] J. Ye and R.P. Baldwin, Anal. Chem., 65 (1993) 3525.

[25] I.C. Chen and C.-W. Whang, J. Chromatogr., 644 (1993) 208.

[26] S.S. Ferris, G. Lou and A.G. Ewing, J. Microcol. Sep., 6 (1994) 263.

[27] T.J. O'Shea and S.M. Lunte, Anal. Chem., 66 (1994) 307.

[28] W. Lu and R.M. Cassidy, Anal. Chem., 66 (1994) 200.

[29] A.G. Ewing, J.M. Mesaros and P.F. Gavin, Anal. Chem., 66 (1994) 527A.

[30] F.M. Everaerts, J.L. Beckers and Th.P.E.M. Verheggen, Isotachophoresis. Theory, Instrumentation and Applications, Elsevier, Amsterdam, 1976.

[31] D. Kaniansky, Thesis, Comenius University, Bratislava, 1981.

[32] D. Kaniansky, M. Koval' and S. Stankoviansky, J. Chromatogr., 267 (1983) 67.

[33] M. Koval', D. Kaniansky, M. Hutta and R. Lacko, J. Chromatogr., 325 (1985) 151.

[34] R. Kalvoda, Použití Operačních Zesilovaču v Chemické Instrumentaci, SNTL, Prague, 1974.

[35] K. Štulík, V. Pacáková and M. Podolák, J. Chromatogr., 298 (1984) 225.

[36] S.G. Weber and J.T. Long, Anal. Chem., 60 (1988) 903A.

[37] S. Fredriksson, J. Chromatogr., 188 (1980) 266.

[38] H.M. Liebich and C. Foerst, J. Chromatogr., 525 (1990) 1.

[39] D. Kaniansky and J. Marák, J. Chromatogr., 498 (1990) 191.

ELSEVIER

Capillary zone electrophoretic separation of the enantiomers of dipeptides based on host–guest complexation with a chiral crown ether

Martin G. Schmid and Gerald Gübitz*

Institute of Pharmaceutical Chemistry, Karl-Franzens University of Graz, Universitätsplatz 1, A-8010 Graz, Austria

Abstract

The enantiomeric separation of racemic glycyldipeptides and diastereomeric dipeptides by using capillary zone electrophoresis and (+)-18-crown-6-tetracarboxylic acid (18C6H$_4$) as a chiral selector added to the electrolyte is described. The separation of dipeptides with two stereogenic centres into four peaks by using capillary zone electrophoresis is reported for the first time. Chiral discrimination is attributed to the formation of a diastereomeric host–guest complex which leads to different interactions for each enantiomer. Owing to the differences in stability of the complexes, the four optical isomers elute at different migration times, allowing the chiral separation. The influence of buffer composition, crown ether concentration and the addition of organic modifiers was studied. All glycyldipeptides were resolved and for most of the diastereomeric dipeptides four baseline-separated peaks were observed.

1. Introduction

Capillary electrophoresis has been found to be a very useful tool for the separation of enantiomers [1–3]. The principle of host–guest complexation using chiral crown ethers, successfully applied in the HPLC separation of enantiomers [4–10], has recently been adapted also to capillary zone electrophoresis for the separation of enantiomers of amino acids [11–13] and amino alcohols [13,14].

This paper describes the optical resolution of dipeptides by (+)-18-crown-6-tetracarboxylic acid (18C6H$_4$) added as a chiral selector to the electrolyte. Hilton and Armstrong [7] resolved some dipeptides by HPLC using a crown ether column at different temperatures. Obviously, dipeptides are basic and essential components in biological systems either as individual compounds or as constituents of proteins [15,16]. The development of methods for the direct resolution of compounds having more than one chiral centre is therefore of great interest for enantiomeric purity control. Further, peptide syntheses often require the presence of only one enantiomer.

In previous papers [11–14], the potential of 18C6H$_4$ for enantioseparation and the recognition mechanisms were described. The aim of this study was to investigate the influence of the buffer composition, the crown ether concentra-

---

* Corresponding author.

tion and organic modifiers such as methanol on the chiral separation of dipeptides.

2. Experimental

2.1. Methods

Capillary electrophoresis was performed using a Prince capillary electrophoresis instrument (Lauerlabs, Netherlands) equipped with an on-column UV detector (Lambda 1000; Bischoff Analysentechnik, Leonberg, Germany). Separations were carried out at ambient temperature in a fused-silica capillary tube (80 cm × 75 μm I.D., effective length 71 cm). Samples were injected hydrodynamically (20 mbar) for 6 s, which led to an injection volume of about 12 nl. The potential during analysis was 20 kV unless stated otherwise. Dipeptides were detected by UV absorption at 206 nm. An Axxiom 737 system (Moorpark, CA, USA) was used for data acquisition.

2.2. Materials

All reagents were of analytical-reagent grade unless indicated otherwise. (+)-18-Crown-6-tetracarboxylic acid, citric acid, tartaric acid, sodium dihydrogenphosphate and methanol (additionally doubly distilled) were purchased from Merck (Darmstadt, Germany). All dipeptides, N-tris(hydroxymethyl)methylglycine (tricine), 3-(cyclohexylamino)-1-propanesulfonic acid (CAPS) and tris(hydroxymethyl)aminomethane (Tris) were obtained from Sigma (Deisenhofen, Germany).

Sample solutions were prepared by dissolving the dipeptides (1 mg) in doubly distilled, deionized water (1 ml); samples and buffer solutions were filtered through a 0.45-μm pore-size filter (Schleicher & Schüll, Dassel, Germany) and degassed with helium 5.0.

3. Results and discussion

18-Crown-6 is a macrocyclic polyether ring [17,18]. Six oxygen atoms link six ethylene groups to build a cavity suitable to potassium ions (K^+), ammonium ions (NH_4^+) or protonated primary alkyl amines (RNH_3^+). The mechanism of chiral recognition has already been widely discussed [4–6,8,10–14,19]. Briefly, hydrogen bonds forming a tripod arrangement and an optical barrier caused by the asymmetric substituents are responsible for the chiral discrimination. Lehn and co-workers [20,21] synthesized a useful derivative, (+)-18-crown-6-tetracarboxylic acid (Fig. 1), which seems to be a very suitable chiral additive. In this case, in addition to the chiral barrier formed by the carboxylic acid pairs, electrostatic interactions might support the chiral separation [13].

3.1. Optimization of the buffer system

Generally, separations were carried out either with the crown ether only or with an additional electrolyte. Different buffer systems were investigated to optimize the separation conditions.

Using a background electrolyte, 10 mM $18C6H_4$ with 10 mM Tris–citrate, gave the fastest and best results concerning the peak sharpness. According to Kuhn et al. [12], the mobility of this buffer system fits the chiral selector because of the minimization of electrophoretic dispersion. Tris was considered to have similar migration properties to amino acids without forming a complex with the crown ether. CAPS adjusted to pH 2.0 with tartaric acid gave peak tailing and a poor peak shape. A solution of 1 mM sodium dihydrogenphosphate (higher phosphate levels resulted in too high current values) failed, possibly because of interaction of the Na^+ cation with $18C6H_4$. A test experiment with DL-leucyl-DL-leucine using 10 mM Tris–citrate without the chiral selector resulted in only
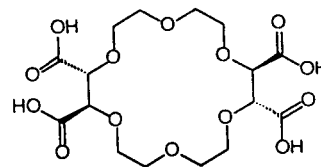
Fig. 1. Structure of (+)-18-crown-6-tetracarboxylic acid.

two peaks: the first peak consisted of L-leucyl-L-leucine (L-Leu-L-Leu) and D-leucyl-D-leucine (D-Leu-D-Leu), the second peak of L-leucyl-D-leucine (L-Leu-D-Leu) and D-leucyl-L-leucine (D-Leu-L-Leu). The migration order was verified by sampling the four pure enantiomers.

3.2. Resolution of glycyldipeptides

The elution sequence for glycyl-DL-valine was investigated by sampling the enantiomers. Gly-L-Val migrated faster, indicating that 18C6H$_4$ forms stronger complexes with glycyl-D-enantiomers than with Gly-L-antipodes. Kuhn et al. [11] found amino acids to show same behaviour.

Separation data are given in Table 1 and an example is shown in Fig. 2. Generally, each glycyldipeptide tested was separated although the chiral centre is in the δ-position to the primary amine. Using HPLC, dipeptides with a C-terminal glycine, where the chiral C atom is located in the α-position to the primary amine, are found to be resolved much better [7]. This type of dipeptide was not included in our investigations. Fig. 3 demonstrates the relationship between the molecular mass (M_r) of each glycyldipeptide and its separation factor $\alpha(t_2/t_1)$. The experiment was carried out using 25 mM 18C6H$_4$ without any additional background electrolyte. The higher the M_r, the more efficient was the resolution of the enantiomers. Moreover, the comparison of Gly-DL-Leu with Gly-DL-Nle and of Gly-DL-Val with Gly-DL-Nva [observed when using 10 mM 18C6H$_4$ and 10 mM tris–citrate (pH 2.0)] showed another effect: straight-chain alkyl groups were resolved worse than their branched isomers.

3.3. Separation of diastereomeric dipeptides

We examined the chiral resolution of a series of different dipeptides having two optically active centres. Analyses were performed using either 10 mM 18C6H$_4$ and 10 mM Tris–citrate (pH 2.0) as a buffer system or 25 mM 18C6H$_4$ without any additional background electrolyte.

Most of the diastereomeric dipeptides were separated into their four enantiomers. Separa-

tion data are given in Table 2. As the pure enantiomers for the other dipeptides were not available, the elution order was only investigated for Leu-Leu. In contrast to the glycyldipeptides, the molecular masses do not seem to be correlated with separation factors. Dipeptides consisting of amino acids with bulky substituents were better resolved than those with small substituents, e.g. DL-leucyl-DL-leucine or DL-leucyl-DL-phenylalanine compared with DL-alanyl-DL-valine. In some cases the use of only 10 mM 18C6H$_4$ with additional background electrolyte resulted in baseline resolution, connected with a decreased migration time and sharper peaks. For example, Fig. 4 shows the separation of DL-leucyl-DL-phenylalanine into its four enantiomers using 10 mM 18C6H$_4$ and 10 mM Tris–citrate (pH 2.0) as a buffer system. In this case, the number of theoretical plates was about 30 000.

We optimized the chiral resolution of a DL-leucyl-DL-leucine racemate, applying different amounts of 18C6H$_4$ in water without adding any additional electrolyte. At concentrations below 5 mM 18C6H$_4$, only three completely resolved peaks were obtained: L-Leu-L-Leu migrating fastest, followed by a mixture of D-Leu-L-Leu and L-Leu-D-Leu. The third peak was D-Leu-D-Leu. At a concentration of about 5 mM 18C6H$_4$, a partial separation of L-Leu-D-Leu and D-Leu-L-Leu was observed. Optimum resolution was obtained at 25 mM 18C6H$_4$, whereby D-Leu-L-Leu migrated faster than L-Leu-D-Leu. A further increase in the chiral additive resulted in a decrease in the resolution factor. Using an 18C6H$_4$ concentration higher than 55 mM, the three-peak constellation was reobtained. This is generally confirmed by a theoretical model, indicating that the degree of separation depends on the concentration of the chiral selector and that there is an optimum concentration [22]. Fig. 5 shows the change in R_s (L-Leu-D-Leu/D-Leu-L-Leu) versus the concentration of the crown ether.

Besides increasing the concentration of the chiral selector, the addition of methanol was found to improve the resolution in some cases (Table 3). Without adding methanol, a 25 mM 18C6H$_4$ solution was necessary for the resolution

Table 1
Separation data for optically active glycyldipeptides using chiral 18C6H$_4$ (25 mM): resolution (R_s), separation factor ($\alpha = t_2/t_1$) and migration time of the first-eluted enantiomer (t_1)
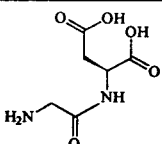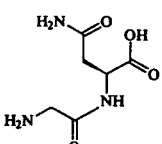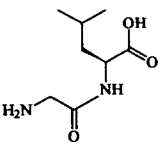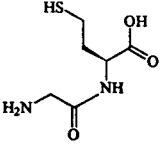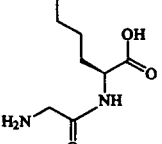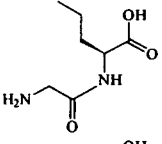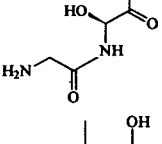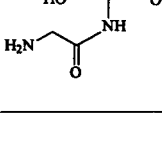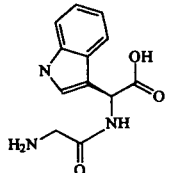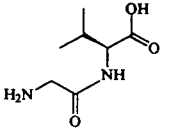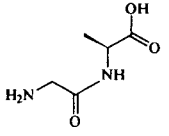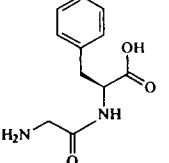
Compound	Formula	t_1 (min)	α (t_2/t_1)	R_s
Glycyl-DL-aspartate		28.11	1.040	1.57
Glycyl-DL-apraragine		26.53	1.028	0.96
Glycyl-DL-leucine		28.03	1.041	1.57
Glycyl-DL-methionine		28.97	1.048	1.79
Glycyl-DL-norleucine		28.63	1.032	1.47
Glycyl-DL-norvaline		27.91	1.026	1.15
Glycyl-DL-serine		27.72	1.019	0.90
Glycyl-DL-threonine		28.14	1.029	1.21

Table 1 (continued)

Compound	Formula	t_1 (min)	α (t_2/t_1)	R_s
Glycyl-DL-tryptophan		33.07	1.064	1.94
Glycyl-DL-valine		32.56	1.026	0.98
Glycyl-DL-alanine		28.20	1.006	0.30
Glycyl-DL-phenylalanine		30.99	1.056	1.75

of DL-leucyl-DL-leucine to obtain four baseline-separated peaks, whereas the addition of 20% (v/v) methanol to a 15 mM solution of 18C6H$_4$ gave the same result (Fig. 6).

Using HPLC and a Crownpak CR(+) column, Hilton and Armstrong [7] obtained at ambient temperature only three peaks for the separation of Leu-Leu, whereas at low temperature the dipeptide was completely resolved. Interestingly,
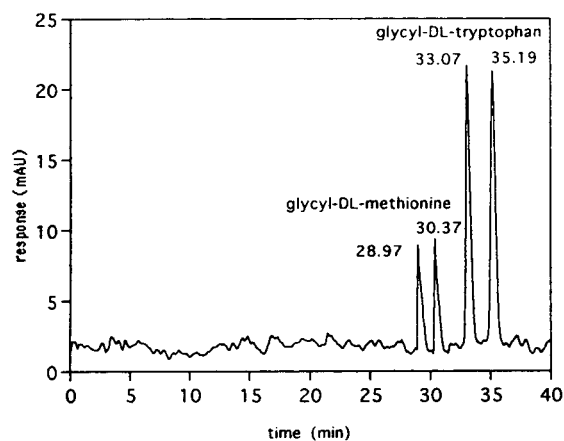
Fig. 2. Separation of the enantiomers of glycyl-DL-methionine and glycyl-DL-tryptophan using 25 mM 18C6H$_4$ (pH 2), 20 kV.
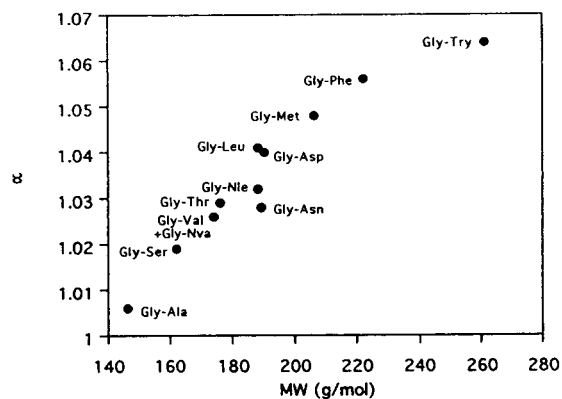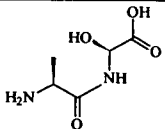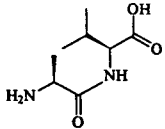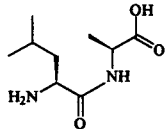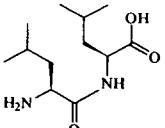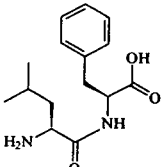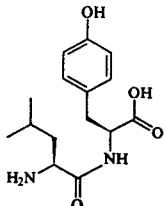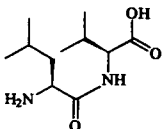
Fig. 3. Relationship between the molecular mass of a glycyldipeptide and its separation factor $\alpha(t_2/t_2)$. Buffer system: 25 mM 18C6H$_4$ without any background electrolyte.

Table 2
Separation data for optically active dipeptides (buffer: 25 mM 18C6H$_4$): migration time for the first-eluted enantiomer (t_1) and separation factors of the 1st and 2nd, the 2nd and 3rd and 4th peaks, $\alpha_{1/2}$, $\alpha_{2/3}$ and $\alpha_{3/4}$ respectively

Compound	Formula	Peaks	t_1 (min)	$\alpha_{1/2}$	$\alpha_{2/3}$	$\alpha_{3/4}$
DL-Alanyl-DL-serine		4	22.81	1.031	1.017	1.028
DL-Alanyl-DL-valine		2	19.27	1.104	–	–
DL-Leucyl-DL-alanine		4	21.41	1.026	1.043	1.122
DL-Leucyl-DL-leucine		4	27.38	1.030	1.032	1.195
DL-Leucyl-DL-phenylalanine		4	21.16	1.123	1.078	1.116
DL-Leucyl-DL-tyrosine		2	26.26	1.166	–	–
DL-Leucyl-DL-valine		3	23.44	1.035	1.073	1.015
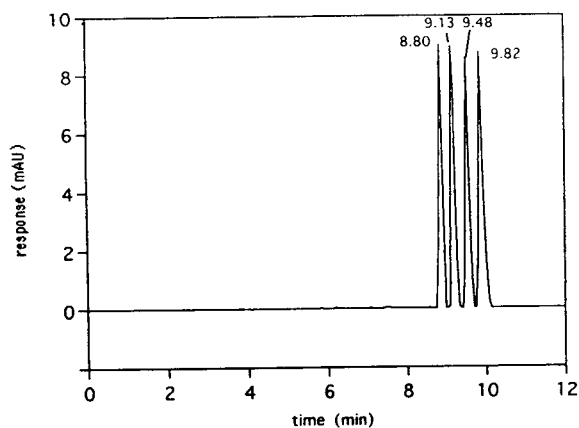
Fig. 4. Electropherogram of the chiral resolution of DL-leucyl-DL-phenylalanine [buffer: 10 mM 18C6H$_4$–10 mM Tris–citrate (pH 2.0)], U = 30 kV.
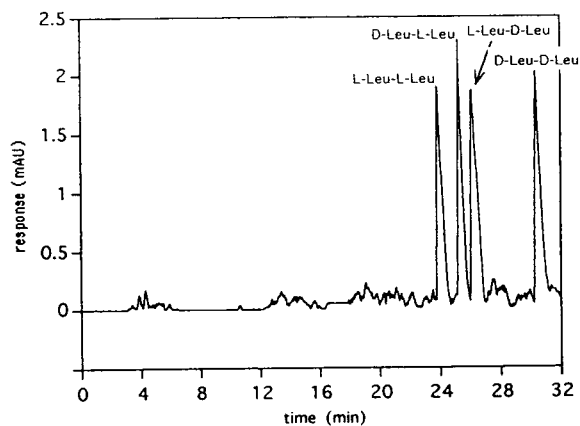
Fig. 6. Electropherogram of the chiral resolution of DL-leucyl-DL-leucine [buffer: 15 mM 18C6H$_4$, –10 mM Tris–citrate, 20% (v/v) methanol], U = 30 kV.
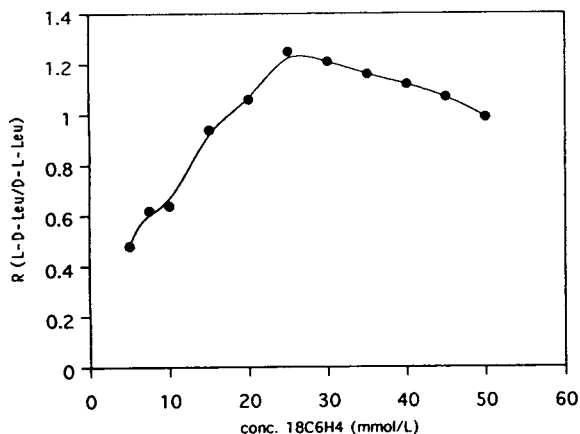
Fig. 5. Resolution of the leucylleucine enantiomer L-leucyl-D-leucine and D-leucyl-L-leucine as a function of 18C6H$_4$ concentration.

compared with our results, the elution order was reversed.

4. Conclusion

The potential of 18C6H$_4$ as a selector for chiral separation of dipeptides into their enantiomers using capillary zone electrophoresis has been demonstrated. The formation of diastereomeric inclusion complexes determines different migration times for each enantiomer of a racemic compound.

Twelve glycyldipeptides and seven dipeptides with two chiral centres were resolved by a simple separation system. At ambient temperature each glycyldipeptide was at least partially resolved and more than half of the diastereomeric dipeptides were separated into four peaks. Our

Table 3
Separation data for resolving the peaks of D-leucyl-L-leucine and L-leucyl-D-leucine by increasing the proportion of methanol in 15 mM 18C6H$_4$ (pH 2)

Methanol added to 15 mM 18C6H4 (%)	Resolution factor, R_s(L–D-Leu/D–L-Leu)	Separation factor, α(L–D-Leu/D–L-Leu)
0	0.921	1.020
5	0.978	1.027
20	1.14	1.035

investigations have shown that in addition to the concentration of 18C6H$_4$, the addition of organic modifiers and added electrolytes has a marked effect on the resolution.

We also investigated the influence of the structure of glycyldipeptides on the resolution. The selectivity is usually optimum when the amino functionality is adjacent to the stereogenic centre. However, such dipeptides have their chiral centre in the δ-position to the amino group. As the NH$_3^+$ residue fitting into the cavity of the crown ether is located at the glycyl part, no steric hindrance can be expected from branched alkyl groups. A relationship between the molecular mass of glycyldipeptides and their separation factor α was demonstrated.

Acknowledgement

References

[1] T.J. Ward, Anal. Chem., 66 (1994) A633.
[2] M.M. Rogan, K.D. Altria and D.M. Goodall, Chirality, 6 (1994) 25.
[3] M. Novotny, H. Soioni and M. Stafansson, Anal. Chem., 66 (1994) A646.
[4] G. Dotsevi, E. Soga and D.J. Cram, J. Am. Chem. Soc., 97 (1975) 1259.
[5] E.P. Kyba, J.M. Timko, L.J. Kaplan, F. de Jong, G.W. Gokel and D.J. Cram, J. Am. Chem. Soc, 100 (1978) 4555.
[6] S. Motellier and I.W. Wainer, J. Chromatogr., 516 (1990) 365.
[7] M. Hilton and D.W. Armstrong, J. Liq. Chromatogr., 14 (1991) 3673.
[8] M. Hilton and D.W. Armstrong, J. Liq. Chromatogr., 14 (1991) 9.
[9] P.M. Uddvarhelyi and J.C. Watkins, Chirality, 2 (1990) 200.
[10] T. Shinbo, T. Yamaguchi, K. Nishimura and M. Sugiura, J. Chromatogr., 405 (1987) 145.
[11] R. Kuhn, F. Stoecklin and F. Erni, Chromatographia, 33 (1992) 32.
[12] R. Kuhn, C. Steinmetz, T. Bereuter, P. Haas and F. Erni, J. Chromatogr., 666 (1994) 367.
[13] R. Kuhn and F. Erni, T. Bereuter and J. Häusler, Anal. Chem., 64 (1992) 2815.
[14] E. Höhne, G.-J. Krauss and G. Gübitz, J. High Resolut. Chromatogr., 15 (1992) 698.
[15] G. Sosnovsky, I. Prakash and N.U.M. Rao, J. Pharm. Sci., 82 (1993) 1.
[16] G. Sersa, S. Novakovic and A. Stalc, Mol. Biother. 4 (1993) 188.
[17] C.J. Pedersen, J. Am. Chem. Soc., 89 (1967) 2495 and 7017.
[18] C.J. Pedersen, J. Inclus. Phenom., 8 (1988) 337.
[19] G. Gübitz, Chromatographia, 30 (1990) 555.
[20] J.M. Dietrich, J.M. Lehn and J.P. Sauvage, Tetrahedron Lett., (1969) 2885.
[21] J.M. Lehn, J. Inclus. Phenom. 8 (1988) 351.
[22] S.A.C. Wren and R.C. Rowe, J. Chromatogr., 603 (1992) 235.

Enantiomeric separation by capillary electrophoresis using a soluble neutral β-cyclodextrin polymer

Benno A. Ingelse[a,1], Frans M. Everaerts[b], Claudia Desiderio[a], Salvatore Fanali[a,*]

[a]Istituto di Cromatografia del CNR, Area della Ricerca di Roma, P.O. Box 10, 00016 Monterotondo Scalo (Rome), Italy
[b]Laboratory of Instrumental Analysis, Department of Chemistry, Eindhoven University of Technology, P.O. Box 513, 5600 MB Eindhoven, Netherlands

Abstract

Enantiomers of several racemic basic compounds of pharmaceutical interest and three tryptophan derivatives were investigated by capillary electrophoresis employing a soluble β-cyclodextrin polymer and native β-cyclodextrin. The effects of the concentration of the polymer added to the background electrolyte and of the pH of the buffer on the effective mobility and resolution of the studied compounds were examined. The β-cyclodextrin polymer showed a higher stereoselectivity than the parent β-cyclodextrin. Enantioselectivity and resolution were influenced by the concentration of the β-cyclodextrin polymer and the background electrolyte. A pH study, carried out in the pH range 2.7–6, showed that an increase in pH caused a general decrease in both resolution and selectivity. The best results for the enantiomeric separation of the basic compounds studied were obtained at pH 2.7.

1. Introduction

The development of new chiral substances, especially in the pharmaceutical field, places increasing demands on analytical methods for the separation of these kinds of isomers for, e.g., the chiral purity control of drugs and pharmacokinetic studies.

Enantiomers are optical isomers possessing similar physico-chemical properties and thus difficult to separate from each other. Their separation can be obtained using a chiral environment that interacts with the enantiomers either before or during the separation process forming stable diastereoisomers or labile diastereomeric complexes, respectively.

Analytical methods used so far for the enantiomers separation include high-performance liquid chromatography (HPLC) [1–3], thin-layer chromatography (TLC) [4], gas chromatography (GC) [5] and capillary electrophoresis (CE) [6–17].

CE is a recent separation technique that allows rapid separations to be performed with high resolution and high efficiency, and requiring only

---

* Corresponding author.
[1] Permanent address: Laboratory of Instrumental Analysis, Department of Chemistry, Eindhoven University of Technology, P.O. Box 513, 5600 MB Eindhoven, Netherlands.

small amounts of buffer and sample. Among the chiral selectors used for the resolution of enantiomers by CE, buffer additives such as chelator–metal complexes [16], chiral crown ethers [10–12], proteins [8,9,13], bile salts [14,15], cyclodextrins (CDs) and their derivatives [6,7,18,19], etc., have been widely applied.

Native CDs (α, β and γ) and their derivatives (methylated, carboxymethylated, methylamino, hydroxypropylated, etc.) have been successfully utilized in many applications [6,7,18,19]. These chiral selectors have been mainly used in capillary zone electrophoresis (CZE) and in several instances the combination of CDs and micellar electrokinetic chromatography (CD–MEKC) allowed the enantiomeric resolution of neutral compounds.

When CDs or their derivatives are used, the chiral resolution is based on selective complexation with analytes. Hydrophobic interactions between analytes and the CD cavity and hydrogen bonds with hydroxy (or modified) groups on the CD rim can lead to the formation of labile diastereoisomeric complexes with different stability constants. The most stable complex formed moves with a lower effective mobility.

Linear or cross-linked polymers have been mainly used in CE as sieving media for improving the selectivity of the separation of high-molecular-mass compounds of biological origin such as proteins and nucleic acids [20]. Recently we used a chargeable β-cyclodextrin polymer for the enantiomeric resolution of several basic compounds [21] and Nishi et al. [22] studied the enantiomeric resolution of trimetoquinol hydrochloride and related substances using uncharged β-cyclodextrin polymer.

In this work, we investigated the effect of a soluble uncharged β-cyclodextrin polymer for the separation of enantiomers of several basic compounds by CE. The effect of the chiral polymer concentration on the effective mobility, the resolution and the selectivity was investigated. Further, the effects of the pH and of the concentration of the background electrolyte were also studied.

2. Experimental

2.1. Chemicals

Soluble β-cyclodextrin polymer (EP-β-CD) was purchased from Cyclolab (Budapest, Hungary), β-cyclodextrin from Fluka (Buchs, Switzerland), sodium hydroxide, acetic acid, phosphoric acid, sodium dihydrogenphosphate and citric acid from Carlo Erba (Milan, Italy) and standards of analytical-reagent grade from Sigma (St. Louis, MO, USA). Doubly distilled water (Menichelli, Rome, Italy) was used to prepare all solutions.

The background electrolyte (BGE) containing EP-β-CD was filtered by using nylon filters of 0.45 μm pore size (Lida, Kenasha, WI, USA). Stock solutions of standard samples (10^{-4} M) were prepared and stored at 4°C. The concentration of injected racemic mixtures was 10^{-5} M for propranolol, terbutaline, isoproterenol and ester tryptophan derivatives and that of all other standards was $5 \cdot 10^{-5}$ M. For the electrophoretic experiments performed with the laboratory-made electrophoresis apparatus, 25 mM of the following buffers were used: phosphate, pH 2.7; citrate, pH 3.5; acetate, pH 4.5; and phosphate, pH 6.0.

2.2. Apparatus

Experiments were carried out using a laboratory-made electrophoresis apparatus. The electrode chamber in which the detection end of the capillary was connected to a refilling block were as described previously [17]. The electrophoretic separations were performed at room temperature in untreated fused-silica capillaries obtained from Supelco (Bellefonte, PA, USA), 560 mm × 50 μm I.D., with an effective length of 360 mm. The apparatus included a Spellman (Rockford, IL, USA) CZE1000R power supply and a Spectra FOCUS variable-wavelength UV detector (Thermo-Separation, San Jose, CA, USA). The detector was operated at 206 nm, and connected to a ChromJet integrator (Thermo-Separation). Before applying the sample, the capillary was

filled with the background electroyte (BGE) containing the polymer. No chiral polymer was present in the electrode chambers. The injection of the sample was performed hydrodynamically at the anodic end of the capillary for 10 s; the difference between the liquid level in the electrode chamber and the sample vial was set to 20 cm. The applied voltage was 15 kV. The electroosmotic flow was measured injecting benzyl alcohol ($10^{-4}M$).

The experiments for the study of the effect of the concentration of BGE on the resolution of enantiomers of bupivacaine were performed in a P/ACE 2200 capillary electrophoresis system (Beckman, Fullerton, CA, USA) with UV detection at 214 nm. A fused-silica capillary (Microquartz, Munich, Germany), 370 mm $\times$ 0.05 mm I.D., effective length 300 mm, was used for the experiments and the cartridge temperature was 20°C.

3. Results and discussion

Different basic compounds of pharmaceutical interest, namely adrenergic agonists (ephedrine, epinephrine, norephinephrine, isoproterenol and terbutaline), β-adrenergic blockers (atenolol, metoprolol, oxprenolol and propranolol), anaesthetics (ketamine and bupivacaine), an anorexic (norephedrine) and tryptophan methyl, ethyl and butyl esters were selected for the electrophoretic experiments. Their structures are shown in Fig. 1.

The racemic mixtures of the analytes were run in phosphate buffer at pH 2.7 in the absence of chiral additive and owing to the protonation of nitrogen atom they moved towards the cathode; as expected, no enantiomeric separation was obtained.

For the study of enantiomer resolution, the phosphate buffer was supplemented with different amounts of β-cyclodextrin polymer (for the composition, see Table 1).

Under the experimental operating conditions (pH 2.7) the electroosmotic flow was relatively low compared with the effective mobility of the

cationic samples and thus the chiral selector acted as a quasi-stationary phase.

The effective mobility was calculated using the equation

$$\mu_{eff} = \mu_{app} - \mu_{eof} \tag{1}$$

where μ is the mobility and the subscripts eff, app and eof stand for effective, apparent and electroosmotic, respectively.

The selectivity (S) and resolution (R) were calculated using the following equations:

$$S = \Delta\mu/\mu_m \tag{2}$$

$$R = 2(t_2 - t_1)/(w_2 + w_1) \tag{3}$$

where $\Delta\mu$ is the difference in effective mobility, μ_m the median mobility $[(\mu_2 + \mu_1)/2]$, t the migration time, w the peak width at the baseline and subscripts 1 and 2 represent the two enantiomers.

Fig. 2 shows the effect of the concentration of β-cyclodextrin polymer added to the BGE at pH 2.7 on the effective mobility of racemic β-adrenergic blockers. An increase in the concentration of the complexing additive leads to a general decrease in the effective mobility for all the compounds studied owing to the complexation with the polymer. The analytes formed labile diastereomers during the electrophoretic runs, causing a decrease in the velocity depending on the stability constant of the complex formed. The complexation power of the modified CD used (10–50 mg/ml) decreased in the order propranolol >metoprolol >atenolol >oxprenolol. Wren and Rowe [23] proposed to relate the interaction between β-blockers and cyclodextrin to the hydrophobicity of the analytes. This means that the most hydrophobic compound has the strongest interaction with the hydrophobic cavity of the CD. The influence of the hydrophobicity of the analytes on the inclusion complexation is also illustrated by our results obtained for methyl, ethyl and butyl esters of tryptophan. Fig. 3 shows the effect of the concentration of β-cyclodextrin polymer on the effective mobility of these tryptophan esters. The complexation was very strong for the most hy-
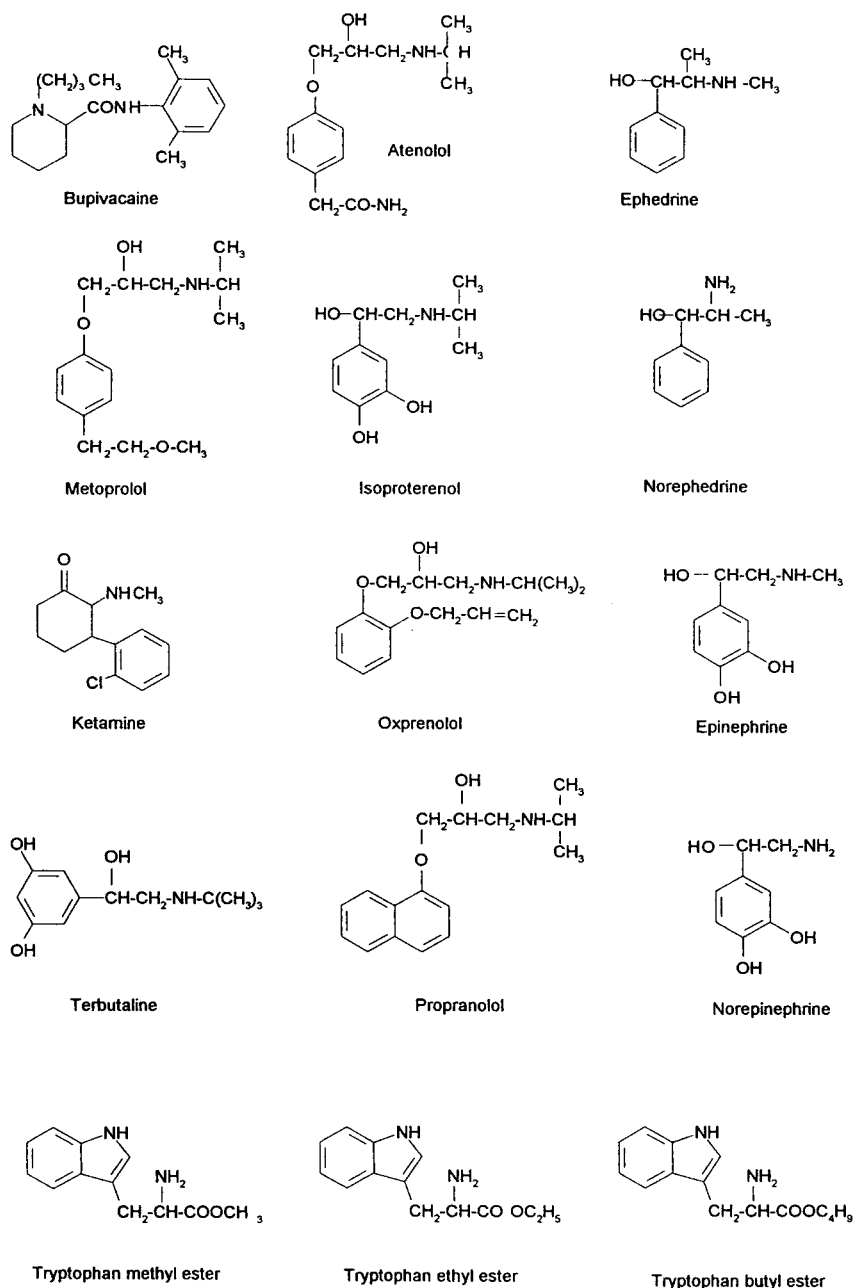
Fig. 1. Structures of the compounds studied.

drophobic compound (butyl derivative). Also in this case an increase in the concentration of the complexing additive caused a general decrease in effective mobility for all three esters. A similar effect was obtained for the two anaesthetics studied, where bupivacaine was more complexed

Table 1
Main properties of β-cyclodextrin polymer

Molecular mass	3000–5000
Solubility in water	>40%
CD content	50–60%
Cross-linking	Epichlorohydrin

Fig. 3. Dependence of the effective mobility of three trypto-phan esters on the β-cyclodextrin polymer concentration. Experimental conditions as in Fig. 2.

than ketamine (results not shown). Finally, the electrophoretic study of adrenergic agonists confirmed the importance of the type and concentration of the CD on the inclusion complexation. In fact, the β-cyclodextrin polymer was found to be a good complexing additive for all the compounds studied. Also in this case an increase in concentration of the modified CD caused a decrease in the effective mobility.

The complexation power at 15 mg/ml of EP-β-CD was found to decrease in the order ter-butaline >epinephrine >norepinephrine >ephe-drine >isoproterenol; an increase in the concentration of the complexing additive caused a reversal of complexing power, e.g., at 50 mg/ml isoproterenol was more complexed than epi-nephrine but less so than terbutaline.

3.1. Effect of concentration of β-cyclodextrin polymer on selectivity and chiral recognition

For the study of chiral recognition, the ana-
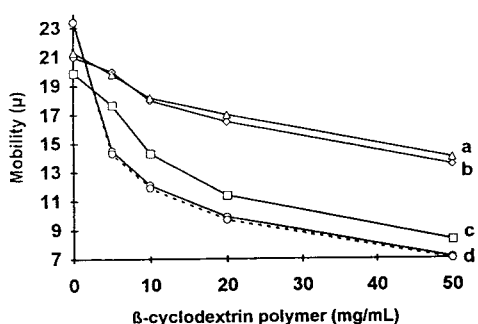
Fig. 2. Effect of β-cyclodextrin polymer concentration on the effective mobility ($\mu \times 10^5$ cm^2 V^{-1} s^{-1}) of β-adrenergic blockers: (a) oxprenolol; (b) atenolol; (c) metoprolol; (d) propranolol). Capillary, 560 mm $\times$ 0.05 mm I.D. (effective length 360 mm), uncoated; applied voltage, 12 kV; background electrolyte, 25 mM phosphate buffer (pH 2.7); β-cyclodextrin polymer was present into the capillary only. For other conditions, see text.

lytes were injected using a BGE at pH 2.7 supplemented with different amounts of β-cyclodextrin polymer in the range 0–50 mg/ml. Resolution of the racemic mixtures into their enantiomers was obtained for terbutaline, iso-proterenol, epinephrine, propranolol and methyl, ethyl and butyl esters of tryptophan ($R \geqslant$ 1). Norepinephrine was only partly resolved ($R = 0.6$ at 50 mg/ml of chiral additive) and no resolution was recorded in the concentration range of CD studied for ephedrine, norephe-drine, ketamine, bupivacaine, atenolol, meto-prolol and oxprenolol.

Fig. 4a and b show the effect of the concentration of EP-β-CD on the resolution factor (R) and selectivity (S), respectively, for propran-olol and butyl, ethyl and methyl esters of trypto-phan.

An increase in the concentration of β-cyclodextrin polymer added to the BGE at pH 2.7 led to a general increase in resolution and selectivity. Among the β-blockers studied, pro-pranolol, the most hydrophobic analyte, was the only to be resolved into its enantiomers even at a relatively low concentration of chiral additive (0.5 mg/ml); Maximum of resolution ($R = 1.8$) and selectivity ($S = 0.0204$) were obtained when 20 mg/ml of chiral agent were used. These data confirm the previous finding [24] and the theoretical model discussed by Wren and Rowe [25] concerning maximum resolution at a certain concentration of chiral selector.
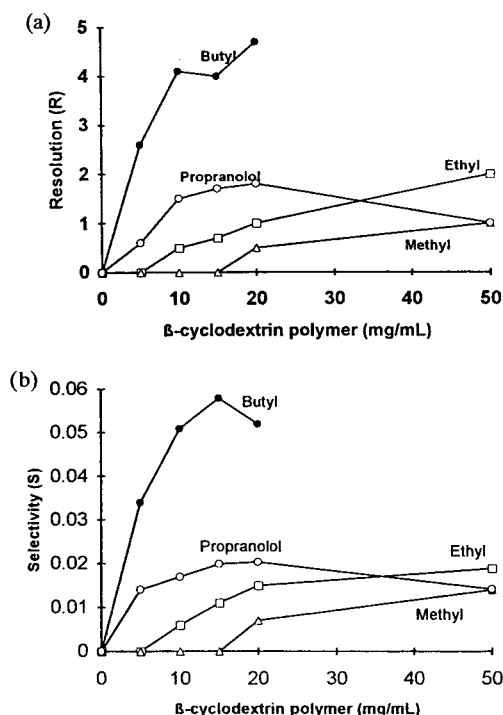
Fig. 4. Effect of the concentration of β-cyclodextrin polymer on (a) resolution, R, and (b) selectivity, S, for three tryptophan esters and propranolol. Experimental conditions as in Fig. 2.

Fig. 5. Electropherograms for the enantiomeric separation of racemic mixtures of (a) butyl, (b) ethyl and (c) methyl esters of tryptophan. Background electrolyte, 25 mM phosphate buffer (pH 2.7) containing 20 mg/ml β-cyclodextrin polymer. Other experimental conditions as in Fig. 2.

An interesting behaviour was found for tryptophan esters, where the resolving power of β-cyclodextrin polymer decreased in the order butyl >ethyl >methyl. The resolution and selectivity increased with increasing concentration of the chiral selector for ethyl and methyl tryptophan derivatives, whereas for the butyl derivative S increased up to 15 mg/ml and then decreased; the resolution showed similar behaviour to that for the other esters with a slight decrease in R at 15 mg/ml. Fig. 5 shows the electropherograms for the enantiomeric separation of racemic butyl, ethyl and methyl esters of tryptophan.

The length of the ester chain had a strong influence on the enantioselectivity. In order to explain the strong complexation and/or the strong enantioselectivity of the racemic butyl ester with the chiral polymer, we have to consider the hydrophobic interaction of the butyl chain with the inside and/or the outside of the CD cavity. Further, the inclusion complex formed is stabilized by stereoselective bonds (hydrogen) between the amino groups of the analyte and hydroxyl groups of the CD.

The effect of the concentration of EP-β-CD on resolution and selectivity is also demonstrated for the enantiomeric separation of adrenergic agonists and anaesthetic compounds. Fig. 6a and b show the effect of the concentration of EP-β-CD on the resolution of norephedrine, norepinephrine, epinephrine, terbutaline and isoproterenol and the selectivity for terbutaline and propranolol, respectively. Both parameters increased with increase in the concentration of the chiral selector added to the BGE, except for norephedrine, which was not resolved at all under the operating conditions (0.50 mg/ml of polymer). The resolving power of EP-β-CD was found to decrease in the order terbutaline >isoproterenol >epinephrine >norepinephrine >norephedrine.

As an example, the electropherograms in Fig. 7 demonstrate the different resolving power of EP-β-CD on the enantiomeric separation of racemic nor-epinephrine, isoproterenol and propranolol; the first was spiked with the (S)-(−)-isomer.

In order to explain the high resolving power of the chiral polymer towards terbutaline, we could
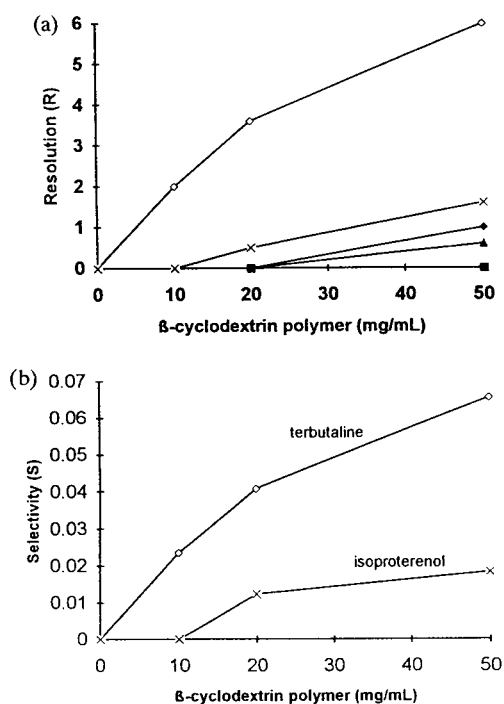
Fig. 6. Dependence of (a) resolution, R, of (■) norephedrine, (▲) norepinephrine, (◆) epinephrine, (×) isoproterenol and (◇) terbutaline and (b) selectivity, S, of terbutaline and isoproterenol on the concentration of β-cyclodextrin polymer. Experimental conditions as in Fig. 2.

remark that the substituent groups on the asymmetric carbons of terbutaline had a strong influence on the enantiorecognition mechanism.
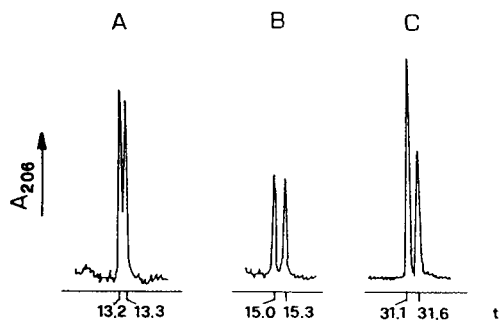
Fig. 7. Electropherograms for the enantiomeric separation of (A) norepinephrine, (B) isoproterenol and (C) propranolol [spiked with (S)-(−)-isomer]. Background electrolyte, 25 mM phosphate buffer (pH 2.7) containing 50 mg/ml β-cyclodextrin polymer. Other experimental conditions as in Fig. 2.

Even though the chiral polymer proved to be a good complexing agent towards the two anaesthetics studied, no enantiomeric resolution was obtained for ketamine and bupivacaine at EP-β-CD concentrations ≤50 mg/ml.

Considering the high solubility (>40%, w/v) of the chiral polymer and the effect of its concentration on resolution, we tried to increase its content to 100, 150 and 200 mg/ml for the enantiomeric separation of those analytes not or poorly resolved in this study. No resolution of metoprolol, atenolol and ephedrine was obtained, norephedrine showed $R = 0.5$ at 100 mg/ml and no improvement in resolution was found at higher concentrations of the chiral selector. Bupivacaine was partly resolved into its enantiomers only at 200 mg/ml of EP-β-CD with $R = 0.5$. Good enantiomeric separation was obtained for ketamine and norepinephrine at 100 mg/ml ($R = 1$).

The migration order of enantiomers was verified for propranol, epinephrine, norepinephrine, isoproterenol and methyl and ethyl esters of tryptophan by spiking the racemic mixtures with the separated optical isomers (commercially available) and performing electrophoresis experiments. The L-isomers of tryptophan esters moved faster than the D-forms. For the other analytes, the (−)-enantiomers moved faster than the (+)-enantiomers, indicating that the (+)-antipodes formed complexes with higher stability constants than their isomers.

The enantiomeric separation power of EP-β-CD was compared with that of native β-CD. The amount of cyclodextrins units per milligram of polymer was calculated according to the specification of the manufacturer (CD content 58.2%, w/w) in order to compare the concentration of EP-β-CD with that of the parent β-CD. Consequently, we compared the resolution of propranolol, terbutaline, butyl ester of tryptophan and epinephrine obtained at 2.5, 5, 10 and 20 mM β-CD with the resolution obtained at 5, 10, 20 and 50 mg/ml [50 mg/ml of EP-β-CD should be compared with 25 mM β-CD (aqueous solutions of <20 mM can be prepared)].

Propranolol and the butyl ester of tryptophan were not resolved at any concentration of β-CD,

whereas epinephrine showed $R = 0.3$ at 20 mM. The three analytes were baseline separated into their enantiomers with a polymer containing less β-CD (propranolol, butyl ester of tryptophan and epinephrine at 10, 5 and 50 mg/ml). Only for terbutaline was the resolving power of native CD greater than that of the polymer; at 2.5 mM β-CD R was 1.26 whereas 5 mg/ml EP-β-CD gave $R = 0.85$. The higher resolving power of the chiral polymer can also be supported by previous results obtained for the methyl ester of tryptophan, which was not resolved with β-CD [26].

The high resolution capability of EP-β-CD toward the compounds studied cannot be interpreted by considering only parameters such as the concentration of CD, hydrophobicity and structure of the analytes; the structure of the chiral selector also has to be taken into account. In fact, the polymerization changes the properties of β-CD units, producing a more rigid and different conformation in comparison with the native CD. Further, the aliphatic chain (due to epichlorohydrin) is probably a source of hydrophobic interactions with the analytes and improves the chiral recognition. Finally, we must also consider the cooperation of two CD moieties of the polymer for inclusion complexation with analytes possessing more than one guest part in their structure [27].

3.2. Effect of pH of BGE on resolution

The effect of the BGE pH on the resolution was investigated using for the electrophoretic experiments four different buffers at pH 2.7, 3.5, 4.5 and 6.0 and containing 10 mg/ml of EP-β-CD. Fig. 8 shows the effect of the pH of the BGE on the resolution of the butyl of ester tryptophan, terbutaline and propranolol. An increase in buffer pH led to a decrease in the resolution factor for all the compounds studied, except for terbutaline, which showed a maximum of R at pH 3.5. One explanation for the decrease in resolution with increasing pH of the BGE is probably the increase in the electroosmotic flow causing a higher apparent mobility of the basic analytes and thus a shorter time of interaction with the chiral selector [28]. It is noteworthy that
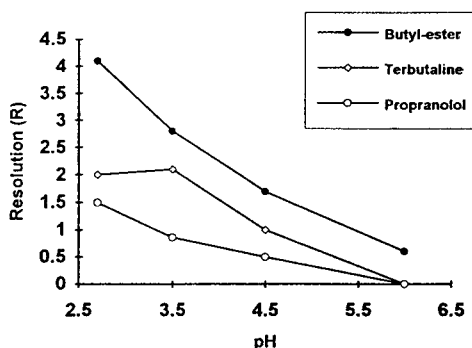
Fig. 8. Influence of the pH of the background electrolyte on the resolution of (●) the butyl ester of tryptophan (◇) terbutaline and (○) propranolol.

at pH 6 the polymer showed interactions with the capillary wall; in some instances the capillary was blocked and the problem could be eliminated by washing with methanol.

3.3. Effect of buffer concentration on resolution of enantiomers

The experiments for the study of the effect of buffer concentration on enantiomeric resolution were carried out on bupivacaine using a thermostated capillary cartridge at 20°C in order to reduce the Joule heat, which can strongly in-
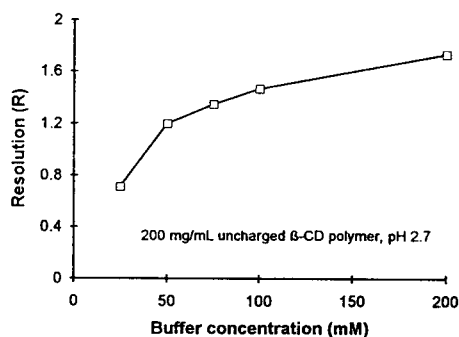
Fig. 9. Dependence of the resolution, R, of bupivacaine on the concentration of background electrolyte. Apparatus, P/ACE 2200; capillary, 370 (300) mm × 0.05 mm I.D.; applied voltage, 15 kV; temperature of cartridge, 20°C; background electrolyte, phosphate buffer (pH 2.7) containing 200 mg/ml β-cyclodextrin polymer; pressure injection at 0.5 p.s.i. × 10 s of 5×10^{-5} M racemic bupivacaine.
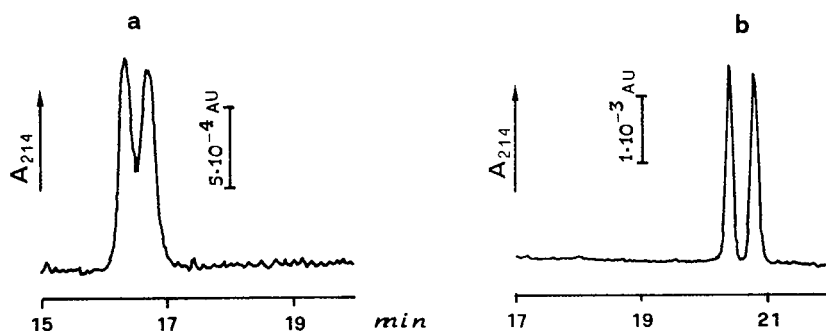
Fig. 10. Electropherograms for racemic bupivacaine at two different concentrations of the background electrolyte. Background electrolyte, phosphate buffer (pH 2.7), (a) 25 and (b) 200 mM, containing 200 mg/ml β-cyclodextrin polymer. Other experimental conditions as in Fig. 9.

fluence the efficiency of the separation. An increase in the buffer concentration caused an increase in the migration time of bupivacaine owing to the influence of the higher ionic strength of the electrophoretic media.

Fig. 9 shows the effect of the buffer concentration, containing 200 mg/ml of β-CD polymer on the resolution of racemic bupivacaine into its enantiomers. Baseline separation of the two antipodes ($R = 1.2$) was obtained at 50 mM phosphate buffer and increased to 1.76 when the buffer concentration was 200 mM. Fig. 10 shows the electropherograms of the enantiomeric separation of bupivacaine at 25 and 200 mM phosphate buffer containing 200 mg/ml β-cyclodextrin polymer.

4. Conclusions

The use of uncharged β-cyclodextrin polymer as a chiral selector in CE allows the enantio-separation of several classes of compounds (β-blockers, α-adrenergic agonists, β-adrenergic agonists, tryptophan esters and anaesthetics).

The complexation, resolution and selectivity are all influenced by the concentration of the β-cyclodextrin polymer added to the BGE. Generally, the higher the concentration of the chiral additive, the greater is the decrease in mobility and the increase in selectivity and resolution, except for propranolol, which shows a maximum of S and R at 20 mg/ml EP-β-CD.

The solubility of the chiral polymer in water–buffer mixtures is relatively high in comparison with that of the native β-CD. The method is cheap because only a few microlitres of chiral polymer solution are used for the electrophoretic experiments (the chiral additive was present only in the capillary).

Further studies will be carried out in order to verify the usefulness of the uncharged chiral polymer for the resolution of other racemic mixtures into their enantiomers and the influence of organic modifiers on the enantioselectivity.

References

[1] J. Debowski, D. Sybilska and J. Jurczak, J. Chromatogr., 282 (1983) 83.
[2] T.J. Ward and D.W. Armstrong, J. Liq. Chromatogr., 9 (1986) 407.
[3] G. Blaschke, J. Liq. Chromatogr., 9 (1986) 341.
[4] D.W. Armstrong, Faulkner, Jr., and S.M. Han, J. Chromatogr., 452 (1988) 323.
[5] C.P. Granville, B. Gehrcke, W.A. Konig and I.W. Wainer, J. Chromatogr., 622 (1993) 21.
[6] T. Schmitt and H. Engelhardt, Chromatographia, 37 (1993) 475.
[7] A. Nardi, A. Eliseev, P. Bocek and S. Fanali, J. Chromatogr., 638 (1993) 247.
[8] R. Vespalec, V. Sustacek and P. Bocek, J. Chromatogr., 638 (1993) 255.
[9] L. Valtcheva, J. Mohammed, G. Pettersson and S. Hjerten, J. Chromatogr., 638 (1993) 263.
[10] R. Kuhn, F. Stoecklin and F. Erni, Chromatographia, 33 (1992) 32.

[11] R. Kuhn and S. Hoffstetter-Kuhn, Chromatographia, 34 (1992) 505.

[12] E. Hohne, G.J. Krauss and G. Gubitz, J. High Resolut. Chromatogr., 15 (1992) 698.

[13] S. Busch, J.C. Kraak and H. Poppe, J. Chromatogr., 635 (1993) 119.

[14] H. Nishi, T. Fukuyama, M. Matsuo and S. Terabe, J. Microcol. Sep., 1 (1989) 234.

[15] S. Terabe, H. Shibata and Y. Miyashita, J. Chromatogr., 480 (1989) 403.

[16] P. Gozel, E. Gassmann, H. Michelsen and R.N. Zare, Anal. Chem., 59 (1987) 44.

[17] S. Fanali, L. Ossicini, F. Foret and P. Bocek, J. Microcol. Sep., 1 (1989) 190.

[18] A. Guttman, A. Paulus, A.S. Cohen, N. Grinberg and B.L. Karger, J. Chromatogr., 448 (1988) 41.

[19] S. Fanali, J. Chromatogr., 474 (1989) 441.

[20] F. Foret, L. Krivankova and P. Bocek, Capillary Zone Electrophoresis, VCH, Weinheim, 1993, pp. 74–79.

[21] Z. Aturki and S. Fanali, J. Chromatogr., 680 (1994) 137.

[22] H. Nishi, K. Nakamura, H. Nakai and T. Sato, J. Chromatogr., 678 (1994) 333.

[23] S.A.C. Wren and R.C. Rowe, J. Chromatogr., 609 (1992) 363.

[24] S. Fanali, J. Chromatogr., 545 (1991) 437.

[25] S.A.C. Wren and R.C. Rowe, J. Chromatogr., 603 (1992) 235.

[26] A. Nardi, L. Ossicini and S. Fanali, Chirality, 4 (1992) 56.

[27] A. Harada, M. Furue and S. Nozakura, Polym. J. 13 (1981) 777.

[28] S.A.C. Wren, J. Chromatogr., 636 (1993) 57.

Capillary zone electrophoresis of serum proteins: study of separation variables

Vladislav Dolník

Institute of Analytical Chemistry, Academy of Sciences of the Czech Republic, Veveří 97, CZ-61142 Brno, Czech Republic

Abstract

Electrophoresis of serum proteins is one of the traditional applications of zone electrophoresis. Whereas electrophoresis in supporting media uses usually 5,5′-diethylbarbiturate at pH 8.6 as the buffer, in capillary zone electrophoresis with on-line UV detection, this electrolyte is of little use because of its high UV absorbance. For that reason, a number of operational electrolytes differing in composition were tested for use in capillary electrophoresis of serum proteins. The influence of the pK_A of co-ions and counter ions and the concentration of the operational electrolyte was examined. If 0.1 M methylglucamine–0.1 M ϵ-aminocaproic acid or 0.1 M methylglucamine, –0.1 M γ-aminobutyric acid is used as the operational electrolyte, capillary electrophoresis separates serum proteins into more than ten zones.

1. Introduction

Electrophoresis of serum proteins has been among the classical methods in clinical chemistry for many years. Usually paper, agar or cellulose acetate served as the separation bed, and serum proteins were separated into about five fractions: albumin, α_1-globulin, α_2-globulin, β-globulin and γ-globulin. More than 20 years ago, agarose brought a significant improvement, enabling more protein zones to be separated [1,2]. The method has since been modified [3–9] and the separated zones were assigned to the individual proteins: prealbumin, albumin, α_1-lipoprotein, α_1-antitrypsin, α_2-macroglobulin, haptoglobulin, β-lipoprotein, transferrin, C_3-complement and γ-globulin [2,5,7]. The clinical interpretation of electropherograms is based on variation in their content [6,7,10,11]. In all these methods, veronal (5,5′-diethylbarbiturate) buffer has been used. Since this is a US Drug Enforcement Adminis-

tration controlled drug, Monthony et al. [12] replaced veronal with Tricine and proposed the Tris–Tricine buffer for the electrophoresis of serum proteins. However, with this newly formulated buffer, α_1-fraction co-migrated with albumin in agarose electrophoresis. The better resolution of α_1-fraction and albumin in the barbital buffer seems to be due to the formation of a veronal–albumin complex and this complex exhibits higher mobility than albumin itself because of the higher charge caused by ionization of veronal. An increase in the ionic strength of the buffer by adding NaCl helps to separate albumin and α_1-fraction; however, addition of salicylate or hippurate, which also form complexes with serum albumin, leads to a more pronounced effect [13].

Several papers have been devoted to the electrophoresis of serum proteins in capillary format with on-line detection [14–19]. Whereas Gordon et al. [14] and Reif et al. [19] used

sodium borate as the operational electrolyte, Chen and co-workers [15–18] did not specify the composition of their electrolyte and used the description Beckman protein analysis buffer.

This paper shows the effect of some separation variables, especially the pK_A of both the co-ion and counter ion, on the separation of serum proteins by capillary electrophoresis.

2. Experimental

Bis-Tris and Tricine were purchased from Fluka (Buchs, Switzerland), vinylmagnesium bromide from Aldrich (Milwaukee, WI, USA) and γ-aminobutyric acid, ϵ-aminocaproic acid and N-methyl-D-glucamine from Sigma (St. Louis, MO, USA). All other chemicals were purchased from Lachema (Brno, Czech Republic).

Analyses were performed with a Crystal CE System Model 310 (ATI Unicam, Cambridge, UK) with UV detection using a Spectra 100 variable-wavelength detector (Thermo Separation Products, Palo Alto, CA, USA) at 200 nm. The data were collected by using software 4880 (ATI Unicam).

A fused-silica capillary (J&W Scientific, Fulsom, CA, USA) of dimensions 75 μm I.D. and 360 μm O.D. was used. The total length was usually 55 cm with 45 cm to the detection window. The detection cell was made by cutting off ca. 1 mm of the polyimide layer [20]. In some experiments, coated capillaries were used where the coating was made with polyacrylamide after vinylation of the capillary surface with vinylmagnesium bromide [21].

Whole blood was drawn from healthy volunteers (members of this laboratory) and used to prepare serum. Serum was used immediately after centrifugation; however, in some cases it was kept at -26°C before its use.

3. Results and discussion

The aim of this work was the experimental testing of a series of various operational elec-

trolytes. The particular zones were identified according to the generally known migration order of serum proteins in agarose gels. Analysis of serum proteins from different individuals was helpful in this respect. Staining of lipoproteins with Sudan Black with subsequent electrophoresis and detection at 570 nm showed only limited possibilities for the identification of lipoproteins. If the fractions were resolved into several subfractions, α_1-antitrypsin, α_2-macroglobulin and transferrin were considered as the main components of α_1-globulin, α_2-globulin and β-globulin, respectively, and their mobilities were used to express the mobility of the whole fraction. (Proteins behave as anions under given conditions and the negative values of the mobility correspond to this fact. However, for sake of simplicity, "higher mobility" here means a higher absolute value of mobility.) Substances differing in pK_A suitable as both counter ion and co-ion were sought. Finally, the co-ions were chosen according to their pK_A to cover the pH range which preliminary experiments had shown to be the most important, i.e., $pK_A \approx 8$–11. Three counter ions were used in these experiments: Na^+, Tris and methylglucamine. The pK_A values of the substances in question, and also the pH of the operational electrolytes, which were prepared by simple mixing of weighed substances without any further pH adjustments, are given in Table 1.

In the first series of experiments, operational electrolytes containing 50 mM NaOH and 0.1 M co-ion were used. As NaOH is a strong base, the pH of the electrolyte is equal to the pK_A value of the individual co-ions. The dependence of absolute value of mobility of the main serum protein fractions on the pK_A of the co-ions is given in Fig. 1: all fractions of serum proteins migrate with a higher velocity with increasing pK_A of the co-ion, i.e., with increasing pH of the operational electrolyte. The separation of the albumin–α_1-fraction pair is crucial, as pointed earlier. With increasing pH, the mobility difference between albumin and α_1-fraction increases, whereas the β-globulin and α_2-globulin mobility window is reduced even when the β-globulin–α_2-globulin separation is not deteriorated.

Table 1
pH of operational electrolytes

Component	Na$^+$	Tris ($pK_A = 8.1$)	MGA ($pK_A = 9.9$)
Tricine ($pK_A = 8.1$)	8.12	8.06	9.10
Asparagine ($pK_A = 8.72$)	8.91	8.41	9.47
Boric acid ($pK_A = 9.24$)	9.24	8.17	9.20
Glycine ($pK_A = 9.78$)	9.86	8.84	9.92
GABA ($pK_A = 10.46$)	10.58	9.27	10.26
EACA ($pK_A = 10.80$)	10.93	9.36	10.62

Fig. 2 shows the sample plot when the counter ion Na$^+$ is replaced with Tris. If an equimolar mixture of Tris and the appropriate acid is used, the pH of the operational electrolyte is theoretically equal to the mean of the pK_As of Tris and the co-ion, as Tris is a weak base. The ionization also influences the ionic strength of the solution. That is why it is more reasonable to plot mobilities vs. pK_a instead of the traditional pH. The real values of pH for the prepared operational electrolytes are given in Table 1. We can observe similar effects as with electrolytes containing
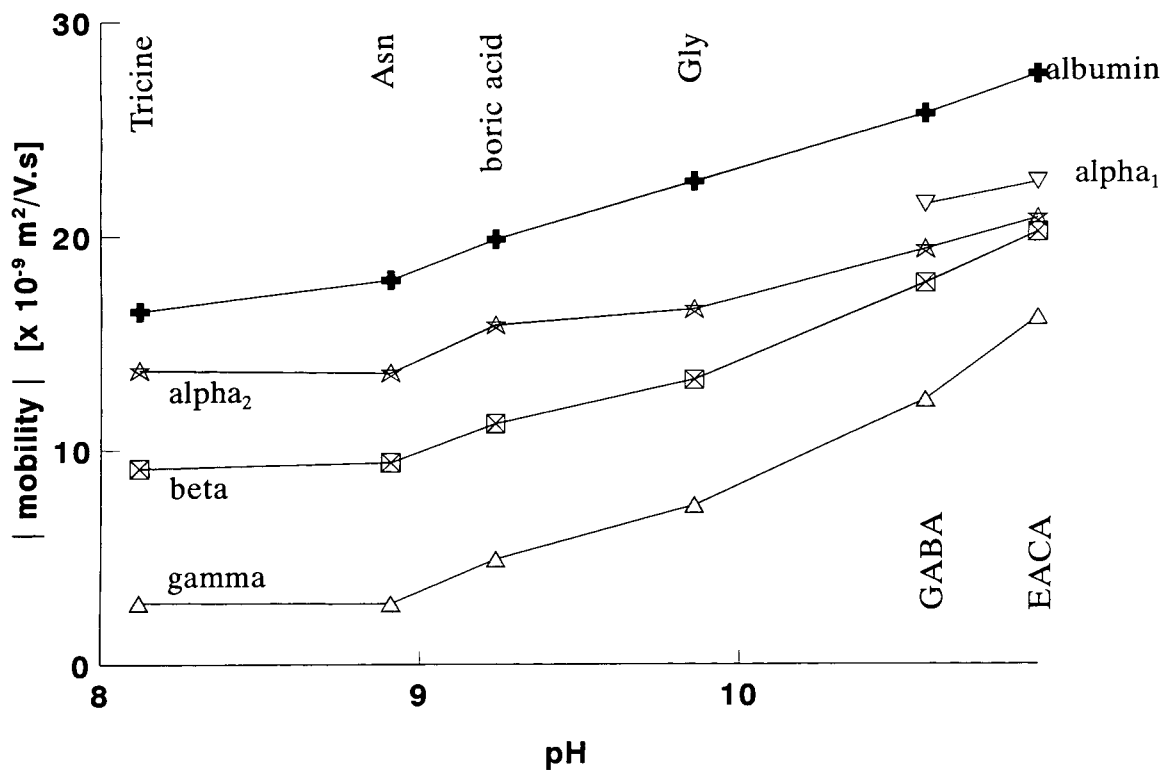
Fig. 1. Effect of pH on the mobility of serum proteins. Experimental conditions: uncoated capillary, 75 μm I.D. $\times$ 360 μm O.D., total length 550 mm, effective length 450 mm; operational electrolyte, 50 mM NaOH–100 mM co-ion; voltage, 11 kV. Fourfold diluted serum sampled with a pressure of 10 mbar for 3 s.
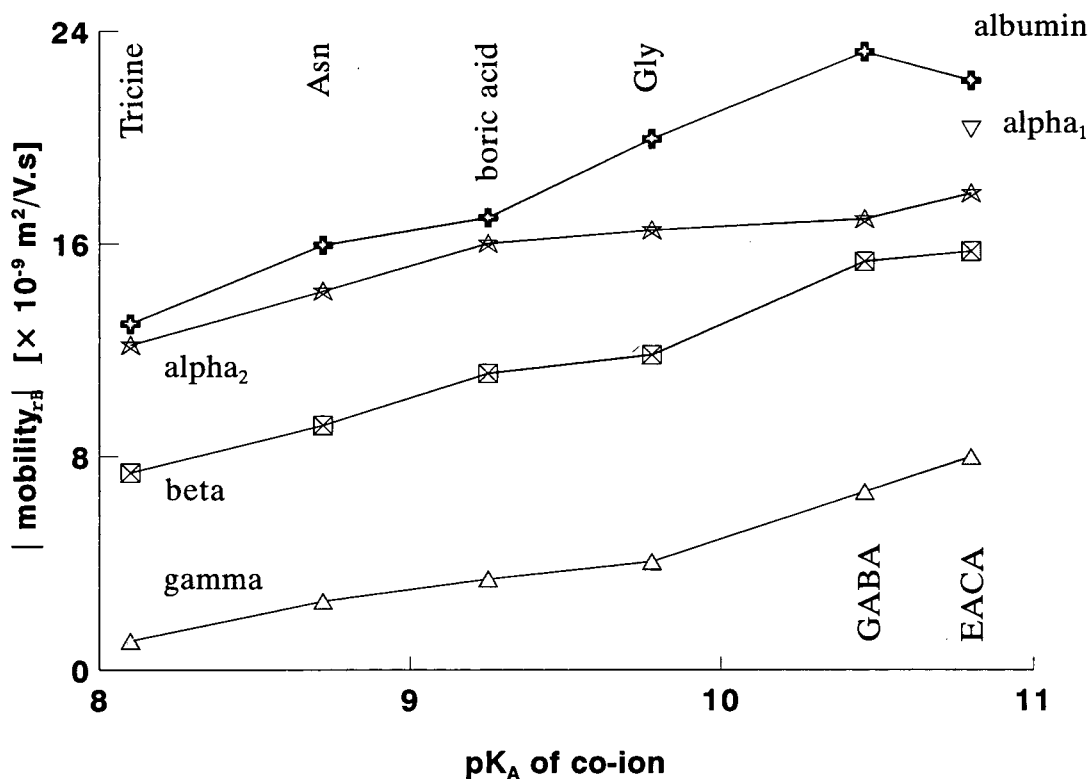
Fig. 2. Effect of pK_A of co-ion on the mobility of serum proteins with Tris as counter ion. Operational electrolyte: 0.1 M Tris–0.1 M co-ion. Other experimental conditions as in Fig. 1.

sodium, i.e., an increase in the co-ion pK_A or pH results in a better resolution between albumin and α-fractions and a lower resolution of β- and γ-globulins. However, in this case, the α_1-globulin peak is obtained with Tris–ϵ-aminocaproic acid exclusively.

The best results were obtained when methylglucamine (MGA) was used as the counter ion in the operational electrolyte formulations. Therefore, the corresponding electropherograms are discussed individually (Fig. 3). In 0.1 M MGA–Tricine (Fig. 3a), the most remarkable effect is the low mobility of γ-globulin, which results in co-migration of this zone with the system peak indicating zero mobility. This is surprising, since in Na–Tricine, γ-globulin migrates anodically to the full extent, although the pH is significantly lower than in 0.1 M MGA–Tricine. This is probably caused by the

interaction of the counter ion with γ-globulins forming ion associates and/or ion pairs, which results in charge reduction and hence a decrease in mobility. In the α_2-globulin–β-globulin area, there is a good resolution of the appropriate subfractions. The peak close to albumin (t_m = 22.98 min) does not correspond to α_1-globulin, as α_1-globulin provides in our sera a significantly smaller peak than the α_2-fraction.

The use of 0.1 M MGA–asparagine provides an electropherogram similar to that with 0.1 M MGA–Tricine (Fig. 3b). A smaller portion of γ-globulins appears on the cationic side of the electropherogram. The UV absorption of asparagine results in a significant decrease in the signal-to-noise ratio.

Use of the popular boric acid as the co-ion failed in the separation of serum proteins in conjunction with MGA (Fig. 3c). This is caused
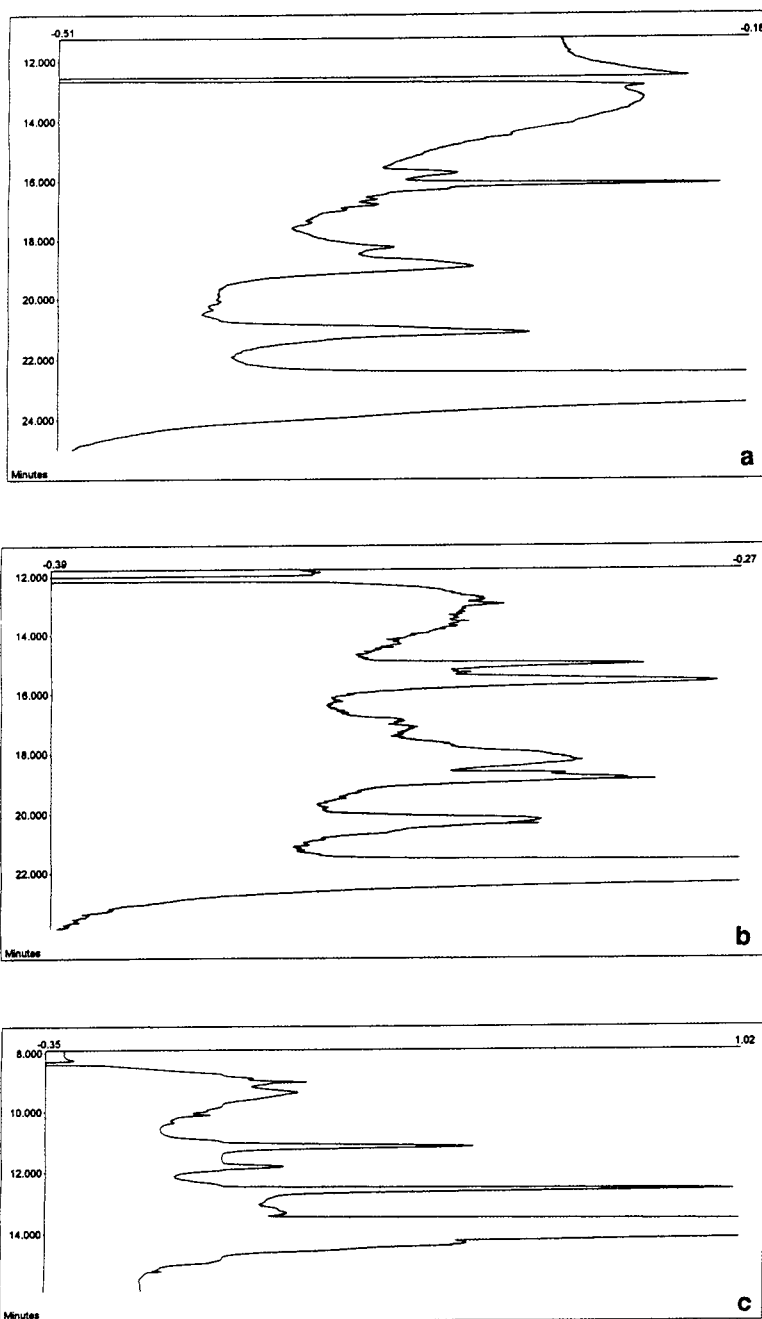
Fig. 3. (*continued on p. 104*).

by the complexation of boric acid with hydroxy groups of MGA, which results in a shift of the pK_A of boric acid and a complicated acid–base equilibrium manifested in a significant deviation of the real pH of the operational electrolyte from the theoretical value.
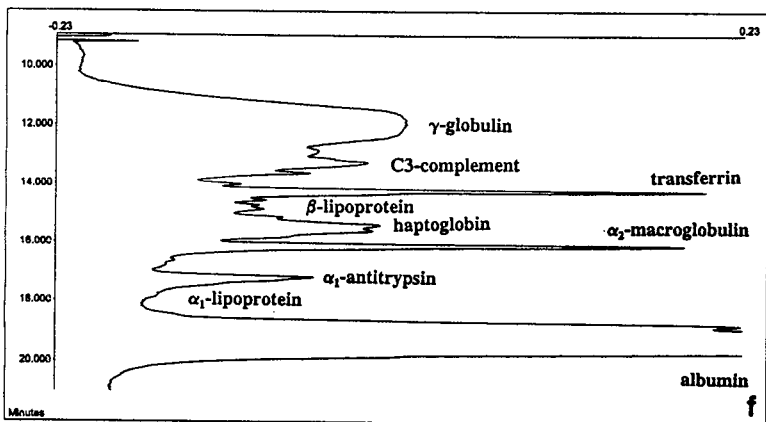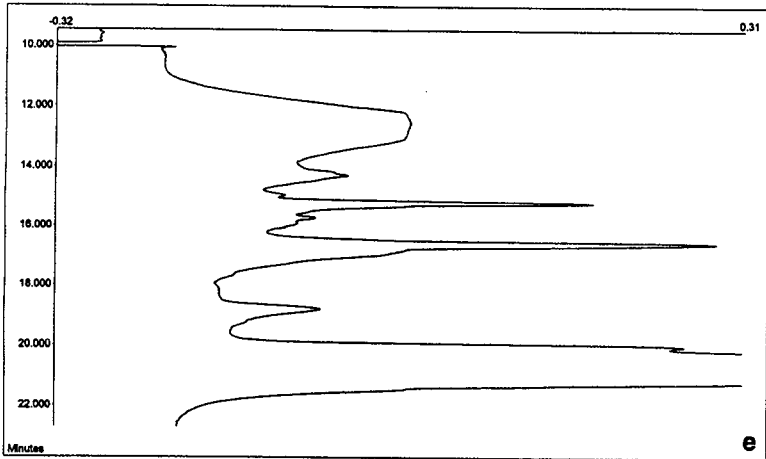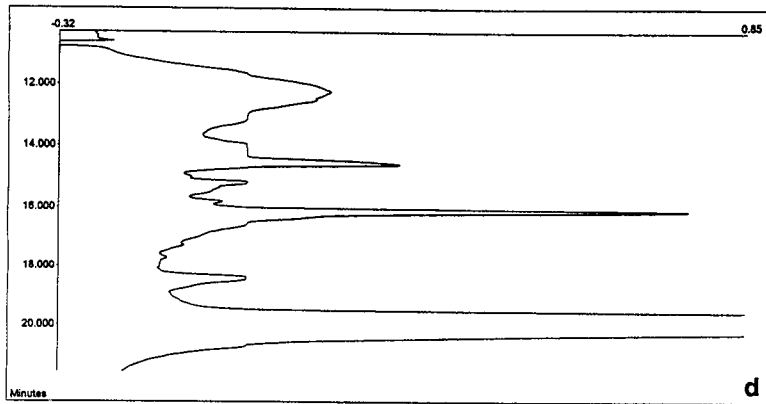
Fig. 3. Electropherogram of serum proteins in operational electrolyte containing 0.1 M methylglucamine as counter ion. Co-ion: (a) 100 mM Tricine; (b) 100 mM asparagine; (c) 100 mM boric acid; (d) 100 mM glycine; (e) 100 mM γ-aminobutyric acid (GABA); (f) 100 mM ϵ-aminocaproic acid (EACA). Other experimental conditions, as in Fig. 1. Ordinate: absorption at 200 nm.

A further increase in pK_A or pH by using glycine as the co-ion leads to an improvement in resolution, primarily by the independent migration of α_1-fraction (Fig. 3d). All the zones, which are known from electrophoresis in agarose, can be found in the electropherogram obtained with 0.1 M MGA–glycine.

Similarly, all fractions were found if γ-aminobutyric acid (GABA) (Fig. 3e) and ϵ-aminocaproic acid (EACA) (Fig. 3f) were used as the co-ion. With the highest mobility, i.e., with the longest migration time, prealbumin appears in the electropherogram. (At least one UV-absorbing non-protein peak with a mobility higher than that of prealbumin can be found in the electropherograms if the separation is performed for a sufficient time. As it was not the aim of this study to analyse all peaks, such as uric acid, no significant attention was devoted to these peaks.) There was a regularly appearing shoulder on the peak of albumin, the identity of which is unknown. In α_1-fraction, the main peak of α_1-antitrypsin can be observed with at least one shoulder, which may correspond to α_1-lipoprotein. Experiments with Sudan Blue-stained serum were not successful in identifying the α_1-lipoprotein peak. With a mobility smaller than that of α_1-globulin, small peaks of group-specific proteins migrate. In α_2-globulin fraction, haptoglobulin and α_2-macroglobulin peaks can be seen. It is not easy to distinguish them, as their migration order varies with the phenotype of the individuals. There are three peaks (series of peaks) in β-fraction: β-lipoprotein, transferrin and C_3-complement. Whereas transferrin migrates as an individual sharp peak, the other subfractions provide several peaks. Both C_3-complement and β-lipoprotein are unstable in serum and decompose. Hence the heterogeneity of these subfractions is at least partially caused by the decomposition.

If we compare the mobilities of the main protein fractions obtained with methylglucamine as the counter ion, a fairly similar plot is obtained as for sodium and Tris (Fig. 4). The mobilities of proteins increase with increasing pH or pK_A; however, the presence of the α_1-fraction makes a significant difference. As

methylglucamine is a weak base, the pH of the operational electrolytes is not identical with the pK_A of the co-ions again. Because the ionic strength varies in the given range, it is advantageous to plot mobility vs. pK_A. The real values of pH for the operational electrolytes are given in Table 1.

When the electroosmotic coefficient from the measurements mentioned above is plotted vs. pK_A (Fig. 5), an interesting plot is obtained. The electroosmotic flow is virtually independent of pH in the given pH range when sodium is used as the counter ion with constant ionic strength. When sodium is replaced with Tris or methylglucamine, a dependence of the electroosmotic coefficient is found, which is more pronounced for methylglucamine. This effect seems to be caused by the decreasing ionization of these organic bases with increasing pH, which results in reduced inter-ionic interaction of these bases with the capillary wall and thus in a higher value of the electroosmotic coefficient.

Further, we were interested in knowing the concentration dependence of the mobilities of serum proteins, with the aim of increasing the operational voltage and hence decreasing the separation time. The dependence of the mobilities of the main serum protein fractions on the concentration of methylglucamine–EACA is plotted in Fig. 6. The plot shows that α_1-fraction disappears from the electropherogram at concentrations below 50 mM. The operational electrolyte 10 mM methylglucamine–EACA enabled an electric field strength of 545 V/cm to be used without any overheating, thus shortening the analysis time significantly. However, it did not help α_1-fraction to appear in the electropherogram and therefore 0.1 M methylglucamine–EACA is recommended as a suitable operational electrolyte for the electrophoresis of serum proteins.

Because of the known effect of hydrophobic acids on the resolution of albumin–α_1-fraction, we decided to investigate this effect in capillary electrophoresis. Unfortunately, the acids, the improving effect of which is known from slab gel electrophoresis, absorb UV radiation and therefore their use in capillary electrophoresis with
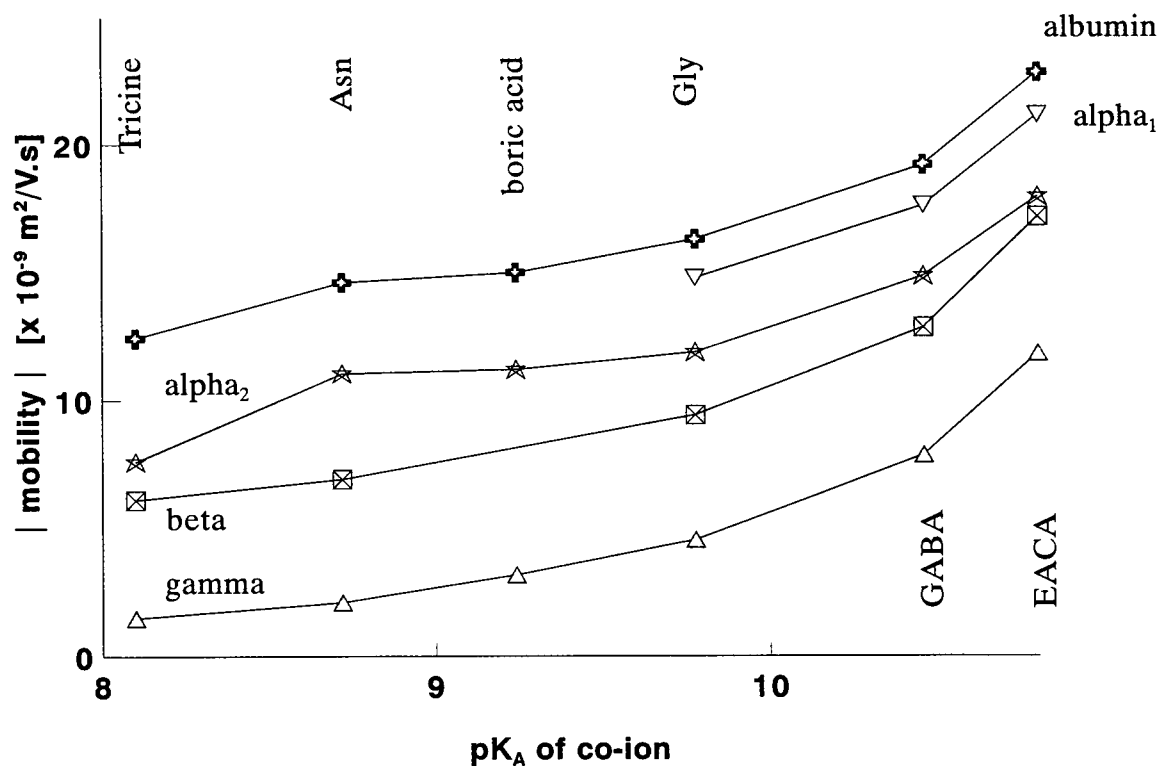
Fig. 4. Effect of pK_A of co-ion on the mobility of serum proteins with methylglucamine as counter ion. Operational electrolyte: 0.1 M methylglucamine–0.1 M co-ion. Other experimental conditions as in Fig. 1.

on-line UV detection is impossible. For that reason, the influence of fatty acids was investigated. Attention was paid primarily to the effect of lauric acid when (i) lauric acid was the only co-ion in the operational electrolyte and (ii) when lauric acid was used in a mixture with another co-ion.

When the operational electrolyte containing 5 mM methylglucamine and 2.5 mM lauric acid was used, α_1-fraction was not resolved from albumin and appeared as a shoulder on the albumin peak. When the concentration of operational electrolyte was doubled, the α_1-globulin–albumin resolution was improved, probably by forming a laurate–albumin complex which exhibits higher mobility than albumin itself. The low ionic strength of this electrolyte enables a high operational voltage to be applied. In the given system, a maximum voltage of 30 kV could be successfully used to shorten the analysis time

whilst maintaining the separation of the main fractions of serum proteins in about 3 min (Fig. 7).

If the concentration of the operational electrolyte is increased further to 60 mM methylglucamine–30 mM lauric acid, the electrophoretic profile of serum proteins is dramatically changed (Fig. 8). Albumin migrates as two split peaks and a number of new peaks appear in the electropherogram. The number of new peaks suggests a good potential for this electrophoresis of serum proteins. However, our optimism is moderate, as a lot of work, primarily in identification and clinical interpretation of electropherograms, must be done in order to introduce this particular analysis into the family of practical applications of capillary electrophoresis. At the given concentration, laurate forms micelles, which should be borne in mind by those who distinguish zone electrophoresis from micellar
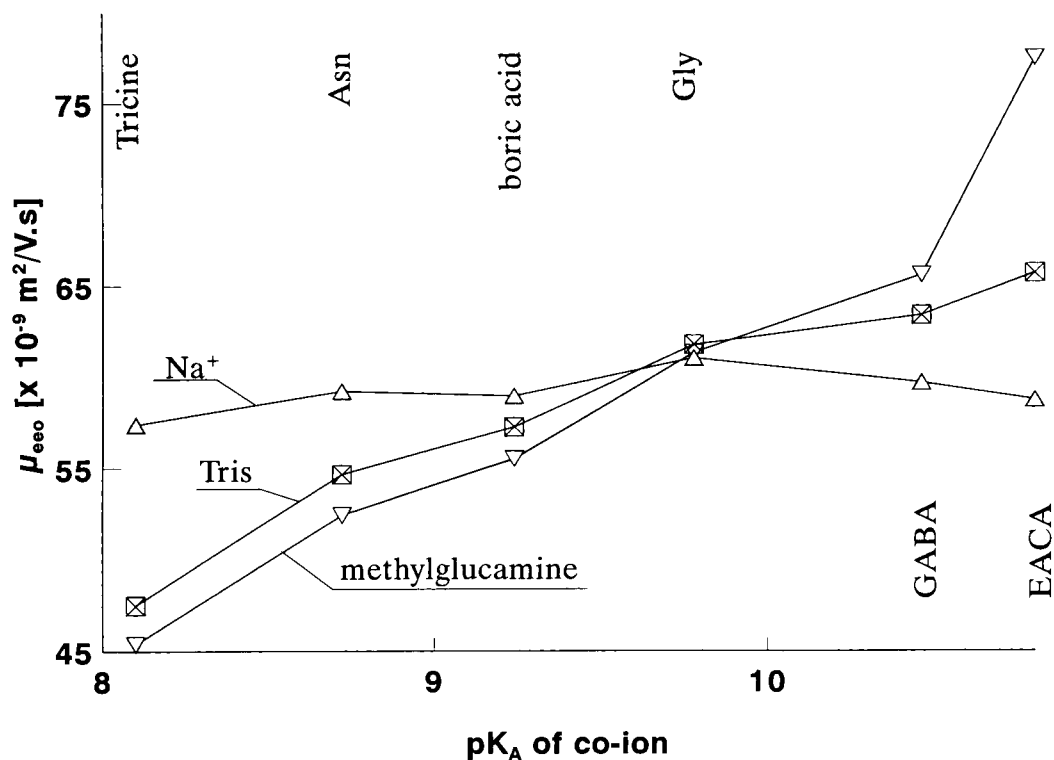
Fig. 5. Effect of pK_A of co-ion on the electroosmotic coefficient with sodium, Tris and methylglucamine as counter ion. Experimental conditions as in Figs. 1, 2 and 4.

electrokinetic chromatography. In our approach, it is sufficient to speak about zone electrophoresis of the protein complexes with laurate. Indeed, the dimensions of protein molecules do not support the simplistic model of spherical micelles with separands incorporated in.

If the operational electrolyte contains lauric acid in the presence of other ions, the detrimental effect of laurate on the integrity of serum proteins starts at lower concentrations. This effect is obvious with an operational electrolyte containing 100 mM methylglucamine–90 mM EACA–5 mM lauric acid (not shown), i.e., at a concentration of lauric acid which, in the absence of other anions did not attack the integrity of serum proteins. This effect is easy to explain: an increase in ionic strength results in increased hydrophobic interactions, and that is exactly what happened in this case. If the content of lauric acid is further increased, the albumin and

γ-globulin peaks are preserved, but a number of new peaks with mobilities higher than that of albumin appear in electropherogram (Fig. 9).

4. Conclusions

Good resolution of serum proteins is achieved by capillary electrophoresis when the operational electrolyte 0.1 M methylglucamine–0.1 M EACA or 0.1 M methylglucamine–0.1 M GABA is used. An operational electrolyte containing 10 mM methylglucamine and 5 mM lauric acid permits the separation of serum proteins with high voltage and the main serum protein fractions can be separated in about 3 min. Capillary electrophoresis in the presence of 60 mM methylglucamine–30 mM lauric acid or 100 mM methylglucamine–80 mM EACA–5 mM lauric acid provides the separation of a large
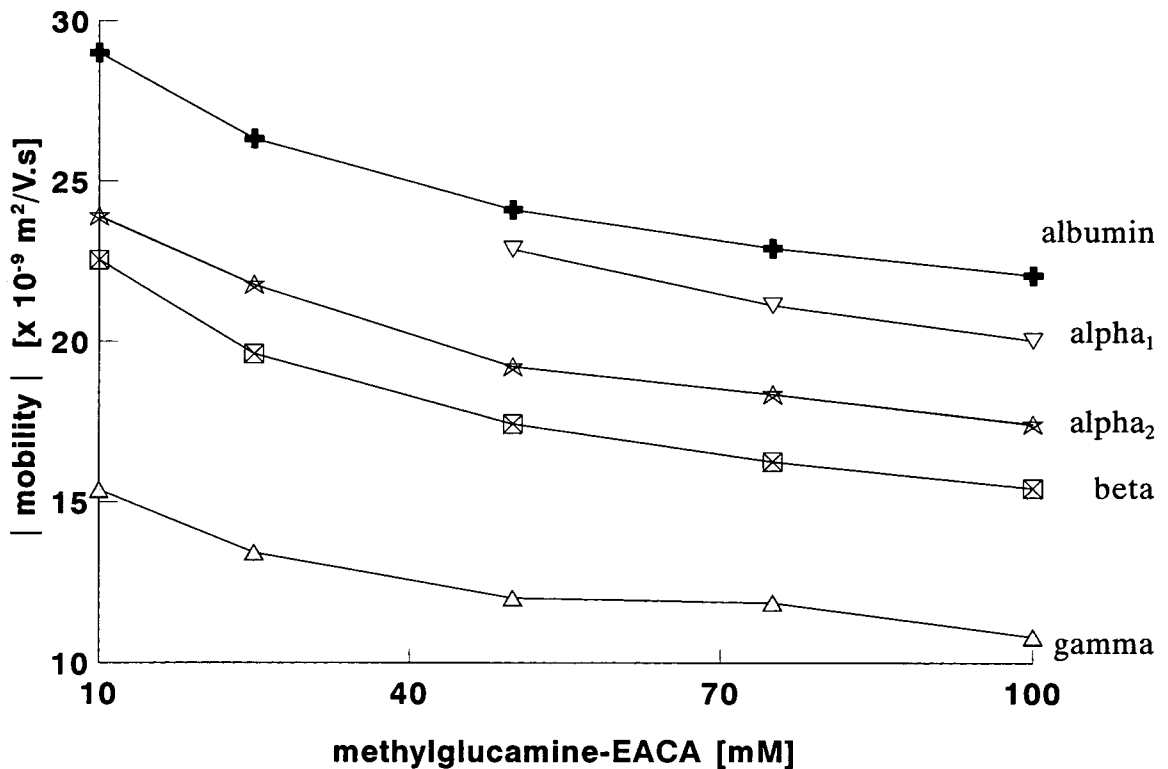
Fig. 6. Effect of concentration of equimolar methylglucamine–EACA on the mobility of serum proteins. Operational electrolyte: 0.01–0.1 M methylglucamine–0.01–0.1 M co-ion. Other experimental conditions as in Fig. 1.
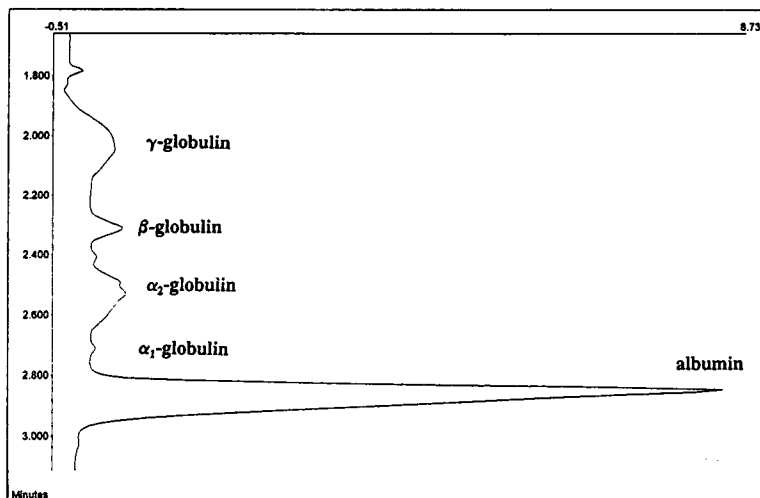
Fig. 7. Electropherogram of serum proteins in operational electrolyte containing 10 mM methylglucamine and 5 mM lauric acid. Voltage, 30 kV. Other experimental conditions, as in Fig. 1. Ordinate: absorption at 200 nm.
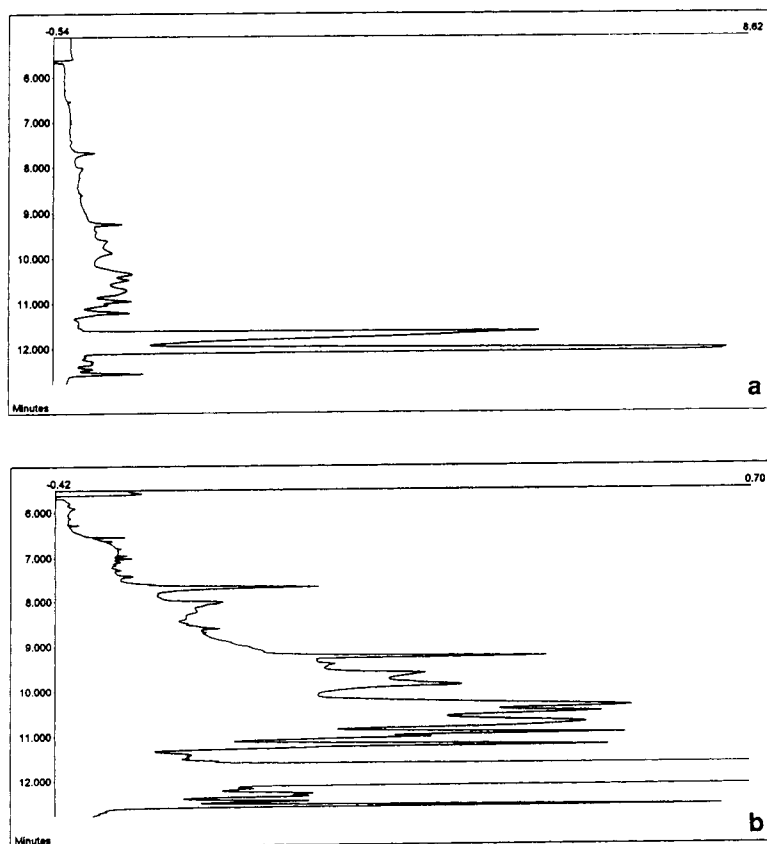
Fig. 8. Electropherogram of serum proteins in operational electrolyte containing 60 m*M* methylglucamine and 30 m*M* lauric acid. Experimental conditions, as in Fig. 1. Ordinate: absorption at 200 nm. (a) and (b) differ by ordinate scale.
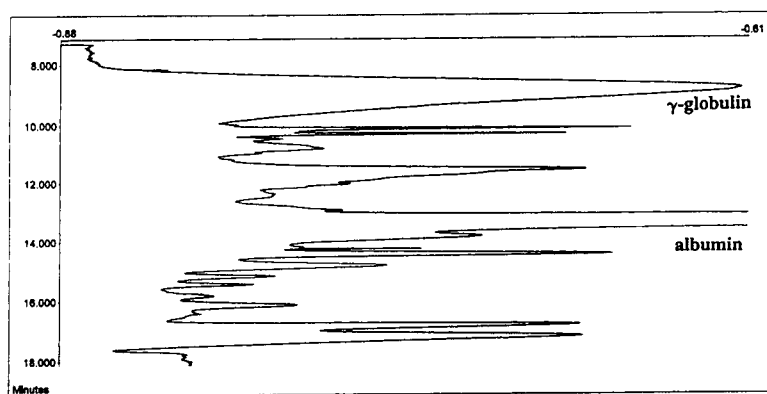
Fig. 9. Electropherogram of serum proteins in operational electrolyte containing 100 m*M* methylglucamine, 80 m*M* EACA and 10 m*M* lauric acid. Experimental conditions as in Fig. 1. Ordinate: absorption at 200 nm.

number of peaks as a result of the disintegration of serum proteins by hydrophobic interactions with laurate. This gives new potential to the electrophoresis of serum proteins.

References

[1] B.G. Johansson, Scand. J. Clin. Lab. Invest., 29, Suppl. 124 (1972) 7.
[2] C.B. Laurell, Scand. J. Clin. Lab. Invest., 29, Suppl. 124 (1972) 71.
[3] J.F. Heremans and P.L. Masson, Clin. Chem., 19 (1973) 294.
[4] R.F. Ritchie and R. Smith, Clin. Chem., 22 (1976) 497.
[5] T. Sun, S.-K. Chan and S. Gross, Am. J. Clin. Pathol., 67 (1977) 247.
[6] T. Sun, Y.Y. Lien and S. Gross, Ann. Clin. Lab. Sci., 8 (1978) 219.
[7] J.-O. Jeppson, C.-B. Laurell and B. Franzén, Clin. Chem., 25 (1979) 629.
[8] K. Ojala and T.H. Weber, Clin. Chem., 26 (1980) 1754.
[9] M. Doren, D. Conlon and L. Blankstein, Clin. Chem., 27 (1981) 200.
[10] M. Engliš, in Z. Deyl (Editor), Electrophoresis, Part B, Elsevier, Amsterdam 1983, p. 201.
[11] E. Gianazza and P.G. Righetti, J. Chromatogr., 569 (1991) 43.
[12] J.F. Monthony, E.G. Wallace and D.M. Allen, Clin. Chem., 24 (1981) 1825.
[13] J. Ambler and M. Rodgers, Clin. Chem., 26 (1980) 1221.
[14] M.J. Gordon, K.-J. Lee, A.A. Arias and R.N. Zare, Anal. Chem., 63 (1991) 69.
[15] F.-T.A. Chen, C.-M. Liu, Y.Z. Hsieh and J.C. Sternberg, Clin. Chem., 37 (1991) 14.
[16] F.-T.A. Chen, J. Chromatogr., 559 (1991) 445.
[17] F.-T.A. Chen, Clin. Chem., 38 (1992) 1651.
[18] F.-T.A. Chen and J.C. Sternberg, Electrophoresis, 15 (1994) 13.
[19] O.W. Reif, R. Lausch and R. Freitag, Int. Lab., June (1994) 10.
[20] V. Dolník and M. Novotny, Anal. Chem., 65 (1993) 563.
[21] K.A. Cobb, V. Dolník and M. Novotny, Anal. Chem., 62 (1990) 2478.

Capillary electrophoresis of hair proteins modified by alcohol intake in laboratory rats

Dita Jelínková[a], Zdeněk Deyl[b],[*], Ivan Mikšík[b], Franco Tagliaro[c]

[a]*Department of Analytical Chemistry, Institute of Chemical Technology, Technická 1905, CZ-16000 Prague 6, Czech Republic*
[b]*Institute of Physiology, Academy of Sciences of the Czech Republic, Vídeňská 1083, CZ-14220 Prague 4, Czech Republic*
[c]*Institute of Forensic and Legal Medicine, University of Verona, Verona, Italy*

Abstract

A capillary zone electrophoretic method was used to obtain profiles of solubilized rat hair keratin proteins. The same methodology was used to reveal the presence of additional protein peaks in alcohol-consuming rats. Two types of separation were investigated. Alkali-solubilized keratins from hair of rats treated for 5 weeks with 5% ethanol and 2 weeks with 10% ethanol (instead of drinking water) and from controls were analysed. Whereas under alkaline conditions (pH 9.2, 50 mM borate) an additional fraction of "low-sulphur" keratins with the highest anodic mobility of this keratin category was shown in alcohol-treated animals, acid electrophoresis carried out at pH 3.5 in phosphate buffer (50 mM) revealed the presence of two sharp peaks absent in the controls. These findings were confirmed by two-dimensional separations of carboxymethylated keratin samples. An attempt was made to identify further one of the newly occurring fractions in alcohol-consuming animals. It was revealed that the tryptic hydrolysate of "low-sulphur" proteins obtained from alcohol-consuming animals contained a peptide not found in controls.

1. Introduction

Hair analysis is gaining considerable popularity in situations where the past history of drug abuse rather than the present state needs to be investigated [1,2]. Whereas morphine, cocaine and a number of other drugs can be extracted from hair after acid, alkaline or solvent treatment of the matrix (for reviews, see Refs. [3 and 4]) (the nature of the way of binding these drugs to the hair matrix remains unknown), apparently there are other metabolites that can interact with the hair keratins. In a previous paper we showed that profiling of the organic phase-extractable material from acid-treated hair may be used as a

---

* Corresponding author.

diagnostic tool in animals predisposed to alopecia areata [5]. Biochemical studies of wool filaments and their associated matrix material have led to the realization that there are three major classes of hair proteins: the low-sulphur keratins (designated 40–60 K), the high-sulphur keratins (designated 10–25 K) and the high glycine–tyrosine proteins (designated 10–25 K). The analysis of solubilized hair keratins by standard gel electrophoresis [6] reveals two fractions (one doublet and one triplet) of probably low-sulphur keratins in the relative molecular mass (M_r) regions of $44/46 \cdot 10^3$ and of $56/59/60 \cdot 10^3$. In the case of keratin characterization by two-dimensional gel electrophoresis, six low-sulphur (M_r 55 500–76 000) and seven high-sulphur (M_r 26 500–43 000) major proteins [7] were

found. It is likely that the molecular masses of these fractions are higher than the real values. Although, as shown also in this report, two-dimensional gel electrophoresis offers valuable separations in profiling hair keratins, capillary zone electrophoresis (CZE) appears more rugged and faster and offers complementary information.

The idea behind investigating hair keratin of alcohol-treated animals is that long-term alcohol intake may cause metabolic alterations that could be expressed and accumulated in long-lived proteins; the production of acetaldehyde (the first metabolite of ethanol) should be the first to be considered. It has been reported that ethanol administration leads to free amino group modification in this way [8]. The objection that the amount of acetaldehyde released is too small to cause any alterations in long-lived proteins should be abandoned not only because of the results just mentioned [8], but also because our experience indicates [9] that even minute concentrations of oxo-containing compounds lead to protein modifications that can be demonstrated, e.g., by decreased solubility.

In this work, we investigated the possibility of separating hair keratins by capillary electrophoresis and attempted to show the differences in keratin protein profiles in hair of rats consuming alcohol.

2. Experimental

2.1. Animals

Two sets of male Wistar rats were housed three per cage (twelve altogether) and fed ad libitum a standard pelleted diet. They were taken into the experiment when 60 days old. Alcohol was administered by replacing water with 5% ethanol solution for 35 days and with 10% ethanol solution for the following 14 days. After this time period the hair from the dorsal region was shaved (about 2.2 g) and subjected to further analysis. The same number of animals (two cages, three animals each) kept on tap water served as controls. The alcohol-treated animals did not differ in the growth curve in

comparison with the controls, but the liquid and food intake was decreased in the experimental group, representing 71% and 78% of the controls (at the end of the experiment), respectively.

2.2. Preparation of samples

The hair sample (about 2.2 g) taken from the dorsal part of the experimental animal was washed stepwise with ethanol and 0.01 M phosphate buffer (pH 6.0) on a Büchner funnel. Two approaches for solubilizing hair proteins were used. At the beginning we used incubation (1.1 g) with 1 M NaOH (125 ml) at 40°C overnight, as is the procedure often used in forensic analyses [10]. The insoluble residue was filtered and the solubilized fraction was extracted three times with 125 ml of chloroform–2-propanol (9:1, v/v) (the aqueous phase was injected). At a later stage, hair samples after the Büchner funnel wash were minced into 2–3-cm pieces and incubated under nitrogen in 8 M urea–200 mM Tris-HCl buffer (pH 9.5)–2 mM mercaptoethanol for 2 h. After this, the swollen hair samples were homogenized and the incubation was continued for a further 2 h at 40°C. The insoluble residue was spun off (10 000 g, 10 min) and the supernatant was stored frozen in small aliquots until used. As the profiles obtained by these two approaches did not differ, the latter procedure was mostly used. For two-dimensional gel separations, the dissolved proteins in 50-μl aliquots were radiolabelled at pH 8.0 by S-carboxymethylation of a proportion of the cystein residues with [2-^{14}C]iodoacetic acid (6 μCi). After 10 min at room temperature, excess iodoacetate was added to complete the modification of the cysteine residues. Excess iodoacetate remaining after 10 min was reacted with 2-mercaptoethanol [11,12].

2.3. Capillary zone electrophoresis (CZE)

The electrophoretic separations were carried out in a 50-μm fused-silica capillary (Polymicro Technologies, Tucson, AZ, USA) mounted in a Model 350, CZE apparatus (ISCO, Lincoln, NE, USA) run routinely at 15 kV (45 μA) with UV detection at 220 nm. Separations were per-

formed under both alkaline and acidic conditions with two kinds of buffers. For the alkaline runs, 50 mM borate buffer (pH 9.2) was used, whereas the acidic separations were run in 50 mM phosphate buffer (pH 3.5). The capillary was occasionally rinsed with 0.1 M NaOH (by aspiration), whereas it was rinsed with the run buffer before each run. Routinely, 7 μl of samples were injected through a 1:1000 split-stream port with an HPLC-type syringe into the ISCO apparatus. Samples were sonicated for 15 min prior to analysis, diluted appropriately (see Results) and filtered through a Millex HV 0.45-μm filter (Waters–Millipore, Milford, MA, USA). Omitting these operations leads at least to a noisy baseline or may spoil the run completely.

The acidic runs were much slower than under alkaline conditions, owing to the large difference in the electroosmotic flow. The positions of individual peaks varied very little (less than 5% R.S.D. of the retention time, except for the slow peaks in the acidic, long-lasting runs). Alkalisolubilized hair from alcohol-treated animals and alkali-solubilized hair from controls were subjected to analysis.

2.4. Polyacrylamide gel electrophoresis

Radiolabelled protein extracts were examined by two-dimensional polyacrylamide gel electrophoresis. Two systems were used in the first dimension separation, being different in each case. Protein separation was carried out in 8 M urea at pH 8.9 or pH 3 in an apparatus with glass tubes (130 × 3.0 mm). The second-dimension separation was according to the apparent M_r by sodium dodecyl sulphate (SDS) electrophoresis in a slab (140 × 120 × 1.5 mm).

For the separation at pH 8.9, the procedure of Davis [13] was used, except that 8 M urea was incorporated into the gels. The proteins (10 μl of protein extract) were separated on polyacrylamide gel rods consisting of 10-mm 4% stacking gel and 100-mm 7.5% separation gel. These gels were prepared from a stock 29.2% acrylamide–0.8% N,N'-methylenebisacrylamide solution, and polymerized using ammonium peroxodisulphate. The electrophoresis was run at 40 V for approximately 18 h until bromophenol

blue tracking dye (loaded on a similar gel rod or added to the upper electrode buffer) had travelled the length of the gel rod.

For electrophoresis at pH 3, the system reported by Marshall and Gillespie [12] was used. The proteins (5 μl of protein extract and 10 μl of acid sample solution) were separated on 110 × 3.0 mm 8% polyacrylamide gel rods [acrylamide–N,N'-methylenebisacrylamide (27:1)] containing 4.7 M acetic acid and 8 M urea. Electrophoresis was performed towards the cathode at 80 V until the crystal violet tracking dye had travelled the length of the gel rod (approximately 18 h).

SDS electrophoresis was carried out according to Laemmli [14] and O'Farrell [15]. Polyacrylamide gel slabs were prepared from a stock 29.2% acrylamide–0.8% N,N'-methylenebisacrylamide solution and polymerized using ammonium peroxodisulphate. A stepwise acrylamide concentration was used by Marshall and Gillespie [12]. The lower 20 mm of the separation gel slab consisted of 15% polyacrylamide and the upper 75 mm 10% polyacrylamide. The first-dimension gel rod was held in place above the 20-mm stacking gel (4.5% polyacrylamide) by 1% agarose [15]. Gel rods after electrophoresis at pH 3 were equilibrated for 45 min with the SDS sample buffer (buffer 0 in Ref. [12]), but this equilibration step was not necessary after isoelectric focusing or pH 8.9 electrophoresis. Electrophoresis was performed at 100 V for 1 h, then at 200 V until the bromophenol blue tracking dye (added to upper electrode buffer before commencement of electrophoresis) had travelled about 10 mm through the 15% polyacrylamide gel. Full details of the procedures were given by Marshall and Gillespie [12].

After SDS electrophoresis, radiolabelled proteins were located by fluorography [16].

2.5. Ion-exchange separation of solubilized keratins

Ion-exchange separation was carried out by passing 5 ml of the supernatant containing alkalisolubilized keratins through a Bio-Rad (Richmond, CA, USA) AG 50W-X8 filter, the cation-exchange bead was flushed with distilled water (5

ml) and the retained fraction was eluted with 0.1 M triethylamine (5 ml). After evaporation (at 50°C in vacuo), the residue was reconstituted in 2 ml of Milli-Q-purified water and after overnight dialysis the sample was ready for further analysis.

2.6. Trypsin digestion

The retained fraction from the Bio-Rad AG 50W-X8 cartridge was prepared as described above except that the dry residue was reconstituted in 50 mM NH_4HCO_3–1 mM $CaCO_3$. Trypsin solution was prepared in the same buffer and the sample was digested at an enzyme-to-protein ratio of 1:10 at 37°C overnight. After stopping further hydrolysis, the digest was either used directly for reversed-phase chromatography or, after drying on a Speed Vac Centrifuge, used for mass analysis.

2.7. HPLC of the trypsin-released peptides [17]

The peptides were separated on a reversed-phase column (Vydac C_{18}, 7 μm, 250 × 0.42 cm I.D.). A linear gradient from 100% A to 70% B within 1 h was applied, where A = 0.10% trifluoroacetic acid (TFA) in water and B = 0.10% TFA in 70% acetonitrile. The flow-rate was 1 ml/min. Collected fractions containing peptides were taken to dryness in a Speed Vac centrifuge.

2.8. Plasma desorption mass spectrometry (PDMS) [18]

Peptides separated by reversed-phase HPLC were dissolved in 8 μl of 0.1% TFA–20% methanol and applied to nitrocellulose-covered targets. Targets were then washed in 10 μl of water (UHQ) to remove salt and PDMS was performed on a Model 20 plasma desorption mass spectrometer (Biolon, Uppsala, Sweden). Each spectrum was accumulated for 10^6 fission events using an acceleration voltage of 15 kV and calibrated with H^+ and NO^+ ions.

3. Results

In contrast to acid extraction [5], alkaline treatment solubilizes much of the hair matrix (about 85%). For capillary electrophoretic analysis, the protein concentration had to be adjusted prior to analysis (50–100 μl to 5 ml of Milli-Q-purified water).

Typical electropherograms of the rat hair keratin fractions obtained from both alcohol-treated and control animals are shown in Fig. 1, where the results are compared with both one- and two-dimensional electrophoresis. Two groups of peaks are seen in the capillary separations: the first group (two peaks in controls, three peaks in alcohol-treated animals) corresponds to the fast-moving zone in plate A_1. The other set of peaks moving with retention 7.5–10 min and two additional peaks moving with retention 15 and 18 min represent the other (smearing zone) seen in one-dimensional electrophoresis.

In two-dimensional gel separations, two categories of protein spots can also be seen, a fast, cathodically moving set of keratin proteins and a long diagonal smear. In accordance with literature data, the two fast-moving peaks in extracts from controls (three in alcohol-consuming rats) were tentatively identified as "low-sulphur" keratins, whereas the rest corresponding to the diagonal smear were assumed to represent the "high-sulphur" keratin proteins.

By passing the keratin protein extract through the Bio-Rad cation-exchange filter, both categories of hair proteins can be separated: the "low-sulphur" proteins are retained whereas the "high-sulphur" proteins are not, as can be seen from Fig. 2; the retained fraction (released by washing the filter with 2 ml of 0.1 M triethylamine, followed by overnight dialysis of the filtrate) corresponds to the first two (or three in alcohol-treated animals) fractions appearing during the capillary electrophoretic runs (see Fig. 2, plates A and C). The unretained proteins correspond to the remaining, more anodically moving peaks. Amino acid analysis of both fractions (data not presented) indicated a higher proportion of sulphur-containing amino acids in the
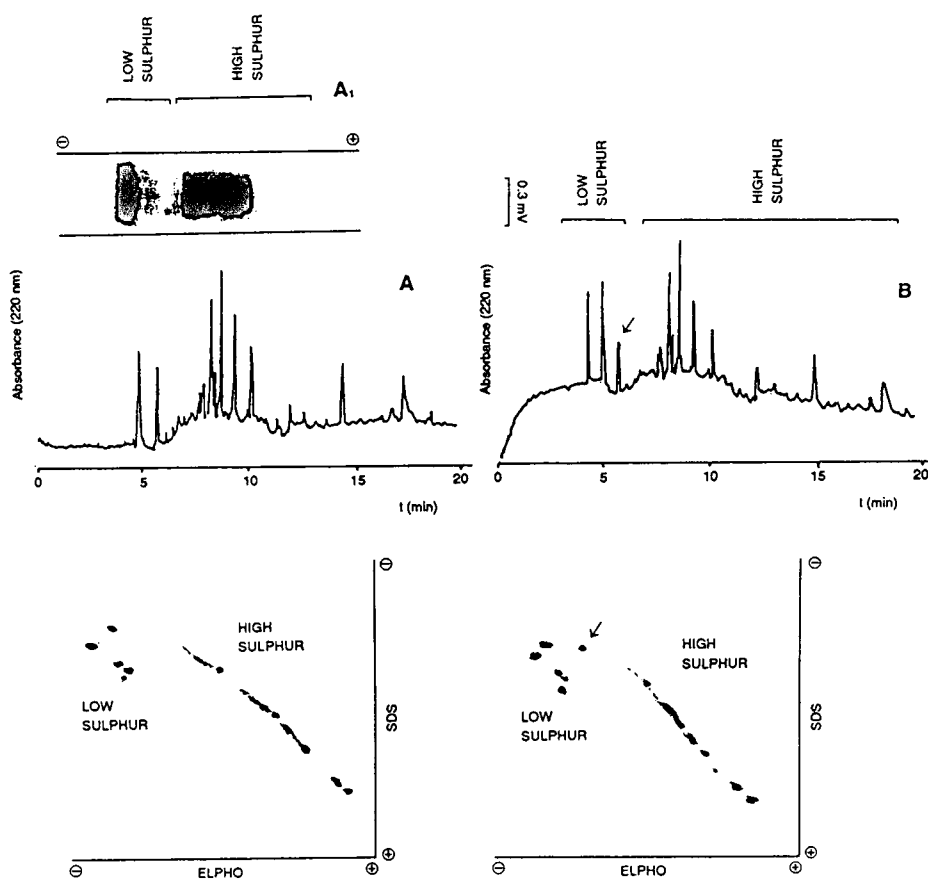
Fig. 1. Comparison of capillary electrophoretic profiles (pH 9.2) of hair keratin samples obtained from (A) control rats and (B) alcohol-treated rats. The dilution of extracts was 50 μl to 5 ml. The position of the peak present in the alcohol-treated animals but absent in controls is indicated by an arrow. Assignment of "high-sulphur" and "low-sulphur" proteins is based on the results shown in Fig. 2. CZE conditions as specified under Experimental.

unretained fraction, justifying the classification of the two sets of protein fractions as "low-sulphur" and "high-sulphur" types.

From the profiles shown in Fig. 1, it is evident that the profiles obtained from controls (plate A) and alcohol-treated animals (plate B) differ in the arrow-indicted peak. The additional fraction belongs, according to its electromigration behaviour, between the "low-sulphur proteins" and has an apparent M_r of $70 \cdot 10^3$.

Further investigation of the "high-sulphur" proteins by two-dimensional electrophoresis under alkaline conditions was not possible owing to the smearing character of the "high-sulphur protein" zone. Therefore, separations run at pH

3.5 as visualized in Fig. 3 were run. These indicated the presence of two spots in the M_r $25 \cdot 10^3$–$30 \cdot 10^3$ region in two-dimensional electrophoresis. In CZE separations (Fig. 3, plates A and B) run at pH 3.5, two distinct peaks appeared at run times between 10 and 20 min in alcohol-treated animals (indicated by arrows) which were absent in control runs. When the fraction retained on the Bio-Rad AG 50W-X8 filter was run under similar conditions, the picture shown for plate C was obtained. By comparison of plate C with plates A and B, the peaks moving at 12 min and less in CZE can be identified as "low-sulphur" and those moving more rapidly to the anode represent the "high-
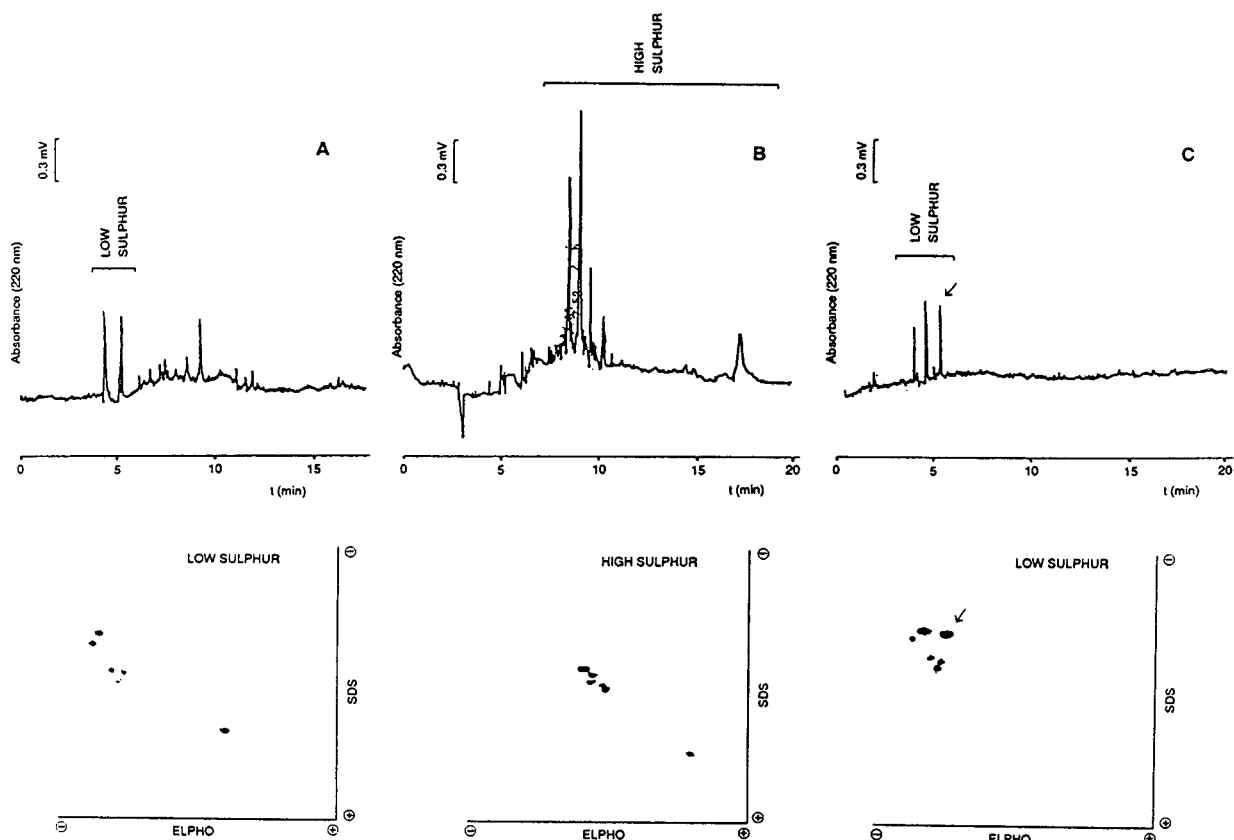
Fig. 2. CZE profiles (pH 9.2) of the retained (plate A) and unretained (plate B) fractions obtained after passing the crude extract through a Bio-Rad AG 50W-X8 filter. "High-sulphur" proteins were recovered in the filtrate whereas "low-sulphur" proteins were released by 0.1 M triethylamine. Comparison with the two-dimensional gel separations is visualized under each CZE run. The position of the fraction of "low-sulphur" proteins occurring in alcohol-treated animals but absent in controls is indicated by an arrow. Profile of proteins retained on the cation-exchange cartridge from the alcohol-treated rat hair preparation is shown on plate C. CZE conditions as specified under Experimental.

sulphur" fraction. It appears that of the three additional peaks occurring with in animals treated for 7 weeks with alcohol, two belong to the category of "high-sulphur" proteins whereas the third fraction can be traced within the "low-sulphur" protein fraction (alkaline separation conditions).

The easy separation of the "low-sulphur" fraction containing an extra peak in alcohol-treated rats (Fig. 1, plate A), the presence of which was confirmed by two-dimensional electrophoresis, prompted us to attempt to characterize further the "low-sulphur" keratin fraction observed in alcohol-treated animals. The Bio-Rad

AG 50W-X8-retained fraction was routinely eluted with 0.1 M triethylamine, lyophilized and hydrolysed with trypsin as described under Experimental. The resulting mixture of peptides was separated by reversed-phase chromatography (Fig. 4). This separation resulted in a very complex mixture, in which 23 peaks could be discerned. All of these were collected, taken to dryness and the residue dissolved in 8 μl of 0.1% TFA–20% methanol and investigated by PDMS. Of the 23 fractions, 11 gave non-interpretable spectra (numerous masses). Peak 11 with M_r 1217.6, however, was present in the preparations obtained from alcohol-treated animals only (Fig.
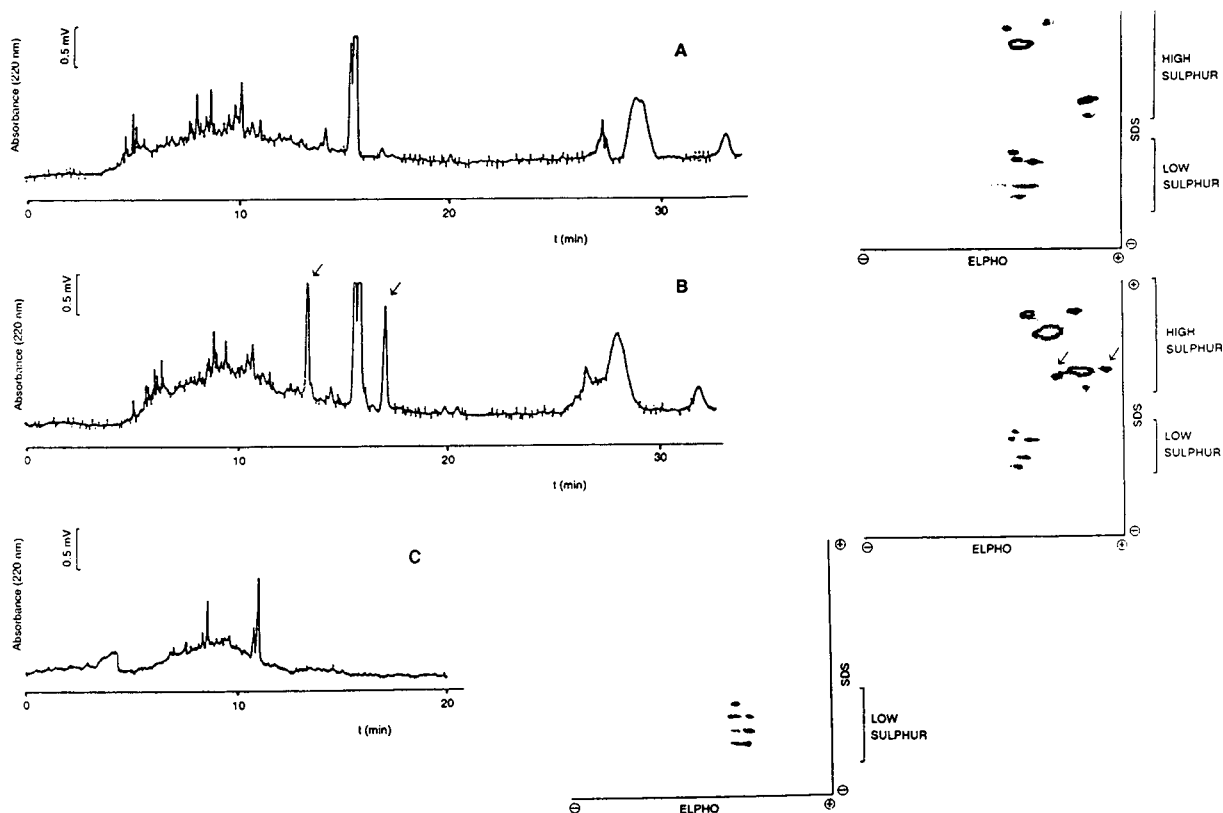
Fig. 3. CZE profiles and two-dimensional electrophoresis of rat hair extracts under acidic conditions. CZE run at pH 3.5, two-dimensional separation at pH 3.0 (see Experimental for details). Plate A, controls; plate B, alcohol-treated, 7 weeks; plate C, fraction of control animals retained on the Bio-Rad AG 50W-X8 filter and released with 0.1 M triethylamine, corresponding to "low-sulphur" proteins.

5) and was absent in preparations obtained from controls.

4. Discussion

CZE can be used not only for the analysis of organic phase-extractable material from hair, as previously reported [5], but also for the analysis of hair proteins. Reproducible profiles were obtained with less than 5% R.S.D. of the retention time on both inter-run and day-to-day bases. The capillary electrophoresis profiles of hair keratins can be separated into two parts: (i) the set of peaks appearing soon before the detector window (two in controls, three in alcohol-consuming rats), which in accordance with

their behaviour in two-dimensional electrophoresis correspond to "low-sulphur" keratins, and (ii) the peaks in the remaining part of the electropherogram, which according to the same comparison could be tentatively identified as "high-sulphur" proteins. These two categories can be easily separated by passing the extract through a cation-exchange cartridge on which the more basic set of peaks is retained. Analysing the filtrate and retentate for the content of sulphur-containing amino acids indicated considerably more (about twice per amino acid nitrogen) sulphur-containing amino acids in the unretained fraction.

In the category of "low-sulphur" proteins, one additional peak in CZE and one additional spot in two-dimensional gel electrophoresis was ob-
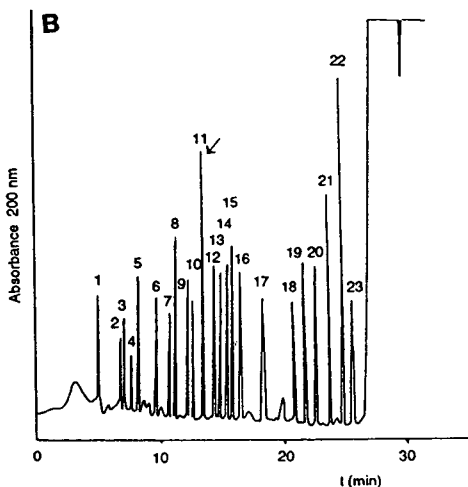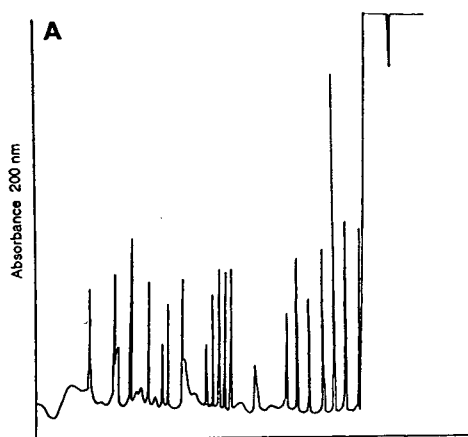
Fig. 4. HPLC of the trypsin hydrolysate of the "low-sulphur" keratin fraction. For preparation, see Experimental. (A) controls; (B) alcohol-treated rats. Note the absence of peak 11 (see arrow) in controls.

Fig. 5. PD mass spectrum of the HPLC fraction present in the alcohol-treated animals only (peak 11, Fig. 4B).

served. This protein fraction exhibited the highest anodic mobility of the proteins constituting the "low-sulphur" category and, according to the gel electrophoretic behaviour, possessed an apparent M_r of $70 \cdot 10^3$. When the separations were run at acidic pH, the profiles of controls and treated animals differed in two peaks (zones) present in the "high-sulphur" region both in the CE runs and in two-dimensional gel electrophoresis.

Fractionation of peptides obtained of trypsini-

zation of the "low-sulphur" proteins indicated the presence of a peptide of M_r 1217.6, which was absent in preparations obtained from untreated animals.

The nature of the protein fractions occurring in alcohol-treated animals should reflect either metabolic changes or post-translational modifications of normally synthesized proteins, or both. To express a definite conclusion in this respect is difficult at present, although some idea can be obtained from the MS data. The peptide found in the "low-sulphur" protein trypsin hydrolysate of alcohol-treated animals was not found in controls. Whether this reflects the presence a metabolite-modified protein is difficult to say.

The fact that it was possible to detect three additional protein fractions in alcohol-treated animal hair keratin preparations appears to indicate a polytopic effect of alcohol consumption on hair keratin. Although no proof has been obtained that these additional fractions represent three different proteins, it seems to be so as the additional "low-sulphur" fraction may not be revealed under acidic separations and, on the other hand, the two "high-sulphur" protein fractions may not be revealed alkaline conditions of electrophoresis (both CE and two-dimensional gel electrophoresis).

From the separation point of view, CZE may serve as an additional tool in separating keratin proteins. This paper represents, to our knowledge, the first attempt in this respect. Although

comparison of carboxymethylated and untreated proteins (i.e., the results of two-dimensional electrophoresis and CZE) may be the subject of discussion because of the structural changes introduced into the protein molecule by carboxymethylation, here we attempted to categorize the peaks occurring in the CZE separations according to a recognized separation procedure.

5. Conclusions

CZE was applied to a category of proteins not previously investigated by this method. Two basic categories of alkali-extractable keratins, namely the "high-" and "low-sulphur" fractions, were easily separated, each of these categories exhibiting multiple peaks. Comparison with two-dimensional electrophoresis revealed lower selectivity, e.g., in the region of "low-sulphur" proteins (five zones separated by two-dimensional gel electrophoresis while only two peaks were obtained by CZE). This, however, may be caused by the fact that in CZE underivatized extracts were used whereas in the two-dimensional gel separations the samples of proteins were carboxymethylated. Certainly further investigations are needed to make CZE generally applicable to the separation of keratins. On the other hand, CZE was capable of revealing the differences in keratin protein profiles caused by alcohol intake over a period of 7 weeks in laboratory rat hair. The differences regarding the number of peaks in which the individual profiles differed were confirmed by two-dimensional gel electrophoresis. It can be concluded that CZE profiling of rat hair keratins is capable of discerning three peaks that occur only in alcohol-consuming animals, whereas no such peaks were obtained for preparations obtained from controls.

References

[1] W.A. Baumgartner, V.A. Hill and W.H. Blahd, J. Forensic Sci., 34 (1989) 1433.
[2] H. Matsuno, T. Uematsu and M. Nakashima, Br. J. Clin. Pharmacol., 29 (1990) 187.
[3] M.R. Harkey and G.L. Henderson, in R.C. Baselt (Editor), Advances in Analytical Toxicology, Vol. 2, Year Book Medical Publishers, Boca Raton, FL, 1989, p. 298.
[4] M. Chiarotti, Forensic Sci. Int., 63 (1993) 161.
[5] Z. Deyl, F. Tagliaro and I. Mikšík, J. Chromatogr. B, 653 (1994) 47.
[6] M.H. Lynch, W.M. O'Guin, C. Hardy, L. Mak and T.-T. Sun, J. Cell Biol., 103 (1986) 2596.
[7] R.C. Marshall, J. Invest. Dermatol., 80 (1993) 519.
[8] O. Niemala, Scand. J. Clin. Lab. Invest., 53 (1993) 45.
[9] Z. Deyl and I. Mikšík, Nutr. Res., submitted for publication.
[10] W.A. Baumgartner and V.A. Hill, Forensic Sci. Int., 63 (1993) 124.
[11] R.C. Marshall, J. Invest. Dermatol., 80 (1983) 519.
[12] R.C. Marshall and J.M. Gillespie, J. Forensic Sci. Soc., 22 (1982) 377.
[13] B.J. Davis, Ann. N.Y. Acad. Sci., 121 (1964) 404.
[14] U.K. Laemmli, Nature, 227 (1970) 680.
[15] P.H. O'Farell, J. Biol. Chem., 250 (1975) 4007.
[16] W.M. Bonner and R.A. Laskey, Eur. J. Biochem., 46 (1974) 83.
[17] H.H. Rasmussen, J. Van Damme, M. Paype, G. Gesser, J.E. Celis and J.E. Vandekerckhove, Electrophoresis, 12 (1991) 873.
[18] H.H. Rasmussen, E. Mortz, M. Mann, P. Roepstorff and J.E. Celis, Electrophoresis, 15 (1994) 406.

Haemoglobin analysis by capillary zone electrophoresis

Ahmet Şahin*, Yahya R. Laleli, Recep Ortancıl

Düzen Laboratories, Atatürk Bulvarı 237/39, Kavaklıdere 06680, Ankara, Turkey

Abstract

The analysis of haemoglobin is routine in medical laboratories for the purpose of assessing blood disorders and related pathologies. Haemoglobin is structurally diverse and possesses many variant forms, some disease-producing. With recent improvements in technology, capillary electrophoresis is now being adapted in the clinical laboratory. This paper describes the analysis of haemoglobin variants using uncoated fused-silica capillaries. The effects of using different buffer salts at different concentrations with different buffer pH values to separate haemoglobin variants in these capillaries are described.

1. Introduction

Analysis of haemoglobin (Hb) variants from patients' blood samples is of medical importance and, for this reason, is an essential procedure in the clinical laboratory. Hb is a heterotetramer which is formed from the association of two pairs of identical subunits. The predominant Hb variant in normal adult blood is Hb A1, a heterotetrameric protein with two α-chains and two β-chains. Hb A2 is also a normal variant present in smaller amounts. Hb F is a form composed of two α- and two γ-globin chains and is normally expressed during foetal development; its presence is gradually replaced by Hb A usually 6 months after birth. The Hb S and C variants are isoelectric variants as a result of single amino acid changes in one of the globin chains (β), and such changes induce alterations in the structural–functional relationships of the Hb subunits to one another, such that at certain blood pH and

level of blood oxygenation, the Hb tetramer undergoes an irreversible conformational shift which manifests itself as a change in the shape of the red blood cell (the classical sickle shape in sickle-cell anaemia). Hundreds of Hb variants, some producing no symptomatic disease, have been identified by various analytical methods.

The demands for clinical laboratories to provide accurate analyses with timely results makes new methodologies which achieve such goals very welcome. Capillary zone electrophoresis (CZE) is finding many uses in clinical chemistry applications [1–6], and there is the potential to apply CZE in Hb variant analysis also. CZE offers some important advantages over other conventional electrophoretic techniques. Besides requiring very small amounts of sample and electrolyte, its potential for automation makes this technique time and labour effective for clinical laboratories.

Several reports have already appeared in which normal and pathological states were assessed based on Hb variant analysis using capillary electrophoretic methods. Particular methods

---

* Corresponding author.

focused on the analysis of intact Hb molecules [2], globin chains [3] or tryptic digests of haemoglobin molecules [4]. Hb variant analysis has also been examined by isoelectric focusing methods using coated [5] and uncoated capillaries [6]. In this study we attempted to establish optimum conditions for Hb variant analysis using CZE with uncoated capillaries.

2. Experimental

The capillary electrophoresis system was a BioFocus 3000 (Bio-Rad, Richmond, CA, USA) equipped with a fused-silica capillary [36 cm (30 cm to the detector) × 50 μm I.D.]. Sample injection was by positive pressure [$34.45 \cdot 10^7$ Pa (5 p.s.i.) for 2 s], with sample loaded at the anode end of the capillary. The applied potential was 10 kV for all analyses. All reagents for preparing electrolytes were of analytical-reagent grade (Merck, Darmstadt, Germany). A capillary wash solution (Bio-Rad) was used to purge the capillaries between runs. Preparation of the capillary for each run involved an automated purging cycle with capillary wash solution, water and running electrolyte in that order, for 1 min each. Detection was at 415 nm using a tungsten lamp source.

Human Hb samples were prepared from whole blood collected in EDTA-containing evacuated tubes. Red blood cells were washed with normal (0.9%) saline four times. An aliquot of a washed cell suspension was mixed with four aliquots of distilled water. Haemolysis was made complete by freezing in a deep freezer for 10 min. Samples were centrifuged at ca. 600 g for 10 min. The supernatant was diluted tenfold in running electrolyte, and the sample was made ready by filtering it through 0.45-μm cellulose ester (Syrfil-MF; Costar, Cambridge, MA, USA).

As an external reference for haemoglobin species variants, the Beckman Paragon electrophoresis system and Hb variant standard kit (Beckman Instruments, Brea, CA, USA) was also used to analyse samples.

3. Results and discussion

The basis for the separation of the Hb variants using CZE is the charge differences in the globin polypeptides. The structure of all variants are such that they possess a net negative charge, under the conditions of CZE separation, and thus the inherent electrophoretic mobility of the Hb species will be directed towards the anode. However, the use of uncoated fused silica at pH values in the neutral or alkaline range creates a significant electro-endoosmotic flow (EOF) directed towards the cathode. The magnitude of the EOF is such that the net mobility of all Hb species is towards the cathode. This property means that Hb species having higher isoelectric points (pI values) (i.e., species with less net negative charge) should be detectable first inasmuch as the electrostatic repulsive forces in the opposite direction are less than for Hb species having lower pI values, and they would show a higher net mobility towards the cathode.

Satisfactory separation of analytes using CZE is highly dependent on a suitable electrophoresis buffer–electrolyte. In addition to ensuring overall stability of the system, the buffer determines the migration behaviour of analytes. Several different buffers have been used for haemoglobin separations in traditional free zone electrophoresis applications. Some methods employ a single weak acid or base to provide the buffering at the running pH; others consist of a mixture of weak acids or bases. As the pI values of haemoglobin species variants are between 7.00 and 7.50 (Hb A1, 7.15; Hb A2, 7.40; Hb F, 7.15; Hb S, 7.25), preparation using buffers with the pH adjusted above these values becomes necessary. Tris and borate buffers are commonly selected because of their buffering capacity ranges between pH 8.0 and 9.5. Veronal (barbital) buffers also possess a buffering capacity in this range and are commonly used in electrophoretic systems involving the use of commercially available agarose gels to analyse Hb variants. We tested Tris, borate and veronal buffers at three different concentrations and at different pH values. Analysis with a Tris–HCl electrolyte was carried

out at 0.5, 1.0 and 1.5 *M*, sodium borate was tested at 20, 30 and 40 m*M* and veronal (sodium barbiturate) at 25, 50 and 75 m*M*. For each of these concentrations for each of the indicated salts, three different pH values were tested, namely pH 8.0, 8.5 and 9.0.

The electropherogram in Fig. 1 illustrates how the molecular charge difference between the Hb S and Hb A1 species affects their separation by CZE. This separation of these variants was also generally observed under a variety of conditions in which all permutations for the three different buffer salts, concentrations and pH were tested. The Hb A2 species is seen to migrate ahead of Hb S in Fig. 1. We found that the degree of separation of Hb S from Hb A1 was not significantly different for any change in the pH (8.0, 8.5, 9.0) of the salts tested, but there were certainly changes in migration times, an increase in pH producing shorter migration times for all species. The inset in Fig. 1 shows a densitometric scan of stained haemoglobin variants observed using the Beckman agarose gel electrophoresis system. Although we did not confirm the identity of Hb variant species during the CZE analysis of our samples using certified standards, the agarose gel analysis operates under identical principles to CZE and the densitometric scan of stained proteins in the gel compares favourably with the absorbance changes during CZE in which detection is specific for the Hb prosthetic group.

The variant Hb F has no significant charge difference from Hb A1 (only 0.05 pH unit separates these variants), and this presents the most difficult challenge to manipulating conditions to separate common variants. Fig. 2 shows the separation of Hb F and Hb A1 from a patient's sample using a 50 m*M* veronal system buffered at pH 8.5. An observable separation of these species was achieved for all pH values tested, but the resolution appeared better at pH 8.0 and 8.5 than at pH 9.0, demonstrating an effect of pH on this separation. Again, the
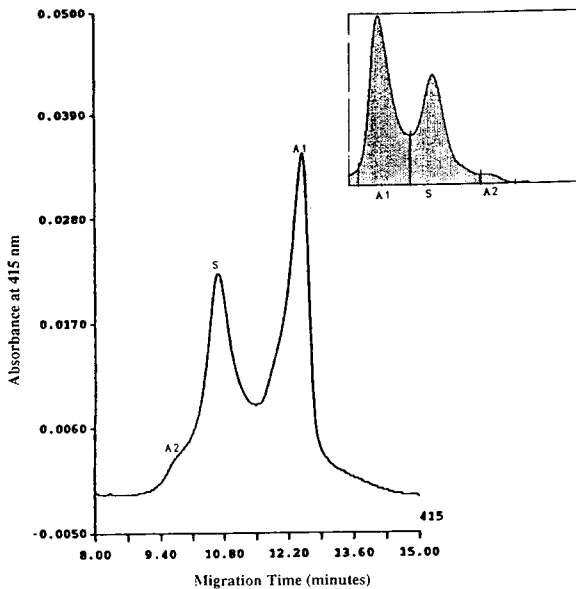
Fig. 1. Electropherogram of a sample from a patient with sickle-cell disease. Electrolyte, 1.0 *M* Tris–HCl (pH 8.0). Other conditions as described under Experimental.
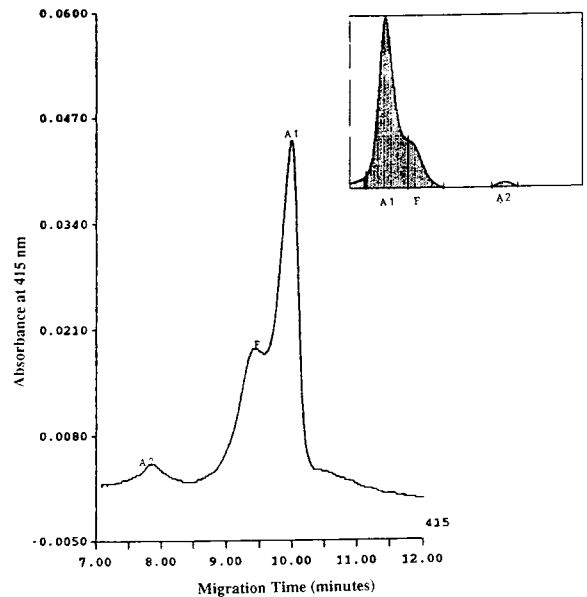
Fig. 2. Electropherogram of a patient's sample with a significant Hb F fraction. Electrolyte, veronal (sodium barbital) (pH 8.5).

proportions of the amounts of Hb species present in this sample agreed with the agarose gel determination (inset).

Fig. 3 is an electropherogram of another patient's sample in which Hb variants were separated using 20 m*M* sodium borate (pH 8.5). The Hb variants A2, S, F and A1 were all detectable. These particular conditions resolved these four variants the best, although we did observe the separation of these variants using this buffer at other pH values. For selecting particular buffer salts to be used in such CZE separations, we found the best concentration for Tris to be 1.0 *M*, for veronal 50 m*M* and for borate 20 m*M*.

Variations in the migration times of the species for replicate analyses were a significant problem and make routine clinical use difficult, in that species identification depends on consistent migration times (much as component identification in high-performance liquid chromatography depends on consistent retention times). We made attempts to stabilize the EOF, which we believe is the factor responsible for such irreproducibili-

ty, but we were unable to obtain more optimum conditions. As the Hb A1 variant is usually a constant in all analyses, its identification can be made initially and then used as a reference for identifying other variants. Fig. 4 is an electropherogram of a normal adult blood sample with Hb A1 present as the major species. There are other cases in which Hb A1 may not be the major species present, as shown in Fig. 5 (identification of Hb species in CZE were made by comparison with separated zones seen in agarose gel electrophoresis, a routine method in our laboratory as well as in many others). Such cases might present some confusion for the analyst. Nevertheless, the experienced analyst would know the relative order of migration of the typical species present in the population, and variations in routine electropherogram patterns can be easily discerned. Alternatively, unknown patients' samples can be run with internal standards (e.g., with commercially available Hb variant standards) to make Hb variant identification unambiguous.

Changes to the conditions of buffering (selection of the ideal salt and therefore of the ideal

Fig. 3. Electropherogram of a patient's sample containing significant proportions of variants Hb A1, A2, S and F. Buffer, sodium borate (pH 8.5).
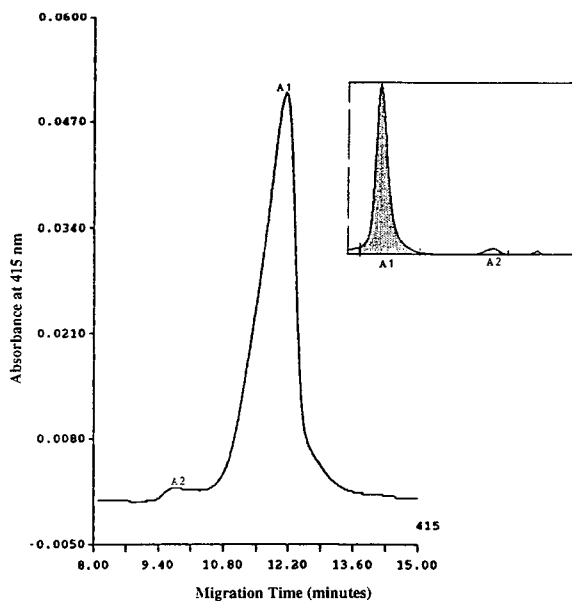
Fig. 4. Electropherogram of a sample obtained from a healthy adult. Buffer, veronal (pH 8.5).
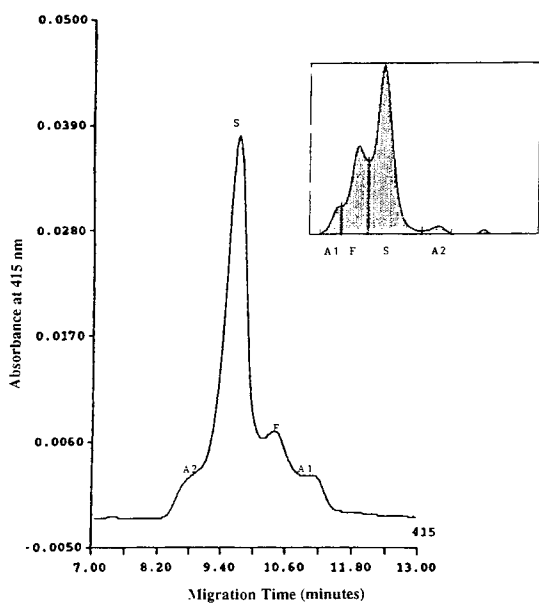
Fig. 5. Electropherogram of a sample from a patient with sickle-cell disease. Buffer, veronal (pH 8.5).

pK_a, electrolyte pH and buffer concentration), in addition to selection of modifying agents which dynamically coat the capillary walls in order to alter protein adsorption and to reduce the EOF to negligible levels, are future considerations for further work to understand and control the considerable variations of migration times observed in replicate analyses.

References

[1] F.A. Chen, C.M. Liu, Y.Z. Hsieh and J.C. Steinberg, Clin. Chem., 37 (1991) 14.
[2] N. Ishioka, N. Iyori, J. Noji and S. Kurioka, Biomed. Chromatgr., 6 (1992) 224.
[3] C.N. Ong, L.S. Liau and H.Y. Ong, J. Chromatogr., 576 (1992) 346.
[4] G.A. Ross, P. Lorkin and D. Perret, J. Chromatogr., 636 (1993) 69.
[5] M. Zhu, T. Wehr, V. Levi, R. Rodriguez, K. Shiffer and Z.A. Cao, J. Chromatogr. A, 652 (1993) 119.
[6] S. Molteni, H. Frischknecht and W. Thormann, Electrophoresis, 15 (1994) 22.

Effects of alkylamines on electroosmotic flow and protein migration behaviour in capillary electrophoresis

Danilo Corradini*, Gianfranco Cannarsa, Emanuela Fabbri, Claudio Corradini

Istituto di Cromatografia del CNR, Area della Ricerca di Roma, P.O. Box 10, I-00016 Monterotondo Stazione (Rome), Italy

Abstract

This paper reports the use of four closely related alkylamines as running electrolyte additives in capillary electrophoresis that permit the control of electroosmotic flow and protein migration behaviour in uncoated capillaries. At pH 2.5 the direction of the electroosmotic flow was anodic with all additives and at constant ionic strength its magnitude increased with increasing alkylamine concentration. The observations are in qualitative agreement with a previous reported theoretical model that correlates the electroosmotic mobility with the charge density in the Stern region of the electric double layer, arising from the adsorption of the additive, and the charge density at the capillary wall due to dissociation of silanols.

1. Introduction

The electric double layer at the interfacial region between the inner wall of the capillary tube and the electrolyte solution gives rise to two fundamental phenomena in capillary electrophoresis: the electroosmotic flow, which is the flow of the electrolyte solution along the capillary tube generated by the electric field applied tangentially to the electric double layer, and the attraction of charged analytes by the oppositely charged groups or ions that form the immobilized part of the electric double layer.

When the capillaries are made of fused silica, the inner wall is negatively charged in the pH range where the silanol groups are dissociated. Under these conditions the electroosmotic flow is directed toward the cathode and positively charged analytes, such as basic proteins, can interact strongly with the capillary wall, leading

to poor efficiency, low resolution and irreproducibility of the retention times.

Many different approaches to control the electroosmotic flow in capillary electrophoresis have been addressed. These include chemical coating of the capillary wall [1–4], extremes of electrolyte pH [5,6], the application of applied radial voltage to the capillary wall [7,8] and the addition to the running electrolyte solution of organic solvents [9], surfactants [10], neutral salts [11] or other additives. Several of these additives have been reported to attenuate protein–capillary wall interactions [12–18] and a few of them also to reverse the direction of the electroosmotic flow [15–18].

Reversal of the direction of the electroosmotic flow in fused-silica capillaries occurs when specific adsorption of counter ions in the immobilized region of the double layer, the so called Stern layer, takes place. In this case, the potential at the plane of shear between the Stern layer and the diffuse layer, ψ_δ, which can be

---

* Corresponding author.

approximated to the zeta potential, ζ, becomes positive and the electroosmotic flow is directed towards the anode.

Alkylamines are generally believed to interact strongly with silanol groups [19] and their effectiveness at masking silanophilic activity in both HPLC [20,21] and capillary electrophoresis [17–18,22] has been reported.

In this work, the effect of cationic additives on the control of the electroosmotic flow and on protein migration behaviour in bare fused-silica capillaries was further investigated by using four closely related alkylamines, differing in the number of ethanol groups replacing the ethyl groups in the molecule of triethylamine. The investigation was performed at pH 2.5 in order to have all alkylamines full protonated and therefore behaving as monovalent cations of similar chemical composition and with gradual differences in their molecular size and hydrophobicity.

2. Experimental

2.1. Samples and chemicals

Cytochrome c (from horse heart), lysozyme (from chicken egg white), ribonuclease A (from bovine pancreas) and α-chymotrypsinogen A (from bovine pancreas) were supplied by Sigma (St. Louis, MO, USA) and 5-(hydroxymethyl-2-furaldehyde by Aldrich (Milwaukee, WI, USA). Triethylamine, N,N-diethylethanolamine, N-ethyldiethanolamine and triethanolamine were purchased from Fluka (Buchs, Switzerland) and were used without further purification. Analytical-reagent-grade phosphoric acid, hydrochloric acid, sodium hydroxide, sodium chloride and HPLC-grade water and methanol were obtained from Carlo Erba (Milan, Italy).

2.2. Apparatus

All experiments were performed using a P/ACE Model 2100 capillary electrophoresis unit, operated under System Gold Version 7.11 control, data acquisition and analysis software (Beckman, Fullerton, CA, USA). A fused-silica

capillary (Quadrex, New Haven, CT, USA) of 0.075 mm I.D. and 0.375 mm O.D. and with a total length of 37 cm (30 cm to the detector) was mounted in the cartridge. The capillary tube temperature was maintained at $25 \pm 1°C$ by means of a fluorocarbon liquid continuously circulating through the cartridge. A deuterium light source with either a 214- or 280-nm bandpass filter was used. The samples were injected by applying 0.5 p.s.i. (1 p.s.i. = 6894.76 Pa) pressure for 1 s, and the approximate sample volume of 9 nl was calculated according to the literature [23].

2.3. Electrophoresis

All experiments were carried out without any chemical coating of the inner wall of the fused-silica capillaries. Prior to use, the untreated capillary was flushed successively with 0.5 M sodium hydroxide (30 min), water (10 min) and 0.1 M hydrochloric acid (30 min), followed by a second treatment with sodium hydroxide (0.5 M for 30 min) and water (10 min), and then rinsed with the running electrolyte.

The running electrolyte was renewed after five or six runs, and before each run the capillary was rinsed with the running electrolyte for 3 min. For storage the capillary was rinsed with water for 10 min and then dried by flushing nitrogen for 10 min.

The capillary tube was flushed with 0.5 M sodium hydroxide (3 min) and water (3 min) each time a running electrolyte of new composition was used. All experiments were carried out by applying a constant voltage of 10 kV. Protein solutions of 1.0–3.0 mg/ml were prepared in HPLC-grade water.

2.4. Electroosmotic mobility measurements

The electroosmotic mobility was determined by measuring the migration time of 5-(hydroxymethyl)-2-furaldehyde, used as an inert tracer, detected at 280 nm at the anodic end of the capillary, on reversing the polarity. The inert tracer was dissolved in methanol–water (1:10, v/v) at a concentration of 1.0 mg/ml. All measurements of electroosmotic mobility were made

in triplicate. Running electrolytes at various additive concentration and constant ionic strength were made by adding the appropriate amount of sodium chloride to the electrolyte solution, containing 50 mM phosphate buffer (pH 2.5), for compensation of the changes in the additive concentration. All solutions were filtered through a Type HA 0.22-μm membrane filter (Millipore, Bedford, MA, USA) and degassed by sonication before use.

3. Results and discussion

The dependence of the electroosmotic mobility on the concentration in the running electrolyte of cationic species which adsorb at the interfacial region between the capillary wall and the electrolyte solution was investigated by using four closely related tertiary alkylamines, namely triethylamine (TEA), N,N-diethylethanolamine (DEEOHA), N-ethyldiethanolamine (EDEHOA) and triethanolamine (TEOHA). At pH 2.5 the direction of the electroosmotic flow, measured with 5-(hydroxymethyl)-2-furaldehyde as a neutral marker, was anodic with all additives and at constant ionic strength (123 mM) its magnitude increased with increasing the alkylamine concentration.

In a previous paper [18] we presented a theoretical model that correlates the electroosmotic mobility with the charge density in the Stern region of the electric double layer, arising from the adsorption of counter ions, and the charge density at the capillary wall, due to dissociation of silanols. According to this model, we can express the dependence of the electroosmotic mobility on the concentration of the cationic additive in the running electrolyte under otherwise identical conditions as

$$\mu_{eo} = \frac{4\pi}{\kappa\eta} \left\{ \frac{zen_0 \dfrac{C}{55.6} \exp\left(\dfrac{ze\psi_\delta + \Phi}{kT}\right)}{1 + \dfrac{C}{55.6} \exp\left(\dfrac{ze\psi_\delta + \Phi}{kT}\right)} - \left(\frac{\gamma}{1 + \dfrac{[H^+]}{K_a}}\right)\right\} \quad (1)$$

where κ is the reciprocal of the Debye length, η is the viscosity of the electrolyte solution, e is the elementary charge, z is the valence of the adsorbing ion, k is the Boltzman constant, T is the absolute temperature, n_0 is the number of accessible sites in the Stern layer, ψ_δ is the potential at the Stern plane, Φ allows for any specific adsorption potential, γ is the sum of the ionized and protonated surface silanol groups, $[H^+]$ is the bulk electrolyte hydrogen ion concentration and K_a is the silanol dissociation constant.

Eq. 1 suggests that at constant ionic strength and pH the electroosmotic mobility would depend mainly on the surface density of adsorbed counter ions in the Stern region of the double layer, which should follow a Langmuirian-type adsorption model. The good agreement between the theoretical prediction of Eq. 1 and the experimental trends in the data is illustrated in Fig. 1 by plots of the electroosmotic mobility against the concentration of the additive in the running electrolyte. These curves, the slopes of which decrease with increasing additive concentration, are Langmuirian or quasi-Langmuirian
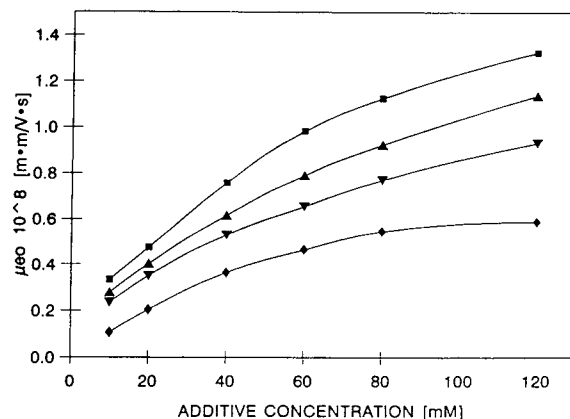
Fig. 1. Dependence of the electroosmotic mobility on the concentration of additive in the running electrolyte at constant ionic strength (123 mM) and pH (2.5). Capillary, fused silica, 0.075 mm I.D. × 370 mm total length (300 mm to the detector); applied voltage, 10 kV; temperature, 25°C; neutral marker, 5-(hydroxymethyl)-2-furaldehyde; detection wavelength, 280 nm at the cathodic end. Additives: ☐ = triethylamine; ▲ = N,N-diethylethanolamine; ▼ = N-ethyldiethanolamine, ◆ = triethanolamine.

Table 1
Molecular volumes of alkylamines calculated by the Chem-X
1990 Molecular Modelling Program

Additive	Molecular volume ($Å^3$)
Triethylamine	98.5
N,N-Diethylethanolamine	104.9
N-Ethyldiethanolamine	111.1
Triethanolamine	117.3

in shape [22]. The differences in the slopes of the four plots in Fig. 1 can be accounted for by differences in either the specific adsorption energy (Φ) or the molecular size of the additives, or both.

The four additives are closely related tertiary alkylamines differing only in the number of hydroxyl functions, which vary from one to three according to the number of ethanol groups which replace the ethyl groups in TEA. The replace-

ment of one, two or three ethyl groups by a corresponding number of ethanol groups is expected to lead to alkylamines with proportionally lower hydrophobic character and larger molecular size. Three-dimensional molecular modelling of the four alkylamines was performed with the Chem-X 1990 Molecular Modelling Program (Chemical Design, Oxford, UK) in order to estimate their relative molecular size by the theoretical molecular volume calculated for a single molecule over its Van der Waals surface [24] and the results are reported in Table 1.

The electroosmotic mobilities obtained with the four alkylamines at different concentrations were plotted against the number of hydroxyl groups present in each additive (Fig. 2A) and against the molecular volumes calculated by the Chem-X 1990 Molecular Modelling Program (Fig. 2B). In both cases the plots obtained were almost linear, with negative slopes. These ob-
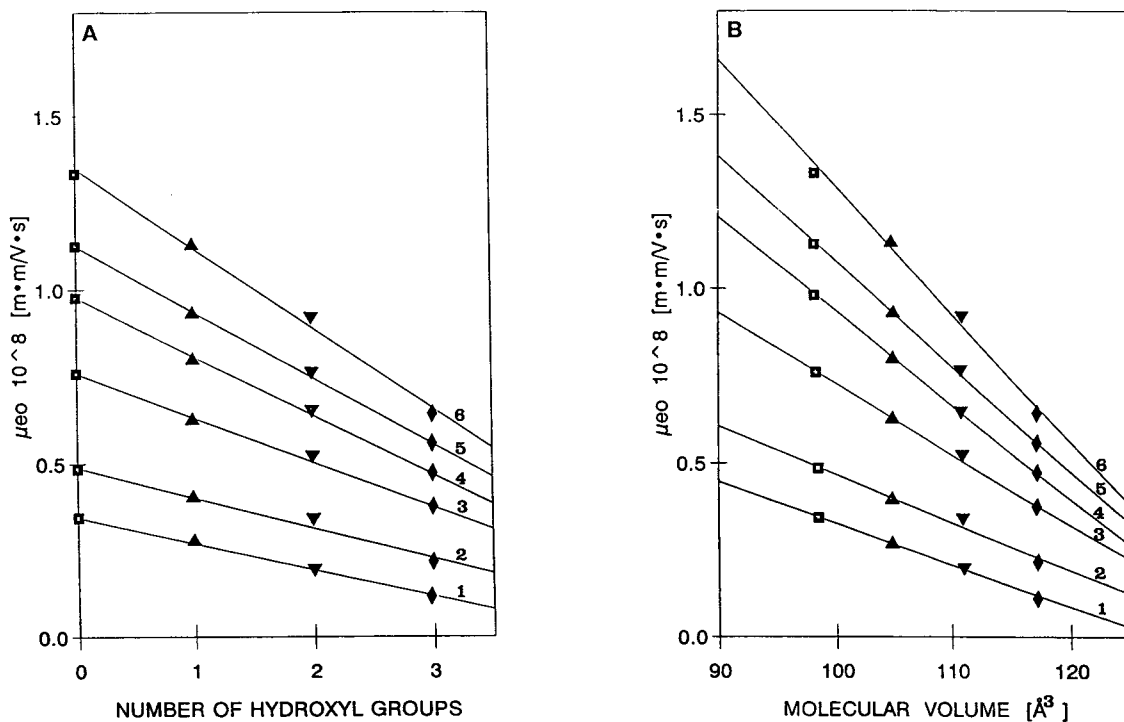
Fig. 2. Dependence of the electroosmotic mobility at different additive concentrations on (A) the number of hydroxyl groups present in each additive and (B) their molecular volumes calculated by the Chem-X Molecular Modelling Program. Additive concentrations (from line 1 to 6): 10, 20, 40, 60, 80 and 120 mM; ionic strength, 123 mM; symbols and other conditions as in Fig. 1.

servations suggest that in addition to the contribution arising from the specific adsorption energy (Φ), which is expected to vary with the different content of hydroxyl groups of the four additives, the electroosmotic mobility may depend on the molecular size of the adsorbing counter ions in such a way that the number of accessible sites (n_0) in the Stern layer can be occupied by a limited number of counter ions, which will be larger for additives of smaller molecular size.

The beneficial effect of controlling the electroosmotic flow by the addition of the four alkylamines to the running electrolyte on the migration behaviour of four basic proteins was also investigated. All experiments were performed under the same conditions as employed to study the effect of these additives on the electroosmotic flow, except that proteins were detected at the cathodic end of the capillary tube.

The four basic proteins cytochrome c (Cyt), lysozyme (Lys), ribonuclease A (RNase) and α-chymotrypsinogen A (Chy) have isoelectric points ranging from 9 to 11 and therefore at pH 2.5 they are positively charged and moved towards the cathode. In the absence of the alkylamines in the running electrolyte, the four basic proteins comprising the mixture test were resolved in a very narrow separation space and migrated with poorly reproducible migration times as fairly symmetric peaks. The poorly reproducible migration times may arise either from protein–capillary wall interactions, which would affect the electroosmotic mobility and consequently the migration times, or from the difficulty of maintaining a constant electroosmotic flow in bare fused-silica capillaries, as evidenced by Cohen and Grushka [25], or both. The narrow separation space is a consequence of full protonation of proteins, which diminishes charge differences between species.

In the presence of the additives, the four basic proteins moved towards the cathode against the electroosmotic flow, which travelled in the opposite direction. Consequently, the apparent mobility of proteins, which is the resultant of the oppositely directed vectors of the protein elec-
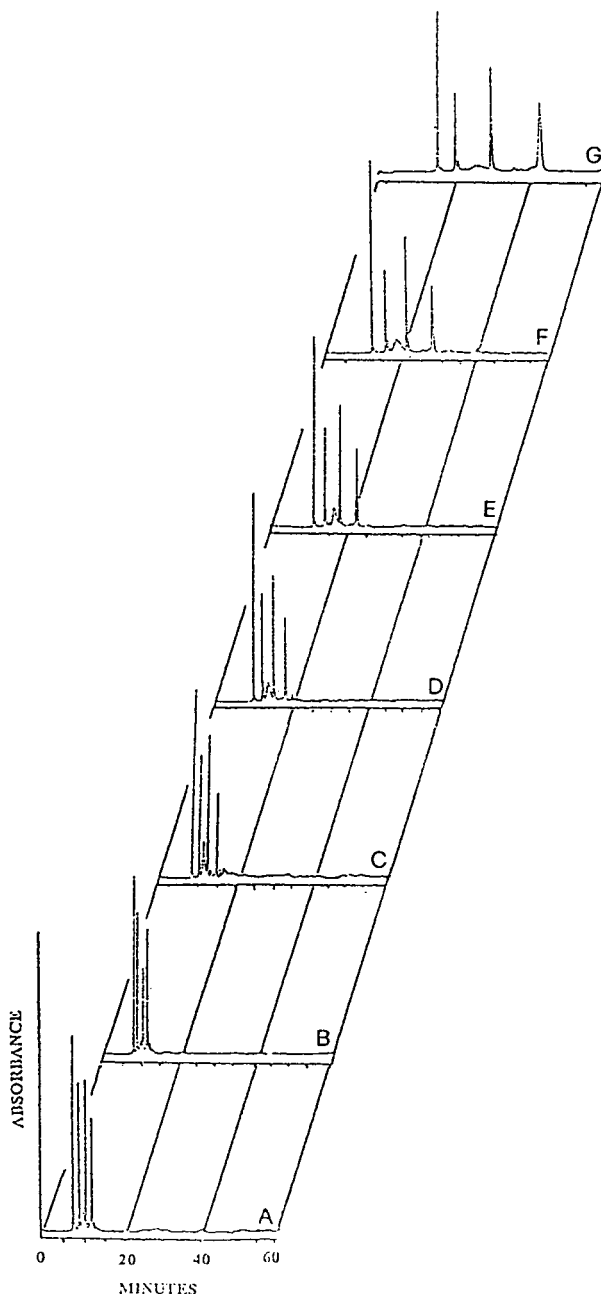
Fig. 3. Electropherograms of standard basic proteins obtained with N,N-diethylethanolamine as the additive at pH 2.5, constant ionic strength (123 mM) and concentrations of (A) 4, (B) 10, (C) 20, (D) 40, (E) 60, (F) 80 and (G) 120 mM. Migration order of proteins as in Fig. 4. Experimental conditions as in Fig. 1, except detection at 214 nm.
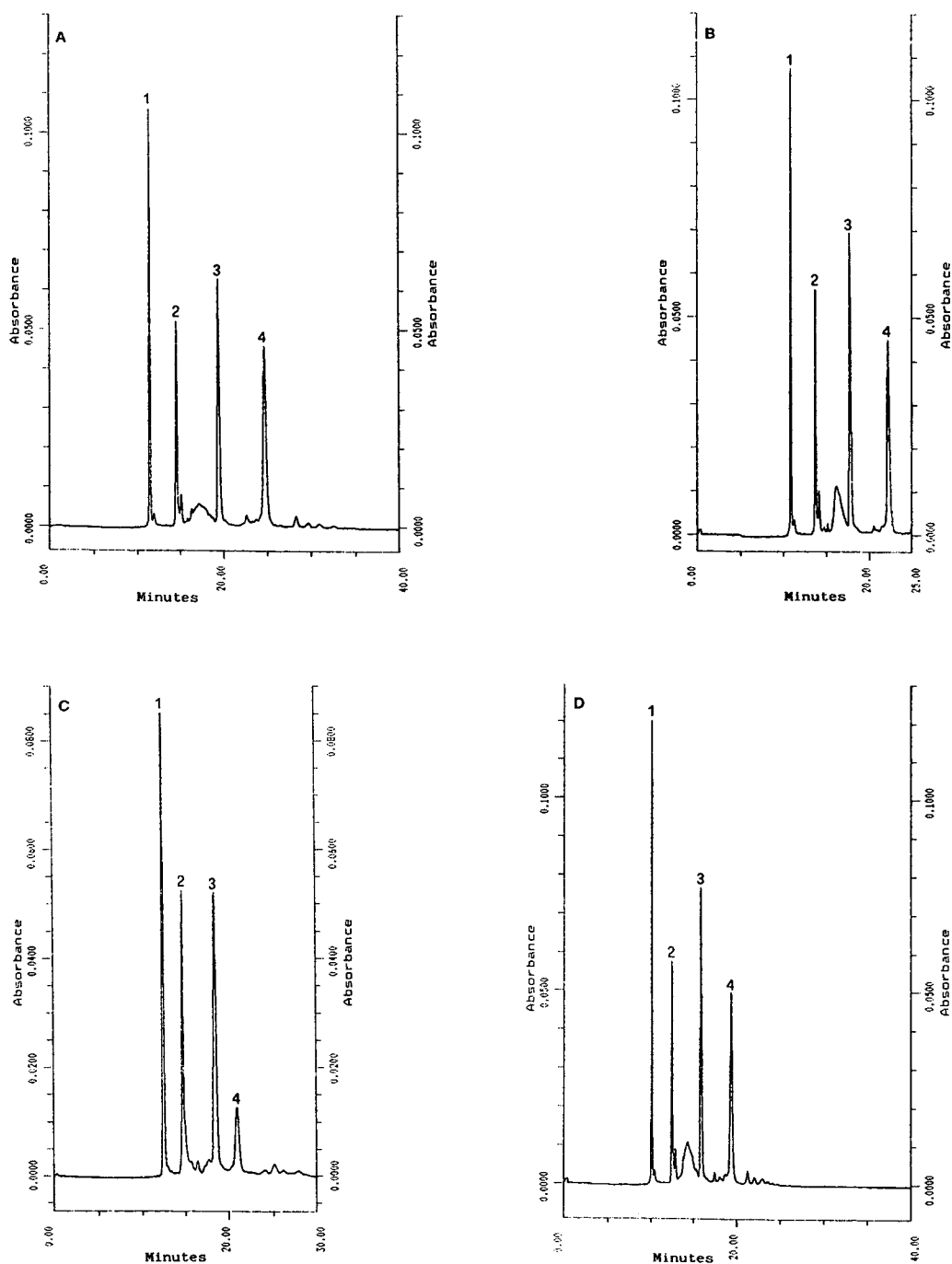
Fig. 4. Electropherograms of standard basic proteins obtained with different additives at the same concentration (60 mM), ionic strength (123 mM) and pH (2.5). (A) Triethylamine; (B) = N,N-diethylethanolamine; (C) N-ethyldiethanolamine; (D) triethanolamine. Proteins: 1 = cytochrome c; 2 = lysozyme; 3 = ribonuclease A; 4 = α-chymotrypsinogen A. Other conditions as in Fig. 3.

trophoretic mobility and of the electroosmotic mobility, varied on changing the additive and for all of them decreased with increasing additive concentration in the running electrolyte. Thus, as shown in Fig. 3 for DEEOHA, an increase in the additive concentration led to an increase in the protein migration times and in the separation space. However, the electrophoretic mobility of proteins was independent from the additive type and concentration, as it varied within 3.0% when measured with each of the four additives over the whole investigated concentration range, and within 5.5% when measured with either additive over the same concentration range. For this the absence of interactions between the investigated proteins and the additives can be inferred.

The effect of using different additives on the separation of a model mixture of the four basic proteins, under otherwise identical conditions, is depicted in Fig. 4. All separations were carried out in the same capillary tube at an applied voltage of 10 kV and with running electrolytes containing the different additives at the same concentration (60 mM), ionic strength (123.5 mM) and pH (2.5). The values of the measured current were 160 ± 5 μA.

Comparison of the four electropherograms shows that the separation of the four basic proteins was improved and the speed of analysis was decreased by using the additive which generated the highest counter electroosmotic flow, i.e., TEA.

The effectiveness of the four alkylamines in preventing protein–capillary wall interactions was investigated by multiple injections ($n = 5$) of this protein mixture into the same capillary using the above running electrolytes and experimental conditions. No washing of the capillary was performed between runs in order to detect irreversible protein adsorption that would affect the electroosmotic flow and consequently the migration times. Under these conditions, the reproducibility of the protein migration times obtained with all additives was better than 2.0% (R.S.D.). These results indicate that the four alkylamines are effective in preventing capillary wall interactions, as can also be inferred from the absence of peak tailing in the electropherograms displayed in Fig. 4.

4. Conclusions

We have further investigated the effect of cationic additives on the electroosmotic flow in bare fused-silica capillaries. Our experimental results showed that the dependence of the anodic electroosmotic flow on the concentration of alkylamines in the electrolyte solution maintained at pH 2.5 and constant ionic strength is described by a Langmuirian-type relationship.

At any given additive concentration, the magnitude of the electroosmotic flow increases according to the order of increasing basicity and decreasing molecular size. This indicates that the observed differences in the electroosmotic flow may reflect differences in the adsorbability of the four closely related alkylamines, which is believed to depend on their specific adsorption energy (Φ) and molecular size [26]. Further, in addition to controlling the electroosmotic flow, the four alkylamines were shown to be effective at preventing protein–capillary wall interactions without affecting the electrophoretic mobilities of these biopolymers.

Acknowledgements

References

[1] S. Hjertén, J. Chromatogr., 347 (1985) 191.
[2] J.W. Jorgenson and K.D. DeArman Lukacs, Science, 222 (1983) 266.
[3] S.A. Swedberg, Anal. Biochem., 185 (1990) 51.
[4] W. Nashabeh and Z. El Rassi, J. Chromatogr., 559 (1991) 367.
[5] R. McCormick, Anal. Chem., 60 (1990) 2322.
[6] J.S. Green and J.W. Jorgenson, J. Chromatogr., 478 (1989) 63.
[7] C.S. Lee, W.C. Blanchard and C.T. Wu, Anal. Chem., 62 (1990) 1550.
[8] M.A. Hayes and A.G. Ewing, Anal. Chem., 64 (1992) 512.

[9] B.B. VanOrman, G.G. Liversidge, G.L. McIntire, T.M. Olefirowicz and A.G. Ewing, J. Microcol. Sep., 2 (1990) 176.

[10] A. Emmer, M. Jansson and J. Roeraade, J. Chromatogr., 547 (1991) 544.

[11] M.M. Bushey and J.W. Jorgenson, J. Chromatogr., 480 (1989) 301.

[12] M. Zhu, R. Rodriguez, D. Hansen and T. Wehr, J. Chromatogr., 516 (1990) 123.

[13] H.H. Lauer and D. McManigill, Anal. Chem., 58 (1986) 166.

[14] J.A. Bullock and L.C. Yuan, J. Microcol. Sep., 3 (1991) 241.

[15] J.E. Wiktorowicz and J.C. Colburn, Electrophoresis, 11 (1990) 769.

[16] A. Emmer, M. Jansson and J. Roeraade, J. High Resolut. Chromatogr., 14 (1991) 738.

[17] W. Nashabeh and Z. El Rassi, J. Chromatogr., 596 (1992) 251.

[18] D. Corradini, A. Rhomberg and C. Corradini, J. Chromatogr. A, 661 (1994) 305.

[19] K.-G. Wahlund and A. Sokolowski, J. Chromatogr., 151 (1978) 299.

[20] K.E. Bij, Cs. Horváth, W.R. Melander and A. Nahum, J. Chromatogr., 203 (1981) 65.

[21] W.R. Melander, D. Corradini and Cs. Horváth, J. Chromatogr., 317 (1984) 67.

[22] C. Chiesa and Cs. Horváth, J. Chromatogr., 645 (1993) 337.

[23] R.S. Bush and B.L. Karger, Technical Bullettin TIBC-104, Beckman Instruments, Spinco Division, Palo Alto, CA, 1990.

[24] G. Del Re, E. Gavuzzo, E. Giglio, F. Lely, F. Mazza and V. Zappia, Acta Crystallogr., Sect. B, 33 (1977) 3289.

[25] N. Cohen and E. Grushka, J. Chromatogr. A, 678 (1994) 167.

[26] P.C. Hiemenz, Principles of Colloid and Surface Chemistry, Marcel Dekker, New York, 1986, pp. 722–726.

Detection of traces of a trisulphide derivative in the preparation of a recombinant truncated interleukin-6 mutein

Jerôme Breton[a], Nilla Avanzi[a], Barbara Valsasina[a], Laura Sgarella[a],
Anna La Fiura[a], Umberto Breme[a], Gaetano Orsini[a], Elisabeth Wenisch[b],
Pier Giorgio Righetti[b,*]

[a]*Pharmacia Farmitalia, BioScience Center, via Giovanni XXIII, I-20014 Nerviano, Italy*
[b]*Department of Cell Biology, University of Calabria in Arcavata di Rende, Cosenza, Italy*

Abstract

A new mutein of interleukin-6, called Δ22-IL-6 Cys 3,4, characterized by the deletion of the first 22 amino acids at the N-terminal end and by the substitution of the first two cysteines (Cys^{23} and Cys^{29}) with serine residues, was produced in *Escherichia coli* and was found to maintain the structural and functional properties of the human native form. A partially purified preparation still showed in isoelectric focusing a minor acidic component (p*I* 6.10) and a more basic component (p*I* 6.70), the native form having a p*I* of 6.56. This preparation was further fractionated in a multi-compartment electrolyser with isoelectric membranes, which allowed the collection of the more alkaline species for characterization. Mass spectra of the p*I* 6.70 form gave an additional mass of 32 atomic mass units (amu), suggesting the addition of two oxygen atoms (a potential oxidation of two methionine residues to sulphoxide). However, the five methionine residues in this higher p*I* form were identified after enzymatic hydrolysis and peptide mapping and were found to be in a reduced state. In addition, the p*I* 6.70 form was quickly converted into the native form by mild reductive treatment. On digestion and fingerprinting, the peptide from residues 50 to 65 of the p*I* 6.70 species (containing the only two cysteine residues of the molecule) exhibited a more hydrophobic behaviour in reversed-phase high-performance liquid chromatography and retained a mass increase of 32 amu. These experimental findings more likely suggest the addition of an extra sulphur atom to the only disulphide bridge to give an unusual protein trisulphide molecule.

1. Introduction

In the production of recombinant proteins, structural variations of the final product can arise at genetic and/or post-translational level or can be induced by process conditions; common

* Corresponding author. Address for correspondence: L.I.T.A., via Fratelli Cervi 93, I-20090 Segrata (Milan), Italy.

changes in the covalent structure of recombinant proteins which depend on the operative conditions are, for example, deamidation of glutamine and asparagine side-chains, scrambling of disulphide bonds, generation of ragged ends by partial proteolysis or oxidation of sensitive residues [1,2]. Recently, a new post-translational modification consisting in a trisulphide cross-link (with an additional sulphur atom inserted into the Cys_2 disulphide bond) was independently discovered by two research groups as a side-

product of recombinant human growth hormone biosynthesized in *Escherichia coli* [3,4].

The identification of process-related modifications of recombinant proteins is an important issue for the characterization and validation of the final preparations. In addition, by knowing the chemico-physical nature of the induced modification it is possible to study a specific purification process which eventually results in the elimination of unwanted heterogeneous forms.

Interleukin-6 (IL-6) is a pleiotropic cytokine which can act on a wide variety of tissues. Depending on the nature of the target cells, IL-6 can exert growth promotion, growth inhibition, differentiation and induction of specific gene expression [5]. The full length form of human IL-6 consists of 185 amino acid residues starting with alanine at position 1 and contains four cysteine residues at positions 45, 51, 74 and 84 [6]. In certain cell types, IL-6 is also produced as a 184 amino acid protein with proline instead of alanine as the first amino acid [7].

Investigations of the relationship between the structure and biological function of IL-6-related proteins have demonstrated that the first 28 amino acids of mature human IL-6 are dispensable for biological activity [8] and that cysteine residues 45 and 51 could be substituted by serine residues without any impairment of the activity [9]. Bacterial expression of IL-6 derived muteins with N-terminal truncation and differential retention of the two disulfide bonds has recently been described [10]. Based on these previous results, we have studied the production of an IL-6 mutein characterized by the deletion of the first 22 amino acids at the N-terminal end and by the substitution of the first two cysteine (Cys[23] and Cys[29]) residues with serine residues, while the other two cysteine residues (Cys[52] and Cys[62]) were retained and gave a disulphide bridge (see Fig. 7: primary structure).

This new mutein, which is called Δ22-IL-6 Cys 3,4 and is under investigation for therapeutic application, was expressed in a recombinant strain of *E. coli* and was found to maintain the structural and functional properties of the human full length IL-6 [11]. In this paper, we demon-

strate some unique structural modifications of a minor, higher p*I* component detected in partially purified preparations of Δ22-IL-6 Cys 3,4, suggesting the formation of a novel protein derivative with a trisulphide bridge.

2. Experimental

2.1. Equipment and chemical for electrophoresis

All analytical immobilized pH gradient (IPG) experiments were performed in a Multiphor II electrophoresis unit equipment with a Macrodrive 5 power supply and Multitemp thermostatic unit (Pharmacia Biotech, Uppsala, Sweden). Acrylamide, N,N'-methylenebisacrylamide, ammonium peroxodisulphate and N,N,N',N'-tetramethylethylenediamine were obtained from Bio-Rad (Hercules, CA, USA). The Immobiline species used, p*K* 3.6, 4.6, 7.0 and 8.5, were from Pharmacia Biotech. HEPES [N-(2-hydroxyethyl)piperazine-N'-2-ethanesulphonic acid] and L-histidine (free base) were supplied by Sigma (St. Louis, MO, USA).

2.2. Preparation of analytical immobilized pH gradients

The gels were of 240 × 110 × 0.5 mm size. An IPG pH of 5.0–8.0 was set in a 5%T, 4%C polyacrylamide matrix [12]. After preparing the two limiting, acidic and basic mixtures, they were titrated (with weak acids and bases) to pH values close to neutrality, to ensure uniform polymerization and efficient monomer conversion throughout the pH gradient. On gel washing (4 × 30 min) in distilled water, all added titrants (and also catalysts and ungrafted monomers) were efficiently removed. The gels were then washed for 30 min in 20% glycerol, dried in air and reswollen in different additives.

2.3. Optimizing the additive concentrations

The use of dry gels allows the formation of an additive gradient at right-angles to the pH gra-

dient. This is of particular value when optimizing the additive concentrations in preliminary experiments. By applying and focusing the sample along the additive gradient, the optimum additive concentration can be determined in a single experiment.

Place the dry gel with its supporting film on a glass plate. Apply the U-frame (reswelling cassette for dry gels) on top of the gel. Clamp the glass plates together. A linear concentration gradient additive is formed by using a gradient mixer. Place 7.3 ml of rehydrating solution into each chamber of the gradient former and allow the gradient to flow from the top of the vertically standing cassette under gravity. The gels are rehydrated overnight. The protein samples (about 50 μg in 50 μl) are applied in surface wells both close to the anode and to the cathode. The electric focusing conditions are as follows: 1 h at 500 V, followed by 5000 V (maximum setting: 1 mA, 5 W) for 14 h at 10°C. Staining is carried out with Coomassie Brilliant Blue R-250 in copper sulphate solution [13].

2.4. Preparative IPGs in a liquid vein

Preparative runs were performed in a multicompartment apparatus equipped with isolectric membranes (IsoPrime from Hoefer Sci., San Francisco, CA, USA) supported by glass-fibre filters [14,15]. After determining the pI values of the IL-6 isoforms in different additive solutions in analytical IPG pH 5–8 gels, eight isoelectric membranes were made with the following pI values: 5.50, 5.95, 6.47, 6.53, 6.57, 6.65, 6.92 and 7.35. The first and last membrane, being adjacent to anolyte and catholyte compartments, respectively, were made in a 10%T, 4%C matrix, whereas the other six were polymerized as 5%T, 4%C polyacrylamide matrices. The membranes had a diameter of 4.7 cm and a thickness of about 1 mm. After casting, the membranes were incubated 20 min in 100 mM ascorbic acid (pH 4.5) so as to eliminate potentially harmful N-oxides [16]. After washing and equilibrating the membranes in 20% glycerol, the multi-compartment apparatus was assembled and the protein (10 mg per 6.5 ml) was loaded into chamber

3. In order to avoid sample dilution, no reservoirs were connected to the chamber, so that the sample volume was limited to 6.45 ml per chamber [17]. After an initial, low-voltage run (maximum setting: 500 V, 1 mA, 1.5 W for 1 h) to eliminate salt in the sample, purification was continued at 3000 V, 3 mA, 1.5 W maximum for 6–16 h. The anolyte was 52 mM HEPES (pH 5.3, conductivity $1.5 \cdot 10^{-3}$ S m^{-1}). The supporting solution in all chambers was 20% glycerol (pH 5.3, conductivity $5 \cdot 10^{-4}$ S m^{-1}). No circulating coolant was utilized and Joule heat was dissipated in air in the cold room.

2.5. Preparation of IL-6 mutein

Δ22-IL-6 Cys 3,4 was expressed as cytoplasmic inclusion bodies by fermentation of a recombinant *E. coli* strain. Insoluble proteins recovered after mechanical cell breakage were dissolved in 6 M guanidine hydrochloride and refolded by tenfold dilution in pH 8 buffer solution. The presence of IL-6-related contaminants was studied using a preparation of Δ22-IL-6 Cys 3,4 partially purified starting from the refolded solution treated with 1.4 M ammonium sulphate and separated by column chromatography on phenyl-Sepharose (Pharmacia Biotech).

2.6. Reversed-phase high-performance liquid chromatography (RP-HPLC)

RP-HPLC was performed using a Vydac C_4 column (250 × 4.6 mm I.D.; particle size 5 μm) at a flow-rate of 1 ml min^{-1}. Mobile phase A was 0.1% trifluoroacetic acid (TFA) (Pierce, Rockford, IL, USA) in water and mobile phase B was 0.07% TFA in 80% acetonitrile (Carlo Erba, Milan, Italy). Elution was performed with a 30-min gradient from 40 to 100% B and monitored with a UV detector at 220 nm.

2.7. Sodium dodecyl sulphate polyacrylamide gel electrophoresis (SDS-PAGE) and immunoblotting

Discontinuous SDS-PAGE in 15% separating gel was performed according to Laemmli [18].

Samples were boiled in 2% SDS–0.025 *M* Tris (pH 6.8) with or without 5% β-mercaptoethanol. Gels were stained with Coomassie Brilliant Blue or silver stain. Immunoblotting was carried out according to the procedure of Towbin et al. [19] with some modifications. Following SDS-PAGE the proteins were electrotransferred to polyvinylidene difluoride membranes (Millipore) using a Multiphor semi-dry blotting apparatus (Pharmacia Biotech) according to the manufacturer's instructions. After blocking, overnight, the non-specific sites with 5% skim milk in Tris-buffered saline, immunostaining was performed by incubation for 1 h at room temperature with the primary antibody anti-human IL-6 (1 μg ml^{-1}) followed by incubation with the secondary antibody goat anti-rabbit IgG horseradish peroxidase conjugate (Bio-Rad, Richmond, CA, USA) diluted 1:1500. Detection was performed by enhanced chemiluminescence (Amersham International, Amersham, UK) according to the manufacturer's instructions.

2.8. Chemical modification of partially purified $\Delta22$-1L-6 Cys 3,4

The oxidation was performed with 4% H_2O_2 for 1 h at room temperature and pH 7.4. The reduction was performed with 10, 5, 1 or 0.5 m*M* dithiothreitol (DTT) at pH 7.4 for 5 min at room temperature. The reaction (oxidation or reduction) was stopped by removing the reagent solution by gel filtration on disposable NAP5 columns (Pharmacia Biotech) equilibrated with 10 m*M* Tris–acetate (pH 7.4).

2.9. Peptide mapping and sequencing

Approximately 20 μg of protein were digested with 0.4 μg of sequencing grade endoproteinase-Lys C (Boehringer, Mannheim, Germany) by overnight incubation at 37°C in 1 *M* urea–0.1 *M* Tris (pH 8) buffer. The resulting peptidic fragments were separated by RP-HPLC on a C_{18} Vydac column; mobile components phase A (0.1% trifluoroacetic acid) and B (95% acetonitrile–0.07% trifluoroacetic acid) were

used with linear gradient elution from 5 to 75% B in 60 min at a flow-rate of 1 ml min^{-1}. Eluted peaks were collected manually and submitted to N-terminal sequence analysis using a Model 477A pulsed-liquid phase sequencer with a Model 120A on-line analyser (Applied Biosystems, Foster City, CA, USA) for the detection of phenylthiohydantoin amino acids; standard manufacturer's programmes were used with minor modifications.

2.10. Electrospray mass spectrometry (ES-MS)

Samples collected after separation by RP-HPLC were injected at a flow-rate of 2 μl min^{-1} into a Hewlett-Packard Model 5989A single quadrupole mass spectrometer equipped with a Hewlett-Packard Model 59987A electrospray interface. Mass spectra were recorded in the positive-ion mode.

2.11. Bioassay

The biological activity of IL-6-related proteins was assayed using a proliferation test with murine hybridoma IL6-dependent cell line 7TD1 and employing spectrophotometric detection with the vital dye 3-(4,5-dimethylthiazol-2-yl)-2,5-diphenyltetrazolium bromide (Sigma) as described [20].

3. Results

A new recombinant mutein of interleukin-6, $\Delta22$-IL-6 Cys 3,4, was expressed in *E. coli* as insoluble aggregate inclusion bodies which were separated from soluble host proteins by cell breakage and centrifugation. The soluble and biologically active molecule was then obtained through a cycle of dissolution in chaotropic agent and dilution in renaturating buffer. Two simple purification steps consisting in ammonium sulphate precipitation of most of the contaminating proteins and hydrophobic interaction chromatography of the supernatant solution gave a product with a purity of about 90% when assessed by
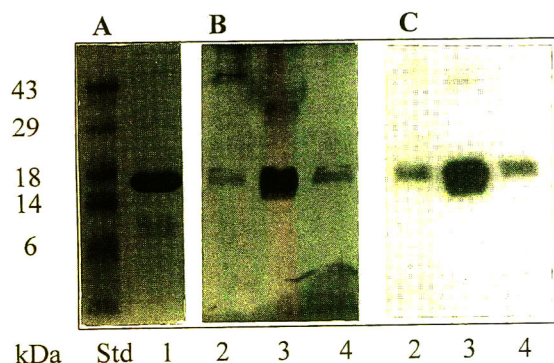
Fig. 1. Electrophoresis of truncated IL-6 muteins. 15% SDS-PAGE of partially purified Δ22-IL-6 Cys 3,4 (lane 1) and Δ22-IL-6 Cys 3,4 forms purified with the multi-compartment electrolyser: acidic form (lane 2), major form (lane 3) and basic form (lane 4). Standard protein markers (lane Std) are reported with their mass values shown on the left. Gel A was stained with Coomassie Brilliant Blue, gel B with silver stain; immunoblotting was performed on gel C using polyclonal anti-human IL-6 antibodies and chemiluminescence detection.

SDS-PAGE (Fig. 1, lane 1) and RP-HPLC analysis (Fig. 2).

However, IPG-isoelectric focusing (IEF) showed the presence of two minor product-related proteins with more basic ($pI = 6.70$) and more acidic ($pI = 6.10$) properties than the main component Δ22-IL-6 Cys 3,4 ($pI = 6.56$). In order to obtain some chemical evidence on the composition of the minor components with different pI values, it was necessary to set up a
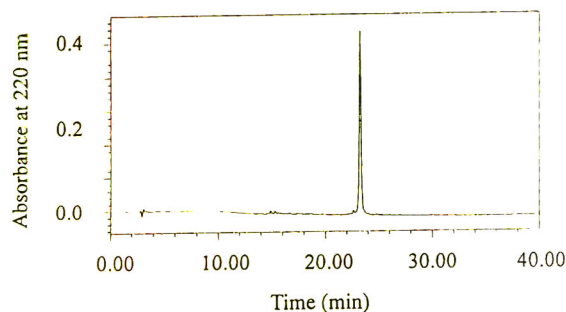
Fig. 2. RP-HPLC of a partially purified preparation of Δ22-IL-6 Cys 3,4. The sample was applied to a Vydac C$_4$ column and eluted with a linear gradient from 32 to 80% of acetonitrile. The chromatographic purity of the preparation was 88%, as calculated from peak areas.

high-resolution preparative IEF technique. The IsoPrime equipment, allowing for the preparative purification of protein isoforms in between sets of isoelectric membranes, was adopted for this task. However, as proteins at their pI values have minimum solubility, it was necessary to explore the solubilizing power of different non-denaturing agents added to the solvent. According to Hjertén [21], compounds such as ethylene glycol and propylene glycol can have a beneficial influence in preventing protein aggregation and precipitation. According to Timasheff and Arakawa [22], glycerol also appears to be a protein-stabilizing agent, as it seems to be excluded from protein surfaces by solvophobic effects. We therefore explored a number of such solubilizers, compatible with a focusing process, by running a continuous sample streak against a concentration gradient of such additives.

As shown in Fig. 3, Δ22-IL-6 Cys 3,4 is compatible with up to about 50% additive. Above this level, two phenomena occur. If the sample has been applied at the cathodic gel side, it still moves to the pI position. However, the protein seems to shift its pI to a more alkaline value (possibly by partial unfolding) and the zone is blurred, indicating sample precipitation in the proximity of the pI region. The second phenomenon, which occurs on anodic sample application, is massive precipitation of the protein and denaturation directly at the application site, just around and above the 50% (v/v) ethylene glycol concentration threshold.

A similar phenomenon occurs in a propylene glycol concentration gradient: on anodic sample application, above 45–50% additive concentration, protein denaturation and precipitation at the deposition site take place (Fig. 4B). In contrast, Δ22-IL-6 Cys 3,4 seems to be compatible with up to 70% (v/v) glycerol level in the solvent (Fig. 4C). Dimethyl sulphoxide shows a similar behaviour to ethylene glycol and propylene glycol (Fig. 4A): on anodic application, Δ22-IL-6 Cys 3,4 begins to change its pI and starts to precipitate at the deposition site, although the phenomenon is much less pronounced than in the case of the two glycols.

Based on the above information, preparative
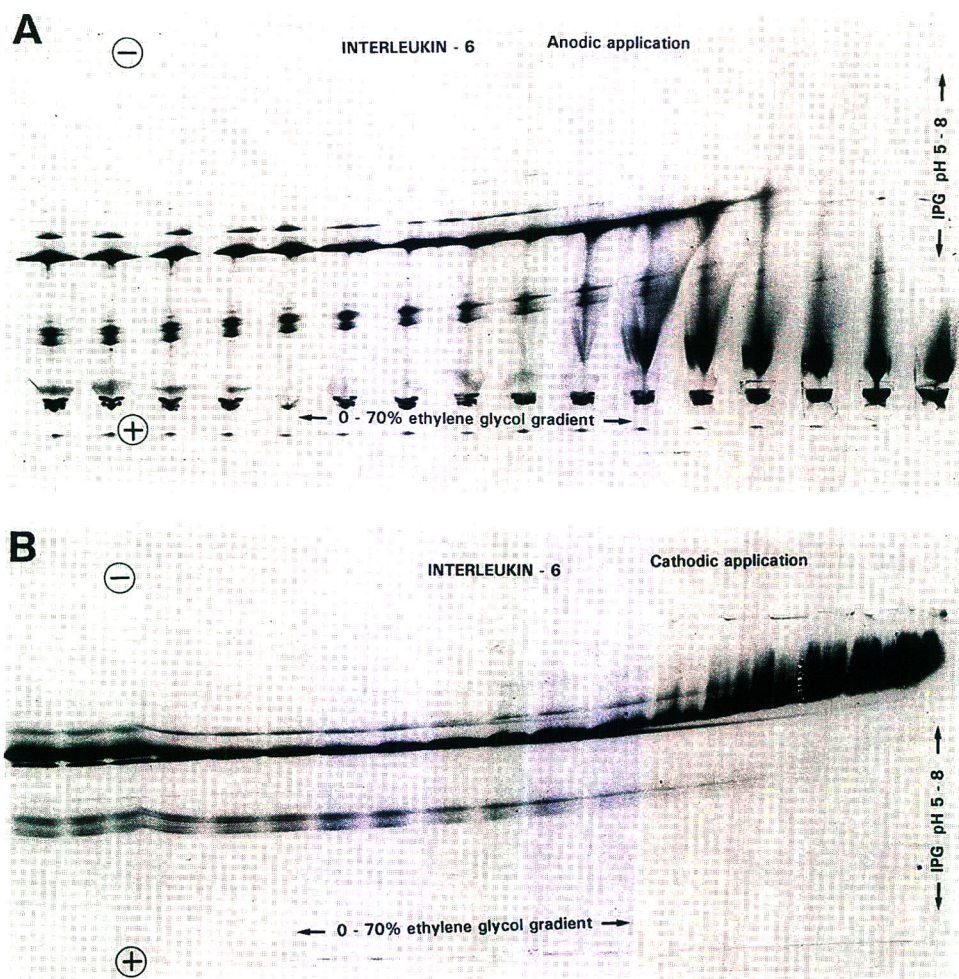
Fig. 3. Effect of ethylene glycol as solubilizer of Δ22-IL-6 Cys 3,4 isoforms at their p*I* values. IPG pH 5.0–8.0 linear gradient, reswollen in an ethylene glycol gradient (from 0 to 70%) perpendicular to the pH gradient. Both gels are made as 5%T, 4%C matrices. Sixteen samples (50 μg per sample) were applied along the acidic gel side (A) or along the basic gel side (B) and focused to the steady state (run at 5000 V for a total of 70 000 V h). Staining with Coomassie Brilliant Blue R-250 in the presence of Cu^{2+}.

runs in the IsoPrime electrolyser were conducted in presence of 20% glycerol as a solubilizing agent. Fig. 5 shows the results of such a preparative run. The main component (p*I* 6.56) was trapped in chamber 3, between two membranes having p*I*s of 6.53 (anodic) and 6.57 (cathodic). The p*I* 6.10 isoform was collected in chamber 2 (between a p*I* 5.95 and a p*I* 6.47 membrane) and the p*I* 6.70 in chamber 4 (between the p*I* 6.65 and p*I* 6.92 membranes). When analysed by

SDS-PAGE (Fig. 1) both of these two minor components exhibited the same relative molecular mass (M_r) as the major Δ22-IL-6 Cys 3,4 form and were recognized by the same antibody, suggesting that they are modified Δ22-IL-6 Cys 3,4 species. Moreover, both minor components were eluted with virtually the same retention time in RP-HPLC (see Table 1). It can also be appreciated (Fig. 1, lane 1) that endogenous contaminants not related to IL-6 and having a
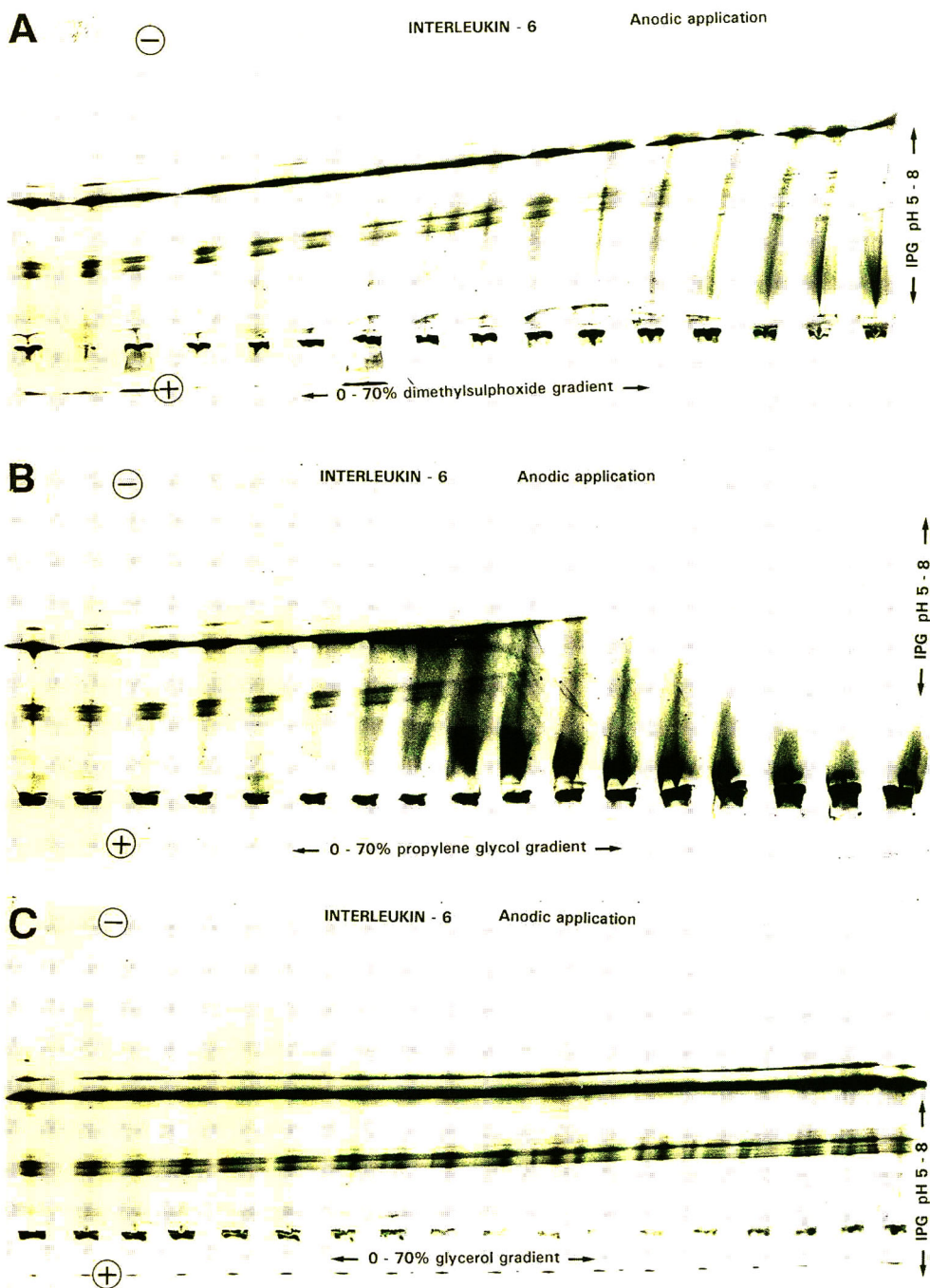
Fig. 4. Effect of different solubilizers on Δ22-IL-6 Cys 3,4 isoforms at their p*I* values. IPG pH 5.0–8.0 linear gradient, reswollen in an (A) dimethyl sulphoxide, (B) propylene glycol or (C) glycerol gradient (from 0 to 70%) perpendicular to the pH gradient. All gels are made as 5%T, 4%C matrices. Sixteen samples (50 µg per sample) were applied along the acidic gel side and focused to the steady state (run at 5000 V for a total of 70 000 V h). Staining with Coomassie Brilliant Blue R-250 in the presence of Cu^{2+}.
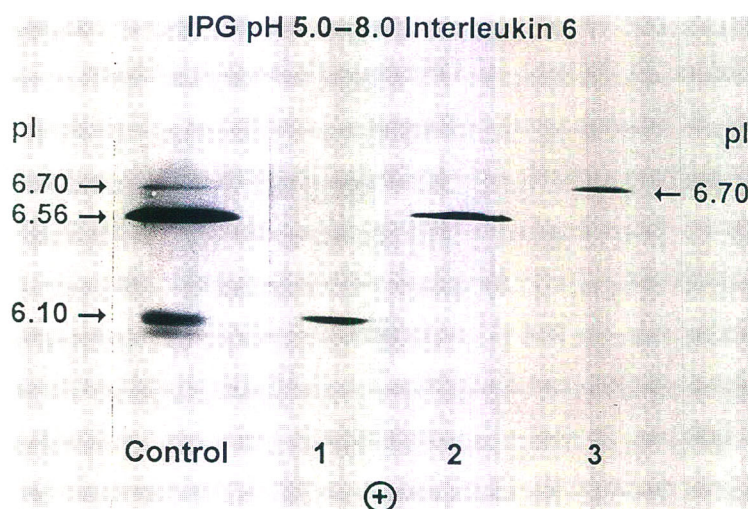
Fig. 5. Analytical IPG-IEF of isoforms of Δ22-IL-6 Cys 3,4 as recovered from the IsoPrime purification process. Analytical gel: IPG pH 5–8 linear gradient, in a 5%T, 4%C matrix, reswollen in 20% glycerol. All samples were applied in surface well (cathodic load) as 70-μl droplets (with variable amounts of proteins, from 10 to 50 μg). Focusing at 10°C, 5000 V (after an initial period of 1 h at 500 V) for 12 h. The cathode is uppermost. Staining with Coomassie Brilliant Blue R-250 in the presence of Cu^{2+}. Control = unfractionated, starting material; 1 = content of chamber 2 (pI 6.10 isoform); 2 = content of chamber 3 (pI 6.56, major component); 3 = content of chamber 4 (basic isoform, with pI 6.70).

lower M_r were efficiently removed in the Iso-Prime run.

The biological activity of the three Δ22-IL-6 Cys 3,4 forms was determined by measuring their ability to induce proliferation of the IL-6-dependent 7TD1 cells. The results showed the same high specific activity for Δ22-IL-6 Cys 3,4

and the acidic form, while the activity of the basic form was about 75% lower (Table 1).

It has been widely reported that acidic derivatives of proteins can be formed by deamidation of the side-chain of glutamine or asparagine, as a spontaneous slow reaction or induced by environmental conditions [23]; however, the occur-

Table 1

Characterization of Δ22-IL-6 Cys 3,4 and its derivatives separated by preparative immobilized pH gradient isoelectric focusing (IPG-IEF)

Sample	RP-HPLC retention time (min)	IPG-IEF, pI	Mass spectrometry, M_r	Bioassay relative potency (%)
Starting preparation	23.2	–	18 695	100
Acidic form	23.1	6.10	n.d.[a]	100
Main form	23.9	6.56	18 695	100
Basic form	23.7	6.70	18 727 (+32)	25

The three Δ22-IL-6 Cys 3,4 forms with different pI, purified with the multi-compartment electrolyser, showed the same retention time in RP-HPLC. The more basic form showed a lower in vitro biological activity than the other forms (EC_{50} for the starting material was about 10 pg ml^{-1}). The relative molecular mass (M_r) of the main form matched the calculated value of 18 696, while the basic form showed a 32 amu increase.

[a] Not determined.

rence of a protein derivative with more basic properties is much less documented.

For this reason, we focused our interest on the elucidation of the modification of the basic form. Determination of relative molecular mass by ES-MS analysis of the major component prepared by IPG-IEF gave an M_r value of 18 695, which corresponds to the calculated value of 18 696 for Δ22-IL-6 Cys 3,4, while the basic form gave a shift of +32 atomic mass units (amu), suggesting the addition of two oxygen atoms. These data, at first, seemed compatible with the oxidation of one methionine residue to methionine sulphone or alternatively with the oxidation of two residues to methionine sulphoxide, which is a covalent modification likely to occur during the production of recombinant proteins [24,25].

Peptide fragments of Δ22-IL-6 Cys 3,4 containing the five methionine residues of the molecule were therefore identified by sequence analysis after endoproteinase-Lys-C digestion and peptide mapping; the same was done on a sample of Δ22-IL-6 Cys 3,4 extensively oxidized in vitro by incubation with H_2O_2. As reported in Table 2, the peptide fragments containing the oxidized methionine residues were eluted with a slightly shorter retention time owing to the decrease in hydrophobicity induced by the formation of methionine sulphoxide. However,
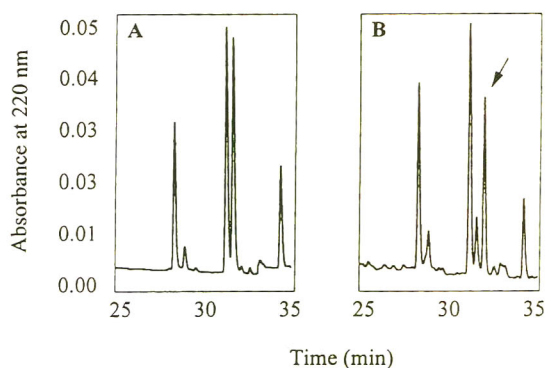
Fig. 6. Comparison of peptide mapping of Δ22-IL-6 Cys 3,4 and its more basic form. Partial elution profile (25–35 min) from a C_{18} HPLC column of endoproteinase-Lys-C digestion products of Δ22-IL-6 Cys 3,4 (A) and of the higher pI 6.70 isoform (B). At time 32.0 min [as indicated by the arrow in (B)] is shown the peak which is not present in native Δ22-IL-6-Cys 3,4 or in in vitro oxidized Δ22-IL-6 Cys 3,4 digest.

enzymatic digestion and peptide mapping of the basic form only showed the presence of the five peptides containing non-oxidized methionine residues (Table 2), ruling out the possibility that the 32 amu increase of this form was due to methionine oxidation.

Interestingly, the only difference between the peptide mapping of Δ22-IL-6 Cys 3,4 and its more basic form was a shift in the RP-HPLC

Table 2
Identification of oxidized methionine residues (Met-SO) in Δ22-IL-6 Cys 3,4 after in vitro treatment with H_2O_2 and in the basic form separated by preparative IPG

Peptide	RP-HPLC retention time (min)	Δ22-IL-6 Cys 3,4[a]		
		Control	H_2O_2 treated	Basic isoform
46–49 (Met[46])	4.9	+	[b]	+
26–33 (Met[28])	5.9	+	[b]	+
151–163 (Met[163]-SO)	33.0	−	+	−
151–163 (Met[163])	36.8	+	−	+
130–150 (Met[140]-SO)	37.6	−	+	−
130–150 (Met[140])	42.0	+	−	+
66–69 (Met[96]-SO)	47.0	−	+	−
66–69 (Met[96])	47.5	+	−	+

[a] + and − indicate the detection or not, respectively, of the corresponding peak in peptide mapping.
[b] After H_2O_2 treatment peptides containing Met[28]-SO and Met[46]-SO are not detectable because they are eluted in the flow-through.

1	SERIDKQIRY	ILDGISALRK	ETSNKSNMSE	SSKEALAENN
41	LNLPKMAEKD	GCFQSGFNEE	TCLVKIITGL	LEFEVYLEYL
81	QNRFESSEEQ	ARAVQMSTKV	LIQFLQKKAK	NLDAITTPDP
121	TTNASLLTKL	QAQNQWLQDM	TTHLILRSFK	EFLQSSLRAL
161	RQM			

Fig. 7. Primary structure of Δ22-IL-6 Cys 3,4. The amino acid sequence is reported as one-letter codes. The location of the single disulphide bond between cysteine 52 and 62 is shown. Underlined residues, from amino acid residues 50–65, represent the modified site found in the more basic form of Δ22-IL-6 Cys 3,4.
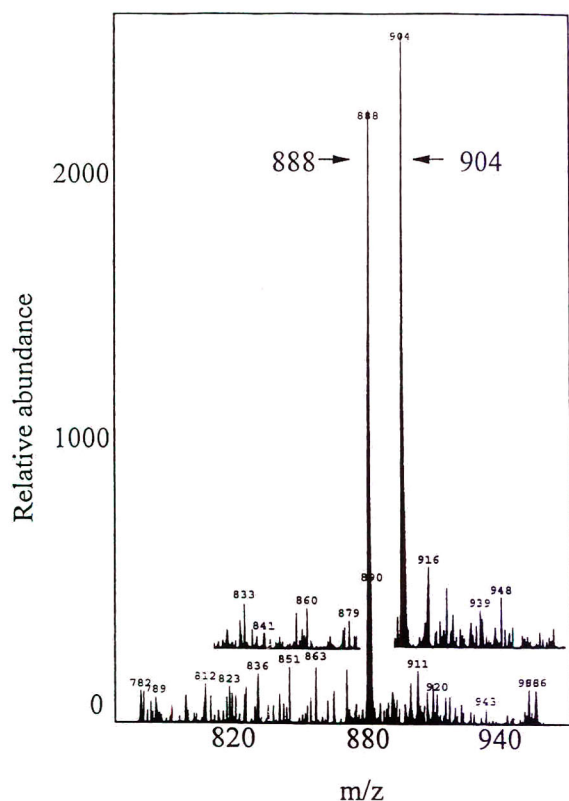
Fig. 8. Mass spectrometry of peptide 50–65. Overlay mass spectra of peptide 50–65 from Δ22-IL-6 Cys 3,4 showing a peak at $(m + 2H)^{2+} = 888$, corresponding to 1774 amu and from the higher pI derivative (pI 6.70) showing a peak shift to $(m + 2H)^{2+} = 904$, corresponding to 1806 amu.

elution profile of the peak corresponding to the peptidic fragment from residue 50 to 65 (Fig. 6), with the peptide of pI 6.70 species exhibiting a more hydrophobic behaviour. The sequence of the peptide 50–65 is as follows: H$_2$N-D-G-X-F-Q-S-G-F-N-E-E-T-X-L-V-K-OH (where X represents a cysteine residue which is not detectable by direct sequencing) and in Δ22-IL-6 Cys 3,4 a disulphide bond links the two cysteine residues present in positions 52 and 62 (Fig. 7, primary sequence).

Sequence analysis of the peptide 50–65 derived from Δ22-IL-6 Cys 3,4 and its corresponding shifted peptide from the more basic form confirmed the sequence identity. ES-MS analysis gave a single signal at m/z 888 and 904 for the peptidic fragment 50–65 from Δ22-IL-6 Cys 3,4 and from the more basic form, respectively (Fig. 8); these peaks can be assigned to a doubly charged molecule $(m + 2H)^{2+}$ corresponding to 1774 amu for peptide 50–65 from Δ22-IL-6 Cys 3,4 (whose calculated mass is 1775 amu) and to 1806 (+32 amu) for the corresponding peptide 50–65 from the higher pI (6.70) form.

Inspection of the amino acid sequence of peptide 50–65 and the fact that the more basic pI 6.70 form of Δ22-IL-6 Cys 3,4 can be easily transformed into the main pI 6.56 form by mild
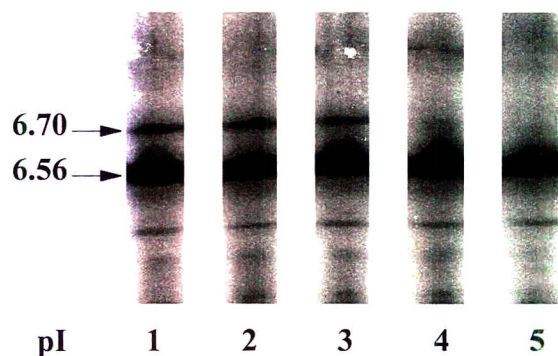
Fig. 9. Reduction of Δ-IL6 Cys 3,4 more basic form. Analytical IPG pH 6.2–7.1 linear gradient of partially purified Δ22-IL-6 Cys 3,4 not incubated (lane 1), and incubated for 5 min with 0.5 mM (lane 2), 1 mM (lane 3), 5 mM (lane 4) and 10 mM dithiothreitol (lane 5). Isoelectric points are indicated on the left. The more basic form pI 6.70 was reduced with 5 mM dithiothreitol.

reductive treatment (Fig. 9) strongly suggest a modification on the Cys_2 cross-link.

4. Discussion

Expanding commercial applications of genetic engineering techniques in the 1980s have led to the manufacture of a large number of protein products in recombinant systems. The production process of recombinant proteins can expose them to conditions which potentially are able to induce conformational alterations or covalent modifications of amino acid side-chains.

The identification of minor protein modifications usually requires the application of different analytical methodologies with high resolving power, e.g., SDS-PAGE, RP-HPLC, peptide mapping and mass spectrometry. Isolectric focusing techniques are increasingly being used for these analyses owing to their capability to detect even very minor charge heterogeneity of proteins. It has been relatively simple to attribute lower p*I* components to modifications such as deamidation, glycosylation, sulphation, phosphorylation and to all the array of surface charge modifiers that lower the net surface charge. However, higher p*I* components have gone unexplained up to the present time. The higher p*I* form of the IL-6 mutein described in this paper displayed a measured mass increase of 32 amu, which, in principle, could arise from the addition of two oxygen atoms (32.00) or of a single sulphur atom (32.07). The peptide fragment 50–65 isolated from the p*I* 6.70 form retained the 32 amu mass increase; the lack of any methionine residue in this fragment excluded the oxidative modification of methionine and restricted the mass modification to the Cys^{52}–Cys^{62} bridge.

A vast literature exists on the oxidation of thiols in aliphatic and aromatic compounds [26]. Whereas in protein chemistry we usually deal with only three oxidation states of cysteine (free thiol, disulphide and, in extreme cases, cysteic acid), in reality thiols are oxidized by a variety of reagents to a whole series of intermediate oxidation products, depending on the specific reaction conditions. Perhaps the best known oxidation

pathway for thiols is via molecular oxygen. The ease of oxidation of thiols on exposure to air is well known, as is the sensitivity of this reaction to catalysts, such as metal ions, UV radiation and other initiators of radical reactions. It is also reported that auto-oxidation is accelerated by bases. In the case of cysteine, between the two oxidation states Cys_2 and cysteic acid, except for the very labile sulphenic acid, a number of stable intermediates exist: mono-, di-, tri- and tetra-sulphone intermediate products have been reported [27].

Following this reasoning, we could speculate that the mass increase observed in the p*I* 6.70 form could be due to the addition of two oxygen atoms to give a cysteine sulphone derivative. However, the peptide 50–65 isolated from the p*I* 6.70 form exhibited a more hydrophobic behaviour than the unmodified peptide 50–65, which is not compatible with the formation of a more oxygenated form. Recently, Canova-Davis [3] and Jespersen et al. [4] described a novel post-translational modification of proteins, identified in recombinant growth hormone preparations, characterized by a 32 amu increase due to the addition of a sulphur atom to a Cy–S–S–Cy bridge (where Cy represents cysteine minus an SH group) to give the trisulphide Cy–S–S–S–Cy. The trisulphide proteins or peptide fragments are, as expected, more hydrophobic than the corresponding unmodified molecules and are easily reverted to the Cy–S–S–Cy form by mild reductive treatment [4]. Our experimental results and the above literature data allow us to propose a trisulphide modification of the single Cys^{52}–Cys^{62} bridge for the more basic Δ22-IL-6 Cys 3,4 form isolated as a minor contaminant of Δ22-IL-6 Cys 3,4 mutein produced in *E. coli*. We have excluded the possibility of an artefactual modification of cysteine residues due to the IPG technique on the grounds that the isolated bands do not redistribute on re-focusing, as is evident from the analytical gels in Fig. 5 (cf., the track of the p*I* 6.56 and 6.70 components).

The mechanism of trisulphide formation in proteins is unknown, although it has been suggested [4] that disulphide bridges of proteins produced in *E. coli* as inclusion bodies and

recovered by cell disruption could be exposed to and cleaved by HS^- ions in a disulphide exchange reaction forming a hydrogen disulphide derivative of one cysteine, which could then react with the other free cysteine to form a trisulphide bond. Trisulphide derivatives of both the growth hormone reported previously [3,4] and Δ22-IL-6 Cys 3,4, reported here, have only been identified in recombinant proteins expressed as cytoplasmic inclusion bodies in *E. coli*. We do not know at present if such an increment in p*I* values, in the case of a modified disulphide bridge to trisulphide, can be a general mechanism valid also for other proteins, but certainly it is a novel finding worth considering when confronted with higher p*I* isoforms in recombinant proteins.

Acknowledgements

References

[1] V.R. Anicetti, B.A. Keyt and W.S. Hancock, Trends Biotechnol., 7 (1989) 342.

[2] D. Naveh, Biopharm., 3 (1990) 28.

[3] E. Canova-Davis, 8th Symposium of the Protein Society, July 9–13, 1994, San Diego, CA (USA), Poster M.

[4] A.M. Jespersen, T. Christensen, N.K. Klausen, P.F. Nielsen and H.H. Sorensen, Eur. J. Biochem., 219 (1994) 365.

[5] J. Van Snick, Annu. Rev. Immunol., 8 (1990) 253.

[6] J. Van Damme, G. Opdenakker, R.J. Simpson, M.R. Rubira, S. Cayphas, A. Vink, A. Billiau and J. Van Snick, J. Exp. Med., 165 (1987) 914.

[7] T. Hirano, K. Yasukawa, H. Harada, T. Taga, Y. Watanabe, T. Matsuda, S. Kashiwamura, K. Nakajima, K. Koyama, A. Iwamatsu, S. Tsunasawa, F. Sakiyama, H. Matsui, Y. Takahara, T. Taniguchi and T. Kishimoto, Nature, 324 (1986) 73.

[8] J.P.J. Brakenhoff, M.H. Hart and A.L. Aarden, J. Immunol., 143 (1989) 1175.

[9] J.N. Snouwaert, F.W. Leebeek and D.M. Fowlkes, J. Biol. Chem., 266 (1991) 23097.

[10] S. Dagan, C. Tackney and S.M. Skelly, Protein Expression Purif., 3 (1992) 290.

[11] J. Breton, A. La Fiura, F. Bertolero, G. Orsini, B. Valsasina, R. Ziliotto, V. De Filippis, P. Polverino de Laureto and A. Fontana, Eur. J. Biochem., 227 (1995) 573.

[12] P.G. Righetti, Immobilized pH Gradients: Theory and Methodology, Elsevier, Amsterdam, 1990.

[13] P.G. Righetti and J.W. Drysdale, J. Chromatogr., 98 (1974) 271.

[14] P.G. Righetti, E. Wenisch, A. Jungbauer, H. Katinger and M. Faupel, J. Chromatogr., 500 (1990) 681.

[15] P.G. Righetti, E. Wenisch and M. Faupel, J. Chromatogr., 475 (1989) 293.

[16] M. Chiari, C. Chiesa, P.G. Righetti, M. Corti, T. Jain and R. Shorr, J. Chromatogr., 499 (1990) 699.

[17] E. Wenisch, P.G. Righetti and W. Weber, Electrophoresis, 13 (1992) 668.

[18] U.K. Laemmli, Nature, 227 (1970) 680.

[19] H. Towbin, T. Staehelin and J. Gordon, Proc. Natl. Acad. Sci. U.S.A., 76 (1979) 4350.

[20] T. Mosmann, J. Immunol. Methods, 65 (1983) 55.

[21] S. Hjertén, in N. Catsimpoolas (Editor), Methods of Protein Separation, Vol. 2, Plenum Press, New York, 1974, p. 233.

[22] S.N. Timasheff and T. Arakawa, in T.E. Creighton (Editor), Protein Structure, IRL Press, Oxford, 1989, p. 331.

[23] P.G. Righetti, Isoelectric Focusing: Theory, Methodology and Applications, Elsevier, Amsterdam, 1983.

[24] M. Kunitani, P. Hirtzef, P. Johnson, R. Halembeck, A. Boosman and K. Koths, J. Chromatogr., 359 (1986) 391.

[25] G. Forsberg, G. Palm, A. Ekebache, S. Josephson and M. Hartmanis, Biochem. J., 271 (1990) 357.

[26] G. Capozzi and G. Modena, in S. Patai (Editor), The Chemistry of the Thiol Group, Wiley, Chichester, 1974, p. 785.

[27] F. Freeman, Chem. Rev., 84 (1984) 117.

Modification of a tunable UV–visible capillary electrophoresis detector for simultaneous absorbance and fluorescence detection: profiling of body fluids for drugs and endogenous compounds

Jitka Caslavska[a], Ernst Gassmann[b], Wolfgang Thormann[a],[*]

[a]*Department of Clinical Pharmacology, University of Berne, Murtenstrasse 35, CH-3010 Berne, Switzerland*
[b]*Ciba-Geigy, Corporate Analytical Research, CH-4002 Basle, Switzerland*

Abstract

Using fused-silica optical fibres for fluorescence light collection and bandpass filters for selection of emission wavelengths, a capillary electrophoresis detection cell of a conventional, tunable UV–Vis absorbance detector was adapted for simultaneous fluorescence (at selected emission wavelength) and absorbance (at selected excitation wavelength) detection. Detector performance is demonstrated with the monitoring of underivatized fluorescent compounds in body fluids by micellar electrokinetic capillary chromatography with direct sample injection. Compared with UV absorption detection, fluorescence detection is shown to provide increased selectivity and for selected compounds also up to tenfold higher sensitivity. Examples studied include screening for urinary indole derivatives (tryptophan, 5-hydroxytryptophan, tyrosine, 3-indoxyl sulfate and 5-hydroxyindole-3-acetic acid) and catecholamine metabolites (homovanillic acid and vanillylmandelic acid) and the monitoring of naproxen in serum, quinidine in serum and urine and of salicylate and its metabolites in serum and urine.

1. Introduction

Laser-based fluorescence has produced spectacular results for solute detection in capillary electrophoresis (CE) [1,2], with detection limits of model compounds in the yoctomole (10^{-24} mol) range [2]. Lasers suffer from a number of inherent limitations, including the availability of excitation wavelengths and high cost. The non-laser-based fluorescence detectors constructed for CE, such as those (in order of decreasing performance) using xenon arc [3] (detection limit

10^{-20} mol), mercury–xenon arc [4] (10^{-16} mol), pulsed xenon [5], deuterium [6] and tungsten [6] lamps, provide much poorer sensitivity but allow for wavelength selection over a wide range. Using such incoherent excitation sources, solute monitoring by simultaneous absorption and fluorescence detection has been described [5], but no detector of this kind is currently available.

Fluorescence detection in CE of low-molecular-mass compounds in body fluids has been shown to provide improved selectivity and often also sensitivity when compared with absorption detection. Examples discussed in the literature include the determination of urinary porphyrins [7] and thiols in blood [8], the assessment of

---

* Corresponding author.

metabolic disorders via the determination of urinary cysteine and homocysteine, taurine in biopsy samples of the myocardium and gluthathione in red blood cell lysates [9] and the monitoring of serum levels of methotrexate [10], anthracyclines [11], naproxen [12] and retinol [13]. It is interesting that in work dealing with endogenous compounds, mostly non-laser-based fluorescence detection was applied via adaptation of HPLC fluorescence detectors to CE, whereas drug monitoring was effected via the use of laser-induced fluorescence detection.

The laboratory in Berne has specialized in applying CE and micellar electrokinetic capillary chromatography (MECC) to the determination of drugs and metabolites in body fluids [14–20]. In view of the high potential of using fluorescence detection for drug monitoring and clinical analysis, the construction of an inexpensive, versatile, non-laser-based fluorescence detector for CE was undertaken. The cell of a conventional, tunable UV–Vis absorbance detector was adapted for simultaneous fluorescence and absorbance detection. The modification implemented is similar to that described by Albin et al. [6], using optical fibres for fluorescence light collection, optical bandpass filters for selection of emission wavelengths and a photomultiplier module for emission light detection. In this set-up, the detector can be employed (i) for simultaneous fluorescence and absorption detection where the wavelengths for excitation of fluorescence and absorption detection are identical, or (ii) for multi- or single wavelength absorption detection, for which the detector was originally designed. In both operational modes, computerized data acquisition, handling and storage are employed. Fluorescence detector performance is demonstrated with the monitoring of endogenous low-molecular-mass compounds, such as urinary indole derivatives and catecholamine metabolites. Further, combined fluorescence and absorption detection is shown to be an interesting approach for the monitoring of drugs in body fluids, including naproxen in serum, quinidine in serum and urine and salicylate and its metabolites in serum and urine.

2. Experimental

2.1. Chemicals, origin of samples and routine methods of analysis

All chemicals were of analytical-reagent or research grade. The drugs naproxen, salicylate and quinidine were of European Pharmacopoeia quality. Salicyluric acid, tyrosine (Tyr), tryptophan (Trp), 5-hydroxytryptophan (5HTrp), 5-hydroxyindole-3-acetic acid (5HIAA), homovanillic acid (HVA), vanillylmandelic acid (VMA) and 3-indoxyl sulfate (3IXS) were obtained from Sigma (St. Louis, MO, USA). Our own serum and urine were employed as blank matrices. Sera from patients were collected in our routine drug assay laboratory where they were received for drug monitoring. Salicylate and quinidine in serum were determined by automated fluorescence polarization immunoassays (FPIA) on a TDx analyser (Abbott Laboratories, Irving, TX, USA). The immunoassays were performed according to the manufacturer's instructions using their reagent kits. Patients' 0–24-h urine samples with increased concentrations of 5-HIAA, HVA or VMA were obtained from the routine clinical laboratory of the University Hospital (Berne, Switzerland), where they were analysed by HPLC. All samples were stored at −20°C until further analysis.

2.2. Electrophoretic instrumentation and running conditions

The instrument with multi-wavelength detection employed in this work has been described previously [14–17]. If not stated otherwise, it featured a 75 μm I.D. fused-silica capillary of about 50 (70) cm effective (total) length (Product TSP/075/375, Polymicro Technologies, Phoenix, AZ, USA), together with a UVIS 206 PHD fast-scanning multi-wavelength detector and a No. 9550-0155 on-column capillary detector cell (both from Linear Instruments, Reno, NV, USA). The detector allows the selection of wavelengths between 190 and 800 nm (in 1-nm increments; with a deuterium and a tungsten

lamp covering the wavelength ranges 190–365 and 366–800 nm, respectively). For all experiments, the 206 PHD detector was controlled by a Mandax AT 286 computer system (Panatronic, Zürich, Switzerland) and running the 206 detector software package version 2.0 (Linear Instruments) with windows 286 version 2.1 (Microsoft, Redmond, WA, USA). Multi-wavelength data were read, evaluated and stored as described previously [14–17].

Modifications for simultaneous absorbance and fluorescence detection were made in-house. A schematic representation of the assembly is presented in Fig. 1. The body of the detector cell was machined so that two 370 μm O.D. fused-silica optical fibres (Polymicro Technologies) could be mounted at right-angles (as shown in Fig. 1) or at 30° to the capillary axis (right-angles to the optical axis of the excitation light beam in both instances). For positioning of the two fibres in close proximity to the capillary and ball lens, the same sleeve and ferrule mounting (inset in Fig. 1) as for the fixation of the capillary was employed. The ends of the fibres were polished with successively finer grades of wet silicon carbide paper followed by slurries of alumina on microcloth. The optical assembly was cleansed using methanol. The two fibres were united and interfaced to an interchangeable filter holder which was mounted as closely as possible to an HC120-05 photosensor module (Hamamatsu, Bridgewater, NJ, USA). Bandpass (interference) filters for 340, 366, 405, 450 and 520 nm (half-bandwidth 10 ± 2 nm; transmission >30%) were purchased from Balzers (Balzers, Liechtenstein). The output signal of the photomultiplier module was interfaced directly to the data acquisition system. Fluorescence and absorption (at the excitation wavelength) data were registered simultaneously with a two-channel PC Integration Pack (version 3.0; Kontron, Zürich, Switzerland), which features automatic range switching and a dynamic sampling rate allowing sampling every 10 ms for rapidly changing signals. Data
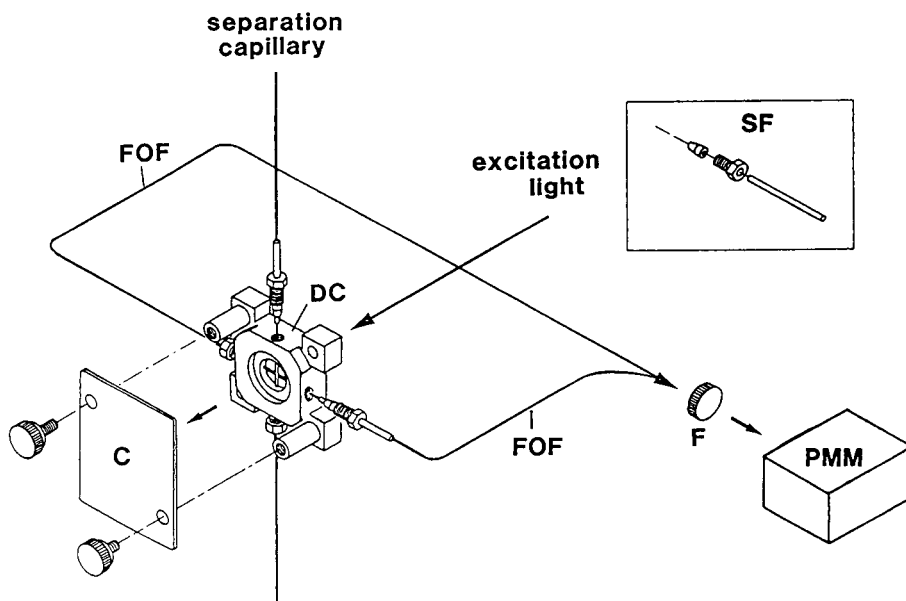
Fig. 1. Schematic representation of the detection cell for simultaneous absorption and fluorescence detection. The inset depicts an exploded view of the sleeve and ferrule mounting for the optical fibres and the separation capillary (adapted from the capillary detector cell manual of Linear Instruments). DC = detector cell body; C = cover plate with photodiode assembly for absorption light detection; FOF = fused-silica optical fibre; F = bandpass or edge filter; PMM = photomultiplier module for fluorescence light detection; SF = sleeve and ferrule mounting.

storage and computations were executed on a Mandax AT 286 computer. For simultaneous fluorescence and absorption detection, the 206 PHD detector was used in the high-sensitivity monochrome mode.

If not stated otherwise, a constant voltage of 20 kV (90 μA) was applied and the cathode was on the detector side. Sample application was effected manually through dipping the anodic capillary end into the sample vial and lifting it by ca. 34 cm for a specified time interval. Conditioning between runs was achieved by rinsing the capillary with buffer for 10 min. A buffer composed of 75 mM sodium dodecyl sulfate (SDS), 6 mM Na$_2$B$_4$O$_7$ and 10 mM Na$_2$HPO$_4$ (pH $\approx$ 9.2) was employed. All standard drug solutions were prepared in buffer or methanol at concentrations of 5–100 μg/ml. Blank and patients' samples were spiked by addition of known aliquots of these standard solutions to the plain body fluids.

3. Results and discussion

As described above, the detector cell constructed uses two optical fibres for fluorescence light collection (Fig. 1). First, employing Trp as a model compound, the performance of the mountings of these fibres at 30° angles was compared with that provided with fixation at right-angles. With excitation at 220 nm and emission monitored at 340 nm, fluorescence monitoring at 30° was determined to provide lower sensitivity compared with emission light collection at right-angles, the difference being attributed to difficulties in the alignment of the collection fibres. With the 90° mounting, the sensitivity was found to be about equal to that obtained by UV absorption detection at the excitation wavelength. Thus, for all the data discussed below, the mounting of the optical fibres at right-angles was employed. The relative magnitudes of the absorption and fluorescence signals are not only dependent on how the emission light is collected, but are mainly dependent on the solute, its chemical environment, and the optical specifications, including the

wavelengths selected for excitation and emission. For example, with fluorescein as the sample, the fluorescence response at 520 nm was determined to be much larger than the absorption signal at 220 nm. Therefore, with fluorescence detection as described here, the detection limit can be improved compared with that obtained by UV absorption detection. Under the experimental conditions investigated, the absorbance and fluorescence detection limits ($S/N = 3$) for fluorescein were determined to be about 6.0 and 0.4 μg/ml, respectively.

As reported previously, CE techniques are attractive methods which permit monitoring of endogenous and exogenous compounds by direct injection of body fluids [15,17–20]. Resolution, however, can be hampered owing to the presence of a large number of endogenous low-molecular-mass components and peak assignment can be difficult when solutes are monitored by UV absorption. This is particularly the case with urine samples. The data presented in Fig. 2A represent an electropherogram obtained after direct injection of a tenfold diluted urine of a healthy individual and absorption detection at 220 nm. Corresponding fluorescence data with an emission band filter of 340 nm are depicted in Fig. 2B and those with the same urine spiked with 5HIAA, HVA and VMA are presented in Fig. 2C. All peaks, including those of Tyr, Trp, 5HTrp and 3IXS, were not only assigned based on their fluorescence, but also on matching multi-wavelength absorption spectra obtained by using the same detector in the fast scanning mode (data not shown).

Indoles, including Trp, 5HTrp, 5HIAA and 3IXS, which are heterocyclic amine compounds, and catecholamine metabolites, such as HVA and VMA, are present in cells and extracellular fluids of living organisms. Determination of such compounds in urine is clinically important and is typically performed by HPLC or GC [21,22]. For example, monitoring of 5HIAA in 0–24-h urine is employed for screening for carcinoid tumours, the normal excretion being <70 μmol per 24 h. The MECC data presented in Fig. 3A were obtained by injection of a tenfold diluted patient's urine, the 5HIAA concentration of which
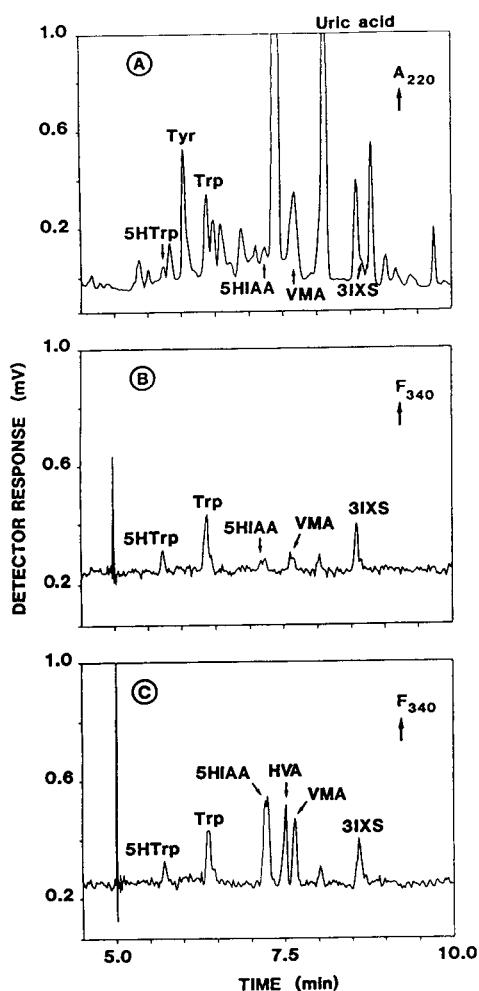
Fig. 2. MECC electropherograms of (A) tenfold diluted urine from a healthy individual obtained via absorption measurement at 220 nm, (B) the simultaneously collected fluorescence data with an emission filter of 340 nm and (C) the fluorescence data obtained with the same tenfold diluted urine but spiked with 5HIAA (5.4 μg/ml), HVA (74 μg/ml) and VMA (31 μg/ml). Sample injection time and applied voltage, 5 s and 20 kV, respectively.

Fig. 3. MECC fluorescence (excitation at 220 nm and emission at 340 nm) data for (A) a tenfold diluted patient's urine with a pathological 5HIAA level and (B) an undiluted patient's urine with elevated concentrations of HVA and VMA. Sample injection times, 5 and 2 s, respectively. Other conditions as in Fig. 2.

was determined to be 332 μM using HPLC (data from the routine clinical laboratory). The urine volume collected was 760 ml and the excretion was calculated to be 252 μmol per 24 h. Comparison of the data in Fig. 3A with those in Fig. 2 reveals the presence of a much enlarged 5HIAA peak in the former case, indicating that elevated, pathological concentrations of 5HIAA

can easily be monitored by MECC with direct injection of plain or diluted urine and on-column fluorescence detection.

HVA and VMA are catabolic products of catecholamines that are excreted in elevated amounts (>34 and >46 μmol per 24 h, respectively) in the urine of patients with various diseases, including neuroplastoma and hepatic encephalopathy [21–23]. The MECC data depicted in Fig. 3B were obtained by injection of an undiluted patient's urine with elevated excretion of HVA and VMA. The presence of both HVA and VMA could be determined unambiguously by MECC and fluorescence detection (Fig. 3B). Compared with the data reported by Issaq

et al. [23], the fluorescence detector described here appears to have higher sensitivity than the UV detector employed by them. These few data suggest that MECC with fluorescence detection could be used for the simultaneous monitoring of pathological urinary levels of Trp, 5HTrp, 5HIAA, HVA and VMA, and thus for the diagnosis of diseases. Further, with extraction prior to application to the capillary, many more basic neurotransmitters and their acidic metabolites could be detected [21,22].

To complement our previous efforts in monitoring drugs by MECC with UV absorption detection and direct sample injection [18–20], the potential of employing simultaneous fluorescence and absorption detection for drug analysis was investigated. Using naproxen, salicylate and quinidine as model drugs, electropherograms of a serum blank and the serum blank spiked with

the three drugs are presented in Fig. 4A and B, respectively. The fluorescence data for the serum blank reveal a sharp peak produced by Trp. Hence this compound can be used as an endogenous marker substance. Further, the response originating from the proteins could easily be allocated. However, the compounds producing the two sharp peaks marked ? could not be identified. As can be seen from the data in Fig. 4B, all three drugs were found to produce satisfactory peaks when injected within plain serum. For naproxen, the fluorescence response with a 366-nm emission filter was found to be much stronger than that obtained with absorption detection at 220 nm. The opposite was true for salicylate, whereas for quinidine the peak height of the fluorescence signal was slightly larger than that of the UV absorption response observed at the excitation wavelength. With

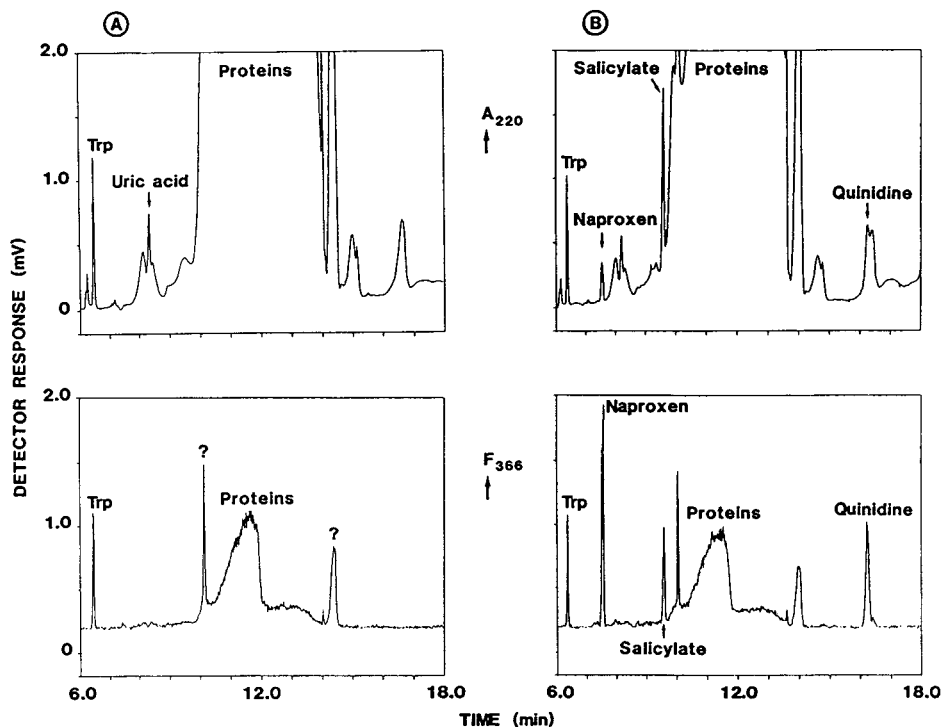

Fig. 4. MECC data for (A) serum blank and (B) serum blank spiked with naproxen (5 μg/ml), salicylate (75 μg/ml) and quinidine (13 μg/ml). The upper graphs represent UV absorption data measured at the excitation wavelength of 220 nm and the lower graphs are the fluorescence data obtained with a 366-nm bandpass filter. Injection time and applied voltage, 2 s and 20 kV, respectively.

direct serum injection, the latter drug was found almost to co-elute with another compound, this being clearly seen in the absorbance data (upper graph of Fig. 4B). However, this unknown endogenous substance appears not to fluoresce and quinidine can easily be determined via evaluation of the fluorescence data. Hence simultaneous gathering of UV absorption and fluorescence data appears to be advantageous for drug monitoring and will be further emphasized with the analysis of patients' samples discussed below.

The MECC data shown in Fig. 5 were obtained via direct injection of serum from a patient undergoing naproxen pharmacotherapy. Using MECC with on-column absorption detec-
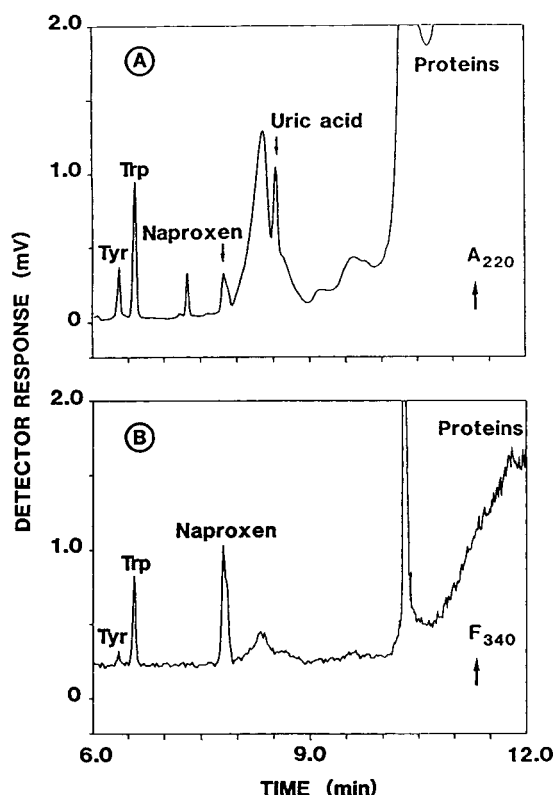

Fig. 5. MECC data for serum from a patient under naproxen pharmacotherapy. The upper graphs represent UV absorption data measured at the excitation wavelength of 220 nm and the lower graphs are the fluorescence data obtained with a 340-nm bandpass filter. Other conditions as in Fig. 4.

tion, the naproxen serum level was determined to be 9.4 μg/ml [19]. As expected, fluorescence detection provides a higher response than that obtained with absorption measurement at the excitation wavelength of 220 nm. Thus, with the simple fluorescence detector sub-μg/ml serum levels of naproxen (detection limit ca. 0.2 μg/ml) can be recognized, the concentration limit being about one order of magnitude lower than that observed with UV absorption detection [19]. However, using laser-induced fluorescence detection and drug extraction, an even lower detection limit was reported [12].

The data presented in Fig. 6A were obtained with a directly injected serum sample from a patient under quinidine pharmacotherapy. Using FPIA, the quinidine serum level in that sample was determined to be 10.7 μM (3.5 μg/ml), this being within the therapeutic range (6–15 μM) of this drug. As suggested according to the absorption data obtained with serum blank spiked with quinidine (Fig. 4B), this drug is co-eluting with matrix compounds (upper graph of Fig. 6A). However, using fluorescence detection with excitation and emission at 220 and 366 nm, respectively (lower graph of Fig. 6A), quinidine could readily be detected (for blank data refer to Fig. 4A). The MECC detection limit ($S/N = 3$) was determined to be 4.6 μM (1.5 μg/ml), hence MECC with direct serum injection and on-column fluorescence detection permits the determination of quinidine serum levels of pharmacological interest.

The electropherograms depicted in Fig. 6B were registered when analysing a twofold diluted urine which was collected 8–16 h after administration of 200 mg of quinidine sulfate (one tablet of Kinidin-Duriles; Astra Pharmaceutica, Dietikon, Switzerland). With urine, hardly any endogenous compounds elute after about 10 min {see Fig. 2A (complete blank data not shown) and to data reported in Refs. [17] and [24]}. Hence urinary quinidine can be monitored by both UV absorption and fluorescence detection. Further, owing to the fluorescence and an apparent similarity of the UV absorption spectrum with that of quinidine (data not shown), the peak eluting after about 14.3 min (peak marked with
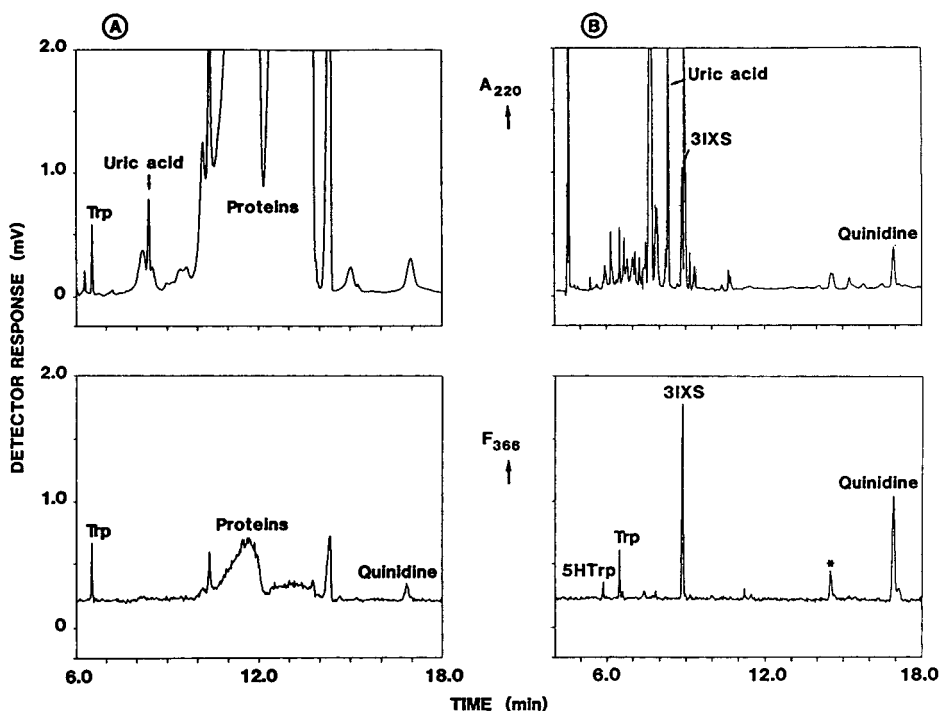
Fig. 6. MECC data obtained for (A) a patient's serum sample and (B) a twofold diluted urine from a test subject who had ingested quinidine. The upper graphs represent UV absorption data measured at the excitation wavelength of 220 nm and the lower graphs are the fluorescence data obtained with a 366-nm bandpass filter. Other conditions as in Fig. 4.

an asterisk in Fig. 6B) could be the response of 2-hydroxyquinidine, a metabolite of quinidine found in urine. Owing to the lack of a standard of this compound, however, this assumption could not be verified.

Although the fluorescence signal of salicylate is smaller than that obtained with absorption detection effected at the excitation wavelength of 220 nm (see Fig. 4B with fluorescence measured at 366 nm), it can be employed effectively for monitoring of this compound. MECC data obtained with a urine and a serum sample from a patient under suspected salicylate intoxication are presented in Fig. 7A and B, respectively. MECC data with multi-wavelength absorption data of these samples have been discussed previously (see Fig. 5 in Ref. [17]), the salicylate concentrations in urine and serum being of the

order of 3 mM each. MECC data for tenfold diluted urine (Fig. 7A) and directly injected serum (Fig. 7B) are depicted. Both UV absorption data (at the excitation wavelength of 220 nm) and the fluorescence data with an emission wavelength of 450 nm [the use of this filter provided a slightly higher response than those employing 366-nm (Fig. 4B) and 405-nm (data not shown) filters] reveal the presence of salicylate in both samples. As discussed before [17], comparison of the urine and serum data (particularly for fluorescence data, lower graphs) reveals the presence of similar salicylate concentrations in these two body fluids. Moreover, fluorescence monitoring shows the presence of molecules of similar structure, including metabolites of drugs. For example, with the aid of the urinary fluorescence data, the presence of the
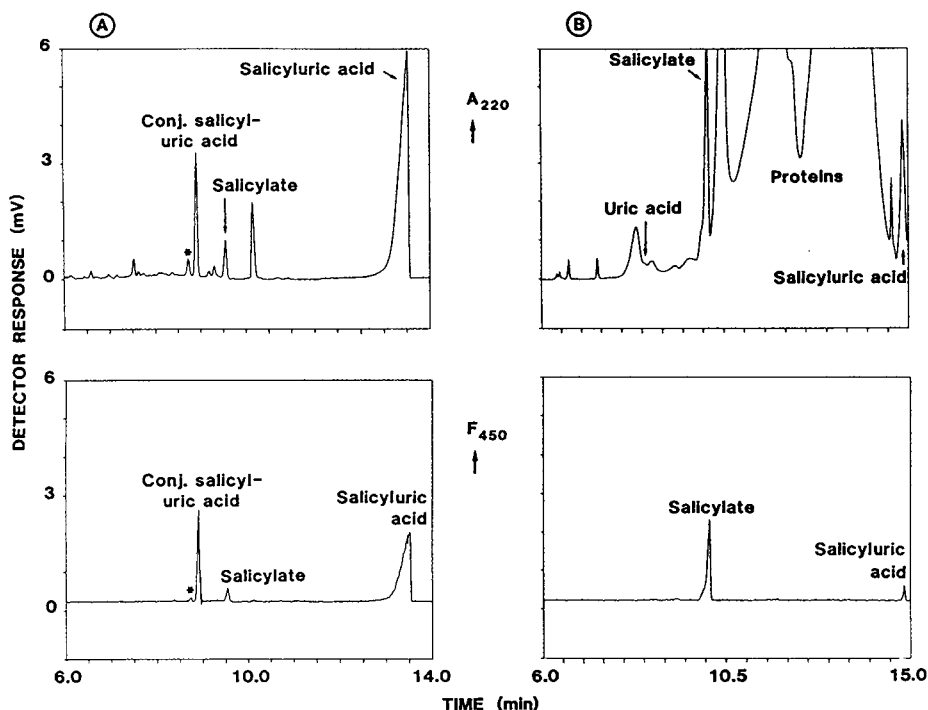
Fig. 7. MECC data obtained for (A) tenfold diluted urine and (B) serum from a patient with salicylate intoxication. The upper graphs represent UV absorption data measured at the excitation wavelength of 220 nm and the lower graphs are the fluorescence data obtained with a 450-nm bandpass filter. Other conditions as in Fig. 4.

major metabolite of salicylate, salicyluric acid and other salicylate metabolites could be suspected. Not surprisingly, using spectral analysis of the UV absorption data and rerunning the urine spiked with salicyluric acid allowed the positive identification of its peak which elutes at 13.6 min. Further, according to the UV spectrum and the fluorescence signal of the peaks eluting at 8.7 and 8.9 min, these peaks were assigned to the glucuronic acid conjugates of salicylate (marked with an asterisk in the lower graph of Fig. 7A) and salicyluric acid, respectively. In the case of the serum data (Fig. 7B), the small peak eluting at about 14.8 min could be assigned to salicyluric acid. Hence simultaneous monitoring of UV absorption and fluorescence provides valuable information both for drug monitoring and for the determination of metabolites.

4. Conclusions

Using direct injection of body fluids and looking at solutes with native fluorescence, monitoring of fluorescence with the simple detector assembly described is shown to provide increased selectivity and for selected compounds also up to tenfold higher sensitivity compared with UV absorption detection. Further, simultaneous UV absorbance (at the excitation wavelength) and fluorescence detection in MECC is shown to be attractive for screening and profiling of body fluids for disease diagnosis and/or confirmation, for therapeutic and diagnostic drug monitoring (including evaluations of intoxications) and for the assessment of drug metabolism. The detector employed allows the selection of excitation wavelengths between 195 and 800 nm (in 1-nm

increments), permits emission wavelength selection with a bandpass or a long-pass (edge) filter, and provides fluorescence and absorption data with the same time axis.

Acknowledgements

References

[1] E. Gassmann, J.E. Kuo and R.N. Zare, Science, 230 (1985) 813.

[2] D.Y. Chen, H.P. Swerdlow, H.R. Harke, J.Z. Zhang and N.J. Dovichi, J. Chromatogr., 559 (1991) 237.

[3] E. Arriaga, D.Y. Chen, X.L. Cheng and N.J. Dovichi, J. Chromatogr. A, 652 (1993) 347.

[4] D.J. Rose and J.W. Jorgenson, J. Chromatogr., 447 (1988) 117.

[5] R.G. Brownlee and S.W. Compton, Am. Biotechnol. Lab., October (1988) 10.

[6] M. Albin, R. Weinberger, E. Sapp and S. Moring, Anal. Chem., 63 (1991) 417.

[7] R. Weinberger, E. Sapp and S. Moring, J. Chromatogr., 516 (1990) 271.

[8] B. Lin Ling, W.R.G. Baeyens and C. Dewaele, Anal. Chim. Acta, 255 (1991) 283.

[9] E. Jellum, A.K. Thorsrud and E. Time, J. Chromatogr., 559 (1991) 455.

[10] M.C. Roach, P. Gozel and R.N. Zare, J. Chromatogr., 426 (1988) 129.

[11] N.J. Reinhoud, U.R. Tjaden, H. Irth and J. van der Greef, J. Chromatogr., 574 (1992) 327.

[12] H. Soini, M.V. Novotny and M.-L. Riekkola, J. Microcol. Sep., 4 (1992) 313.

[13] Y. Ma, Z. Wu, H.C. Furr, C. Lammi-Keefe and N.E. Craft, J. Chromatogr., 616 (1993) 31.

[14] W. Thormann, P. Meier, C. Marcolli and F. Binder, J. Chromatogr., 545 (1991) 445.

[15] W. Thormann, A. Minger, S. Molteni, J. Caslavska and P. Gebauer, J. Chromatogr., 593 (1992) 275.

[16] P. Wernly and W. Thormann, Anal. Chem., 63 (1991) 2878.

[17] J. Caslavska, S. Lienhard and W. Thormann, J. Chromatogr., 638 (1993) 335.

[18] H. Wolfisberg, A. Schmutz, R. Stotzer and W. Thormann, J. Chromatogr. A, 652 (1993) 407.

[19] A. Schmutz and W. Thormann, Electrophoresis, 15 (1994) 1295.

[20] A. Schmutz and W. Thormann, Ther. Drug Monit., 15 (1993) 310.

[21] P.M.M. van Haard and S. Pavel, J. Chromatogr., 429 (1988) 59.

[22] Z. Yi and P.R. Brown, Biomed. Chromatogr., 5 (1991) 101.

[23] H.J. Issaq, K. Delviks, G.M. Janini and G.M. Muschik, J. Liq. Chromatogr., 15 (1992) 3193.

[24] J. Caslavska, E. Hufschmid, R. Theurillat, C. Desiderio, H. Wolfisberg and W. Thormann, J. Chromatogr. B, 656 (1994) 219.

Chiral separation of deprenyl and its major metabolites using cyclodextrin-modified capillary zone electrophoresis

Éva Szökő*, K. Magyar

Department of Pharmacodynamics, Semmelweis University of Medicine, Nagyvárad tér 4, 1089 Budapest, Hungary

Abstract

A capillary electrophoretic method for the enantiomer resolution of deprenyl and its main alkaline metabolites amphetamine, methamphetamine and propargylamphetamine is described. An acidic separation buffer with a suitable chiral complexing agent, heptakis-(2,6-di-O-methyl)-β-cyclodextrin, was used and the optimum separation conditions were determined by changing the concentration of the chiral selector, the applied electric field and the concentration of methanol.

1. Introduction

It is well known, that many drugs display enantioselectivity in their pharmacological activity and metabolism. Using the optical isomer having the therapeutic effect is highly required to avoid unnecessary burdening of the body with the xenobiotic. Since a great number of drugs consist of enantiomers, chiral separation of these appears to be important.

Selegiline [R-(−)-deprenyl] has been used in the treatment of Parkinson's disease. This drug is the antipode of a chiral compound having the higher pharmacological efficacy [1]. Two of its main metabolites are amphetamine and methamphetamine [2,3]. These compounds have strong psychostimulant effects, the S-(+)-enantiomers being more active [4]. It is an issue of debate if the metabolites of deprenyl significantly contribute to its pharmacological effects [5,6]. Also, it has still to be proved that the more efficacious enantiomers of the metabolites are not formed in the body. This necessitates a chiral separation method of these compounds.

As indicated by the many papers published in this field, there is a growing interest in the application of capillary electrophoresis (CE) for enantiomer separations. The chiral selectors are usually applied as buffer additives, the most often used being cyclodextrin (CD) derivatives (uncharged, charged, polymers) [7–10], crown ethers [11], bile salts [12], other optically active detergents [13] or biopolymers [14]. Advantages offered by capillary electrophoresis are direct chiral resolution, high efficiency of the separation, speed, and low cost.

A micellar electrokinetic capillary chromatographic method for the separation of enantiomers of amphetamine, methamphetamine and other phenylethylamine compounds has been developed by Lurie [15]. Successful use of cyclodextrin derivatives for the chiral resolution of phenylethylamines has also been demonstrated [7]. In the present study we elaborated a cyclodextrin-modified CE method for the separation of deprenyl and its main metabolites.

---

* Corresponding author.

SSDI 0021-9673(95)00090-9

2. Experimental

2.1. Apparatus

A Crystal 300 (ATI Unicam, Cambridge, UK) capillary electrophoresis system equipped with a variable-wavelength UV absorbance detector set at 190 nm was used. CE separations were performed in a 70 cm × 75 μm I.D. uncoated fused-silica capillary; the length to the detection window was 55 cm. Samples were introduced by electrokinetic injection. Axxiom 727 software was used for data collection.

2.2. Chemicals

Tris–phosphate pH 2.8 (20 mM) containing 0.1% or 0.5% hydroxypropylmethylcellulose (HPMC) was used as running buffer. Tris and phosphoric acid were purchased from Reanal (Budapest, Hungary), and hydroxypropyl-methylcellulose from Sigma (St. Louis, MO, USA). The chiral selectors β-cyclodextrin and heptakis-(2,6-di-O-methyl)-β-cyclodextrin (DI-MEB) were obtained from Cyclolab (Budapest, Hungary).

The sample mixture contained S-(+)- and R-(−)-deprenyl, S-(+)- and R-(−)-metham-phetamine, R-(−)-amphetamine, and R-(−)-propargylamphetamine. Only one of the antipodes of the two latter compounds were available. These test compounds were kindly pro-

vided by Chinoin Pharmaceutical and Chemical Works (Budapest, Hungary). The chemical structure of deprenyl and the metabolites are shown in Fig. 1.

3. Results and discussion

Achiral separation of deprenyl and its three metabolites was achieved using low pH background electrolyte (Fig. 2.). All of the components are ionized at this pH and their migration is in the direction of the electroosmotic flow. Application of HPMC in the separation buffer improved the resolution of the sample components and the reproducibility of migration times as well.

3.1. Use of chiral additives

For the separation of the enantiomer pairs, the dimethyl substituted derivative of β-cyclodextrin is suitable. The unsubstituted β-cyclodextrin does not fit the chiral resolution of these compounds even in its saturating concentration. Both the deeper hydrophobic cavity of DIMEB and its different capability of hydrogen bond formation [16] may contribute to the different complex formation constants of the enantiomer pairs necessary to achieve their chiral resolution.

Application of DIMEB in the buffer increased the migration time of each sample component.
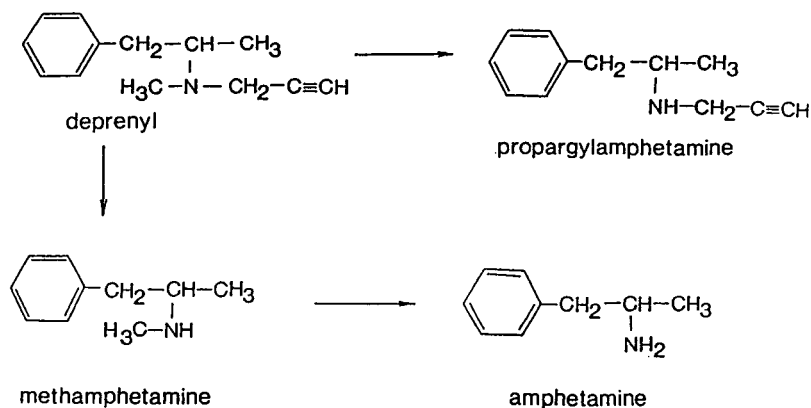
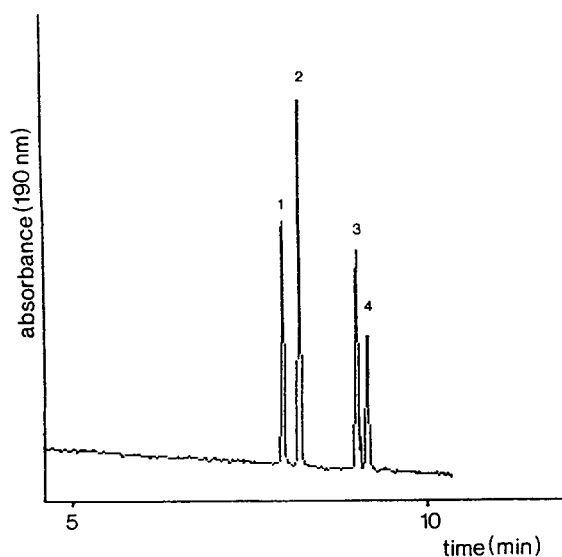Fig. 1. Chemical structures of deprenyl and its metabolites.

Fig. 2. Achiral separation of mixture of racemic deprenyl and its metabolites. Capillary: uncoated fused-silica 70 cm × 75 μm I.D. (55 cm to detector). Buffer: 20 mM Tris–phosphate–0.1% HPMC pH 2.8. Sample: 1 = (−)-amphetamine; 2 = (±)-methamphetamine; 3 = (±)-deprenyl; 4 = (−)-propargylamphetamine; 10^{-5} M each. Injection 3 kV, 12 s. Constant voltage 21 kV; current 32 μA.

This indicated the inclusion complex formation of the analytes with the chiral additive. The complexes formed have lower electrophoretic mobilities than the uncomplexed analytes. The increased migration time results primarily from the complex formation, whilst the slightly increased viscosity of the buffer and the slightly decreased electroosmotic flow do not significantly contribute. Fig. 3. shows the migration times of the sample components in the presence of 3–24 mM DIMEB. The non-linear change observed is characteristic of this kind of separations, just as the existence of a concentration optimum of the chiral selector for each analyte [17,18]. The decline in resolution when using the chiral selector above its optimum concentration has not been really explained so far. Inversion of the migration order of the enantiomers was found and different separation mechanisms at low and high concentrations of the chiral selector have been suggested by Schmitt and Engelhardt [19]. Non-specific hydrophobic interactions [20] and dimerization of CDs [21] have also been discussed as a reason for the loss in resolution at very high concentrations of the CD derivatives.
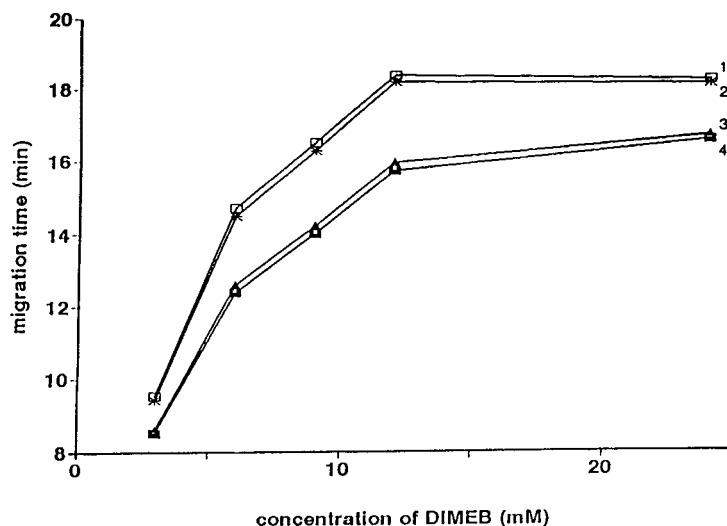

Fig. 3. Plot of migration time vs. concentration of DIMEB in the separation buffer: 1 = (+)-deprenyl; 2 = (−)-deprenyl; 3 = (+)-methamphetamine; 4 = (−)-methamphetamine.

Table 1
Effect of heptakis-(2,6-di-O-methyl)-β-cyclodextrin (DIMEB) concentration on separation selectivity and resolution of enantiomer pairs

Concentration of DIMEB (mM)	Selectivity[a]		Resolution[b]	
	MA[c]	D[d]	MA	D
3	1.007	1.010	0.8	0.9
6	1.014	1.015	2.4	2.9
9	1.014	1.014	2.0	2.2
12	1.014	1.010	2.2	2.4
15	1.010	1.008	1.2	0.7
24	1.008	1.007	0.4	0.3

[a] Selectivity $= \mu_1/\mu_2$, where $\mu_{1,2}$ are the electrophoretic mobilities.
[b] Resolution $= 2 \cdot (t_2 - t_1)/(w_1 + w_2)$, $t_{1,2}$ are the migration time, and $w_{1,2}$ are the peak widths of the enantiomers, respectively.
[c] Methamphetamine.
[d] Deprenyl.

The dependence of the selectivity and resolution of enantiomer pairs on the concentration of the chiral selector is listed in Table 1. For both compounds the (+)-isomers have lower electrophoretic mobility, indicating that their inclusion complex formation constants are higher compared to those of the (−)-isomers. The optimum concentration of the chiral selector for the separation of both enantiomer pairs of deprenyl and methamphetamine was found to be between 6 mM and 12 mM in 20 mM Tris–phosphate, pH 2.8 buffer containing 0.1% HPMC.

3.2. Effect of the electric field

The effect of the electric field on the separation of the enantiomers was considerable. We obtained the best chiral resolution when the separation was performed at 300 V/cm. At a low field strength (100 V/cm) the chiral resolution was totally lost, due to the increased sample diffusion during the long migration time and to the decreased separation efficiency. At a high field strength (400 V/cm) the resolution also decreased, probably because of the effect of heat generated in the capillary. The formation constants of CD–analyte complexes are sensitive to temperature change [22]. With increasing temperature they become smaller and the separation selectivity decreases significantly [23–25].

Separation of the sample mixture with the optimum concentration of the chiral selector and field strength is shown in Fig 4. Although the
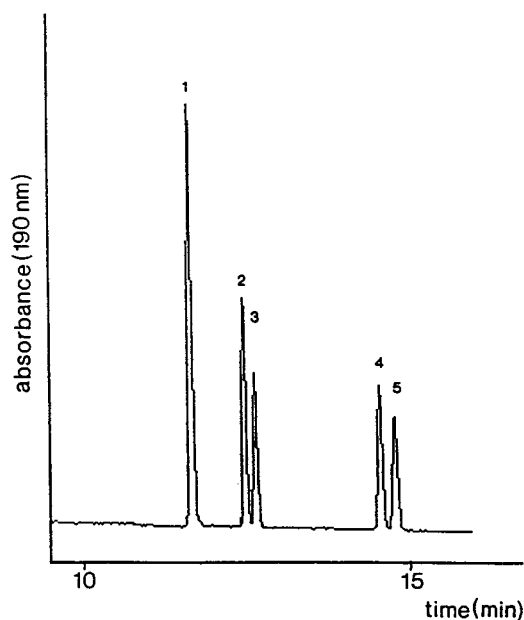

Fig. 4. Chiral separation of the mixture of racemic methamphetamine and deprenyl. Separation buffer as in Fig. 2, containing 6 mM DIMEB. Sample: 1 = (−)-amphetamine; 2 = (−)-methamphetamine; 3 = (+)methamphetamine; 4 = (−)-deprenyl; 5 = (+)-deprenyl; 10^{-5} M each. Injection 3 kV, 12 s. Constant voltage 21 kV; current 32 μA.

separation conditions are suitable for the enantiomer resolution of racemic deprenyl and methamphetamine, co-migration of S-(+)-deprenyl with R-(−)-propargylamphetamine was observed.

3.3. Effect of methanol

Addition of methanol to the separation buffer significantly improved the resolution of deprenyl and propargylamphetamine. This can be explained by the beneficial effect of reduced electroosmotic flow on the resolution of sample components migrating in the direction of the flow and by the differential change in the effective electrophoretic mobility of sample components of different hydrophobicity. However, the enantiomer resolution of methamphetamine and deprenyl slightly decreased as the methanol content of the separation buffer increased. Organic solvents usually reduce the hydrophobic interactions, and they may interact with the hydrophobic cavity of the cyclodextrins [26]. The presence of methanol can influence the complex formation of the analytes with DIMEB, which may also change the difference between the complex formation constants of the enantiomer pairs or the optimum concentration of the chiral additive. The effect of various methanol concentrations on the resolution of the sample components is shown in Fig. 5.

4. Conclusions

The chiral selector heptakis-(2,6-di-O-methyl)-β-cyclodextrin is thought to be an appropriate choice for the separation of optical isomers of deprenyl and its major metabolites by capillary electrophoresis. The use of methanol as an additive in the separation buffer was necessary to achieve the resolution of S-(+)-deprenyl and R-(−)-propargylamphetamine, although its presence slightly decreased the resolution of the enantiomer pairs of the two racemic compounds.

Fig. 5. Effect of methanol [(A) 10%, (B) 15%, (C) 20%] added to the separation buffer on the resolution of the sample components. Sample: 1 = (−)-amphetamine; 2 = (−)-methamphetamine; 3 = (+)methamphetamine; 4 = (−)-deprenyl; 5 = (+)-deprenyl; 6 = (−)-propargylamphetamine; 10^{-5} M each. Separation buffer as in Fig. 2, containing 12 mM DIMEB and various concentrations of methanol.

References

[1] K. Magyar, E.S. Vízi, Z. Ecseri and J. Knoll, Acta Physiol. Hung., 32 (1967) 377.
[2] E.H. Heinonen, V. Myllyla, K. Sotainemi, R. Lammintausta, J.S. Salonen, M. Anttila, M. Savijarvi, M. Kotila and U.K. Rinne, Acta Neurol. Scand., 126 (1989) 93.
[3] H. Kalász, L. Kerecsen, J. Pucsok and J. Knoll, J. Chromatogr., 499 (1990) 589.
[4] K.M. Taylor and S.H. Snyder, Science, 168 (1970) 1487.
[5] S.R. Philips, J. Pharm. Pharmacol., 33 (1981) 739.
[6] G.P. Reynolds, J.D. Elsworth, K. Blau, M. Sandler, A.J. Lees and G.M. Stern, Br. J. Clin. Pharmacol., 6 (1978) 542.
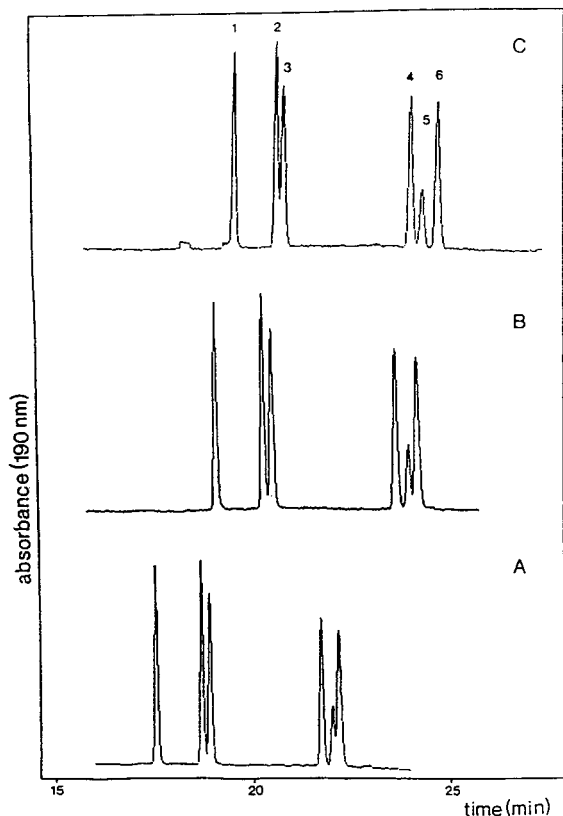[7] S. Fanali, J. Chromatogr., 474 (1989) 441.

[8] J. Snopek, H. Soini, M. Novotny, E. Smolkova-Keulemansova, and I. Jelinek, J. Chromatogr., 559 (1991) 215.

[9] T. Schmitt and H. Engelhardt, Chromatographia, 37 (1993) 475.

[10] S. Fanali and F. Kilár, J. Capillary Electrophoresis, 1 (1994) 72.

[11] R. Kuhn, F. Erni, T. Bereuter and J. Häusler, Anal. Chem., 64 (1992) 2815.

[12] S. Terabe, M. Shibata and Y. Miyashita, J. Chromatogr., 480 (1989) 403.

[13] K. Otsuka, J. Kawahara, K. Tatekawa and S. Terabe, J. Chromatogr., 559 (1991) 209.

[14] S. Busch, J.C. Kraak and H. Poppe, J. Chromatogr., 635 (1993) 119.

[15] I.S. Lurie, J. Chromatogr., 605 (1992) 269.

[16] J.J. Stezowski, M. Czugler and E. Eckle, in J. Szejtli (Editor), Proceedings 1st Int. Symp. on Cyclodextrins, Budapest, September 1981, Akademiai Kiado, Budapest, 1981, p. 151.

[17] S.A.C. Wren and R.C. Rowe, J. Chromatogr., 603 (1992) 235.

[18] S.A.C. Wren and R.C. Rowe, J. Chromatogr., 635 (1993) 113.

[19] T. Schmitt and H. Engelhardt, J. High Resolut. Chromatogr., 16 (1993) 525.

[20] M.J. Sepaniak, R.O. Cole and C. Clark, J. Liq. Chromatogr., 15 (1992) 1023.

[21] M. Heuermann and G. Blaschke, J. Chromatogr., 648 (1993) 267.

[22] S.M. Han and N. Purdie, Anal. Chem., 56 (1984) 2825.

[23] A. Guttman, A. Paulus, A.S. Cohen, N. Grinberg and B.L. Karger, J. Chromatogr., 448 (1988) 41.

[24] W. Schutzner and S. Fanali, Electrophoresis, 13 (1992) 687.

[25] M.W.F. Nielen, Anal. Chem., 65 (1993) 885.

[26] P. Gareil, J.P. Gramond and F. Guyon, J. Chromatogr., 615 (1993) 317.

Ionic strength and charge number correction for mobilities of multivalent organic anions in capillary electrophoresis

Werner Friedl[a], Jetse C. Reijenga[b],[*], Ernst Kenndler[a]

[a]*Institute for Analytical Chemistry, University of Vienna, Währinger Strasse 38, A-1090 Vienna, Austria*
[b]*Department of Chemical Engineering, Eindhoven University of Technology, P.O. Box 513, 5600 MB Eindhoven, Netherlands*

Abstract

An empirical expression was derived for the actual mobility, μ, valid in an extended range of ionic strength, I, between 0.001 and 0.1 mol/l, using a three-parameter exponential fit for the ratio of actual and absolute mobilities (μ_0 at $I = 0$), which consists of two variables: ionic strength of the buffer and charge number, z, of the solute. The charge numbers of the solute anions (21 aromatic sulfonates) ranged between 1 and 6, and the ionic strength was varied in the range mentioned using a sodium acetate buffer. The mobilities were determined at 25.0°C in a coated capillary with suppressed electroosmotic flow. The resulting fitting equation, valid under these conditions, is $\mu/\mu_0 = \exp(-0.77\sqrt{z}I)$. The difference between measured mobilities and mobilities calculated from a tenfold higher or lower ionic strength, using this equation, is within 5% for all experiments. For multivalent ions, μ values can be derived from μ_0 with comparable accuracy.

1. Introduction

The effective mobility, μ_{eff}, of the separands is the physico-chemical property of key importance in capillary electrophoresis (CE). It is given by $\mu_{eff} = \mu_0 f\alpha$ (for monovalent ions), where μ_0 is the absolute mobility (at infinite dilution), α is the degree of dissociation and f is a correction factor counting for the deviation from ideality. The actual mobility, μ, is that of the fully protonated or deprotonated ion at ionic strength I.

The ionic strength includes contributions from all ionic species in solution, including H^+ and OH^-, and with increased contribution of multivalent ions: $I = \frac{1}{2}\sum c_i z_i^2$, where c_i is the equilibrium concentration of species i and z_i the charge. The effective mobility depends on the pH and the ionic strength of the background electrolyte. Whereas its dependence on the pH through α is well defined, the influence of the ionic strength on the correction factor, f, is still under discussion, at least for those concentrations between 0.001 and 0.1 mol/l, which are commonly used in capillary zone electrophoresis (CZE).

Long before CE was introduced, a number of workers published papers on ionic strength and temperature dependence of molar conductivity and transport numbers; readers are referred to standard works on the subject [1]. Data were obtained from conductivity and other measurements under different conditions. In general, these models include $\sqrt{I}$. Their validity is limited to ionic strengths of up to 0.001 mol/l, without

* Corresponding author.

additional data on the sample components. A number of corrections were introduced to increase the concentration range, requiring additional sample-specific data, such as ionic radii. These data are, in general, difficult to obtain.

A further complication is that all of these models refer to the molar conductivity of electrolytes, dissolved at different concentrations, rather than to mobilities of individual ionic species, dissolved in a background electrolyte.

Concerning CE, in most cases some information will be available on the electrophoretic mobility of the solutes in a certain operational system, either from the values of absolute mobilities from the literature, or obtained by measurements with CE at a certain buffer composition. In order to optimize a separation, it will certainly be useful to have some idea of how the mobility will change if the pH or the ionic strength of the background electrolyte is altered. The effect of pH in selectivity tuning is fairly elementary from theory of isotachophoresis [2,3] and has been treated in a number of textbooks on capillary electrophoresis [4,5] and in previous publications [6,7]. The effect of ionic strength on mobility and selectivity in capillary electrophoresis is mentioned in the same textbooks. It is, however, still a matter of discussion, which is reflected by the number of contradictory contributions published on the subject. In some of them, the "overall" mobility (including electroosmosis) is measured as a function of buffer concentration [8,9]. An exponential decrease with increasing ionic strength was found, attributed mainly to a change in electroosmosis. Another publication [10] gives the mobility as being proportional to $1/\sqrt{I}$. In a computational study [11], the data taken from a textbook on the subject [1] are summarized in stating that the mobility (rather than the molar conductivity) is a non-linear function of $-\sqrt{I}$ for 1:1 electrolytes. In a more recent study [12], mobilities of a number of monovalent components were determined in a series of buffers with a limited range of ionic strength and the results were fitted to a linear model. Finally, in a publication on computational simulation of migration and dispersion in zone electrophoresis [13,14], a straightforward

empirical model for the ionic strength dependence of mobilities was introduced:

$$\mu/\mu_0 = \exp(-0.5z^{1.78}\sqrt{I}) \qquad (1)$$

The idea behind the necessity for such an empirical relationship was that a 10% predictability for certain experimental conditions is preferred over a 1% accuracy in a concentration range where zone electrophoretic experiments are commonly not carried out (≤ 0.001 mol/l).

In dealing with these kinds of models presented in the literature [1], one has to be careful in applying them to other systems [10–13]. In addition, the conductivity and mobility data in the literature refer to ionic strengths originating from the ions themselves, not from a buffer with a relatively high concentration (even if ion pairing and complexation can be excluded). Finally, literature data are mostly from inorganic anions and metal ions, which often have rotational symmetry and a high charge density. From the practical point of view, the larger, organic ions with a lower charge density are more interesting for CE. This is another reason why the present study was undertaken. For simplicity, strong acids were chosen as reference compounds in order to avoid effects caused by incomplete protolysis: the separands used are fully dissociated at the operating pH. A choice was made for μ/μ_0 as an exponential function, because it makes it possible to obtain μ_0 by extrapolating ln μ to $I = 0$. In addition, a linearized function (see the $\sqrt{I}$ models above) at higher concentration always leads to an exponential deviation: a linear function is only a special case of the expansion series of an exponential function.

2. Experimental

2.1. Apparatus

The instrument used for the measurements was a P/ACE System 2100 (using System Gold 6.01) (Beckman, Palo Alto, CA, USA) equipped with a UV absorbance detector at 214 nm. The separation capillary was made from fused silica,

75 μm I.D. and 363 μm O.D. (Supelco, Belle-fonte, PA, USA). The total length was 0.269 m and the effective length (the distance from the injector to the detector) was 0.202 m. The capillary was thermostated at 25.0°C. The operating voltage was chosen between 2000 and 5000 V, depending on the ionic strength of the background electrolyte. Injection of the sample was carried out by pressure for 1 s.

2.2. Reagents

Chemicals used for the preparation of the buffer solutions were analytical-reagent grade acetic acid and sodium hydroxide (Merck, Darmstadt, Germany). A number of different dyes with 1–6 sulfonic acid groups were used as model components (see Table 1). The azo dyes were prepared [16] by coupling the diazotized 1-naphthylamine sulfonic acid to the 2-naphtholsulfonic acid. All other components were obtained from commercial sources (Aldrich, Steinheim, Germany; Fluka, Buchs, Switzerland; Merck) in the highest available purity.

2.3. Procedures

The analytes were first titrated in order to verify that the sulfonic acid groups are fully dissociated at the working pH and that no other protolysis is likely to occur in the background electrolyte system used.

The background electrolyte was prepared by adding acetic acid and sodium hydroxide (at a molar concentration ratio of 2:1), resulting in buffers with ionic strengths of 0.1, 0.05, 0.01, 0.005 and 0.001 mol/l and a pH of about 4.75 (which was not further adjusted). This background electrolyte was chosen because complexation or ion pairing between sample and buffer ions was least likely, an obvious requirement for the present investigation. For the same reason, no additives were used.

In order to prevent systematic errors in migration time due to stacking, the sample components were dissolved in background electrolyte. The sample concentration was as low as possible in order to prevent concentration overload.

The mobility was calculated from the migration time t_m using the equation $\mu = L_d L_t / V t_m$, where L_d is the length of the capillary to the detector, L_t the total length and V the voltage. The quality of the determination of the migration times was determined with two anions (iodide and 2,4,5-trichlorobenzenesulfonate) as external reference compounds. The migration times of these standards were constant during the measurements in each particular buffer system to within about 0.2%.

The voltage was chosen in such a way that the temperature rise due to heat development inside the capillary was only 0.1°C or less. This temperature rise was calculated using the previously mentioned simulation program [13]. The coating procedure described by Hjertén [15] was applied.

3. Results and discussion

Some examples of the dependence of the actual mobility on the ionic strength for ions of different charge are shown in Fig. 1. It can be seen that the mobility decreases with increasing I in all cases. The slope of the graphs (especially at low I) is, however, strongly dependent on the charge number; it becomes increasingly steeper with increasing charge number. This leads to the fact that, within the range of measurement, the mobilities of the more highly charged species are reduced nearly by a factor of 2. The monovalent ions behave differently, however: between 0.001 and 0.01 mol/l the mobility remains nearly constant and is finally reduced at 0.1 mol/l by only about 20%. This unexpectedly deviant behaviour of the monovalent solutes will also be reflected in subsequent graphical representations.

3.1. Determination of model parameters

The basic approach to describe the dependence of the actual mobility, μ, on the ionic strength, I, and on the charge number, z, is the following three-parameter fitting equation:
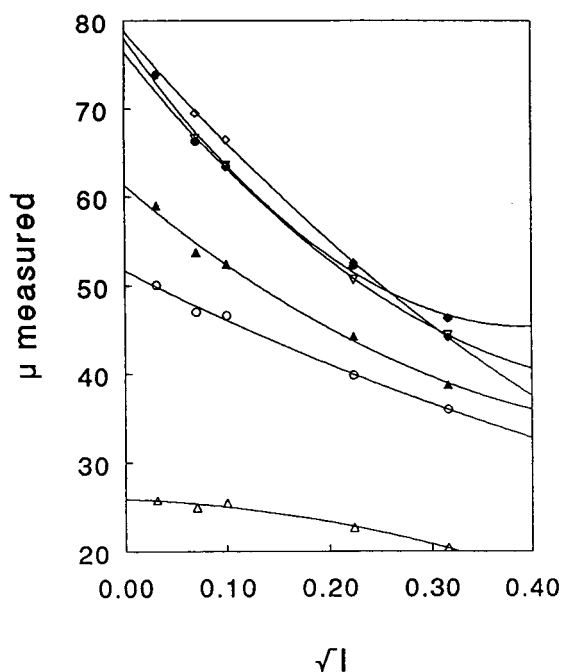
Fig. 1. Dependence of the measured actual mobility, μ, on the square root of the ionic strength, I, used for the determination of the absolute mobility, μ_0, by extrapolating a second-order polynomial fit of μ to $I = 0$. I is given in mol/l and the mobilities are given in 10^{-9} m^2/V·s. Examples of six components with different charge numbers are shown: $\triangle = 1$AN2; $\bigcirc = 2$NA36; $\blacktriangle = 3$IN; $\mathbf{O} = 4$IN; $\triangledown = 5$AZ11; $\diamondsuit = 6$AZ13. See Table 1 for component codes.

$$\mu = \mu_0 f = \mu_0 \exp(-az^b I^c) \qquad (2)$$

As the value of the constant c is expected to be close to 0.5, $\ln \mu$ was plotted vs. $\sqrt{I}$ for each individual component to obtain μ_0 using a second-order polynomial fit. The μ_0 values determined in this way are listed in Table 1. The correlation coefficients are always 0.990 or better.

Conversion of the model Eq. 2 leads to

$$\ln[-\ln(\mu/\mu_0)] = \ln(az^b) + c \ln I \qquad (3)$$

All values of μ/μ_0 were subsequently calculated. The slope of the plot of $\ln[-\ln(\mu/\mu_0)]$ vs. $\ln I$ for each individual solute gives c. The correlation coefficients were 0.997 or better. Some examples of these plots are shown in Fig. 2. The lines corresponding to different charge numbers z are
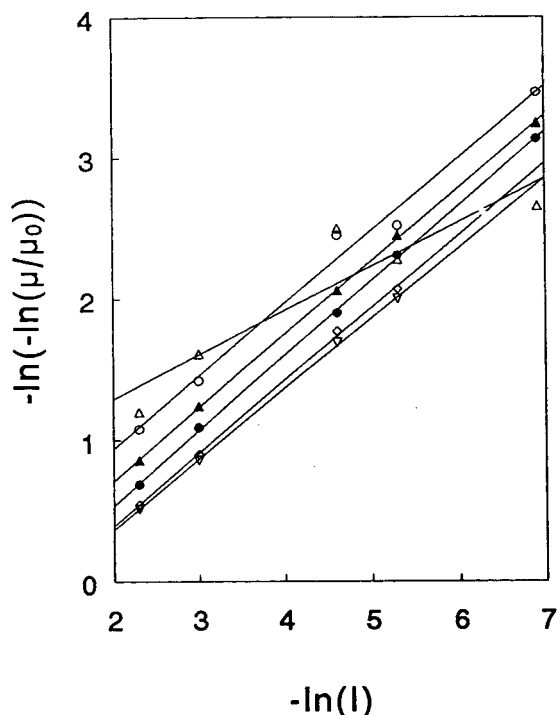
Fig. 2. Examples of the determination of c using components with different charge numbers, according to Eq. 3. See text and the caption of Fig. 1 for further details.

approximately parallel, but they have different intercepts, which are equal to $\ln(az^b)$.

The values of c obtained in this way are shown in Fig. 3. It can be seen that the three monovalent solutes are clearly outliers with c values of about 0.3, in contrast to all other compounds. This deviating behaviour of the monovalent ions (which was mentioned above) is not fully understood. Nevertheless, for the calculation of the parameters, the data from the monovalent solutes were further excluded. An overall average value of 0.52 for c is determined, with a standard deviation σ_c of 0.04 and a 95% confidence interval of 0.02. This value of c is close to that corresponding to the square-root equation, mentioned in the literature [1,13]. Based on the value for c, the model equation can be converted into

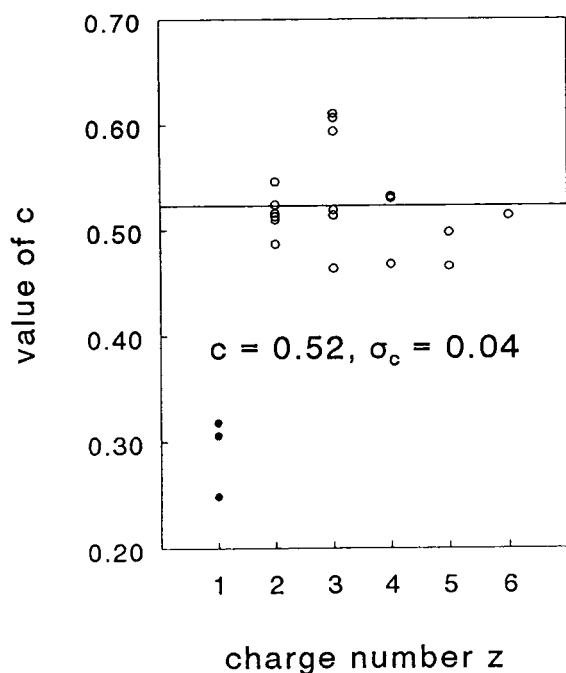$$\ln[-\ln(\mu/\mu_0)/I^{0.52}] = \ln a + b \ln z \qquad (4)$$

Fig. 3. Value of c from all components ($n = 21$) versus charge number z. ● = Outliers.

A plot of $\ln[-\ln(\mu/\mu_0)/I^{0.52}]$ vs. $\ln z$ is given in Fig. 4. After removing only two obvious outliers, the correlation coefficient is fair (0.78). The slope of the plot in Fig. 4 is $b = 0.49$ with a standard deviation σ_b of 0.04. The intercept is $\ln a$, from which $a = 0.85$ is obtained with a standard deviation σ_a of 0.13. The overall equation, valid for ionic strengths between 0.001 and 0.1 mol/l and charge numbers from 2 to 6, thus becomes

$$\mu/\mu_0 = \exp(-0.85z^{0.49}I^{0.52}) \tag{5}$$

Simplification of the fitting equation

As both parameters c and b are relatively close to 0.5, a further simplification of Eq. 5 seems reasonable:

$$\mu/\mu_0 = \exp(-d\sqrt{zI}) \tag{6}$$

In order to evaluate the effect of this simplification on the predictive value of the model, d was determined from all experiments with multivalent ions. The average value of d was 0.77 and
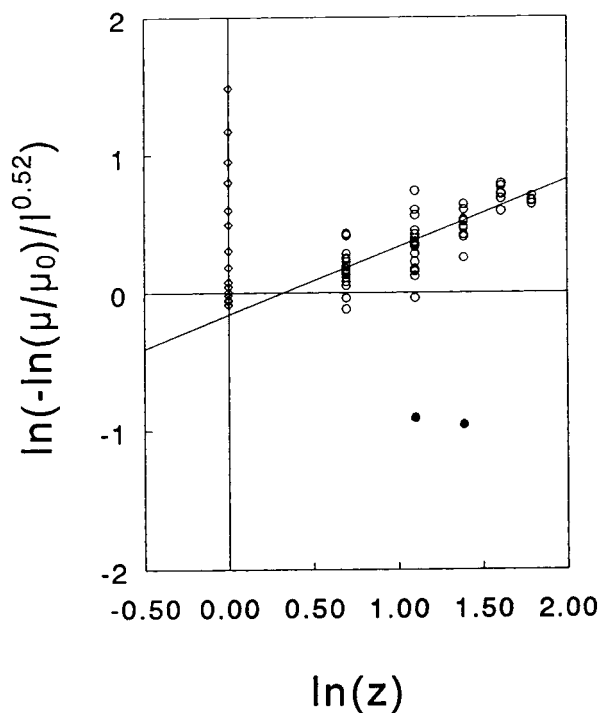

Fig. 4. Determination of b and a (from the slope and the intercept, respectively, according to Eq. 5) for all ionic strengths and all multivalent ions (○). Monovalent ions (◇) and some outliers (●) were omitted from the linear curve fit.

the standard deviation σ_d was 0.11. This is not surprising because both c and b in the model of Eq. 2 do not deviate significantly from 0.5, as seen from their respective standard deviations. In addition, the relative standard deviation of d in Eq. 6 is not larger than that of a in Eq. 5. In view of its inherent simplicity, preference should therefore be given to the model of Eq. 6, which now becomes

$$\mu/\mu_0 = \exp(-0.77\sqrt{zI}) \tag{7}$$

3.2. Evaluation of the model

Two different approaches were applied to evaluate the model by calculating μ values for different ionic strengths and charge numbers from Eq. 7 and to compare the results with the measured data: (i) from the values of the absolute mobilities, μ_0 (Table 1) and (ii) from one

actual mobility determined at a particular ionic
strength. Both approaches are of practical inter-
est, because in practice either the absolute
mobility can be found in the literature, or a
single experiment in a particular buffer gives a
certain mobility value.

The mobilities calculated in these ways were
compared with the data measured at the same
ionic strength.

Approximation of μ from μ_0

For this approximation, μ_0 values determined
with the five-point second-order polynomial fit of
all experiments were used (Table 1). From this
value, actual mobilities μ were calculated for
each component at all ionic strengths. The agree-
ment between measured and calculated mobility
was excellent, as shown in Fig. 5. The linear
correlation coefficient of the line in Fig. 5 is high
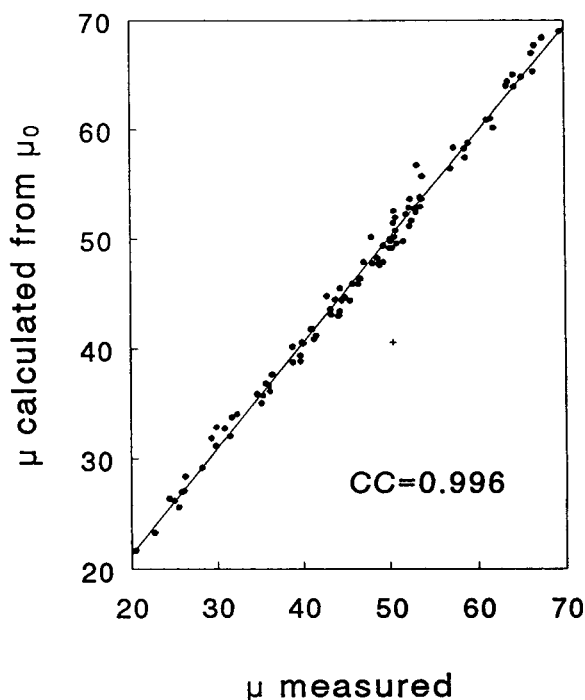(0.996). Differences are of the order of a few

Fig. 5. Correlation between the measured actual mobility
and the actual mobility calculated from μ_0, using the model
described in the text. In this case μ_0 was obtained with a
five-point second-order polynomal fitted to the square-root
model from all ions and all ionic strengths ($n = 100$). There is
one outlier (+). The mobilities are given in 10^{-9} $m^2/V \cdot s$.

Table 1
Model components investigated

Code	$-\mu_0$	Name
1AN2	27.7	Anthraquinone-2-sulfonic acid
1NA2	33.7	2-Naphthalenesulfonic acid
1TO4	34.6	4-Toluenesulfonic acid
2AN15	48.1	Anthraquinone-1,5-disulfonic acid
2AN26	49.5	Anthraquinone-2,6-disulfonic acid
2NA15	55.6	Naphthalene-1,5-disulfonic acid
2NA26	54.9	Naphthalene-2,6-disulfonic acid
2NA36	51.7	Naphthalene-3,6-disulfonic acid
2BE13	63.1	Benzene-1,3-disulfonic acid
3IN	61.3	Indigo-5,5',7-trisulfonic acid
3NA136	67.5	Naphthalene-1,3,6-trisulfonic acid
3AZ05	54.6	AZO-4,3',6'-trisulfonic acid
3AZ06	55.2	AZO-3,6,6'-trisulfonic acid
3AZ07	56.3	AZO-3,6,8-trisulfonic acid
3AZ08	54.8	AZO-3',6',8'-trisulfonic acid
4IN	74.7	Indigo-5,5',7,7'-tetrasulfonic acid
4AZ09	67.1	AZO-3,6,8,6'-tretrasulfonic acid
4AZ10	68.0	AZO-3,6,3',6'-tetrasulfonic acid
5AZ11	76.5	AZO-3,6,8,3',6'-pentasulfonic acid
5AZ12	77.3	AZO-3,6,3',6',8'-pentasulfonic acid
6AZ13	78.9	AZO-3,6,8,3',6',8'-hexasulfonic acid

The first digit of the code is the charge number z. The
absolute mobility μ_0 (in sodium acetate buffer) determined at
25°C by extrapolation to $I = 0$ (see text for further details) is
given in 10^{-9} $m^2/V \cdot s$. AZO = (2-hydroxy-1-naph-
thylazo)naphthalene.

percent. With the purpose of quantifying the
predictability of the model, the results are pre-
sented in a different way.

In Fig. 6, the relative difference between
measured and calculated mobility is shown
plotted against the charge number. What we
observe is a random error of 5% or less for
charge numbers $z = 2$–6. A systematic deviation
(the average of the values is about 5%) and a
slightly larger scatter is observed only for mono-
valent ions, which is not surprising for the
reasons mentioned above.

As mentioned in the Introduction, it is not
advisable to derive μ from μ_0 values obtained
from conductivity measurements and literature
transport numbers: the predictive value of mo-
bilities in buffers obtained in this way is inher-
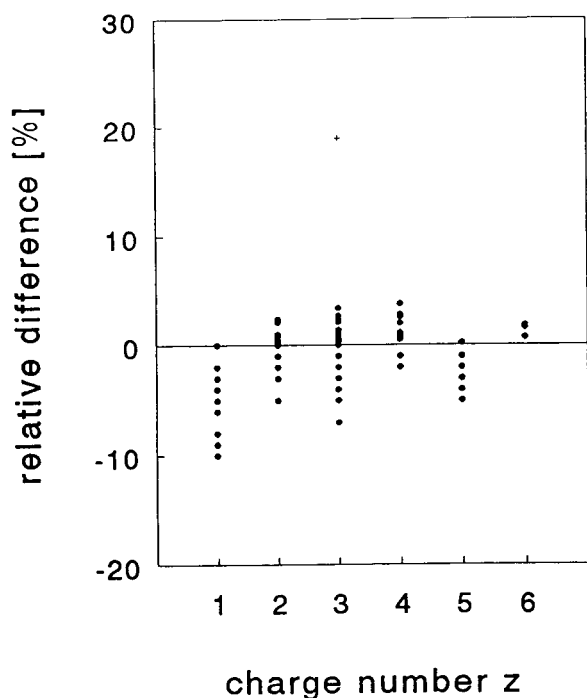ently doubtful. Although calculation of μ_0 is not

Fig. 6. Relative difference between measured and calculated actual mobility (see caption of Fig. 5) as a function of charge number z, using Eq. 5. The mean relative difference is 0.8%; there is one outlier (+).

necessary in order to calculate the mobility at one ionic strength from experiments at another ionic strength in the same buffer system, μ_0 may be useful in comparing results in different laboratories using the same buffer at different ionic strengths. For each condition, only a single experiment is needed. Further electrophoretic behaviour in the chosen buffer can then be predicted using the Henderson–Hasselbach equation and Eq. 7 for the effects of pH and ionic strength, respectively.

Approximation of μ from a different ionic strength

The model can also be used to calculate the mobility at a certain ionic strength from that obtained experimentally at another ionic strength. Obviously, one has to be careful not to go beyond the valid ionic strength range. The form of Eq. 5 makes it possible to do so without

the need to know μ_0 because μ/μ_0 is written explicitly. The mobility calculated from a tenfold higher ionic strength is plotted against the measured mobility in Fig. 7. The correlation is fairly satisfactory (correlation coefficient = 0.995). Comparable or even better results are obtained if μ is calculated from a 2–5-fold lower ionic strength. Here also the relative differences are of the order of a few percent. The deviation is random, not systematic, and the relationship seems valid for charge numbers 2–6.

Comparison with a former approach

When comparing the model Eq. 7 with the previously published model [13,14] (Eq. 1), the following differences can be seen. The square root of I was a good estimate, even at the ionic strengths used in the present investigation. The effect of the charge number was previously
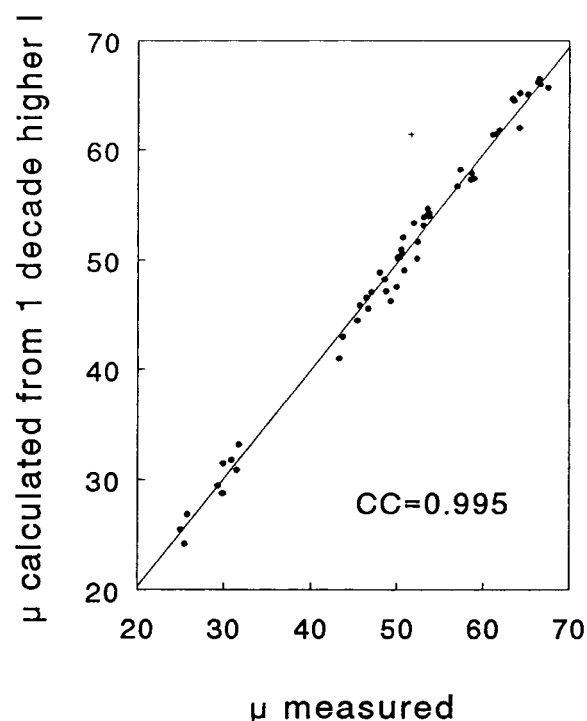

Fig. 7. Correlation between measured actual mobility and actual mobility calculated from experimental data at a tenfold higher ionic strength ($n = 100$), using the model of Eq. 7. Mobilities are given in 10^{-9} $m^2/V \cdot s$ units. There is one outlier (+).

overestimated, although for low charge numbers it was compensated for by the lower value of a. Previous experimental verification [14] of Eq. 1 was satisfactory, however, probably because these experiments were limited to charge numbers 1–3 and an ionic strength of ca. 0.01 mol/l.

4. Conclusions

An empirical model was developed that makes it possible to calculate mobilities of strong, multivalent ions with charge numbers between 2 and 6 in the ionic strength range 0.001–0.1 mol/l either from a single experiment or from the absolute mobility. Calculation of mobilities within one decade of ionic strength in the range mentioned can be carried out with an error of 5% or less, for charge numbers 2–6. Extrapolation from zero ionic strength is also possible, leading to a comparable accuracy, at least for all multivalent ions. Further experiments will have to show if the present model is also valid for other components and weak solutes.

Acknowledgement

References

[1] R.A. Robinson and R.H. Stokes, Electrolyte Solutions, Butterworths, London 2nd ed., 1970, pp. 133–145.

[2] F.M. Everaerts, J.L. Beckers and Th.P.E.M. Verheggen, Isotachophoresis, Theory, Instrumentation and Applications (Journal of Chromatography Library, Vol. 6), Elsevier, Amsterdam, 1976.

[3] P. Boček, P. Deml, P. Gebauer and V. Dolník, Analytical Isotachophoresis (Electrophoresis Library), VCH, Weinheim, 1988.

[4] F. Foret and P. Boček, in A. Chrambach, M.J. Dunn and B.J. Radola (Editors), Advances in Electrophoresis, Vol. 3, VCH, Weinheim, 1989, pp. 273–342.

[5] S.F.Y. Li, Capillary Electrophoresis—Principles, Practice and Applications (Journal of Chromatography Library, Vol. 52), Elsevier, Amsterdam, 1992.

[6] E. Kenndler and C. Schwer, J. Chromatogr., 608 (1991) 161.

[7] W. Friedl and E. Kenndler, Anal. Chem., 65 (1993) 2003–2009.

[8] G.J.M. Bruin, J.P. Chang, R.H. Kulman, K. Zegers, J.C. Kraak and H. Poppe, J. Chromatogr. 471 (1989) 429–436.

[9] W. Nashabeh and Z. El Rassi, J. Chromatogr. 514 (1990) 57–64.

[10] H.J. Issaq, I.Z. Atamna, G.M. Muschik and G.M. Janini, Chromatographia, 32 (1991) 155–161.

[11] J. Heinrich and H. Wagner, Electrophoresis, 13 (1992) 44–49.

[12] R.H.P. Reid, J. Chromatogr. A, 669 (1994) 151–183.

[13] J.C. Reijenga and E. Kenndler, J. Chromatogr. A, 659 (1994) 403–415.

[14] J.C. Reijenga and E. Kenndler, J. Chromatogr. A, 659 (1994) 417–426.

[15] S. Hjertén, Chromatogr. Rev., 9 (1967) 122–219.

[16] J. Gasparic and A. Sedmíková, J. Chromatogr. A, 665 (1994) 197–202.

ELSEVIER

Bidirectional isotachophoretic separation of metal cations using EDTA as a chelating agent

Takeshi Hirokawa*, Takao Ohta, Ken-ichiro Nakamura, Kazuhiro Nishimoto, Fumitaka Nishiyama

Applied Physics and Chemistry, Faculty of Engineering, Hiroshima University, Kagamiyama 1, Higashi-hiroshima 739, Japan

Abstract

An operational electrolyte system using EDTA as a chelating agent was developed for the bidirectional isotachophoresis (ITP) of metal ions. The anolyte used was 20 mM HCl buffered by adding β-alanine at pH 3.6. The catholyte was 20 mM ammonia solution buffered by acetic acid at pH 4.8 and containing EDTA in the range 0–1 mM. In relation to the concentration of EDTA, the isotachophoretic separation behaviour of eighteen metal cations containing equimolar EDTA was studied by using with particle-induced X-ray emission (PIXE). They were Na^+, Li^+, Ba^{2+}, Sr^{2+}, Mg^{2+}, Ca^{2+}, Mn^{2+}, La^{3+}, Ce^{3+}, Co^{2+}, Zn^{2+}, Gd^{3+}, Pb^{2+}, Y^{3+}, Ni^{2+}, Cu^{2+}, Lu^{3+} and Fe^{3+} in increasing order of chelate stability constants. When a catholyte containing 0.1 mM EDTA was used, Na^+, Li^+, Ba^{2+}, Sr^{2+}, Mg^{2+}, Ca^{2+} and Mn^{2+} were completely recovered as cations and La^{3+}, Ce^{3+}, Co^{2+}, Zn^{2+}, Gd^{3+}, Pb^{2+}, Y^{3+}, Ni^{2+}, Cu^{2+} and Lu^{3+} were completely recovered as chelate anions. The recovery was incomplete for a test mixture without adding EDTA, even when the EDTA concentration in the catholyte was 1 mM. Absolute mobilities of several chelates were obtained and the concentration and pH of isotachophoretic zones were simulated to clarify the decomposition during migration.

1. Introduction

When conventional operational systems for isotachophoresis (ITP) [1,2] are used, anions or cations migrate isotachophoretically to form stacked zones. That is, isotachophoretic regulation of separand concentration is restricted to separands of the same charges as the leading ion. However, when an appropriate electrolyte system with dual leading ions and dual terminating ions is used, both anions and cations migrate

isotachophoretically to form stacked zones. That is, isotachophoresis can in principle be bidirectional [3].

We have reported that an operational electrolyte system for bidirectional isotachophoresis (BITP) could be constructed simply by combining a leading electrolyte for anions and that for cations [4]. Considering the limitation of the pH difference between the combined leading electrolytes, we have described fifteen bidirectional electrolyte systems covering the pH range 3–10 [5].

BITP is an effective method for the analysis and fractionation of both anions and cations in a sample. When both components are to be ana-

* Corresponding author.

lysed, the use of a bidirectional operational electrolyte system may considerably shorten the analysis time, although a dual detector system is necessary. Even if such a system is not available, it is very convenient that an electrolyte system can be applied for the analysis of both anions and cations. Moreover, a new separation system may be developed by utilizing BITP.

We have been studying the isotachophoretic separation behaviour of metal cations, including rare earth ions. Recently we reported the selective analysis of alkali ions and alkaline earth metal ions from a test mixture of twenty metal cations using tartaric acid as the complexing agent [6]. The strongly interacting ions contained in the test mixture presumably formed complexes with low effective mobility or non-ionic ones, as they could not be detected as isotachophoretic zones. If mobile anions were formed using an appropriate complex-forming agent, BITP could be applied for the analysis of such a complex mixture.

In this paper, we describe the selective separation of metal ions by means of BITP utilizing EDTA as a chelate-forming agent. The role of EDTA is to reverse the ionic charges of strongly interacting cations into anions. Taking into account previous studies [7,8] on the ITP analysis of EDTA chelates by using unidirectional electrolyte systems, the dependence of the recovery of chelate anions on pH and EDTA concentration was studied for eighteen metal cations by means of ITP with particle-induced X-ray emission (PIXE) [6]. The cations are Na^+, Li^+, Ba^{2+}, Sr^{2+}, Mg^{2+}, Ca^{2+}, Mn^{2+}, La^{3+}, Ce^{3+}, Co^{2+}, Zn^{2+}, Gd^{3+}, Pb^{2+}, Y^{3+}, Ni^{2+}, Cu^{2+}, Lu^{3+} and Fe^{3+} in increasing order of stability constants. The purpose was to clarify how the stability constants should differ for BITP of the metal cations.

The stability of the chelate zone is important from the viewpoint of recovery. The concentrations of the chelate and the free metal ions in the isotachophoretic zone are simulated to describe the stability of the chelate zone. As no mobilities of chelate anions have previously been reported, they were determined by ITP.

2. Theoretical

2.1. Operational electrolyte system for BITP using EDTA

The operational electrolyte system in BITP consists of a leading electrolyte for anions (anolyte) and that for cations (catholyte). The pH buffer in the anolyte plays the role of the terminating cations, and that in the catholyte plays the role of the terminating anions.

Fig. 1 illustrates the electrolyte system for BITP filled in a separation capillary. The anolyte is 20 mM HCl buffered by adding β-alanine at pH 3.6 and the catholyte is 20 mM ammonia solution buffered by adding acetic acid at pH 4.8. The catholyte contains the complexing agent EDTA in the range 0–1 mM. In this system, β-alanine and acetic acid are simultaneously cationic and anionic terminators, respectively.

In previous studies on the ITP separation of EDTA chelates, no EDTA was added to the catholyte [7,8]. As shown later, the addition of EDTA was necessary to obtain complete recovery at pH 3.6.

As in conventional unidirectional ITP, the effective mobility of the terminators should not
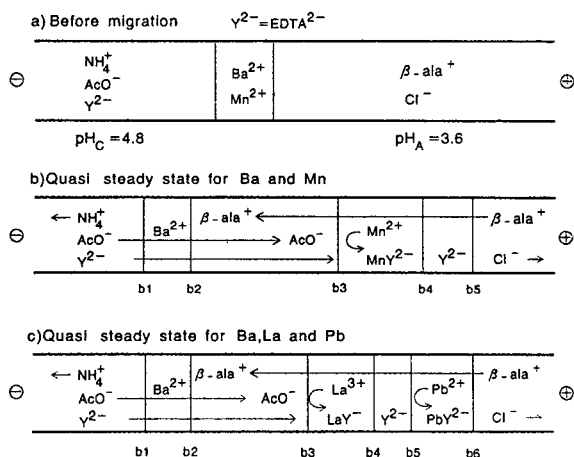

Fig. 1. Schematic diagrams of bidirectional isotachophoresis utilizing EDTA as a chelating agent. The anolyte (anionic leading electrolyte) is HCl buffered by β-alanine and the catholyte (cationic leading electrolyte) is ammonia solution buffered by acetic acid (electrolyte system No. 2 in Table 2).

be too small or too large. Otherwise, ITP is impossible or the effective mobility range of analysable samples become very narrow. Therefore, the pH difference of the electrolyte is not arbitrary [4] and preferably is in the range $0.5 < pH_C - pH_A < 1.5$, where pH_C is the pH of the catholyte and pH_A is that of the anolyte.

2.2. Stability of isotachophoretic zone of EDTA chelates

Let us consider Ba^{2+} and Mn^{2+} as the sample, as shown in Fig. 1a and b. The chelate stability constants with $EDTA^{4-}$ at zero ionic strength were 9.62 and 15.63, respectively. Under the pH conditions used in this study, EDTA may exist as divalent anions, $EDTA^{2-}$ (hereafter abbreviated as H_2Y^{2-}). Then the chelate-forming reaction with metal cations M^{n+} that actually occurs in the isotachophoretic zone can be written as

$$M^{n+} + H_2Y^{2-} = MY^{(n-4)-} + 2H^+$$
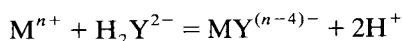
As the conditional stability constants of EDTA chelates are much smaller than the stability constants, weakly interacting Ba^{2+} will be detected as cations forming a steady-state zone, as shown in Fig. 1b. On the other hand, strongly interacting Mn^{2+} is detected as a chelate anion. Accordingly, the recovery as the chelate anion is closely related to the pH of the anolyte (pH_A) and the concentration of EDTA contained in the catholyte.

The other important factor affecting the recovery is the migration order, as discussed in detail by Gebauer et al. [8]. H_2Y^{2-} from the catholyte overtakes the MnY^{2-} zone, because H_2Y^{2-} has a larger effective mobility than that of MnY^{2-}. This migration order for H_2Y^{2-} and the chelate of metal ions may be reversed, depending on the central metal ion. For example, the effective mobility of PbY^{2-} is slightly larger than that of H_2Y^{2-} as shown in Fig. 1c. Obviously, from the concentration regulation in isotachophoresis, the concentration of EDTA is much higher in the EDTA zone than that in the catholyte. In the case of PbY^{2-}, if the chelate decomposes to release free metal ions, they will return to its original zone forming the chelate zone again reacting with H_2Y^{2-}. It should be noted the effective mobility of a monovalent chelate anion, e.g., LaY^-, is always smaller than that of H_2Y^{2-} and therefore such an effect is not expected.

Since H_2Y^{2-} is fed continuously from the catholyte, the EDTA zone between the boundaries b_4 and b_5 (Fig. 1) cannot reach the steady state, that is, the zone length increases with time. Accordingly, the boundaries b_3 and b_4 moves with a smaller velocity than the isotachophoretic velocity. On the other hand, the boundaries b_1, b_2 and b_5 show purely isotachophoretic behaviour.

3. Experimental

3.1. Samples

Table 1 lists the eighteen metal ions and the values of the stability constants (ionic strength =

Table 1
Chelate stability constants of metal cations

$MY^{(n-4)-}$	Log K	$MY^{(n-4)-}$	Log K	$MY^{(n-4)-}$	log K
NaY^{3-}	3.46	MnY^{2-}	15.63	PbY^{2-}	19.70
LiY^{3-}	4.61	LaY^-	17.28	YY^-	19.90
BaY^{2-}	9.62	CeY^-	17.76	NiY^{2-}	20.34
SrY^{2-}	10.50	CoY^{2-}	18.02	CuY^{2-}	20.52
MgY^{2-}	10.65	ZnY^{2-}	18.26	LuY^-	21.62
CaY^{2-}	12.43	GdY^-	19.17	FeY^-	26.82

0). The values were obtained by applying an ionic strength correction to the reported values at ionic strength = 0.1 [9]. An equimolar test mixture was prepared from 20 mM stock solutions of the chlorides obtained from Tokyo Kasei (Tokyo, Japan). The concentration of the component was 1 mM. The pH of the sample solution was adjusted to 4.8 by adding acetic acid. The pH of the sample solution was kept constant just before starting migration, because the sample is injected into the catholyte and the pH was adjusted to 4.8.

A test mixture of the eighteen metal cations containing an equimolar amount of EDTA was also prepared by mixing the above test mixture and 20 mM EDTA solution. The pH of the EDTA solution was adjusted to 4.8 by adding ammonia solution. The component concentration was 0.5 mM.

Small amounts of cationic dyes (toluidine blue and astrazon pink) and an anionic dye [4,5-dihydroxy-3-(p-sulfophenylazo)-2,7-naphthalene-disulfonic acid (SPADNS)] were co-migrated to monitor the migration process and determine the timing of fractionation.

3.2. Operational electrolyte system

Table 2 summarizes the electrolyte systems used. The anolyte was 20 mM HCl and chloride was the leading ion for anions. The pH of the anolyte (pH_A) was adjusted to 3–6 by using appropriate buffers as shown in Table 1. The catholyte was 20 mM aqueous ammonia solution containing EDTA as the complexing agent, and ammonium was the leading ion for cations. The concentration of EDTA was varied as 0.1, 0.25, 0.5 and 1.0 mM. The pH of the catholyte (pH_C) was adjusted to 4.8 by adding acetic acid. The electrolytes used contained 0.1 mass-% of hydroxypropyl cellulose (HPC) (Tokyo Kasei) to suppress electroosmotic flow. The viscosity of a 2 mass-% HPC solution was 1000–4000 cP at 20°C.

All reagents were purchased from Tokyo Kasei. pH measurements were carried using a Horiba (Tokyo, Japan) Model F-7 AD digital pH meter.

Table 2
Operational electrolyte system used in isotachophoresis

Anolytes pH buffers	20 mM HCl (1) Triglycine (pH 3.1) (2) β-Alanine (pH 3.6) (3) ε-Aminocaproic acid (pH 4.4) (4) Histidine (pH 6.0)
Catholytes pH buffers	20 mM ammonia solution (1) Acetic acid (pH 4.8) (2) Caproic acid (pH 4.8) (3) MOPS (pH 6.0)
Chelating agent	EDTA, 0.1–1.0 mM

Operational electrolyte system for BITP

System No.	Anolyte	Catholyte	EDTA concentration (mM)
1	1	1	
2	2	1	
3	3	2	
4	4	3	
5	2	1	0.1
6	2	1	0.25
7	2	1	0.5
8	2	1	1.0

3.3. Isotachophoretic apparatus used for R_E measurement

The detector used for R_E measurement was a high-frequency contactless conductivity detector (HFCCD) [10]. The separation unit of the apparatus used was that of a Labeco (Spiska Nova Ves, Slovakia) ZKI-001 instrument. The separation column used consisted of a preseparation capillary (10 cm × 0.5 mm I.D.) and a main capillary (20 cm × 0.25 mm I.D.). The migration current when detecting zones was 50 μA, which was supplied by a high-voltage power supply for a Shimadzu (Kyoto, Japan) IP-2A instrument. Measurements were carried out at 25°C in a temperature-controlled room.

The qualitative index R_E is defined as the ratio of the potential gradient (E V cm^{-1}) of a sample zone (E_S) to that of a leading zone (E_L) [11]. When a conductivity detector is used, it is equal to the ratio of specific resistance (ρ) of each zone. It is also equal to the ratio of the effective

mobility ($\bar{m}$) of leading ion to that of sample ion in its zone from the equality of the velocity of migrating zones ($v = \bar{m}E$):

$$R_E = E_S/E_L = \rho_S/\rho_L = \bar{m}_L/\bar{m}_S$$

As the output signal of the HFCCD shows a non-linear response to the specific resistance [10], the signal obtained was converted into specific resistance using a fourth-order polynomial expression of output voltage. Picric acid was used as the internal standard to correct the slight drift of HFCCD signals. The simulated R_E value was 2.64 at $pH_A = 3.6$.

3.4. Micro-preparative isotachophoretic analyser

Fig. 2 shows a schematic diagram of the capillary-type micro-preparative analyser modified for BITP. The design and the method of fractionation have already been reported in detail for the unidirectional version [12]. The separated sample zones were fractionated from a nozzle by applying a counter-flow of the anolyte and the catholyte. Two syringe pumps were used for the purpose.

Fig. 2b shows the injection compartment of the analyser. The compartment was made of two blocks of acrylic resin. A semipermeable membrane was inserted between two blocks to prevent hydrodynamic flow in the separation tube.

The separation column used consisted of a PTFE precolumn (46 cm × 1 mm I.D. for anions, 63 cm × 1 mm I.D. for cations) and a PTFE main column (20 cm × 0.5 mm I.D.). The total volume of the column was 0.40 cm^3 for anions and 0.53 cm^3 for cations. The quantity of electric charge integrated until the first sample zone was 1.1 C.

One drop (ca. 5 μl) comprised one fraction, which contained ca. 5 nmol of component. The amount depends on the velocity of the counterflow and migration current. In the present experiments, the former was ca. 30 μl min^{-1} and the latter was 150 μA.

3.5. PIXE analysis

For PIXE spectral measurements, a Van de Graaff accelerator was used (Model AN-2500;
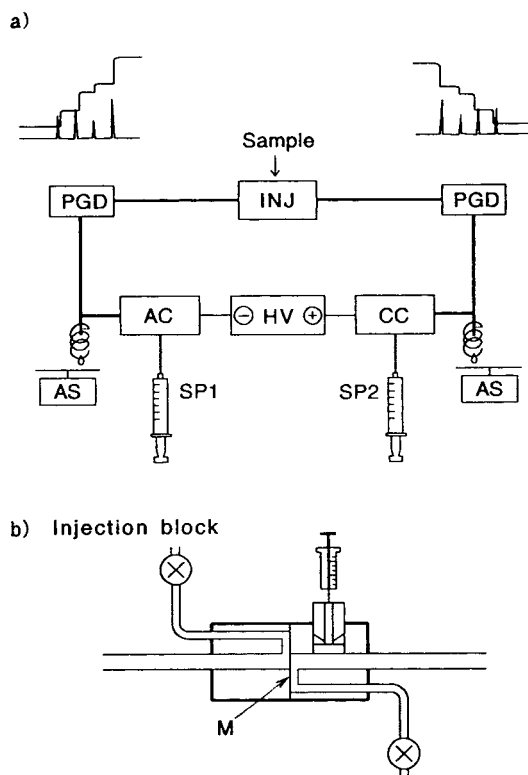
a)

b) **Injection block**

Fig. 2. (a) Schematic diagram of preparative ITP equipment. PGD = potential gradient detector; INJ = sample injection valve; AC = anolyte compartment; CC = catholyte compartment; HV = high-voltage power supply; SP1 and SP2 = syringe pumps making counter flow of anolyte and catholyte; AS = automated sampler. (b) Injection compartment. M = semipermeable membrane.

Nisshin High Voltage, Tokyo, Japan). The energy of the H$^+$ beam was 2 MeV, the beam current was ca. 50 nA and the integrated charge was 10 μC. The detector used was a high-purity Ge detector (an Ortec Model GLP-10180) and the multi-channel analyser was a Laboratory Equipment, (Tokyo, Japan) Model AMS-1000. Owing to the limitations of the X-ray detection system used, light elements below atomic number 14 (Si) could not be detected.

A Nuclepore filter (thickness 5 μm and pore size 0.1 μm) was used as the target backing material, which was mounted on an aluminium flame. The separated zones were fractionated dropwise on the Nuclepore filter. After drying in

a desiccator, the fractions were used as PIXE targets. A typical single run took ca. 200 s to obtain a PIXE spectrum of a fraction. The spectra obtained were analysed by using the spectrum deconvolution software PIXS [13].

4. Results and discussion

4.1. Mobility of EDTA chelates

First, absolute mobilities of EDTA and several EDTA chelates were determined by the best-fitting procedure for the observed and simulated R_E using the least-squares method [14].

Table 3 gives the evaluated absolute mobilities of several chelate anions, R_E values obtained by using electrolyte system No. 2 (pH$_A$ 3.6) and the stability constants. The mobility of H_2Y^{2-} was obtained using three R_E values (2.12, 1.96 and 1.86) obtained by using electrolyte systems Nos. 2, 3 and 4 in Table 2, respectively. It was assumed that the mobility of the ionic component of EDTA increased linearly with increasing charge.

Obviously from Table 3, the mobilities of divalent anions are twice those of the monovalent anions. However, the difference in the mobilities among the monovalent or divalent ions is very small. This is natural because the mobility of these chelates is mostly determined by the bulky ligand, suggesting that only a limited number of chelate anions can be separated at once.

4.2. Migration behaviour of EDTA chelates

The isotachophoretic separation behaviour of EDTA chelates was studied by Yoshida et al. [7] for fourteen metal ions, Mg^{2+}, Ca^{2+}, Ba^{2+}, Mn^{2+}, Co^{2+}, Ni^{2+}, Cu^{2+}, Zn^{2+}, Cd^{2+}, Hg^{2+}, Pb^{2+}, Bi^{3+}, Fe^{3+} and La^{3+}. They concluded that an anolyte (leading electrolyte for anions) of low pH should be avoided in order to obtain good recoveries and the use of specific buffering counter ions was effective for obtaining better separability.

First, the migration behaviour of EDTA chelates was observed using electrolyte systems containing no EDTA. Fig. 3 shows a typical isotachopherogram of LaY^- and PbY^{2-} obtained by using electrolyte system No. 2 (pH$_A$ 3.6) and calibration lines obtained by using various electrolyte systems in the pH range 3.1–6. The stability constants of LaY^- and PbY^{2-} were log $K = 17.3$ and 19.7, respectively. As shown in Fig. 3b, the calibration line at pH$_A$ = 3.6 did not pass through the origin: 5 nmol of LaY^- decomposed during migration with integrated charge 0.33C.

Fig. 3c shows the calibration lines of LaY^- obtained at various pH$_A$, confirming that the LaY^- chelate decomposed at low pH, releasing La^{3+} and H_2Y^{2-}, and the rate of decomposition was large at low pH. On the other hand, the decomposition of PbY^{2-} and LuY^- (log $K = 21.6$) could not be detected even at pH 3.6.

As discussed by Gebauer et al. [8] for NTA–metal complexes, such decomposition was due to the small conditional complex stability constants at low pH, where the chelate was labile depend-

Table 3
Absolute mobilities of EDTA chelates obtained by isotachophoretic method

$MY^{(n-4)-}$	R_E	m_0	$MY^{(n-4)-}$	R_E	m_0
CeY^-	4.20	20.5	AlY^-	3.62	23.5
LaY^-	4.19	20.6	CaY^{2-}	2.28	42.3[a]
YY^-	4.04	21.3	NiY^{2-}	2.31	41.5
LuY^-	4.02	21.4	PbY^{2-}	2.18	43.6
FeY^-	3.70	23.1	H_2Y^{2-}	2.26	44.0

The pK_a values of the EDTA used were 2.11, 3.01, 6.84 and 11.84 at zero ionic strength. These values were obtained by applying an ionic strength correction to the reported values of 2.0, 2.67, 6.27 and 11.0 at ionic strength 0.1.
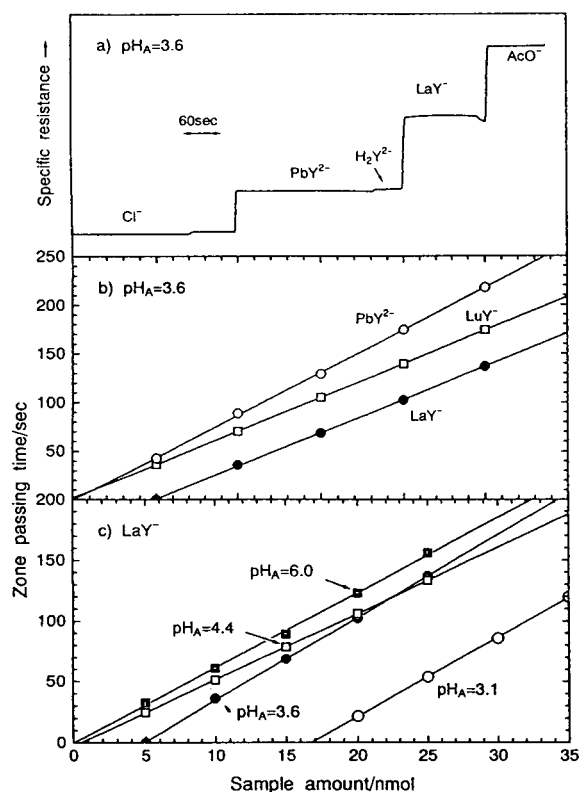[a] Obtained at pH$_A$ = 6.

Fig. 3. (a) Isotachopherogram of LaY$^-$ and PbY^{2-} (Y = EDTA) obtained at pH$_A$ = 3.6; (b) calibration lines obtained at pH$_A$ = 3.6; (c) calibration lines obtained by using various electrolyte systems in the pH$_A$ range 3.1–6. The injected sample amount was 1.2 μl (12 nmol of metal ions). Operational electrolyte systems as in Table 1. Migration current = 50 μA. Quantity of integrated charge = 0.28 C.

ing on the stability constants. In this case, LaY$^-$ gradually decomposed to release La^{3+} and H$_2$Y^{2-} and the released H$_2$Y^{2-} formed the isotachophoretic zone next to the chelate zone as shown in Figs. 1 and 3a. On the other hand, La^{3+} migrates towards the cathode to form an isotachophoretic zone when a bidirectional electrolyte system is used.

The rate of chelate decomposition must be closely related to the conditional stability constants of the chelate and therefore free metal ions in the zone. Using the absolute mobilities evaluated for the chelate ions, the isotachophoretic chelate zones were simulated. Table 4 shows the total concentration of LaY$^-$, LuY$^-$ and PbY^{2-} in the isotachophoretic zones and the concentration of free metal ions at pH$_A$ 3.6. In the LaY$^-$ zone, the free metal ion concentration was only 0.6% of that of the chelate. In spite of this low concentration of free ions, the decomposition could not be neglected. On the other hand, the free metal ion contents of the LuY$^-$ and PbY^{2-} zones were 0.004% and 0.06%, respectively.

4.3. Difference of the stability constants necessary for bidirectional isotachophoretic separation

According to preliminary experiments, MnY^{2-} (log K = 15.63) mostly decomposed to form Mn^{2+} zone when pH$_A$ was 3.1 and there was no

Table 4
Simulated concentration of some chelates and free metal ions in the isotachophoretic zones

MY$^{(n-4)-}$	Log K[a]	pH	Log K'[b]	Concentration (mM)	
				Chelate	Free metal
LaY$^-$	17.28	3.91	−1.36	9.90	0.059
LuY$^-$	21.62	3.89	2.99	10.4	0.00042
PbY^{2-}	19.70	3.74	1.07	7.40	0.0046

[a] Log K = [MY$^{(n-4)-}$]/([M^{n+}][Y^{4-}]).
[b] Log K' = MY$^{(n-4)-}$][H$^+$]^2/([M^{n+}][H$_2$Y^{2-}]).

EDTA in the catholyte. Therefore, MnY^{2-} was selected as the standard chelate to investigate the difference in the stability constants necessary for bidirectional separation. Several two-component mixtures of MnY^{2-} and (lanthanide)Y^- were analysed and the recovery was investigated.

Fig. 4a shows migration scheme for MnY^{2-} and LaY^- releasing Mn^{2+}, La^{3+} and Y^{2-}. Fig. 4b and c show calibration lines obtained for anions and cations by using a bidirectional electrolyte system. The difference in the stability constants between LaY^- and MnY^{2-} was Δ log $K = 1.65$. Obviously from Fig. 4b and c, MnY^{2-} decomposed to migrate as cations and part of the LaY^- and CeY^- also did. When CeY^- (Δ log $K = 2.13$) was co-migrated with MnY^-, the re-

covery as CeY^- was better than that of LaY^-. The anionic increased with increase in the stability constants, and finally complete recovery was obtained for GdY^- (Δ log $K = 3.54$).

It was revealed from this experiment that Na^+, Li^+, Ba^{2+}, Sr^{2+}, Mg^{2+}, Ca^{2+} and Mn^{2+} (log K of $MnY^{2-} = 15.6$) were recovered as cations at pH 3.1 and the metal ions Gd^{3+} (log K of $GdY^- = 19.2$), Pb^{2+}, Y^{3+}, Ni^{2+}, Cu^{2+}, Lu^{3+} and Fe^{3+} were recovered as chelate anions, when the sample contained an equimolar amount of EDTA but no EDTA was present in the catholyte. Among the other metal ions, La^{3+} and Ce^{3+} were detected as both anions and cations. For CoY^{2-}, NiY^{2-} and ZnY^{2-}, no cationic zones were observed. The zone length of these chelates could not be observed accurately, as the step heights overlapped with that of the H_2Y^{2-} zone.

4.4. Recovery of metal cations

Finally, the test mixture of the eighteen metal cations without adding EDTA was analysed by ITP–PIXE using electrolyte systems Nos. 6–8 in Table 2. EDTA was present only in the catholyte. A 10-μl volume of the sample mixture (amount of each component = 10 nmol) was separated and fractionated.

Fig. 5 shows the analytical results for ITP fractions obtained by PIXE. The EDTA concentration was 0.25 mM (Fig. 5a) and 0.5 mM (Fig. 5b). Obviously from Fig. 5, Ba^{2+}, Sr^{2+} and Ca^{2+} were detected as cations and the others were detected as anions. The recoveries of Ba^{2+}, Sr^{2+} and Ca^{2+} were 100%. As Li^+, Na^+ and Mg^{2+} could not be detected using the PIXE detection system used, they are not shown in Fig. 5. All of these cations can be assigned by using a conventional isotachophoretic method using standard samples. The separability of cations were affected by the EDTA concentration.

Concerning the chelate anions, it was found that the recovery was not so good in general. When the EDTA concentration was 0.25 mM, La, Ce and Mn could not be detected either as anions or as cations. When the EDTA concen-

Fig. 4. (a) Migration scheme of MnY^{2-} and LaY^- liberating Mn^{2+} and La^{3+}, and calibration lines obtained for (b) anions and (c) cations by using the bidirectional electrolyte system.
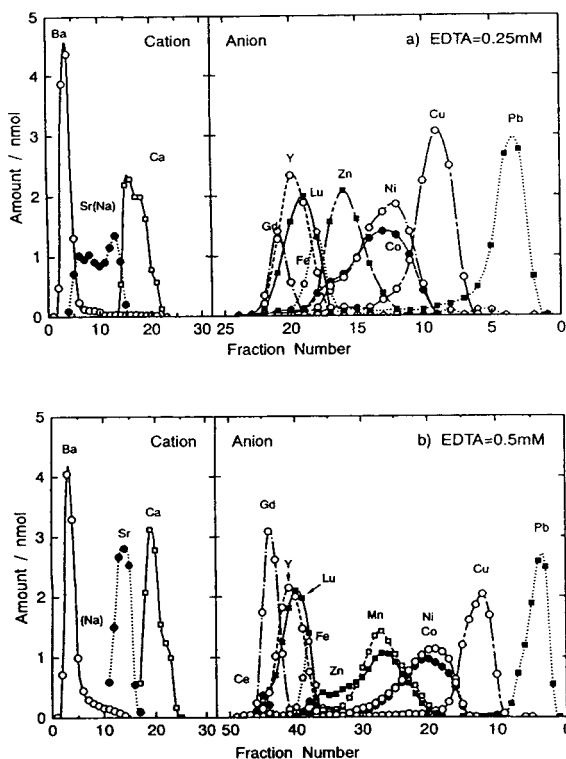
Fig. 5. Analytical results for the fractions of the eighteen metal cations obtained by PIXE. The concentration of EDTA in the catholyte was (a) 0.25 and (b) 0.5 mM. The injected sample amount was 10 μl (10 nmol metal of ions). Operational electrolyte systems Nos. 5 and 6 in Table 1. Quantity of integrated charge = 1.1 C.

Complete recovery was obtained for the chelate anions when the sample solution contained an equimolar amount of EDTA and the catholyte contained EDTA at a low concentration. When a catholyte containing 0.1 mM EDTA was used, Na$^+$, Li$^+$, Ba^{2+}, Sr^{2+}, Mg^{2+}, Ca^{2+} and Mn^{2+} (log K of MnY^{2-} = 15.63) were completely recovered as cations, and La^{3+} (log K of LaY$^-$ = 17.28), Ce^{3+}, Co^{2+}, Zn^{2+}, Gd^{3+}, Pb^{2+}, Y^{3+}, Ni^{2+}, Cu^{2+} and Lu^{3+} were completely recovered as chelate anions.

It should be noted that the addition of 0.1 mM EDTA to the catholyte was sufficient for complete recovery. This is reasonable from the result of simulation that the concentration of free metal ions in the isotachophoretic zone is very small, as shown in Table 4.

Fig. 6 summarizes the recovery of the eighteen metal ions. The sample components were arranged in order of increasing stability constants. Weakly interacting ions of Na$^+$ to Ca^{2+} were always recovered as cations and the recovery was 100%. The others were detected as anions and the recovery was closely dependent on the EDTA concentration in the catholyte. A 100% recovery was obtained for the eighteen metal cations in the presence of an equimolar amount of EDTA.

It is interesting that the recovery was closely

tration was increased to 0.5 mM, a 50% recovery was obtained as MnY^{2-} and a small amount of CeY$^-$ was detected. However, La still could not be detected as the chelate.

In general, the recovery increased when the EDTA concentration was high, as is obvious for, e.g., MnY^{2-} and GdY$^-$ in Fig. 5. However, complete recovery could not be obtained, even when the EDTA concentration was increased to 1 mM. The addition of EDTA at ca. 1 mM was not useful, because non-complexing EDTA disturbed the migration of NiY^{2-}, CoY^{2-}, MnY^{2-} and ZnY^{2-} to form a mixed zone, and the zone length of non-complexing EDTA increased with increase in the EDTA concentration.
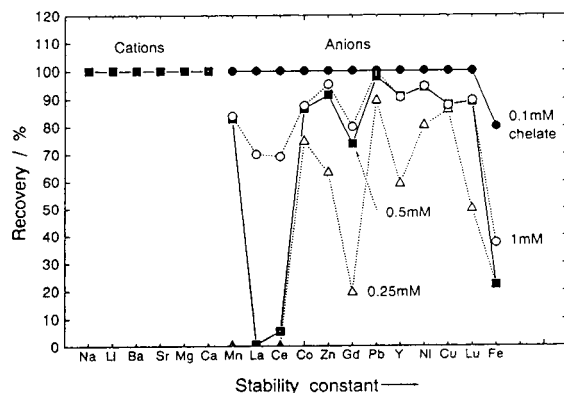

Fig. 6. Recovery of the eighteen metal cations. Operational electrolyte systems Nos. 4, 5, 6 and 7 in Table 1. Quantity of integrated charge = 1.1 C.

dependent on the migration order, confirming the previous study by Gebauer et al. [8]: when the effective mobilities of the chelates were greater than that of EDTA, such as PbY^{2-} in Fig. 3, the observed recovery was much better than the value estimated from the stability constants. Even when the chelate divalent anions have similar effective mobilities to the EDTA anion, the EDTA concentration co-existing with the chelate was high owing to mixed zone formation. Consequently, divalent chelates showed better recoveries than monovalent chelates.

In conclusion, metal cations can be analysed by bidirectional isotachophoresis using EDTA as a complex-forming agent. At pH_A 3.6, the weakly interacting alkali and alkaline earth metal ions were detected as cations and the other metal ions were detected as anions forming chelates. This separation system will be applied to trace element analyses of, e.g., biochemical materials.

Acknowledgement

References

[1] F.M. Everaerts, J.L. Beckers and Th.P.E.M. Verheggen, Isotachophoresis–Theory, Instrumentation and Applications, Elsevier, Amsterdam, 1976.
[2] P. Bocek, M. Deml, P. Gebauer and V. Dolnik, Analytical Isotchophoresis, VCH, Weinheim, 1988.
[3] W. Thormann, D. Arn and E. Schumacher, Electrophoresis 6 (1985) 10.
[4] T. Hirokawa, K. Watanabe, Y. Yokota and Y. Kiso, J. Chromatogr., 633 (1993) 251.
[5] T. Hirokawa, J. Chromatogr., 694 (1995) 355.
[6] T. Hirokawa, W. Xia, K. Nakamura, I. Tanaka, F. Nishiyama, Y. Kiso, B. Gas and J. Vacik, J. Chromatogr. A, 663 (1994) 245.
[7] H. Yoshida, I. Nukatsuka and S. Hikime, Bunseki Kagaku, 28 (1979) 382.
[8] P. Gebauer, P. Bocek, M. Deml and J. Janak, J. Chromatogr., 199 (1980) 81.
[9] L.G. Sillen and A.E. Martell (Editors), Stability Constants of Metal-Ion Complexes (Special Publication No. 17), Chemical Society, London, 1964.
[10] B. Gas, M. Demjanenko and J. Vacik, J. Chromatogr., 192 (1980) 253.
[11] T. Hirokawa, M. Nishino, N. Aoki, Y. Kiso, Y. Sawamoto, T. Yagi and J. Akiyama, J. Chromatogr., 271 (1983) D1.
[12] T. Hirokawa, J. Hu, K. Umeda, G. Kimura, H. Ikeda, F. Nishiyama and Y. Kiso, J. Chromatogr., 513 (1990) 297.
[13] T. Hirokawa, F. Nishiyama and Y. Kiso, Nucl. Instrum. Methods, B31 (1988) 525.
[14] T. Hirokawa and Y. Kiso, Anal. Sci., 8 (1992) 737.

Stability measurements of antisense oligonucleotides by capillary gel electrophoresis

Gerard J.M. Bruin[a,*], K. Olaf Börnsen[a], Dieter Hüsken[b], Ernst Gassmann[a], H. Michael Widmer[a], Aran Paulus[a]

[a]*Corporate Analytical Research, Ciba, CH-4002 Basel, Switzerland*
[b]*Central Research Laboratories, Ciba, CH-4002 Basel, Switzerland*

Abstract

The approach of using antisense oligonucleotides as potential drugs is based on hybridization of a short chemically-modified oligonucleotide with complementary cellular DNA or RNA sequences. A critical question is the stability of chemically modified antisense oligonucleotides in cellular environments. In a model system, resistance against various nucleases was evaluated by capillary gel electrophoresis (CGE). For some of the samples, matrix assisted laser desorption and ionization mass spectrometry (MALDI-MS) was used as an additional analytical tool to perform stability measurements.

Using CGE, the enzymatic degradation of single nucleotides from the oligomer can be followed after different incubation times. 10% T polyacrylamide gels give baseline resolution for oligonucleotides ranging between 5 and 30 bases in length. The kinetic influence of a specific nuclease concentration and the antisense oligonucleotide structure on the cleavage reaction are discussed. Also, a simple desalting method to improve the injection efficiency and sensitivity of the method are described. Examples of measurements of chemically modified antisense 19-mers are presented.

1. Introduction

Short segments of single-stranded oligonucleotides, complementary to a specific gene, have received attention as potential therapeutic agents in recent years [1,2]. The idea behind these antisense or anti-gene agents is that they inhibit a specific gene expression, either in the nucleus by binding to double-stranded DNA and pre-mRNA or in the cytoplasm by binding to mRNA. In this way the production of a specific, harmful protein can be prevented. The main problems associated with a therapeutic development are the delivery of the antisense agents to the cells, uptake across the membrane [3,4], and the in vivo stability against nucleases [5–7]. In order to overcome these stability and uptake problems, several DNA analogues with backbone, desoxyribose, and base modifications have been described. One of the earliest backbone modifications is in the phosphorothioates with the substitution of a sulfur atom for a non-bridging oxygen atom in the phosphodiester [8]. Later, the replacement of the complete deoxyribose-phosphate backbone by an amide functional group [9], which renders so-called peptide nucleic acids (PNA), and mixed phosphodiester–

---

* Corresponding author.

amid bonds [10] are described. In addition to the backbone modifications, several ribose modifications show improved stability under physiological conditions compared with the phosphodiester bond.

The intensive research in the field of antisense oligonucleotides nowadays asks for a fast, reliable, highly-efficient analytical technique in order to perform purity and stability checks of these type of synthesized compounds.

Capillary gel electrophoresis (CGE) has proven to be a suitable analytical method with high resolution for the separation of modified and unmodified oligonucleotides, as demonstrated by several authors [11-14]. Cohen et al. [11,12] indicated that HPLC separations were inferior with respect to resolution compared CGE separations for the analysis of phosphorothioates and phosphodiesters.

Rose [13] studied the binding of peptide nucleic acids to their complementary oligonucleotide with CGE. He showed that CGE was useful in resolving the free and bound species which in turn also allowed the calculation of binding kinetics and the stoichiometry of binding.

The influence of gel concentration, pH and buffer additives, was proven to be critical in obtaining high resolution and gel-to-gel reproducibility for the analysis of phosphorothioates as investigated by DeDeionisio [14].

This paper describes the use of CGE for the stability measurements of antisense oligonucleotides. The influence of various endo- and exonucleases on the stability of unmodified and modified oligonucleotides will be discussed. In order to get a better insight on the cleavage reactions, some of the samples were also analyzed at various incubation times with matrix assisted laser desorption and ionization mass spectrometry (MALDI-MS). This technique allowed identification by molecular mass of the degradants formed.

The ultimate goal of analysing cell extracts was checked by injecting samples with high salt concentrations. It is well known in CGE (and in CE in general) that electrokinetic injection of samples with high conductivity results in a decreased amount of sample. This problem can be partly circumvented by a simple and rapid desalting procedure.

2. Experimental

2.1. Instrumentation

Capillary gel electrophoresis was carried out on a Hewlett-Packard [3D]Capillary Electrophoresis system (Waldbronn, Germany) using polyacrylamide gel-filled capillaries (10% T, 0% C), which were prepared in house according to a previously published method [15]. Data acquisition and data analysis were done with HP [3D]CE analysis software.

The separations were performed in 75 μm I.D. capillaries with 32 cm total length (24 cm effective length), using a separation voltage of -10 kV. The capillary was thermostated at 30.0°C and the sample tray at 24°C. The background electrolyte consisted of 100 mM Tris and 100 mM boric acid at pH 8.4. These conditions resulted in currents between 3 and 4 μA. Injection was done electrokinetically at the cathodic site at 5 kV for 5 s.

Micellar electrokinetic capillary chromatography (MEKC) separations were carried out using a Prince (Lauerlabs, Emmen, Netherlands) capillary electrophoresis system.

MALDI-MS measurements were recorded on a LDI-1700 instrument from Linear Scientific (Reno, NV, USA). The linear time-of-flight mass spectrometer was calibrated with a peptide standard mixture for conversion from flight times to molecular masses. All measurements were carried out in the negative ion mode, using dihydroxyacetophenone – diammoniumhydrogencitrate as a matrix [16].

2.2. Chemicals

p(dT)$_{20}$ and Orange G, which was used as an internal standard in some of the experiments, were obtained from Sigma (St. Louis, MO, USA). The other modified and unmodified oligonucleotides were synthesized in the Central Re-

search Laboratories of Ciba-Geigy or at ISIS (Carlsbad, CA, USA). The phosphodiesterase from *Crotalus durissus* (snake venom nuclease) and the endo/exonuclease Nuclease S1 were purchased from Boehringer (Mannheim, Germany).

Tris(hydroxymethyl)aminomethane (Tris), boric acid, sodium dodecysulfate (SDS), sodium dihydrogenphosphate, dihydroxyacetopheonone and diammonium hydrogencitrate were of analytical grade and obtained from Fluka (Buchs, Switzerland).

2.3. Methods

The general procedure for stability measurements of oligonucleotides involved mixing a small volume of an oligonucleotide solution (dissolved either in water or in buffer), typically between 10 and 20 μl, with 1 to 5 μl of a nuclease solution. Injections into the gel-filled capillary were performed directly from the incubation vial at regular time intervals.

For the MALDI-MS measurements 1.4 μl incubation solution (with the same composition as for the CGE measurements) was mixed with 1.4 μl matrix solution (a mixture of 10 mM 2,6-dihydroxyacetophenone and diammonium hydrogencitrate in acetonitrile). From this, 0.4 μl was placed onto the probe tip and rapidly dried with vacuum to avoid separation during the crystallization process. The complete sample preparation was typical and is described elsewhere [16].

The following procedure, called drop dialysis, was used for desalting samples of interest. About 10 μl reaction mixture were pipetted on a small Millipore filter with a pore size of 0.025 μm, which was placed on top of a water surface. The sample was desalted after approximately 30 min. The desalted aliquot was then put in a sample vial and injection was performed in the usual way.

3. Results and discussion

The mass-to-charge ratio of oligonucleotides decreases rapidly from 2 to 5 nucleotides and reaches a plateau above 10 nucleotides. It implies that separations based on a difference in charge can be carried out in free solution without a problem in case of oligonucleotides smaller than 10 bases in length. However, the electrophoretic mobility in free solution is almost constant for oligonucleotides with more than 10 bases. In the size range between ten and thirty bases, the sieving effect of gels becomes mandatory. This can be seen in Fig. 1A and B. Whereas in the electropherogram in Fig. 1A where the $p(dT)_{2-11}$ mixture is baseline resolved, the resolution for the $p(dA)_{12-18}$ mixture decreased considerably. In both examples SDS was used in order to improve resolution. The addition of Mg(II) or Zn(II) in millimolar concentrations to the background electrolyte, as suggested by Cohen et al. [17], resulted only in small improvements of the $p(dA)_{12-18}$ separation.

These results clearly demonstrate that the use of sieving gels (or suitable polymer solutions [18]) is necessary in order to separate on the basis of a difference in size, rather than on a difference in charge.

3.1. Incubation of $p(dT)_{20}$ with snake venom nuclease

A simple model system has been chosen to develop and evaluate a CGE protocol to study precise kinetics of the degradation of a specific oligonucleotide in various media. It consisted of phosphodiester $p(dT)_{20}$ as model compound which reacts with snake venom nuclease. $p(dT)_{20}$ was chosen for its commercial availability in a pure form and its well-defined reaction products [only $p(dT)s$, smaller than 20 bases in length], which can be baseline resolved with CGE. The exonuclease attacks exclusively at the 3′-end of an oligonucleotide. Immediately after vortex mixing the $p(dT)_{20}$ solution, dissolved in buffer and the snake venom nuclease solution, the first injection was performed. Consecutive injections were done automatically at regular time intervals. The $p(dT)_{20}$ concentration was $4 \cdot 10^{-3}$ μg/μl in 40 mM Tris–HCl, 4 mM MgCl$_2$, pH 9.0 buffer. A total reaction volume of about 20 μl was used.
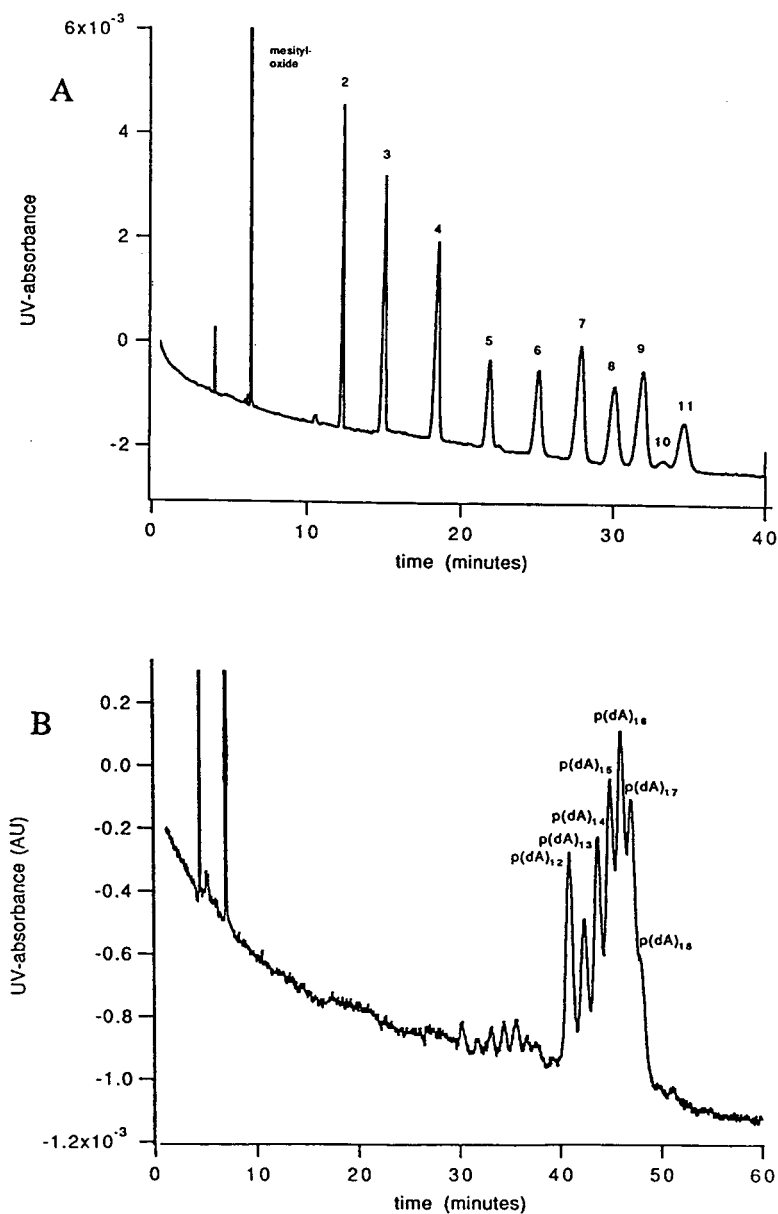
Fig. 1. Electropherograms of small desoxynucleotides in the free solution mode. (A) Separation of oligothymidylic acids $p(dT)_{2-11}$. Background electrolyte: 5 mM Tris, 5 mM NaH$_2$PO$_4$, 50 mM SDS, pH 7.0; Capillary, 55.7 cm × 50 μm I.D., effective length 44.7 cm; $V = 20$ kV, $I = 52$ μA; detection wavelength 260 nm; $T = 22°C$; injection, 15 mbar, 3 s. Numbers indicate the number of bases. (B) Separation of polydeoxyadenylic acids $p(dA)_{12-18}$. Experimental conditions as in (A).

Fig. 2 shows typical electropherograms obtained during the degradation. It can be seen that going from Fig. 2A to C the reaction rate decreases due to the lower exonuclease concentration. In Fig. 2A, where the nuclease concentration is 4 ng/μl, the reaction was nearly
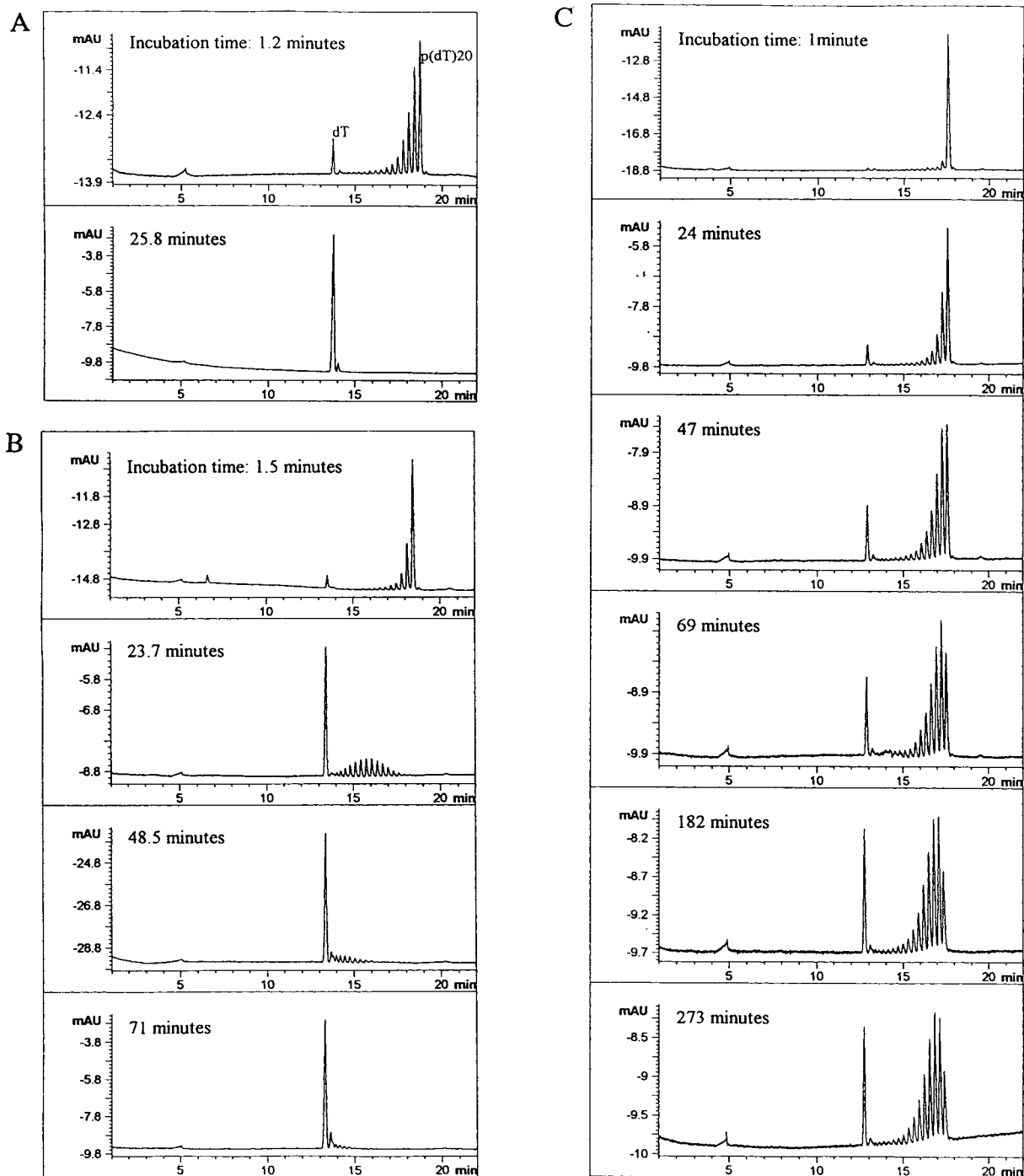
Fig. 2. Separation of p(dT)$_{20}$ and its degradants after incubation with snake venom nuclease. The electropherograms were obtained after injection at the indicated incubation times. Separation conditions: $V = -10$ kV, $I = 3-4$ μA; background electrolyte, 100 mM Tris, 100 mM boric acid, pH 8.5; capillary, 32 cm $\times$ 75 μm I.D., effective length, 24 cm; injection, -5 kV, 5 s. For incubation conditions, see text. Snake venom nuclease concentrations: (A) 4.0 ng/μl, (B) 0.95 ng/μl, (C) 0.22 ng/μl.

completed after 25.8 min incubation. At a concentration of approximately four times less snake venom nuclease, the reaction proceeds at a lower rate, as shown in Fig. 2B. In this case the reaction comes to completion after 71 min. In electropherograms A and B resulting from 1.2 and 1.5 min incubation time in A and B, respectively, baseline resolution between the $p(dT)_{20}$ peak and its degradants $p(dT)_{19}$, $p(dT)_{18}$, etc. can be observed. The increasing peak at 13.5 min is the single nucleotide $p(dT)$. When $p(dT)$s with 2 to 5 bases are also present (at very low concentrations), these fragments coelute, as seen by the somewhat broader peak around 13.7 min.

At a nuclease concentration of 0.22 ng/μl the reaction rates are again slower. The reaction even stops after approximately two hours and no further change in the relative peak areas is observed, as seen in Fig. 2C.

Table 1 summarizes the relative standard deviations of the migration times and relative migration times, $t_r = t_{m,p(dT)n}/t_{m,p(dT)}$, for $p(dT)_{20}$ and some of its degradants. With RSD values between 0.3 and 0.5% an excellent reproducibility is observed. This is further improved by calculating relative migration times, using t_m of $p(dT)$ as internal standard. However, it must be noted that this can only be achieved when the gel-filled capillary does not show bubble formation. In our experience, the gels could withstand between 30 and 50 injections without deteriorating in performance and/or in reproducibility. In our separation system, an indication for bubble formation at the injection side was a current below 3 μA, which could be confirmed under a microscope with 80 × magnification. The de-

creasing currents were accompanied by shifts in migration times and a drop in theoretical plates from ca. 200 000 to below 100 000. The possible problem with regard to identification of the oligonucleotide of interest and its degradants can be easily circumvented by using relative migration times.

The extinction coefficient ϵ of an oligonucleotide increases strongly with its size. For example, the ϵ values for the monomer $p(dT)$ and the 20-mer are $8.70 \cdot 10^3$ and $1.706 \cdot 10^5$ l·mol^{-1}·cm^{-1}, respectively. ϵ values can be calculated according to a method described by Puglisi and Tinoco [19]. An Excel program was used for this purpose in our lab [20]. The relative concentrations of $p(dT)_{20}$ and the degradants were calculated using computed extinction coefficients from the peak areas in the electropherograms as shown in Fig. 2. In Fig. 3, the relative concentrations of $p(dT)$ and $p(dT)_{20}$ are plotted versus the incubation times at various nuclease concentrations.

In the reaction described above, which can be expressed as

$$p(dT)_{20} \xrightarrow{k_1} p(dT)_{19} \xrightarrow{k_2} p(dT)_{18} \xrightarrow{k_3} \ldots \rightarrow dT$$
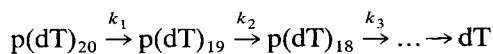
the exponential decay of $p(dT)_{20}$ is given by

$$[p(dT)_{20}] = [p(dT)_{20}]_0 \cdot e^{-k_1 t}$$

where $[p(dT)_{20}]_0$ is the initial concentration and

Table 1
Average migration times and relative standard deviations (RSD), in migration times and relative migration times of four degradation products of $p(dT)_{20}$

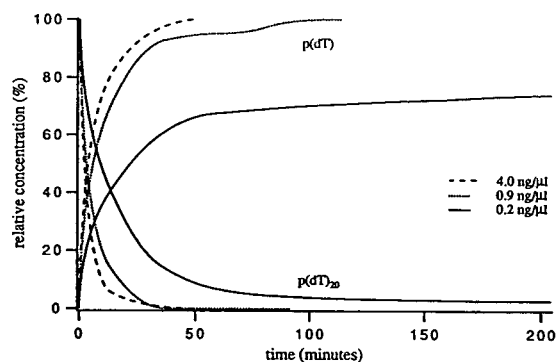|	t_m (min)	RSD, t_m	RSD, t_r
dT	12.80	0.4	–
$p(dT)_{10}$	14.43	0.3	0.19
$p(dT)_{15}$	15.95	0.4	0.15
$p(dT)_{18}$	16.85	0.4	0.11
$p(dT)_{20}$	17.44	0.5	0.17

Fig. 3. Kinetic curves on incubation at three different snake venom nuclease concentrations. For incubation conditions, see text. Relative concentrations of $p(dT)_{20}$ and dT vs. time of incubation.

k_1 is the reaction constant of the first step. The subsequent increase and decrease in concentration of $p(dT)_{19}$ is given by

$$[p(dT)_{19}] = \frac{[p(dT)_{20}]k_1}{(k_2 - k_1)}(e^{-k_1 t} - e^{-k_2 t})$$

For smaller degradants similar equations can be derived.

The half-life time of each species $t_{1/2} = \ln 2/k_n$ can be derived from the computed rate constants.

Under these incubation conditions, $T = 24°C$, 40 mM Tris–HCl, pH 9.0, and the given concentrations of the reactants, the half-life times of $p(dT)_{20}$ were 2.1, 3.3 and 9.3 min, going from 0.4, to 0.95, to 0.22 ng/μl, respectively. It must be emphasized here that the half-life times have a strong dependence on the incubation conditions, such as the pH, type of media, the presence of Mg^{2+} ions, the temperature and the concentration of the reactants. For instance, addition of Mg^{2+} ions at physiological levels more than doubles the rate of degradation [20]. The degradation patterns found are fully in accordance with a 3'-end exonuclease activity and resemble results obtained from HPLC analysis of heterogeneous oligonucleotides as measured by Bacon et al. [6] and Vichier-Geurre et al. [21].

The high ionic strength of the sample solution resulting from buffer ions in the incubation vial largely reduces the amount of sample injected onto the gel-filled capillary. This is a well known phenomenon in CGE [22]. In Fig. 2, the drift and noise in the baseline are much more pronounced than in the case where an injection was made from a salt-free incubation vial (results not shown). In order to get rid of the buffer, and eventually other salts, a desalting step has to be used. This desalting step is strongly recommended for measurements in cell extracts where one has to deal with even higher salt concentrations, typically in the order of 100 mM. The effectiveness of the simple desalting step (see Experimental) is illustrated in Fig. 4A and B. In Fig. 4A, the reaction product p(dT) (from Fig. 2B, last electropherogram) was treated after a

few hours according to the above described procedure and the sample was reinjected. A strong increase in peak area can be observed in Fig. 4B. [Before and during the desalting procedure, the small peaks in the upper electropherogram representing $p(dT)_{2-10}$, reacted all to p(dT).] The gain in peak area for the oligonucleotides between 15 and 20 bases in length is around a factor of 45 (see Fig. 5). Going to smaller fragment sizes the gain decreases because the smaller fragments are partly lost through the pores of the filter. However, even for the monomers a gain in peak area between 6 and 8 could be easily obtained.

Comparable information on degradation kinetics can be obtained with MALDI-MS. It has been shown to be a sensitive method with extremely high resolution for the analysis of both chemically modified and unmodified oligonucleotides [16,23]. MALDI-MS has the advantage that it also renders molecular masses of degradants. However, it is more complicated to perform the experiments with MALDI than in an automated CE fashion as described above, since mixing of the matrix and the sample (ca. 1.4 μl) from the incubation vial is essential before the sample is introduced into the vacuum system of the MALDI-time-of-flight mass spectrometer.

Some mass spectra of $p(dT)_{20}$ at different incubation times are depicted in Fig. 6. The difference between the peaks equals m/z 304, corresponding to the cleavage of p(dT) units from the p(dT)s. Also, peaks for doubly charged species, $(M - H)^{2-}$, and dimers, $(2M - H)^-$, are visible in the mass spectra.

3.2. Incubation of heterogeneous oligonucleotides with snake venom nuclease

With heterogeneous oligonucleotides the electropherograms show more irregular patterns, because both the electrophoretic mobility and thus the resolution and the peak height not only depend on the size of the oligonucleotide, but also on the base sequence [24,25]. This is illustrated in Fig. 7, where a 19-mer 5'-TTC TCG CTG GTG AGT TTC A-3' was mixed with snake venom nuclease in 40 mM Tris–HCl, 4
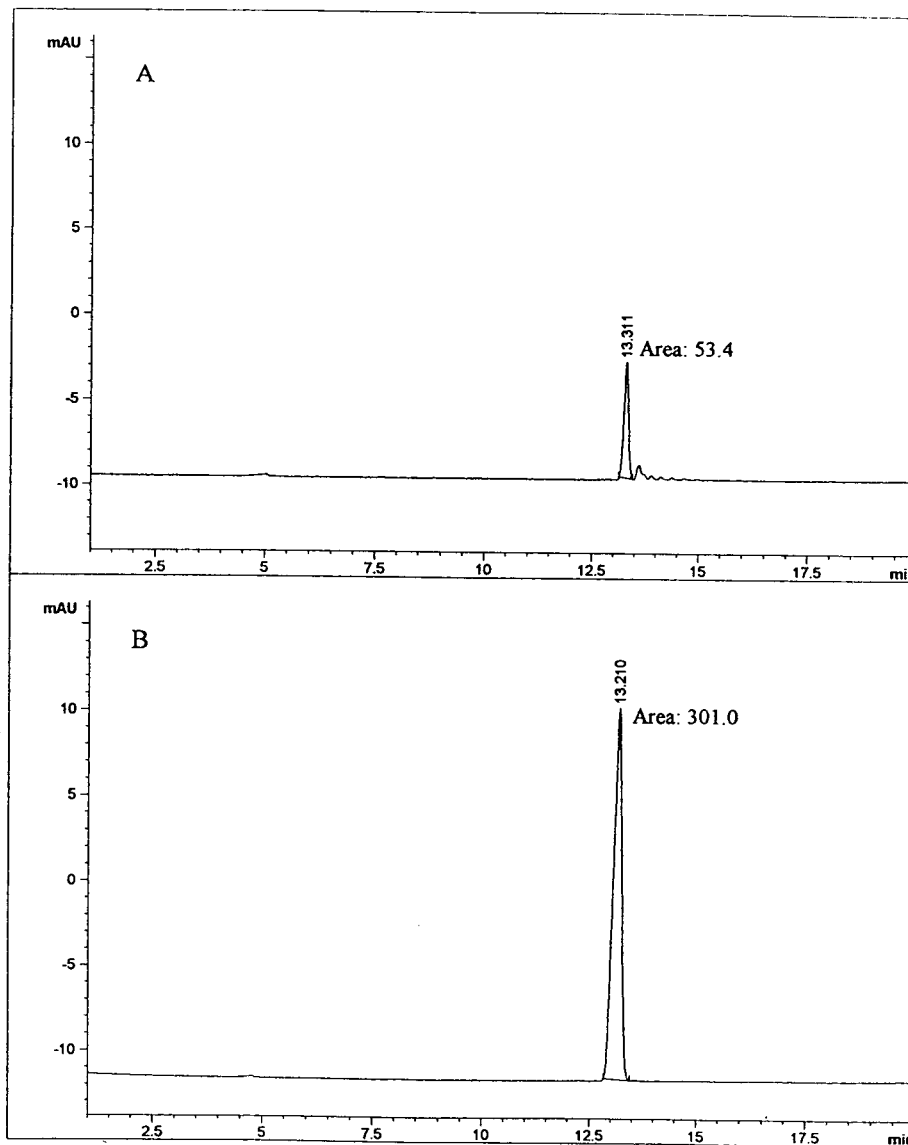
Fig. 4. The influence of sample ionic strength on amount of oligonucleotides injected. (A) Reaction product p(dT), dissolved in incubation buffer 40 mM Tris–HCl, 4 mM MgCl$_2$, pH 9.0, (B) Same sample after desalting.

mM MgCl$_2$, pH 9. The results from this 19-mer, a natural phosphodiester, are shown here and represent a 'reference' oligonucleotide for further experiments with chemically modified antisense oligonucleotides (see below); it consists of the same base sequence and length as the modified ones.

The small peak, migrating before the four monomers, and marked with an asterisk, is the internal standard Orange G. The concentrations in the incubation vial were 0.005 μg/μl for the 19-mer and 4 ng/μl for the snake venom nuclease. In the fourth electropherogram (after 181 min incubation) one can observe the formation of a more or less stable intermediate. This intermediate is still present at much higher
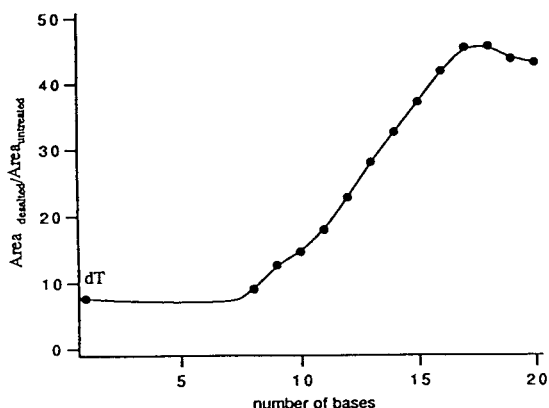
Fig. 5. The gain in peak area after the desalting step. The ratio of the peak areas of the oligothymidylic acids mixture before and after the desalting is plotted vs. the number of bases.
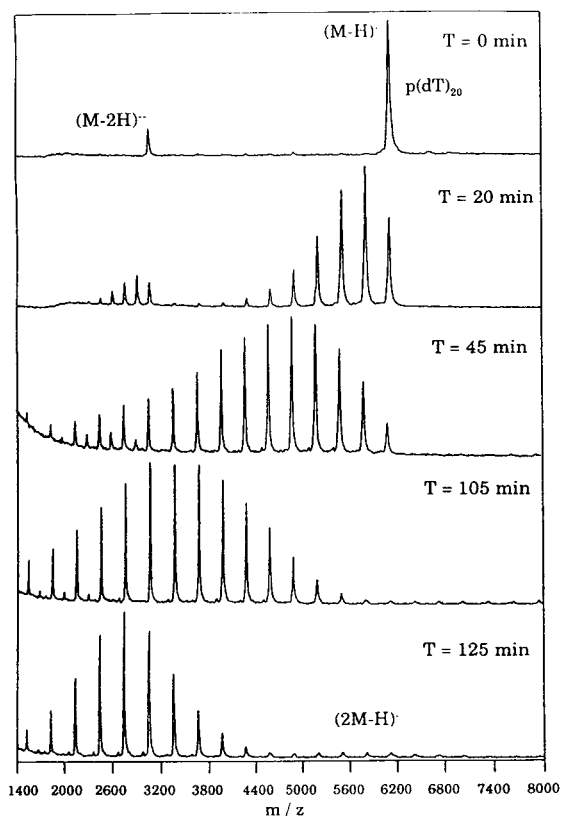
Fig. 6. MALDI-MS spectra of $p(dT)_{20}$ after incubation times with snake venom nuclease, using 2,6-dihydroxy-acetophenon–diammonium hydrogencitrate as the matrix. For incubation conditions, see text.

concentrations than its parent compound and other degradation products. Probably, the presence of a certain base composition at the 3'-terminal residue shows a strong resistance to 3'-exonuclease attack resulting in slow degradation behavior. In the last electropherogram, resulting from 8.5 h incubation, the four remaining reaction products, p(dC), p(dT), p(dG) and p(dA) can be distinguished.

As already mentioned for the degradation of $p(dT)_{20}$ these cleavage reactions can also be followed in time with MALDI-MS. An example of a mass spectrum of a 25-mer 5'-TCA CAG CCT CCA CAC AGA GCC CAT C-3' after 80 min incubation with snake venom nuclease is shown in Fig. 8A. An advantage of MALDI-MS is that it also delivers molecular masses of the reaction products and thus gives more detailed information on reaction products than CE. The differences in m/z values between the main peaks correspond to the loss of one nucleotide subunit structure every time. The masses of pdC, pdT, pdA and pdG subunits are 289.2, 304.2, 313.2 and 329.2, respectively. The achieved mass resolution and molecular mass determination with MALDI-MS allow determination of the sequence of an oligonucleotide as can be seen in Fig. 8A. It must be noted here, that this mass spectrum was recorded without any further sample pretreatment. By desalting and by using an ammonium buffer, the quality and sensitivity can be easily improved [16]. With MALDI-MS, it should also be possible to clarify more complicated reaction schemes, e.g., reactions with nuclease S1 which acts both endo- and exonucleatically.

The physical behavior of digested oligonucleotides does not significantly differ in a time-of-flight mass spectrometer. However, the resolution and detection sensitivity decrease with increasing mass. Also, larger molecules need a higher laser intensity than small molecules. Therefore, quantitative information can be obtained only in a small mass range. Over broader mass ranges, peak intensities cannot be directly compared.

To compare MALDI-MS and CGE, the electropherogram of this oligonucleotide after 77
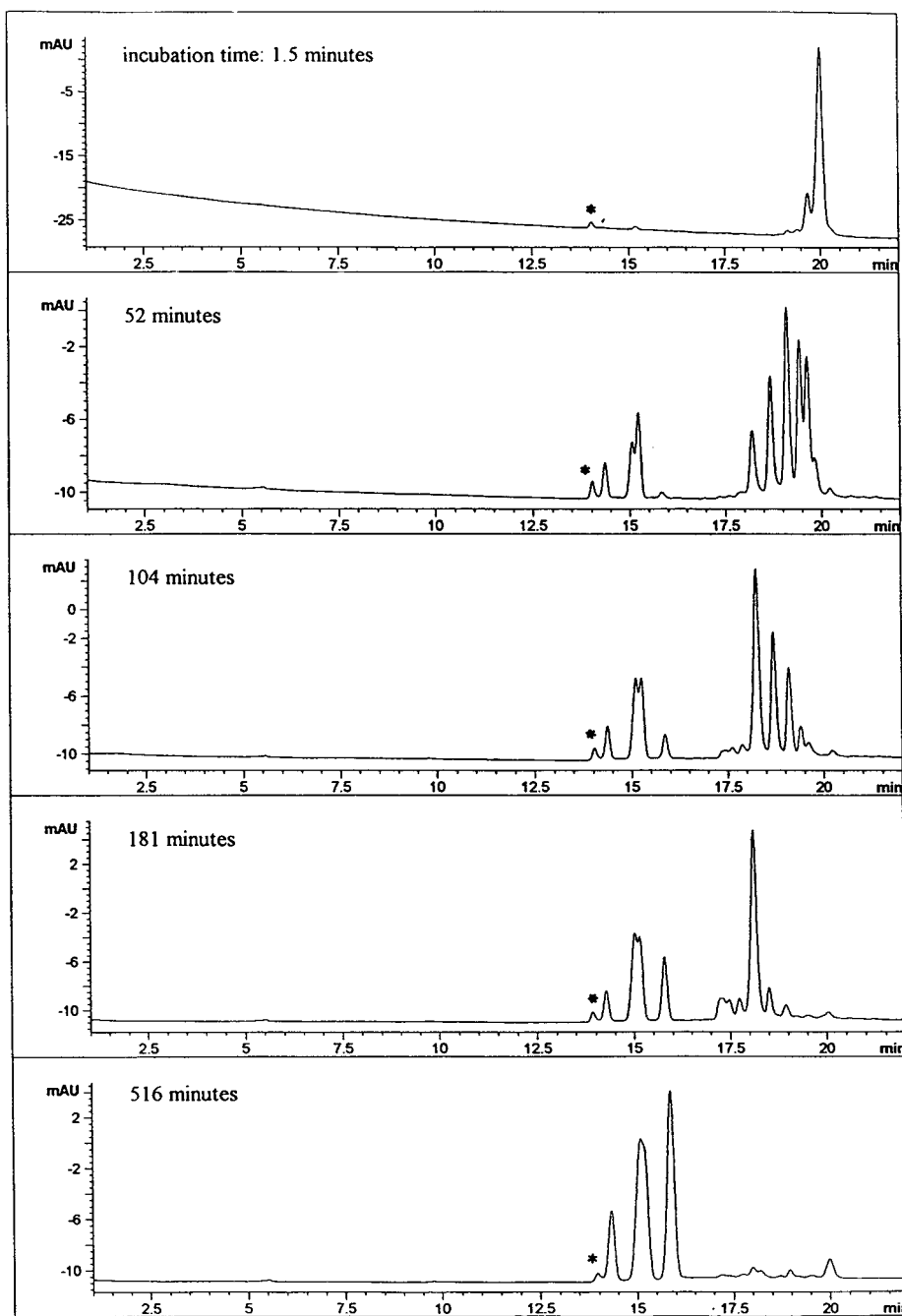
Fig. 7. Electropherograms of the degradation of a 19-mer 5'-TTC TCG CTG GTG AGT TTC A-3' with snake venom nuclease at increasing incubation times. Experimental conditions as in Fig. 2. The Orange G peak is marked with an asterisk.
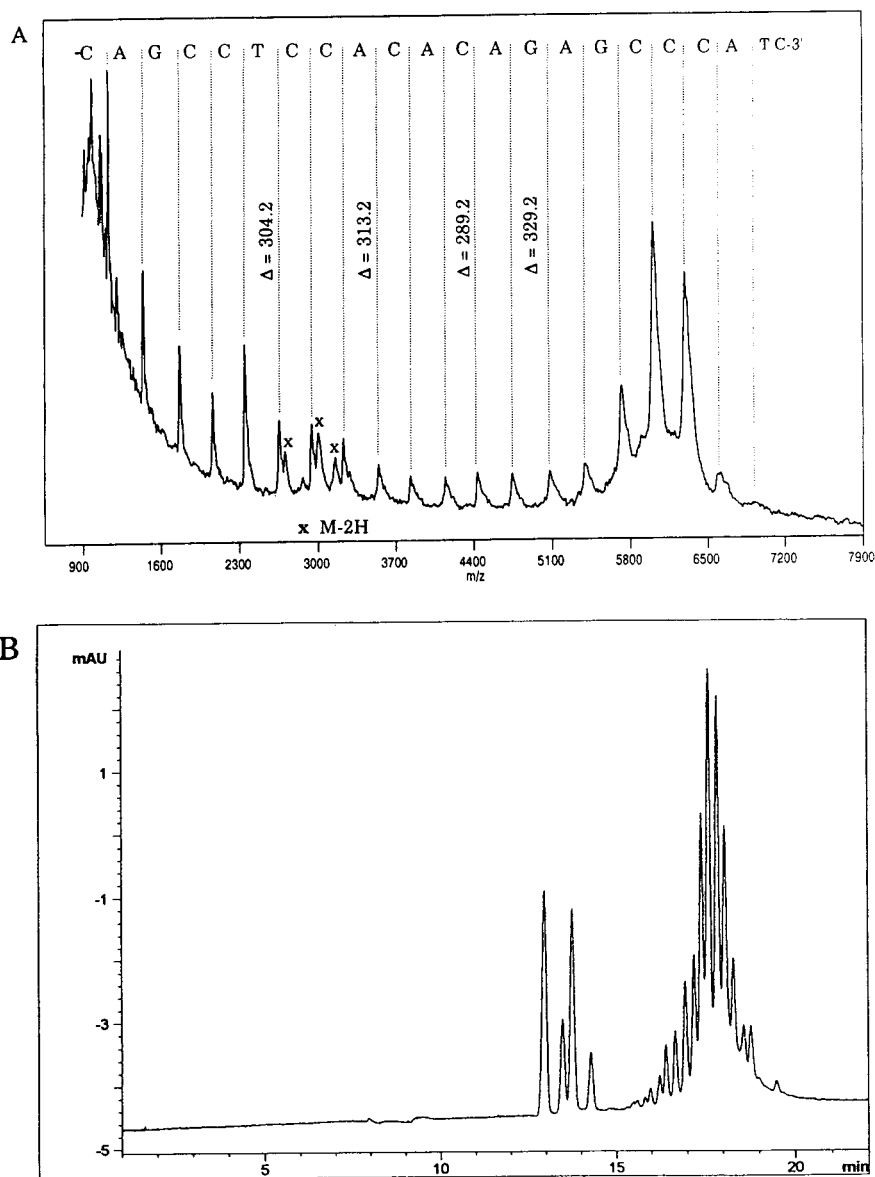
Fig. 8. (A) MALDI-MS spectrum of a 25-mer 5'-TCA CAG CCT CCA CAC AGA GCC CAT C-3' after 80 min incubation with snake venom nuclease. The peaks marked with × are doubly charged fragments. (B) Electropherogram of the 25-mer after 77 min incubation. Experimental conditions as in Fig. 2.

min incubation is depicted in Fig. 8B. Whereas with MALDI-MS a better resolution between the peaks can be obtained, the electropherograms also deliver information about the relative concentrations of the formed monomers. Also, the quantitative interpretation of the data is more straightforward and more reliable than for MALDI-MS.

3.3. Incubation of a heterogeneous 25-mer with nuclease S1

The electropherograms look completely different when nuclease S1 instead of snake venom nuclease is used. Nuclease S1 hydrolyzes single-stranded nucleic acids endo- and exonnucleati-

cally. In the electropherograms in Fig. 9, the reaction mixture consisted of 5.10^{-3} $\mu g/\mu l$ 25-mer 5'-AGT GTC GGA GGT GTG TCT CGG GTA G-3' (complementary to the string from Fig. 8) and 3.6 U/μl Nuclease S1 dissolved in water. The total reaction volume was not more than 11 μl. Only in the first two electrophero-
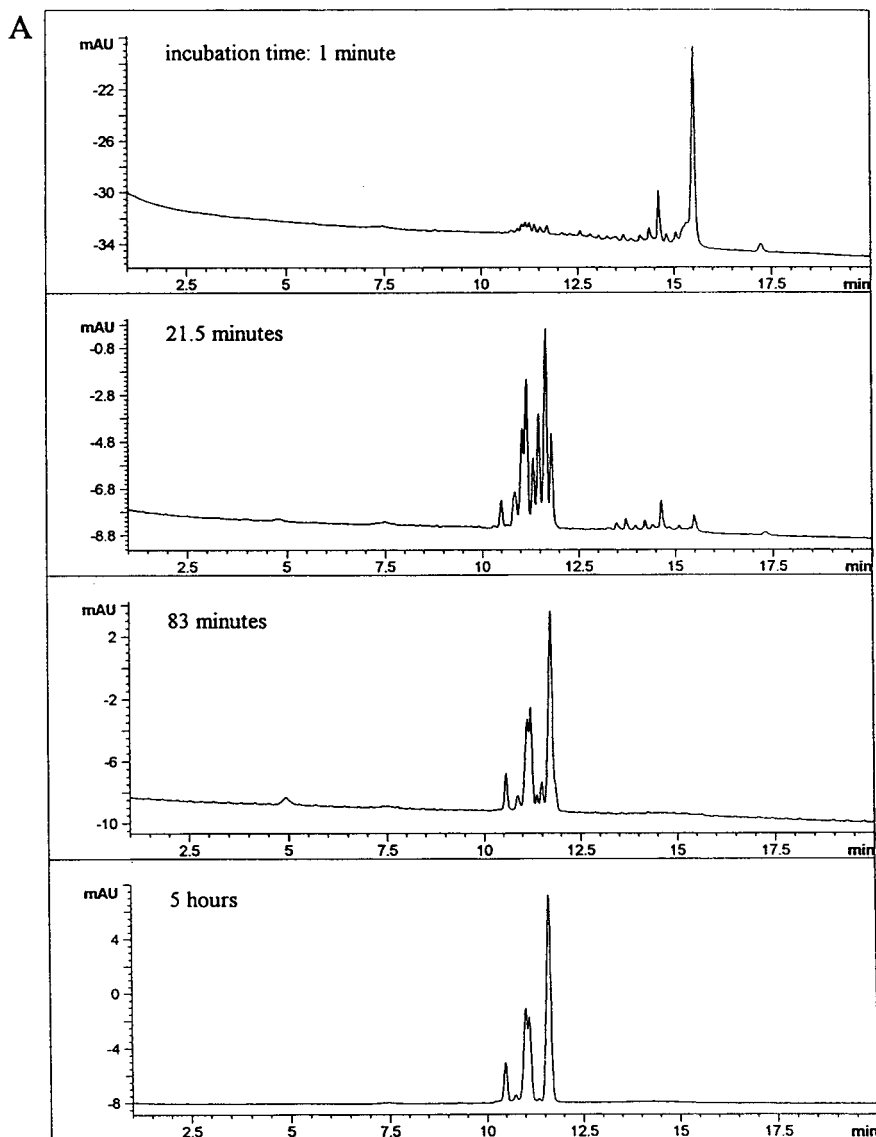
Fig. 9. Electropherograms of 0.005 $\mu g/\mu l$ 25-mer 5'-AGT GTC GGA GGT GTG TCT CGG GTA G-3' after incubation with Nuclease S1. Incubation in water, 3.63 $\mu g/\mu l$ Nuclease S1, reaction volume 11 μl.

grams larger fragments can be observed. Already in an early stage of the degradation process the appearance of small fragments, such as the monomers and dimers, is visible. The last electropherogram shows a comparable peak distribution for the four monomers as in the case of incubation with snake venom nuclease.

3.4. Analysis of modified antisense oligonucleotides

As shown in the electropherograms above, oligonucleotides possessing the natural structure are hardly suitable for therapeutic development, because of quick degradation by various nu-
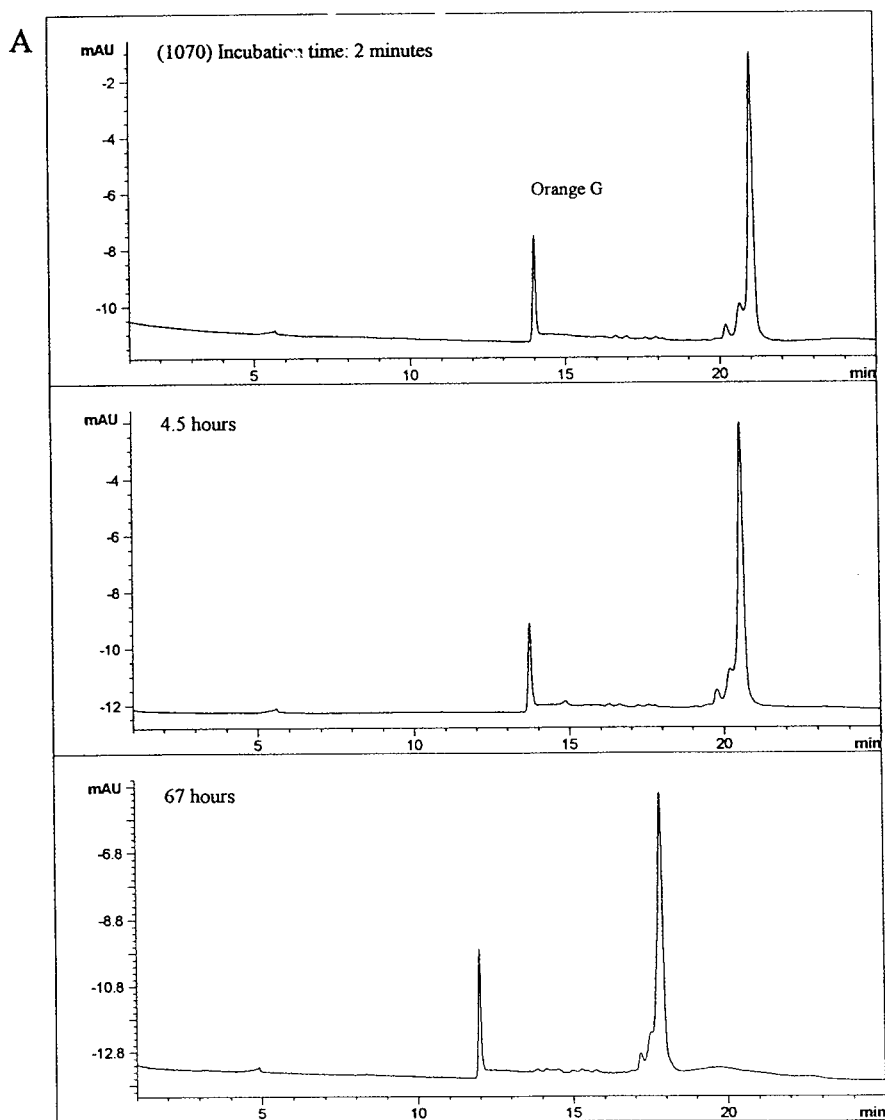
Fig. 10 (*continued on p. 194*).
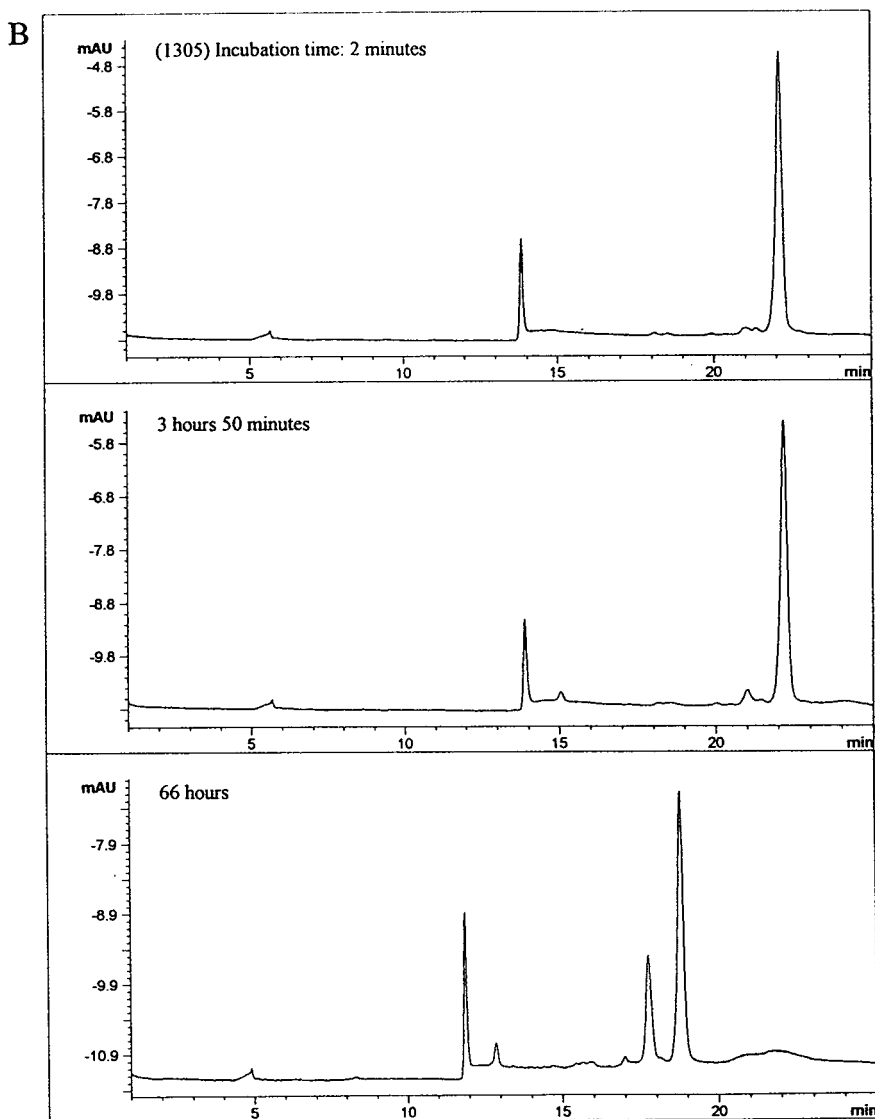
Fig. 10. (A,B) Electropherograms of two chemically modified antisense oligonucleotides after various incubation times. Incubation with snake venom nuclease. Experimental conditions as in Fig. 2.

cleases present in cell extracts. Numeral structural modifications have been proposed and synthesized to improve the resistance to nuclease degradation. Some examples of electropherograms of modified oligonucleotides, resulting from a comparative study, are given here in order to show the difference in stability from the natural phosphodiester. The sequence in these

examples is the same as in Fig. 7. The difference consists of modifications in the base structures and the substitution of non-bridging oxygen by sulfur at various, defined positions in the backbone of the 19-mer. During the stability measurements of a series of modified oligonucleotides, which could be easily done in overnight runs, the unmodified phosphodiester was mea-

sured as well in order to verify reproducible
half-life times with different nuclease and buffer
solutions and capillaries, etc., and test the day-
to-day reproducibility. The electropherograms
are depicted in Fig. 10A and B. As shown, the
oligonucleotide in Fig. 10A was much more
stable than the natural phosphodiester. Whereas
the half-life time of the unmodified oligonucleo-
tide was only three minutes, the modified one
given in Fig. 10A does not show any sign of
degradation with snake venom nuclease after 67
h incubation. The antisense oligonucleotide in
Fig. 10B develops one clearly distinguishable
degradant. Also, the formation of one nucleotide
migrating after the Orange G peak can be
observed in time. The shift in migration time to
lower values in both examples (from the second
to the third electropherogram) is caused by the
somewhat shorter capillary, which was installed
in between those runs.

4. Conclusions

This study has shown that stability measure-
ments of antisense oligonucleotides can be per-
formed with CGE and MALDI-MS. Both meth-
ods have their own advantages and the type of
information is complementary. Excellent repro-
ducibility of migration times can be obtained
with CGE, when care has been taken for a
reproducible production of the gel-filled capil-
laries. In combination with the desalting method
as described above, it is expected that the
analysis of antisense oligonucleotides in cell
extracts will be possible. This is currently under
investigation in our laboratory.

Acknowledgement

References

[1] J. Cohen, in J. Cohen (Editor), Oligodeoxynucleotides, Antisense Inhibitors of Gene Expression, Macmillan Press, New York, 1989, pp. 1–6.
[2] C.A. Stein and Y.-C. Cheng, Science, 261 (1993) 1004.
[3] J.M. Dagle, D.L. Weeks and J.A. Walder, Antisense Res. Develop., 1 (1991) 11.
[4] C. Boiziau and J.J. Toulmé, Biochimie, 73 (991) 1403.
[5] A. Pompon, I. Lefebvre, J.-L. Imbach, Biochem. Pharmacol., 43 (1992) 1769.
[6] T.A. Bacon, F. Mowan, B. Rayner, J.-L. Imbach and E. Wickstrom, J. Biochem. Biophys. Methods, 16 (1988) 311.
[7] B.S. Sproat, A.I. Lamond, B. Beijer, P. Neumer and U. Ryder, Nucleic Acids Res., 17 (1989) 3373.
[8] W.S. Marshall and M.H. Caruthers, Science, 259 (1993) 1564.
[9] P. Wittung, P.E. Nielsen, O. Buchardt, M. Egholm and B. Nordén, Nature, 368 (1994) 561.
[10] A. Demesmaeker, J. Lebreton, A. Waldner and V. Fritsch, Bioorg. Medic. Chem. Lett., 4 (1994) 873.
[11] A.S. Cohen, M. Vilenchik, J.L. Dudley, M.W. Gemborys and A.J. Bourque, J. Chromatogr., 638 (1993) 293.
[12] M. Vilenchik, A. Belenky and A.S. Cohen, J. Chromatogr. A, 663 (1994) 105.
[13] D.J. Rose, Anal. Chem., 65 (1993) 3545.
[14] L. DeDionisio, J. Chromatogr. A, 652 (1993) 101.
[15] A. Paulus, E. Gassmann and M.J. Field, Electrophoresis, 11 (1990) 702.
[16] U. Pieles, W. Zürcher, M. Schär and H. Moser, Nucleic Acids Res., 21 (1993) 3191.
[17] A.S. Cohen, S. Terabe, J.A. Smith and B.L Karger, Anal. Chem., 59 (1987) 1021.
[18] A.E. Barron, H.W. Blanch and D.S. Soane, Electrophoresis, 15 (1994) 597.
[19] J.D. Puglisi and I. Tinoco, in J.E. Dahlberg and J.N. Abelson (Editors), Methods in Enzymology, Volume 180, Academic Press, 1989, p. 304.
[20] L. Cummins, personal communication.
[21] S. Vichier-Guerre, A. Pompon, I. Lefebvre and J.-L. Imbach, Antisense Res. Develop., 41 (1994) 9.
[22] D. Demorest and R. Dubrow, J. Chromatogr., 559 (1991) 43.
[23] B.H. Wang and K. Biemann, Anal. Chem., 66 (1994) 1918.
[24] T. Satow, T. Akiyama, A. Machida, Y. Utagawa and H. Kobayashi, J. Chromatogr. A, 652 (1993) 23.
[25] A. Guttman, A.S. Cohen and N. Cooke, J. Chromatogr., 593 (1992) 297.

Determination of coumarins from *Chrysanthemum segetum* L. by capillary electrophoresis

Renata J. Ochocka, Danuta Rajzer, Piotr Kowalski, Henryk Lamparczyk*

Medical Academy, Faculty of Pharmacy, Gen. J. Hallera 107, PL-80416 Gdańsk, Poland

Abstract

The separation of seven closely related coumarins, i.e., herniarin, coumarin, umbelliferone, aesculetin, dihydrocoumarin, coumarinic acid and 4-hydroxycoumarin, by capillary electrophoresis was studied using different buffer systems. The best conditions chosen were applied for the determination of coumarins in extracts from roots and aerial parts from the plant *Chrysanthemum segetum*.

1. Introduction

The chemical composition of *Chrysanthemum* species is not yet fully elucidated. It was reported that these species contain sesquiterpene lactones [1], flavonoids [2] and coumarins [3]. Coumarins, which are derivatives of benzopyran, are widely distributed in plants and essential oils. They are used as fragrance components in perfumes, toothpastes and tobacco products [4]. Moreover, coumarins are pharmacologically active and have been used in the treatment of a diverse range of diseases, such as brucellosis, burns, rheumatic disease and even cancer [5,6].

A number of techniques have been applied to the determination of coumarins. Most of the previous papers have described results of semiquantitative TLC determinations [3,7–9], but gas chromatography [10], high-performance liquid chromatography [6,9,11] and centrifugal partition chromatography [12] have also been

applied for the separation and determination of coumarins in various natural products.

The great diversity of coumarin structures and their wide range of polarities present special problems for their simultaneous determination. This work represents an attempt to determine coumarins using a modern and fully quantitative capillary electrophoresis (CE) method. The structural formulae of the coumarins under investigation are presented in Fig. 1.

2. Experimental

2.1. Chemicals

Herniarin (7-methoxycoumarin), coumarin, 4-hydroxycoumarin and dihydrocoumarin were obtained from Aldrich-Europe and umbelliferone (7-hydroxycoumarin), aesculetin (6,7-dihydroxycoumarin) and coumarinic acid were purchased from Merck (Darmstadt, Germany).

Methanol, chloroform, lead acetate, boric acid and borax (POCh, Gliwice, Poland) were of

---

* Corresponding author.
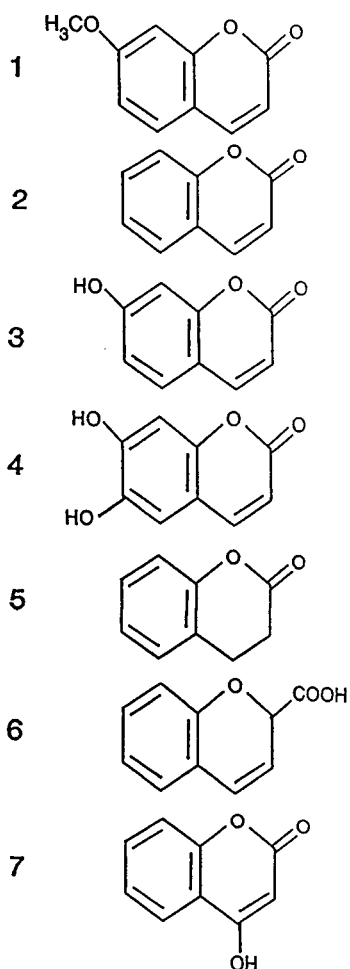
Fig. 1. Structural formulae of investigated coumarins. 1 = Herniarin (7-methoxycoumarin); 2 = coumarin; 3 = umbelliferone (7-hydroxycoumarin); 4 = aesculetin (6,7-dihydroxycoumarin); 5 = dihydrocoumarin; 6 = coumarinic acid; 7 = 4-hydroxycoumarin.

analytical-reagent grade. Water was purified by double distillation.

2.2. Plant material

The plant material was collected from the Gdańsk district (Poland) and identified in the Department of Botany. A voucher specimen is deposited in the herbarium of the Faculty of Pharmacy (Medical Academy, Gdańsk, Poland), International Herbarium Index GDMA.

2.3. Sample preparation

Roots and aerial parts of the plants were dried, powdered and then extracted with methanol. The extract was concentrated in vacuo and the concentrate was diluted with an equal volume of 4% lead acetate solution in water. After standing overnight, the precipitate that formed was removed by filtration. The filtrate was concentrated in vacuo and extracted with chloroform. The chloroform was removed from the extracts and the residue was dissolved in buffer.

2.4. Capillary electrophoresis

Analyses were performed with a Beckman P/ACE 2100 System Gold electrophoresis apparatus with UV detection at 280 nm. The column was a 58 cm × 50 μm I.D. uncoated silica capillary, with a length to the detector of 51 cm. The best overall separation was obtained with 7-s pneumatic injection using a buffer solution of 0.2 M boric acid–0.05 M of borax in water (11:9, v/v) (pH 8.5). The voltage was maintained at 25 kV, which gave a current of 32.6 mA, and the temperature was set at 25°C. Under these conditions the analysis time was 10 min and a baseline separation of herniarin, umbelliferone, esculetin, dihydrocoumarin, coumarinic acid and 4-hydroxycoumarin was achieved.

Stock solutions of standards were prepared in methanol at concentrations of 1 mg/ml. From these solutions, appropriate injection solutions were prepared by mixing the required volume with water.

3. Results and discussion

3.1. Separation of standard mixture

Fig. 2 shows electrophoretic separation of a standard mixture under the conditions described under Experimental. As can be seen, herniarin is not separated from coumarin. Our aim was to develop a method to separate as many compounds as possible. Hence the final conditions
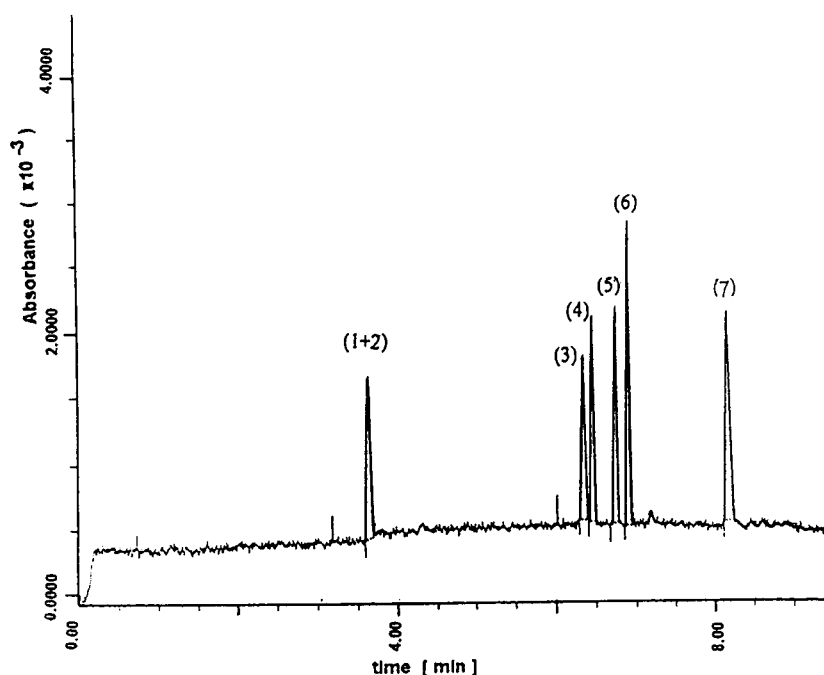
Fig. 2. CE separation of standard coumarin mixture. Conditions as under Experimental. Peaks: 1 + 2 = herniarin and coumarin; 3 = umbelliferone; 4 = aesculetin; 5 = dihydrocoumarin; 6 = coumarinic acid; 7 = 4-hydroxycoumarin.

were not necessarily the best for every type of coumarin mixture, but were selected to provide the best overall separation of the extracts considered. For example, at pH 9.33 the migration time of the last compound (4-hydroxycoumarin) is shorter (6 min), but a separation between umbelliferone and coumarinic acid is not achieved. One of the major advantages of this CE method is that the entire electrophoresis process is relatively rapid, comprising a 7-min analysis time followed by a 3-min wash. In HPLC, for comparison, the retention time of herniarin (7-methoxycoumarin) is 25.27 min [11].

3.2. Chemical composition of the extracts

Fig. 3A shows a typical electrophoretic separation of an extract obtained from aerial parts of *Chrysanthemum segetum* and Fig. 3B shows the electropherogram of the same extract spiked with standards. Fig. 4 illustrates a typical electrophoretic separation of coumarins from roots extract. With our method, coumarin cannot be

separated from herniarin (peaks 1 and 2, Fig. 2); however, most of the plants containing herniarin do not contain coumarin. Using semi-preparative CE and by comparison of UV spectra we found that peak 2 from *Chrysanthemum segetum* extracts represents almost pure herniarin.

The mean concentrations (peak areas) of coumarins found in the aerial part and root samples together with standard deviations (S.D.) and relative standard deviations (R.S.D.) are given in Table 1. The mean concentration values were obtained from six independent extraction runs both for aerial parts and roots of the plant material. The relative standard deviation in each instance is <6%. Therefore, it can be concluded that both the extraction procedure and CE determination are highly reproducible.

As it can be seen in Table 1, 4-hydroxycoumarin was not found in extracts from *Chrysanthemum segetum*. Nevertheless, 4-hydroxycoumarin is an important intermediate product in the biochemical transformation of coumarins to dicoumarol [13]. This transformation is typical of
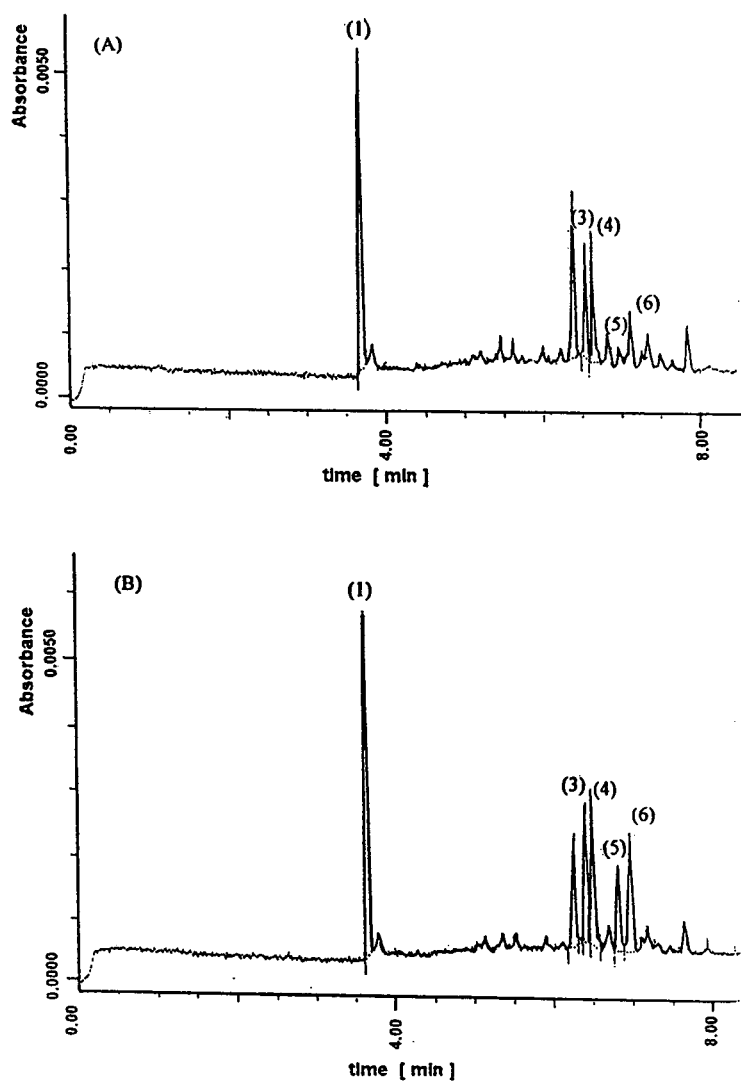
Fig. 3. (A) CE separation of an extract obtained from aerial parts of *Chrysanthemum segetum* L. Peaks: 1 = herniarin; 3 = umbelliferone; 4 = aesculetin; 5 = dihydrocoumarin; 6 = coumarinic acid. (B) The same extract spiked with standards. Conditions as under Experimental.

putrefactive processes. The absence of this compound in the extracts investigated confirms the freshness of the plant material.

It was found that coumarins are distributed differently, both quantitatively and qualitatively, in roots and aerial parts of the plants. The extracts from roots showed abundant herniarin (40%), dihydrocoumarin (30%) and umbel-

liferone (5%). Herniarin (26%) is also the major component of extracts from aerial parts of the plant, but the second highest is umbelliferone (18%) and then esculetin (12%), dihydrocoumarin (11%) and coumarinic acid (4%). Hence it can be concluded that *Chrysanthemum segetum* L. is a herniarin-type species. In the literature there, no quantitative data concerning
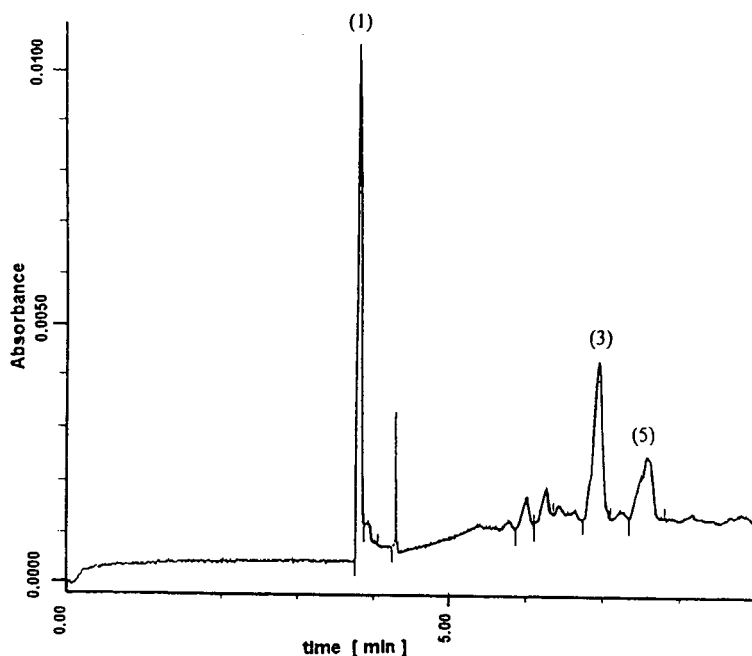
Fig. 4. CE separation of an extract obtained from roots of *Chrysanthemum segetum* L. Conditions as under Experimental. Peaks: 1 = herniarin; 3 = umbelliferone; 5 = dihydrocoumarin.

coumarin contents in *Chrysanthemum segetum* are available. In only one study [3] it was mentioned that herniarin and umbelliferone are the major components of extracts from whole plant material. From this point of view, our conclusions are similar to the results published previously.

The main advantages in the application of CE for the determination of coumarins were the short time of analysis, baseline separation and the low cost of the reagents used in the mobile phase.

Table 1
Contents of coumarins in extracts obtained from aerial parts and roots of *Chrysanthemum segetum* L ($n = 6$)

Compound	Mean content ±S.D. (%)	R.S.D. (%)
Aerial parts		
Herniarin	26.5 ± 0.42	1.6
Umbelliferone	19.0 ± 0.36	1.9
Aesculetin	12.1 ± 0.13	1.1
Dihydrocoumarin	11.3 ± 0.08	0.7
Coumaric acid	4.1 ± 0.0001	0.002
Roots		
Herniarin	39.0 ± 2.2	5.6
Umbelliferone	4.6 ± 0.02	0.4
Dihydrocoumarin	29.9 ± 1.2	4.0

References

[1] B. Drożdż and E. Błoszyk, Planta Med., 33 (1978) 379.
[2] J.B. Harborne, V.H. Heywood and N.A.M. Saleh, Phytochemistry, 9 (1970) 2011.
[3] S. Öksüz and H. Wagner, J. Nat. Prod., 45 (1982) 374.
[4] A.J. Cohen, Food Cosmet. Toxicol., 17 (1979) 277.
[5] H. Wagner, Planta Med., 55 (1989) 235.
[6] D.A. Egan and R. O'Kennedy, J. Chromatogr., 582 (1992) 137.
[7] M.L. Bieganowska and K. Głowniak, Chromatographia, 25 (1988) 111.
[8] S. Cholerton, M.E. Idle, A. Vas, F.J. Gonzalez and J.R. Idle, J. Chromatogr., 578 (1992) 325.
[9] P. Härmälä, H. Vuorela, E.L. Rahko and R. Hiltunen, J. Chromatogr., 593 (1992) 329.

[10] A.C. Arruda, V.E.F. Heinzen and R.A. Yumes, J. Chromatogr., 630 (1993) 251.

[11] P. Gamache, E. Ryan and I.N. Acworth, J. Chromatogr., 635 (1993) 143.

[12] A. Marston, C. Borel and K. Hostettmann, J. Chromatogr., 450 (1988) 91.

[13] J. Kaczkowski, Biochemia Roslin (Plant Biochemistry), Vol. 2, PWN, Warsaw, 1993.

High-performance liquid chromatographic and capillary electrophoretic determination of free nicotinic acid in human plasma and separation of its metabolites by capillary electrophoresis

P.K. Zarzycki, P. Kowalski, J. Nowakowska, H. Lamparczyk*

Medical Academy, Faculty of Pharmacy, Gen. J. Hallera 107, PL-80416 Gdańsk, Poland

Abstract

Two methods are described based on high-performance liquid chromatography and capillary electrophoresis that provide the selective and sensitive determination of nicotinic acid in human plasma. Moreover, the capillary electrophoresis system was used for the separation of nicotinic acid, nicotinamide, nicotinamide N-oxide, N'-methylnicotinamide, 6-hydroxynicontinic acid, nicotinuric acid and barbital (internal standard). The extraction procedure is simple; no gradient elution or derivatization is required. Both methods can be useful for clinical and biomedical investigations.

1. Introduction

Nicotinic acid and its derivatives are widely used in the treatment of hyperlipaemia. In order to determine its concentration in human plasma, spectrophotometric [1–3], paper chromatographic [4], thin-layer chromatographic [5], gas chromatographic [6,7] and high-performance liquid chromatographic (HPLC) [8–13] methods have been described, but some of these methods are currently rarely used. The spectrophotometric method is not specific enough. Generally, planar chromatographic methods are time consuming and are not precise enough. In gas chromatographic methods, nicotinic acid must be derivat-

ized to volatile compounds [6,7]. HPLC methods require either a very long column (50 cm) packed with an ion-exchange stationary phase [9] or the use of an ion-pair chromatographic system [12,13]. Recently, the separation of a standard mixture of eight acids, including nicontinic acid, using electroosmotic flow capillary electrophoresis (CE) was described by Liu and Sheu [14].

The plasma concentration profiles of nicotinic acid and nicotinuric acid after oral administration of 500-mg doses of nicotinic acid was reported by Takikawa et al. [9]. The peak concentrations (C_{max}) of nicotinic acid and nicotinuric acid were ca. 9.2 and 3.0 μg/ml, respectively.

The aim of this study was to evaluate two methods, HPLC and CE, for the determination of nicotinic acid in human plasma.

---

* Corresponding author.

2. Experimental

2.1. Reagents

Nicotinic acid, nicotinamide N-oxide, N'-methylnicotinamide, 6-hydroxynicotinic acid, nicotinuric acid, n-dodecylamine and 3-(N-morpholino)propanesulfonic acid (MOPS) were purchased from Sigma (St. Louis, MO, USA). Nicotinamide was obtained from Koch-Light Laboratories (Colnbrook, Bucks., UK). Barbital, anthranilic acid, sodium tetraborate decahydrate, potassium dihydrogenphosphate, sodium nitrate, phosphoric acid (85%) and hydrochloric acid were obtained from POCh (Gliwice, Poland). Acetonitrile (Merck, Darmstadt, Germany) was of HPLC grade. Methanol and acetone were purchased from POCh; acetone was purified by double distillation from above anhydrous $CaCl_2$. Water was purified by double distillation. Mobile phases and buffers were filtered through a 1.5-μm membrane prior to use. The structures of nicotinic acid metabolites and the internal standards are shown in Fig. 1.
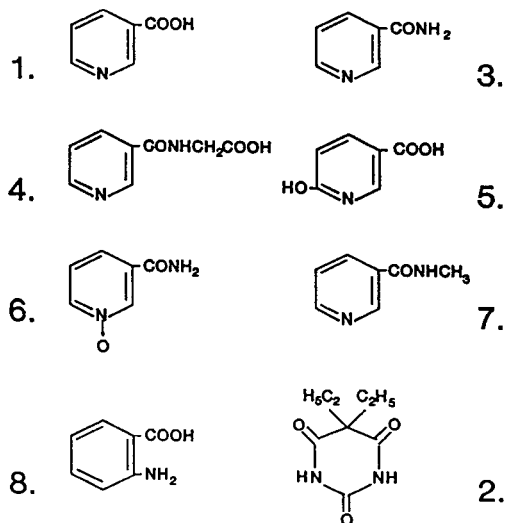
Fig. 1. Structures of nicotinic acid (1), nicotinamide (3), nicotinuric acid (4), 6-hydroxynicotinic acid (5), nicotinamide N-oxide (6), N'-methylnicotinamide (7) and the internal standards barbital (2) and anthranilic acid (8).

2.2. High-performance liquid chromatography

The method employed is based on two methods described by others [12,13]. The mobile phase used was a mixture of acetonitrile and MOPS buffer (10 mM MOPS, pH 5.4) (25:75, v/v). n-Dodecylamine was added to the mobile phase to give a final concentration of 1 mM.

Stock solutions of standards were prepared in acetonitrile at a concentration of 1 mg/ml. From these stock solutions, appropriate injection standard solutions were prepared by mixing the required volume of the stock solution and the chromatographic mobile phase. Typically, 20 μl of these standard solutions were injected.

An ODS-2 column (250 × 4 mm I.D., particle size 5 μm) was obtained from Knauer (Berlin, Germany). The liquid chromatograph consisted of an analytical solvent pump (Knauer A0307), a UV–Vis spectrophotometer (A0293) and a linear recorder (Knauer). A Rheodyne Model 7125 injection valve and a 20-μl loop were used for sample introduction. The UV detector was operated at 262 nm. The flow-rate was 1 ml/min. The column temperature (60 ± 0.1°C) was controlled by immersing the column in a stirred constant-temperature bath containing water used as a heat-exchange medium. The bath was connected to a thermostat. Additionally, the bottle containing the mobile phase was thermostated for 1 h before the experiment in order to obtain proper temperature equilibrium.

2.3. Capillary electrophoresis

A P/ACE 2100 capillary electrophoresis system, from Beckman, equipped with a UV detector operated at 254 nm, was used. The electrophoretic analyses were performed using an unmodified fused-silica capillary (51 cm from injector to detector, 57 cm total length, 50 μm I.D.). Samples were injected by a pneumatic system; the best overall separation was obtained with a 7-s injection. The voltage was maintained at 25 kV and the temperature was set at 25°C. Solutions of 10 mM sodium tetraborate (pH 9.36) or acetonitrile–buffer [10 mM potassium dihydrogenphosphate (pH = 2.50), titrated with phos-

phoric acid] (1:9, v/v) were used for electro-phoretic experiments.

Stock solutions of standards were prepared in acetonitrile at a concentration of 1 mg/ml. From these solutions, appropriate injection solutions were prepared by mixing the required volume of the stock solution with water.

2.4. Sample preparation

The plasma samples (0.5 ml) were spiked with required amounts of nicotinic acid and also, in the case of CE, with nicotinamide. After that, internal standards i.e., 50 μl of anthranilic acid at a concentration of 100 μg/ml or 10 μl of barbital at a concentration 1000 μg/ml for HPLC and CE, respectively, were added. Subsequently, the samples were deproteinized with a 3 ml of acetone–water (2:1, v/v), centrifuged and evaporated to dryness. The residue was dissolved in 0.5 ml of 0.1 M concentrated hydrochloric acid, mixed with 1 ml of methanol and evaporated to dryness. Finally, the residue was dissolved in 200 μl of water or 350 μl of the HPLC mobile phase.

3. Results and discussion

3.1. Samples

Most of the experiments were performed on spiked drug-free plasma samples, although limited numbers of analyses were made using plasma samples from healthy volunteers, after ingestion of a 250-mg dose of nicotinic acid. From the analytical point of view, the results were similar. This can be easily explained, because the protein binding of nicotinic acid is very weak [15].

It is well known that the liquid–liquid extraction of nicotinic acid and some of its metabolites from water or plasma is not effective, because they are very hydrophilic and water soluble at all pH values [9]. In the described purification procedure, the plasma sample was deproteinized with acetone–water and the sample evaporated without extraction by water-immiscible solvent.

3.2. HPLC method

The mechanism of the separation of the acids on the HPLC column is based on the formation of ion pairs between nicotinic acid or anthranilic

Table 1
Numerical data for detection linearity in the HPLC method

Concentration of nicotinic acid (x) (μg/ml)	Peak height (y) (mm)
0.2	3
2.0	21
5.0	70
10.0	145
20.0	276
40.0	548
60.0	768

Regression equation: $y = 7.0\ (\pm 8.0) + 13.0\ (\pm 0.3)x$, $r = 0.9989$.

Table 2
Numerical data for calibration graph for nicotinic acid in the HPLC method with anthranilic acid as internal standard

Concentration of nicotinic acid (x) (μg/ml)	Peak-height ratio (y)
0.5	0.1250
1.0	0.1558
2.0	0.3765
4.0	0.7917
8.0	1.5500
12.0	2.3320

Regression equation: $y = 0.04\ (\pm 0.02) + 0.195\ (\pm 0.003)x$, $r = 0.9997$.

Table 3
Intra-assay precision for the HPLC method

Amount added (μg/ml)	Amount found $\pm$S.D.[a] (μg/ml)	R.S.D.[a](%)
0.5	0.479 $\pm$ 0.07	15.2
1.0	1.068 $\pm$ 0.1	12.1
2.0	2.032 $\pm$ 0.1	6.3
4.0	3.914 $\pm$ 0.3	7.3
8.0	8.324 $\pm$ 0.2	2.7
12.0	12.611 $\pm$ 0.8	6.1

[a] $n = 5$.

acid and *n*-dodecylamine [12,13]. The detection limit of authentic samples for the HPLC method was 0.1 μg/ml and the detection curve was linear over a wide range of nicotinic acid concentration, from 0.2 to 60 μg/ml (Table 1). Numerical data for the calibration graph and its statistics are given in Table 2. The inter-assay variability was determined by analysing five replicates at each concentration in the range 0.5–12 μg/ml (Table 3). The chromatograms of a drug-free plasma sample and a plasma sample spiked with nicotinic acid and internal standard are shown in Fig. 2. The retention time of nicotinic acid, under these conditions, is 7.49 min. The separation between the nicotinic acid and internal

standard peaks is excellent. As can be seen, these peaks do not interfere with the background peaks. However, it was not possible to obtain a satisfactory result with respect to sensitivity and separation for nicotinic acid metabolites from plasma using the HPLC method.

3.3. CE method

The separation between nicotinamide, barbital and nicotinic acid by CE with UV absorbance detection at 254 nm is shown in Fig. 3A. The standards were well separated and their migration times were 2.97, 4.61 and 5.45 min, respectively. Fig. 3B and C show typical electropherograms of a plasma blank and a plasma sample spiked with nicotinomide, barbital (internal standard) and nicotinic acid at concentrations of 12, 20 and 12 μg/ml, respectively. Using 10 mM borax solution as a background electrolyte, the separation between nicotinic acid, barbital, nicotinuric acid and 6-hydroxynicotinic acid is satisfactory. Fig. 4 shows that the nicotinic acid peak does not interfere with the investigated metabolites and internal standard peaks. However, under these conditions no separation is observed between nicotinamide, nicotinamide N-oxide and N'-methylnicotinamide.

The detection curve was linear over a wide range of nicotinic acid concentration, from 1 to 100 μg/ml (Table 4). Table 5 gives numerical data for the calibration together with the statistical evaluation. The inter-assay variability was determined by analysing five replicates at each concentration in the range 1–12 μg/ml (Table 6).

Fig. 5 shows an electropherogram of the investigated compounds using acetonitrile–buffer [10 mM potassium dihydrogenphosphate (pH 2.50), titrated with phosphoric acid] (1:9, v/v) as background electrolyte. The separation between nicotinic acid and its metabolites was greatly improved in comparison with the separation obtained with a borax electrolyte (Fig. 4). However, the migration order of the investigated compounds is changed and the migration times
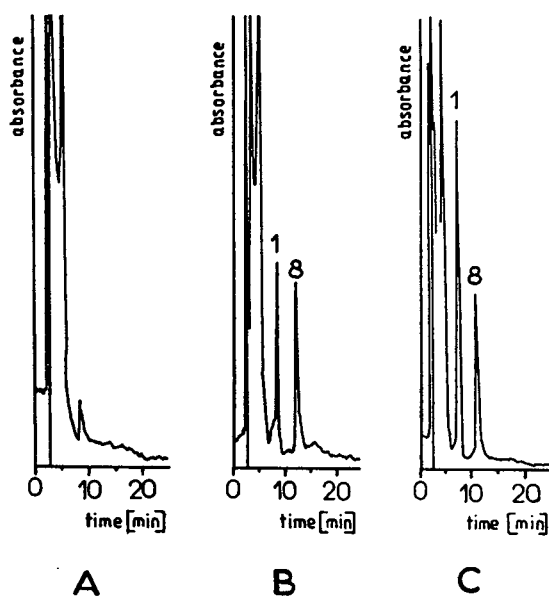
Fig. 2. (A) HPLC of drug-free plasma sample. (B) Chromatogram of a plasma sample containing nicotinic acid at 4 μg/ml and internal standard at 10 μg/ml. (C) Chromatogram of a plasma sample containing nicotinic acid at 8 μg/ml and internal standard at 10 μg/ml. Mobile phase: acetonitrile–10 mM MOPS buffer mM (pH = 5.4) (25:75, v/v), modified by the addition of 1 mM *n*-dodecylamine. Column, Knauer ODS-2 (250 × 4 mm I.D., particle size 5 μm) at 60°C, flow-rate, 1 ml/min; sample loop, 20 μl; UV detection at 262 nm. Peaks: 1 = nicotinic acid; 8 = internal standard (anthranilic acid).
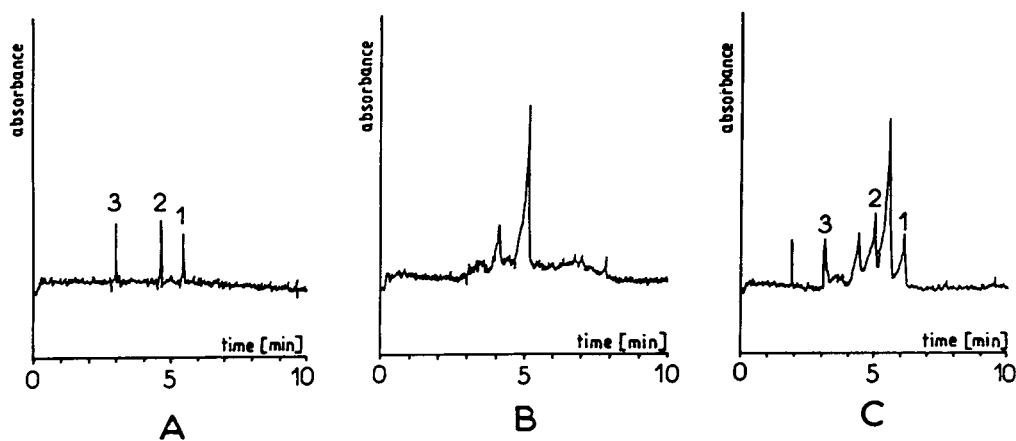
Fig. 3. (A) Electropherogram of a standard solution containing: (1) nicotinic acid, (2) barbital and (3) nicotinamide. (B) Electropherogram of drug-free plasma sample. (C) Electropherogram of a plasma containing (1) nicotinic acid at 12 μg/ml, (2) barbital (internal standard) at 20 μg/ml and (3) nicotinamide at 12 μg/ml. Conditions: applied voltage, 25 kV; 7-s pneumatic injection, unmodified fused-silica capillary (57 cm × 50 μm I.D.) at 25°C; buffer 10 mM, sodium tetraborate decahydrate (pH 9.36); UV detection at 254 nm.
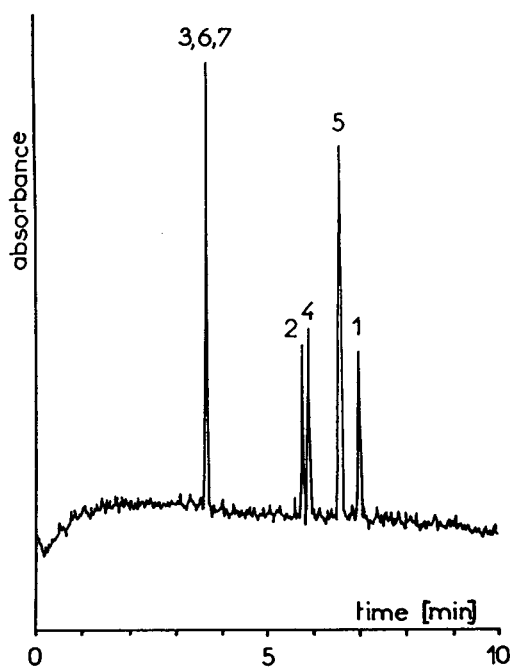
Fig. 4. Electropherogram of a standard solution containing (1) nicotinic acid, (2) barbital and (4) nicotinuric acid at concentrations of 20 μg/ml and (3) nicotinamide, (5) 6-hydroxynicotinic acid, (6) nicotinamide N-oxide and (7) N'-methylnicotinamide at concentrations of 10 μg/ml. Conditions as in Fig. 3.

Table 4
Numerical data for detection linearity in the CE method

Concentration of nicotinic acid (x) (μg/ml)	Peak height (y) (mm)
1	8
2	10
5	19
10	32
20	67
40	136
60	206
100	316

Regression equation: $y = 4.0$ (± 3.0) $+ 3.18$ (± 0.06)x, $r = 0.9989$.

of nicotinamide N-oxide and 6-hydroxynicotinic acid are longer (21.08 and 26.99 min, respectively).

In conclusion, it can be stated that both methods are sensitive, specific and reproducible enough for therapeutic drug monitoring. The main advantage in the application of CE for the determination of nicotinic acid is the low cost of the reagents used in the mobile phase. Moreover, CE gives the possibility of determining nicotinic acid and its metabolites simultaneously.

Table 5
Numerical data for calibration graph for nicotinic acid in the CE method with barbital as internal standard

Concentration of nicotinic acid (x) (μg/ml)	Peak-height ratio (y)
1	0.1110
2	0.1710
4	0.2637
6	0.4075
8	0.5144
10	0.6342
12	0.7270

Regression equation: $y = 0.053 \ (\pm 0.009) + 0.057 \ (\pm 0.001)x$, $r = 0.9982$.

Table 6
Intra-assay precision for the CE method.

Amount added (μg/ml)	Amount found $\pm$S.D.[a] (μg/ml)	R.S.D.[a](%)
1	1.008 ± 0.1	11.5
2	2.059 ± 0.2	9.8
4	3.683 ± 0.4	9.9
6	6.203 ± 0.4	7.1
8	8.074 ± 0.7	9.0
10	10.174 ± 0.7	6.8
12	11.799 ± 1.0	8.3

[a] $n = 5$.
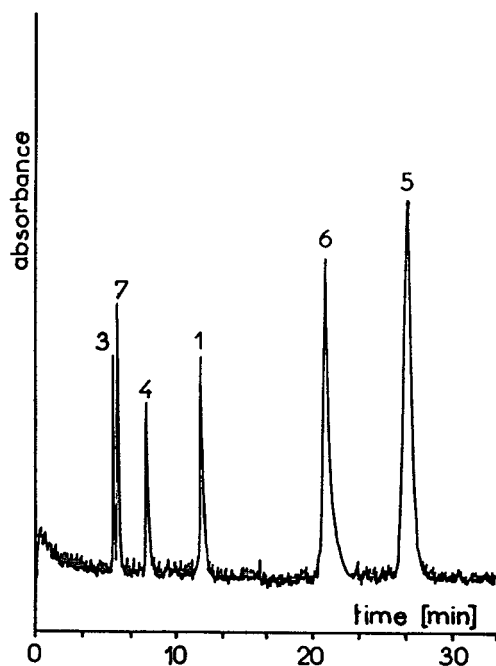
Fig. 5. Electropherogram of a standard solution containing (1) nicotinic acid, (3) nicotinamide, (4) nicotinuric acid (5) 6-hydroxynicotinic acid, (6) nicotinamide N-oxide and (7) N'-methylnicotinamide at concentrations of 20 μg/ml. Electrolyte, acetonitrile–buffer [10 mM potassium dihydrogenphosphate (pH 2.50), titrated with phosphoric acid]. Other conditions as in Fig. 3.

References

[1] E. Bandier and J. Hald, Biochem. J., 33 (1939) 264.
[2] Par M. Lesne, X. Sturbois and M. Mercier, Pharm. Acta Helv., 12 (1976) 367.
[3] L.A. Carlson., Clin. Chim. Acta, 13 (1966) 349.
[4] K.K. Reddi and E. Kodicek, Biochem. J., 53 (1953) 286.
[5] H.R. Bollinger and A. König, in E. Stahl (Editor), Thin-layer Chromatography, Springer, Berlin, 1969, p. 299.
[6] B. Becker and K. Hummel, Arzneim.-Forsch./Drug Res., 40 (1990) 573.
[7] J. Velisek, J. Davidek, J. Zavadil and J. Cerna, Sb. UVITIZ, Potravin. Vedy, 7 (1989) 81.
[8] N. Hengen, V. Seiberth and M. Hengen, Clin. Chem., 24 (1978) 1740.
[9] K. Takikawa, K. Miyazaki and T. Arita, J. Chromatogr., 233 (1988) 343.
[10] Y. Tsuruta, K. Kohashi, S. Ishida and Y. Ohkura, J. Chromatogr., 309 (1984) 309.
[11] K. Shibata, T. Kawada and K. Iwai, J. Chromatogr., 422 (1987) 257.
[12] A. Durrer, B. Walther, A. Racciatti and B. Testa, J. Chromatogr., 495 (1989) 256.
[13] J.L.M. Van de Venne, J.L.H.M. Hendrikx and R.S. Deelder, J. Chromatogr., 167 (1978) 1.
[14] Y.-M. Liu and S.-J. Sheu, J. Chromatogr. A, 663 (1994) 239.
[15] P. O'Connor, J. Feely and J. Shepherd, Br. Med. J., 300 (1990) 667.

Capillary electrophoretic separation of phenolic acids

Giampaolo Cartoni, Franco Coccioli, Renata Jasionowska*

Dipartimento di Chimica, Università degli Studi di Roma "La Sapienza", P. le A. Moro 5, 00185 Rome, Italy

Abstract

Phenolic acids such as syringic, p-coumaric, vanillic, caffeic, 3,4-dihydroxybenzoic and gallic acid, which are present in wines and other alcoholic drinks, were determined by capillary electrophoresis using an uncoated fused-silica capillary. The optimum conditions for their separation were investigated. Examples of electropherograms of phenolic acids contained in some Italian wines are reported.

1. Introduction

Phenolic acids such as syringic, vanillic, caffeic, p-coumaric, gallic and 3,4-dihydroxybenzoic acid are present in wines and other alcoholic drinks [1–3]. Considering the importance of their determination, we studied the possibility of the application of capillary electrophoresis. Many papers have been published on the electrophoretic determination of organic acids [4–8]. The determination of organic aliphatic acids in wine by HPLC and capillary electrophoresis has been reported [9]. Oxalic, citric, tartaric, malic, succinic, formic, fumaric and acetic acid have been determined by indirect detection. The HPLC analysis of wine has been described [10–12]. This paper describes the determination of phenolic acids in wine by capillary electrophoresis using an uncoated fused-silica capillary.

_____

* Corresponding author.

2. Experimental

2.1. Instrumentation

Electrophoresis was carried out using a Spectraphoresis 1000 instrument (Spectra Physics, Palo Alto, CA, USA) with rapid scan spectrophotometric detection. An uncoated fused-silica capillary (SGE, Melbourne, Australia) of I.D. 50 μm and total length 43 cm was used. The distance between the anode end of the capillary, where the sample was injected, and the detector was 36 cm. Sampling was carried out using the hydrodynamic method with times ranging between 2 and 5 s. The volumes of sample solution injected were about 4.5 and 10.0 nl, respectively. The operating temperature was 25°C.

2.2. Reagents

All the reagents used were of high purity. Monobasic phosphate, dibasic phosphate, phos-

phoric acid and sodium carbonate and hydro-gencarbonate were supplied by Carlo Erba (Milan, Italy). Phenolic acid standards were supplied by Fluka (Buchs, Switzerland). The solvents used were methanol and diethyl ether, supplied by Carlo Erba.

2.3. Solutions

Solutions of the acid standards studied were prepared by dissolving the pure compounds in water–methanol (1:1) at concentrations of 0.5 mg/ml each. The following buffers were used as background electrolyte (BGE): phosphate (pH 7.2), hydrogencarbonate (pH 8.3) and carbonate–hydrogencarbonate (pH 9.2 and 10.1). All solutions were filtered before use. Benzyl alcohol was used as a marker of electroosmotic flow.

2.4. Operating conditions

Before carrying out analysis, the capillary was washed for 2 min with 0.1 M NaOH solution and then for 2 min with distilled water, and finally conditioned for 4 min with the buffer solution which was to be used for the analysis. Electro-osmotic flow was then checked by injecting benzyl alcohol. The reproducibility in terms of migration times of the neutral marker was 0.6% (run-to-run) and 3.0% (day-to-day). After ca. 2 weeks the capillary became less active, as detected by a lower electroosmotic flow. Washing with NaOH solution was insufficient to restore the initial activity. Washing with 1 M HCl restored the initial conditions of the electroosmotic flow and migration times. In order to optimize the conditions for the separation of the phenolic acids studied, several tests were carried out by appropriately varying the pH, ionic strength (concentration of BGE) and applied potential. Table 1 summarizes the parameters concerning the experimental conditions of the tests performed.

For the analysis of real wine samples, it was necessary to extract the phenolic acids from the material, as follows. The wine was evaporated under vacuum to eliminate the ethanol. After addition of buffer of pH 8.2 to 2 ml of evapo-rated wine, the sample was extracted with diethyl ether (the ether extract was discarded). After acidification with HCl to pH 1, the wine was extracted three times with diethyl ether. The ether extract was evaporated under nitrogen and the residue was dissolved in 50 μl of water–methanol (1:1). Electrophoretic analysis was carried out on this sample. Extraction with diethyl ether at pH 8 allowed the separation of the neutral and basic substances present in the undissociated form. The ionized phenolic substances remained in the acqueous phase. Later, after acidification, the phenolic substances were in undissociated form and were thus extractable with diethyl ether.

Table 1
Experimental parameters

pH	V (kV)	C (mM)
7.2	10	50
		100
	15	50
		100
8.3	10	20
		50
		80
	15	20
		50
		80
	20	20
		50
		80
9.1	10	50
		80
		100
	15	50
		80
		100
	20	50
		80
10.1	15	50

3. Results and discussion

Phenolic acids are weak carboxylic acids. They are partly dissociated and hence present in
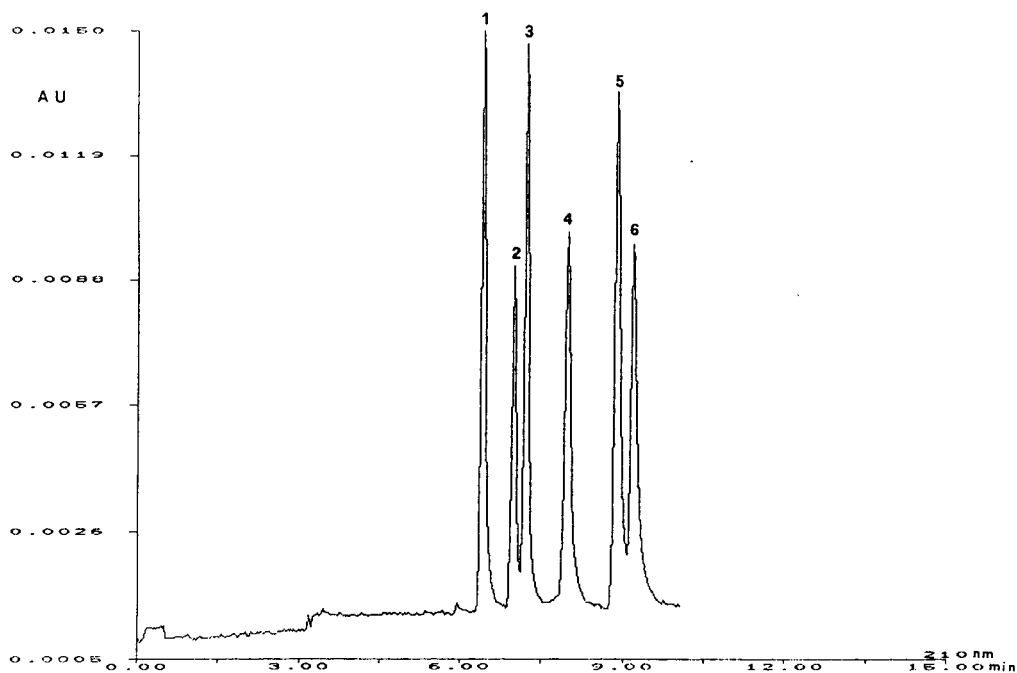
Fig. 1. Electropherogram of standard acid mixture obtained under optimum conditions: pH = 8.3; V = 15 kV; BGE concentration = 50 mM hydrogencarbonate buffer; current = 25 μA. Peaks: 1 = syringic acid; 2 = p-coumaric acid; 3 = vanillic acid; 4 = caffeic acid; 5 = 3,4-dihydroxybenzoic acid; 6 = gallic acid.

anionic form. In an electric field they migrate towards the anode. By carrying out electrophoretic analysis in an uncoated fused-silica capillary, there is an electroosmotic flow. Under these conditions the anions move towards the cathode and it is then possible to detect them. Other experimental parameters being equal, the higher the electroosmotic flow the higher is the
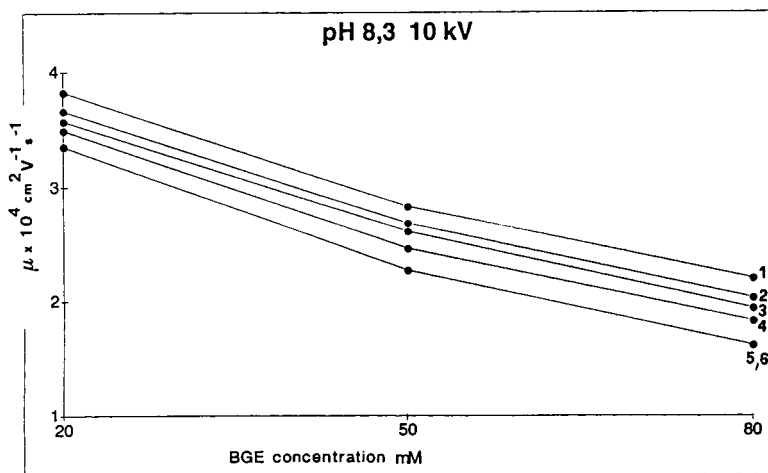
Fig. 2. Apparent mobility of phenolic acids. Conditions: pH = 8.3; V = 10 kV.
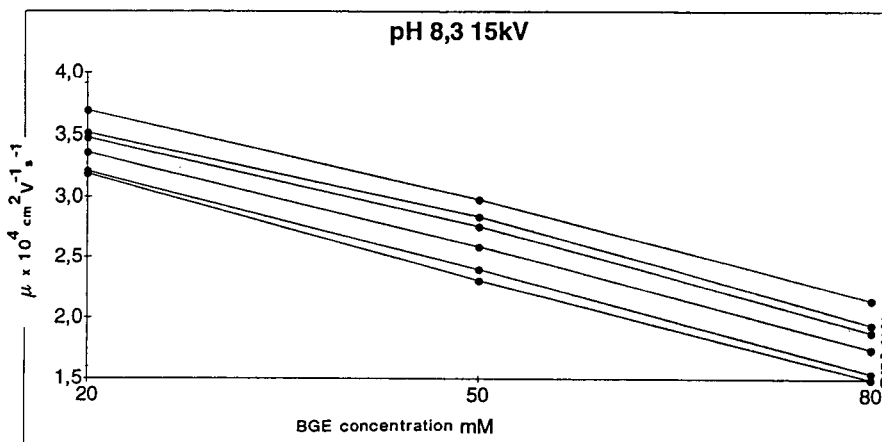
Fig. 3. Apparent mobility of phenolic acids. Conditions: pH = 8.3; V = 15 kV.

anion migration velocity [13,14]. Separation tests on phenolic acids carried out under different conditions (see Table 1) demonstrated that the optimum conditions were pH = 8.3 (hydrogen-carbonate buffer), BGE concentration = 50 mM and applied potential = 15 kV. Only these conditions allowed an electropherogram with six distinct peaks (Fig. 1). The results obtained using a longer capillary (76 cm total length) did not significantly change the separation. Figs. 2–4) show the variation of the apparent mobility of the phenolic acids with BGE concentration. As can be seen, the apparent μ decreases as the BGE concentration rises. This is probably due to the greater screening of the capillary walls by the BGE and, as a result, a decrease in electro-osmotic flow. Fig. 5 shows the variation of the apparent mobility with pH. The experimental data show that the apparent mobility decreases as the pH rises. Since the electroosmotic flow was not significantly influenced by the hydrogen ion concentration in the pH range explored (7–
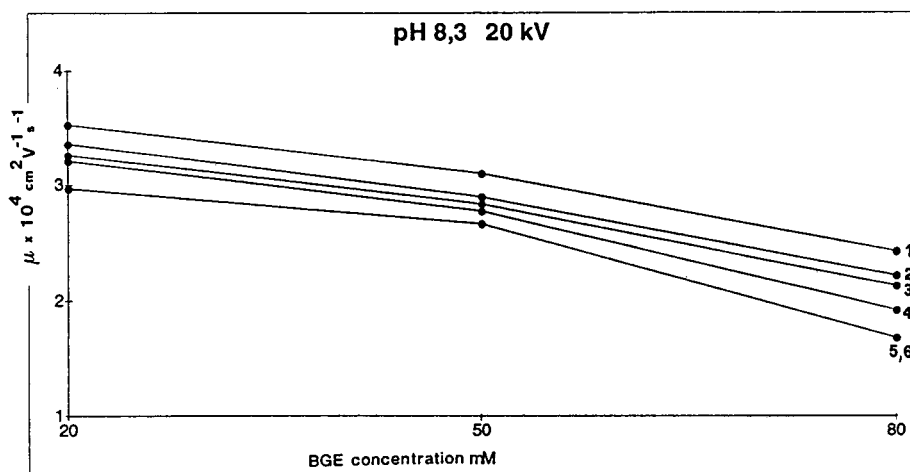
Fig. 4. Apparent mobility of phenolic acids. Conditions: pH = 8.3; V = 20 kV.
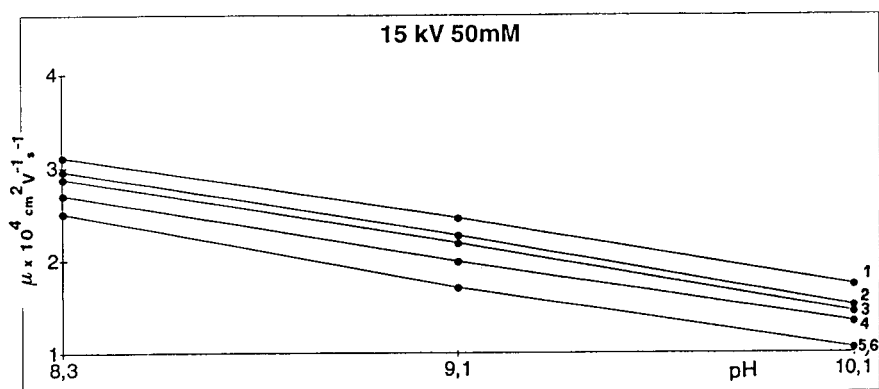
Fig. 5. Apparent mobility of phenolic acids. Conditions: BGE = 50 mM; V = 15 kV.

10), the decrease in the apparent mobility of the acids was probably due to the greater dissociation of the molecules studied (with the resulting "braking" effect of anions with a greater negative charge).

In order to check the reproducibility of the experimental data, the relative standard deviation (R.S.D.) was calculated for the migration times of the acids in the mixture. This value (run-to-run) was always less than 1%. Peak-area integration was carried out on the electropherograms relative to the phenolic acid standard mixture. The peak-area reproducibility (run-to-run) was R.S.D. 1.0–2.2%. Two electrophero-
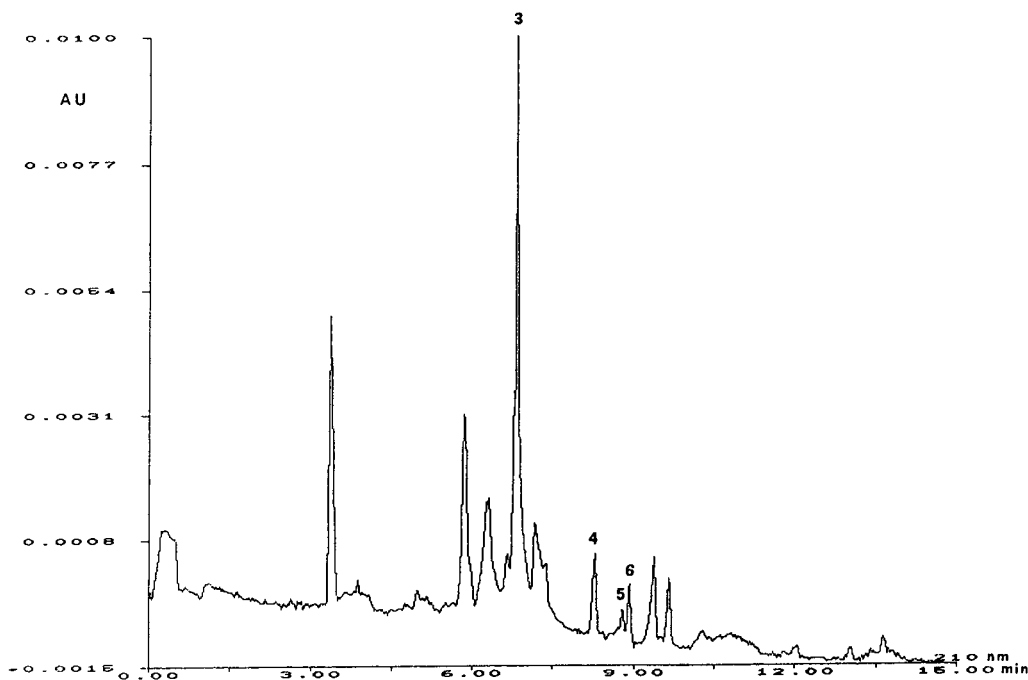
Fig. 6. Electropherogram of sample extracted from Corvo wine. Conditions as in Fig. 1.
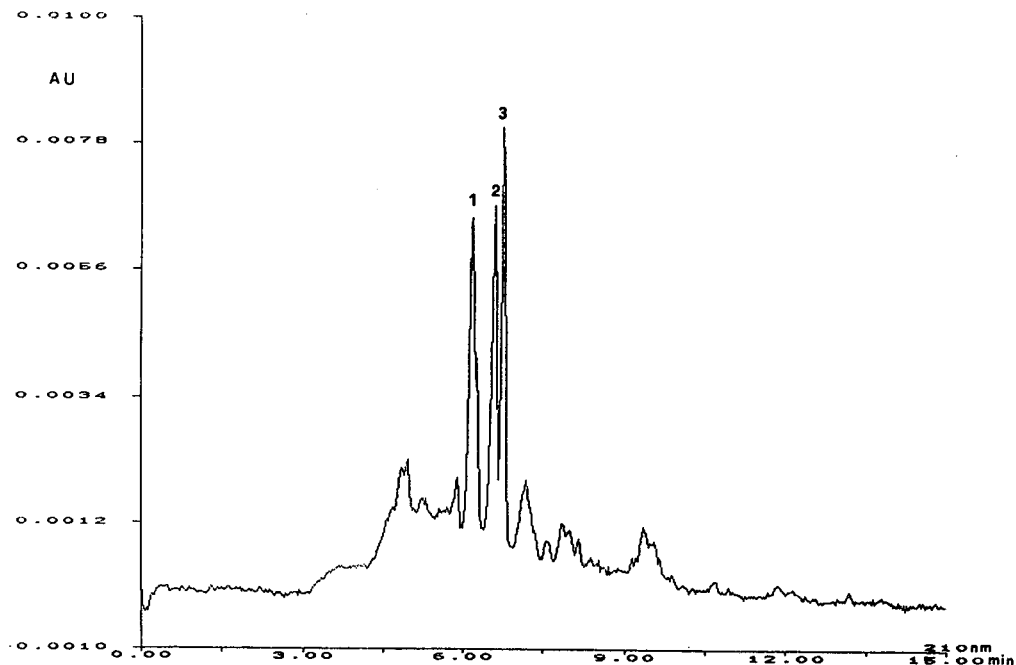
Fig. 7. Electropherogram of sample extracted from Chianti wine. Conditions as in Fig. 1.

grams of samples extracted from Italian red wines are shown: Corvo (Fig. 6) and Chianti (Fig. 7).

References

[1] L.W. Wulf and C.W. Nagel, J. Chromatogr., 116 (1976) 271–279.
[2] C.S. Ough and M.A. Amerine, Methods for Analysis of Musts and Wine, Wiley, New York, 1988, pp. 196–200.
[3] A.A. Qureshi, N. Prentic and W.C. Burger, J. Chromatogr., 170 (1979) 343–353.
[4] W.R. Jones and P. Jandik, J. Chromatogr., 608 (1992) 385–393.
[5] S.C. Smith and M.G. Khaledi, J. Chromatogr., 632 (1993) 177–184.
[6] J. Karovicova, J. Polonsky, M. Drdak, P. Simko and V. Vollek, J. Chromatogr., 638 (1993) 241–246.
[7] S.C. Smith and M.G. Khaledi, Anal. Chem., 65 (1993) 193–198.
[8] Y. Liu and S.J. Sheu, J. Chromatogr., A 663 (1994) 239–243.
[9] V. Levi, T. Wehr, K. Talmadge and M. Zhu, Int. Chromatogr. Lab., 15, September (1993) 4.
[10] K.V. Castleele, H. Geiger and C.F. Van Sumere, J. Chromatogr., 258 (1983) 114–124.
[11] C.G. Barroso, R.C. Torrijos and J.A.P. Bustamante, Chromatographia, 17 (1983) 249–252.
[12] D.A. Roston, P.T. Kissinger, Anal. Chem., 53 (1981) 1695–1698.
[13] T. Tsuda, K. Nomura and G. Nagakawa, J. Chromatogr., 264 (1983) 385–392.
[14] J. Kohr and H. Engelhardt, J. Microcol. Sep., 3 (1991) 491–495.

ELSEVIER

Capillary electrophoretic study of atrazine photolysis

Ph. Schmitt[a,*], D. Freitag[a], Y. Sanlaville[b], J. Lintelmann[c], A. Kettrup[c]

[a]GSF Institut für Ökologische Chemie, Schulstrasse 10, D-85356 Attaching/Freising, Germany
[b]Laboratoire de Photochimie Industrielle, Université Claude Bernard Lyon I, 43 Boulevard du 11 Novembre 1918, 69622 Villeurbanne/Lyon, France
[c]GSF-Institut für Ökologische Chemie, Ingolstädter Landstrasse 1, D-85764 Neuherberg/Oberschleissheim, Germany

Abstract

Capillary electrophoresis in its free solution mode (FSCE) has been used as a rapid analysis tool for the quantification of hydroxytriazines during the photodegradation of atrazine under nitrogen and oxygen atmosphers in the presence or absence of humic substances in aquatic media. Hydroxyatrazine was found to be the main photodegradation product. The presence of dissolved humic substances influenced the photodegradation pathway of atrazine by dealkylation reactions. FSCE has been found effective in the separation of the cationic hydroxytriazines from the anionic humic polyelectrolytes during the analysis without cleanup procedures.

1. Introduction

Atrazine [2-chloro-4-(ethylamino)-6-(isopropylamino)-s-triazine] is widely used over the world as a selective herbicide against broad weed leaves and annual grass. Many studies of atrazine and other s-triazine pesticides over the last two decades have provided a good understanding of their metabolic fate in different matrices under variable conditions (abiotic and biological degradation in soils or sediments and decay through the effect of UV radiation in water). s-Triazines have been found to degrade by dealkylation of the side chains in surface position 4 and 6 and by hydrolysis of the substituent in position 2.

One objective of photochemical studies is the understanding of the environmental relevance of this abiotic degradation pathway [1]. In more recent studies, an additional objective is the optimisation of UV degradation systems in combination with reactive oxygen precursors (O_3, H_2O_2) for decontamination/desinfection of drinking waters [2]. In both cases humic substances can have a significant effect on pesticide decay as a reaction sensitizer or inhibitor [3,4] during photochemical reactions.

The hydroxy metabolites of s-triazines are significant natural degradation products in soils [5] and their occurrence in streams and water reservoirs [6] may occur after slow release from soils or after photolysis of s-triazines in surface waters [7]. Their analysis in environmental matrices is still a challenge; they have to be derivatized for gas chromatography [8] and only a few quantitative techniques based on LC [9,10], HPLC [11–15] or enzyme-linked immunosorbent assay [16,17] are found in the literature.

High-performance capillary electrophoresis (HPCE) is a recent analytical technique that has rapidly found application in biomedical sepa-

* Corresponding author.

rations [18] as well as in environmental sciences [19]. HPCE in its free solution mode (FSCE) has proven useful in pesticide analysis [20,21] and in the separation of s-triazine compounds [22,23].

The present paper has two objectives: first, to examine the photochemical behavior of atrazine in the presence and absence of humic substances, under oxygen and nitrogen atmospheres in aquatic media; second, to show for the first time the application of FSCE as a rapid analysis tool for hydroxy-s-triazines in environmental matrices.

2. Materials and methods

Aqueous solutions of atrazine were prepared at 5 ppm and placed in a cylindrical vessel into which a Philips HPK 125 W high-pressure mercury vapor lamp, with a cooled Pyrex housing to block wavelengths shorter than 290 nm, was inserted. Humic acids were added to some of the aqueous solutions to a concentration of 5 ppm just before they were transferred to the reactor. The pH of the solution was controlled and eventually adjusted to pH 7.0 to ensure solubility of humic acids. Nitrogen or oxygen was bubbled through a sintered glass joined to the bottom of the vessel to keep the solutions saturated with gas during photodegradation experiments. The reaction temperature was kept under these conditions at 20–25°C. The same pesticide solutions were also irradiated under simulated sunlight (xenon lamp) in a Heraeus Suntest apparatus at 30–35°C, with and without fulvic acids (5 ppm). Aliquots of 1 ml were sampled during irradiation and kept in the refrigerator for future analysis. Blanks (pesticide solution with and without humic substances) were analysed to ensure that pesticide degradation was due to photochemical processes only.

The disappearance of the pesticide from reaction mixtures and the appearance of the dealkylated chloro metabolites were monitored by HPLC (Hewlett-Packard, Munich, Germany; HPLC Series 1050). Detection was with an UV filter at 220 nm. A reversed-phase column, 250

mm × 4.6 mm I.D., packed with Hypersil (RP C_{18}, 5 μm) was used for analysis. The mobile phase was acetonitrile–water (50:50) with a flow-rate of 1.0 ml/min in the isocratic mode.

The qualitative and quantitative analyses of the hydroxy metabolites employed a Beckman P/ACE 2100 Series HPCE, assisted by Beckman Gold Chromatography Software. The fused-silica non-coated CE column, 57 cm (50 cm to detector) × 375 μm 0.0 × 75 μm I.D., was obtained from Beckman Instruments (Munich, Germany). The separation runs were done at constant temperature (30°C) and voltage (20 kV) with UV detection at 230 or 214 nm.

Direct sample injection by the hydrodynamic (pressure) mode was used for all experiments; injection times were typically 10 to 20 s. Samples were systematically spiked with standards to assure identification of the hydroxy metabolites. A standard curve was prepared for each hydroxy metabolite for quantitative analysis of their degradation products.

An acetate buffer was used for qualitative and quantitative measurements since such a buffer at 50 mM and pH 4.65 has been shown to give good separation of different dealkylated hydroxy metabolites of atrazine [23]. Buffers were made by mixing one volume glacial acetic acid (0.1 M), one volume sodium acetate (0.1 M), and two volumes water.

Pesticide stock solutions were prepared by dissolving 5.0 mg of pesticide/metabolite in 100 ml of pesticide-grade methanol. If necessary dilutions were done in water (for standard curves) and these solutions were immediately used for CE. All buffers and stock solutions were kept under refrigeration at 4°C.

For an additional confirmation of the identity of atrazine and its metabolites thermospray liquid chromatography–mass spectrometry (LC–TSP-MS) analyses of the reaction solutions obtained after photodegradation in the presence and absence of humic and fulvic acids were carried out.

LC–TSP-MS and LC–TSP-MS-MS have been applied to the determination of polar pesticides and different metabolites of polar nature formed during photodegradation and microbial degra-

dation processes [24–28]. The use of these methods offers the advantage of the direct analysis of polar hydroxy metabolites and direct injection of photodegraded solutions into the LC–MS system.

All LC–TSP-MS experiments were performed using a Finnigan-MAT TSQ 700 triple quadrupole MS–MS system (Bremen, Germany) equipped with a Finnigan-MAT thermospray interface. Conditions were as follows for all analyses: vaporizer temperature was 100°C, source block temperature was kept at 240°C. Ionisation was done in the filament-on mode with an electron current of 600 μA and an electron energy of 600 eV. Multiplier voltage was set at 1200 V. Spectra were acquired by scanning from m/z 100 to 500 every 1 s. The instrument was used in the positive ion mode.

The HPLC pump combined with the mass spectrometer was a Waters gradient pump 600-MS (Milford, USA). The eluent consisted of methanol–water (50:50, v/v) at a flow-rate of 1 ml/min. Injection volume of the samples was 50 μl. Flow injection analysis without chromatographic separation prior to MS analysis was performed. Because similar results were obtained for all samples investigated only one mass spectrum is shown representatively in Fig. 1.

It is well known that LC–TSP-MS spectra of most pesticides are characterized by the presence of $[M + H]^+$ base peaks. Fragmentation of the molecules is hardly found. This observation was also valid for our investigations. As expected the most intense peak is observed at m/z 216 deriving from atrazine, corresponding to $[M + H]^+$. Further compound-specific ions were found for hydroxyatrazine at m/z 198 $[M + H]^+$ and desethylatrazine at m/z 188 $[M + H]^+$. Ameline [M = 127] could not be identified unequivocally because $[M + H]^+$ at m/z 128 was found only with a very small intensity.

The fragments at m/z 174 and 146 are probably stemming from atrazine and desethylatrazine due to a loss of their isopropyl group [M − iso-$C_3H_6]^+$. In contrast to the ethyl group of these compounds the elimination of the isopropyl group is favored and can take place even under soft ionization conditions [24,29]. The presence or absence of chlorinated substances can be verified looking at the typical isotopic ratios (m/z
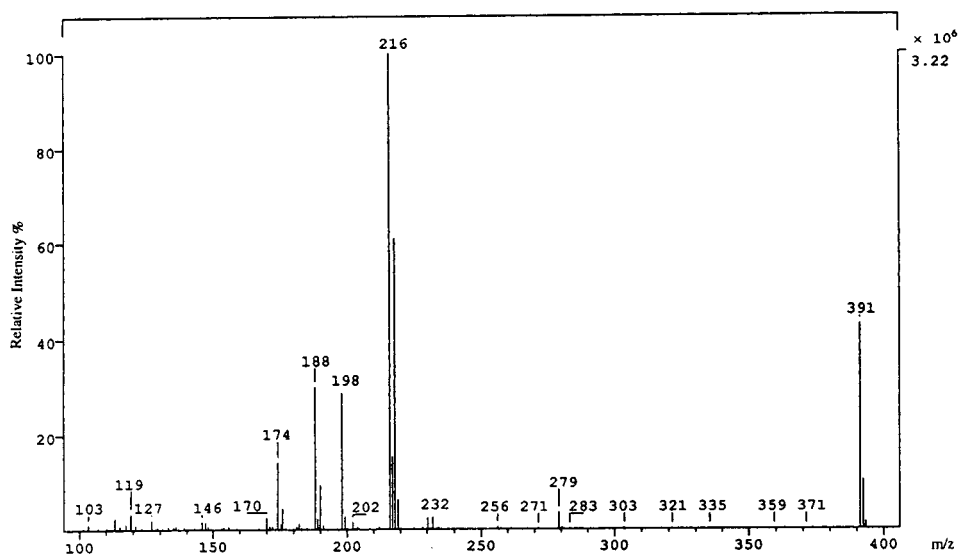
Fig. 1. TSP mass spectrum of atrazine treated with O_2 in the presence of humic acid. The spectrum was obtained after background subtraction.

Table 1
Elemental analysis and acidity data of HA and FA

	C(%)	H(%)	N(%)	O(%)	Ash(%)	C/N	$H/C_{(at.)}$	$O/C_{(at.)}$
FA	44.71	3.44	2.59	43.26	6	17.26	0.92	0.72
HA	48.3	4.04	4.44	39.52	3.7	10.88	1.01	0.61

Total acidity FA: 4, 0 meq uiv. g; HA: 2.42 meq uiv. g.

216 and 218 for atrazine, m/z 188 and 190 for desethylatrazine).

2.1. Chemical source and purity

Chloro- and hydroxy-s-triazines were purchased in greater than 99% purity grade from Dr. Ehrenstorfer GmbH, Augsburg, Germany or from Riedel-de Haen (Pestanal grade), Munich, Germany. All solvents, HCl, glacial acetic acid and sodium acetate (all analytical-reagent grade) were obtained from E. Merck, Darmstadt, Germany.

Humic acids (HA) and fulvic acids (FA) were extracted and isolated from the Ao horizon (0–15 cm) of a cultivated brown soil (Scheyern, Germany) according to the methods of the International Humic Substances Society (IHSS) [30,31]. Elemental analysis and functional group analysis is given in Table 1. Spectroscopic data (NMR, Fourier transform IR, pyrolysis–field ionization mass spectrometry) will be given elsewhere.

3. Results and discussion

3.1. Quantitative measurement of hydroxyatrazine

HPCE in its free zone mode has shown good potential for the analysis of s-triazinic herbicides [23]. This recent analytical technique allows separation of substances as cations on the basis of their relative electrophoretic mobility at a chosen buffer pH. Hydroxy-s-triazines are weakly basic compounds protonating at acidic pH according to Fig. 2 with dissociation constants between 4.5 and 5.2 [32].

The best buffer (signal-to-noise ratio) was found to be acetate at pH 4.5. Under those conditions, the hydroxytriazines were separated in less than 6 min with good quantitative reproducibility.

The relative standard deviations (R.S.D.s) of quantitative measurement of hydroxyatrazine in the current study were 3 and 5% at 230 nm detection wavelength and 5 and 8% at 214 nm detection wavelength for the areas and peak heights, respectively. The R.S.D. of retention times under these experimental conditions was less than 0.2% for all hydroxy metabolites studied.

Standard curves were measured for hydroxyatrazine in a range of 5 ppm to 50 ppb with UV detection at 230 or 214 nm. Peak area was the quantitative parameter chosen for this study with detection at 230 nm, which gave the best reproducibility and sensitivity (Fig. 3).

An example of separation with 50 mM acetate buffer at pH 4.65 is given in Fig. 4a. The five hydroxytriazines are separated in less than 5 min and are detected as cations in this buffer. The electroosmotic flow, corresponding to the speed of the neutral compounds, is indicated in this example by the negative peak at 5 min. Anions migrate after the neutral peak. Humic substances are known to be polyacids with an average pK_a around 3–4. At a buffer pH of over 4, they are partially present as anions and can be fraction-
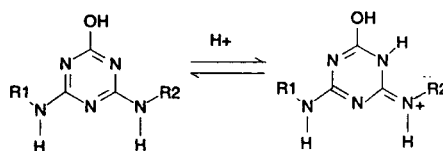
Fig. 2. Protonation of hydroxy-s-triazines at acidic pH [11].
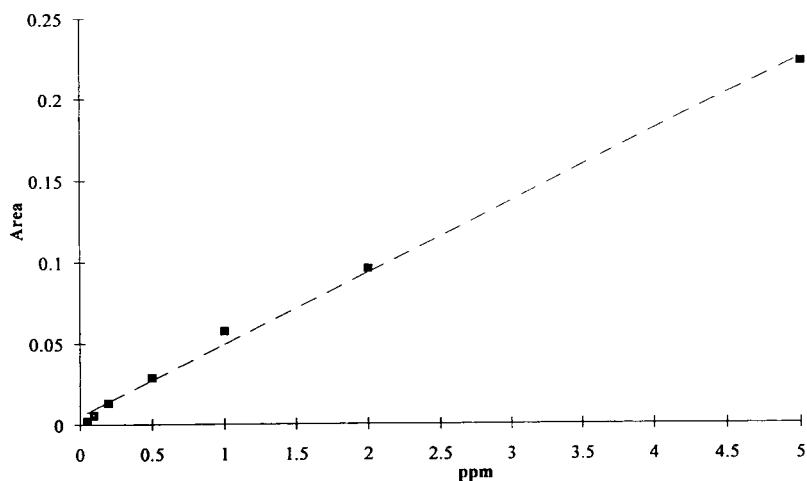
Fig. 3. Standard curve found with hydroxyatrazine. $y = 0.044021x + 0.005$; $r^2 = 99.6$

ated by FSCE on the basis of their electrophoretic mobility (relative charge-to-mass ratio). Previous studies have shown that HPCE can be a useful tool in humic substance characterizations [33] and Fig. 4b shows an electropherogram of the fulvic and the humic acids used in this study, using a 50 mM acetate buffer at pH 5.3 (similar experimental conditions as for the hydroxytriazines). In these conditions the electropherograms of humic substances show an average electrophoretic mobility (AEM) of negatively charged molecules.

One can see by this example that HPCE in its free zone mode is a good technique for the quantitative analysis of hydroxy-*s*-triazines, because potentially interferring humic substances in the sample matrix are separated. Sample clean-up before analysis to separate background matrix material (as in HPLC), is minimized thus avoiding loss of important information.

3.2. Photodegradation kinetics of atrazine

Under oxygen and nitrogen atmospheres, the disappearance of atrazine follows first-order kinetics with rate constants of $22.21 \cdot 10^{-3}$ and $18.32 \cdot 10^{-3}$ h^{-1}, respectively (Table 2). The oxygen atmosphere does not significantly enhance the kinetic rate. When irradiated in the Heraeus Suntest apparatus, the kinetic order is

also first order; but the calculated half-lives are double those found with the high-pressure mercury lamp because of lower light intensity.

The addition of humic material to the solutions did not alter kinetic order but accelerated degradation rates by a factor of 54% under oxygen and 38% under nitrogen (Fig. 5a). Humic substances play an important role in photosensitizing processes via electronic energy transfer [34] and are precursors for the production of oxygen reactive species such as hydrated electrons [35], peroxide radicals, singlet oxygen, hydrogen perodide and OH radicals [36]. Oxygen is involved in sensitizing reactions with dissolved humics and thus the degradation rate is higher in oxygen compared to the experiment with nitrogen. With the Heraeus Suntest apparatus and dissolved fulvic acids, the atrazine degradation rate was also increased by a factor of 33% (Fig. 5b and Table 2).

3.3. Dealkylated and hydroxylated photoproducts

The analysis of hydroxylated photoproducts gave good, rapid results with HPCE without sample pretreatment. Hydroxyatrazine produced by photosubstitution of chlorinated atrazine is the major photoproduct formed without humic substance addition under simulated sunlight and
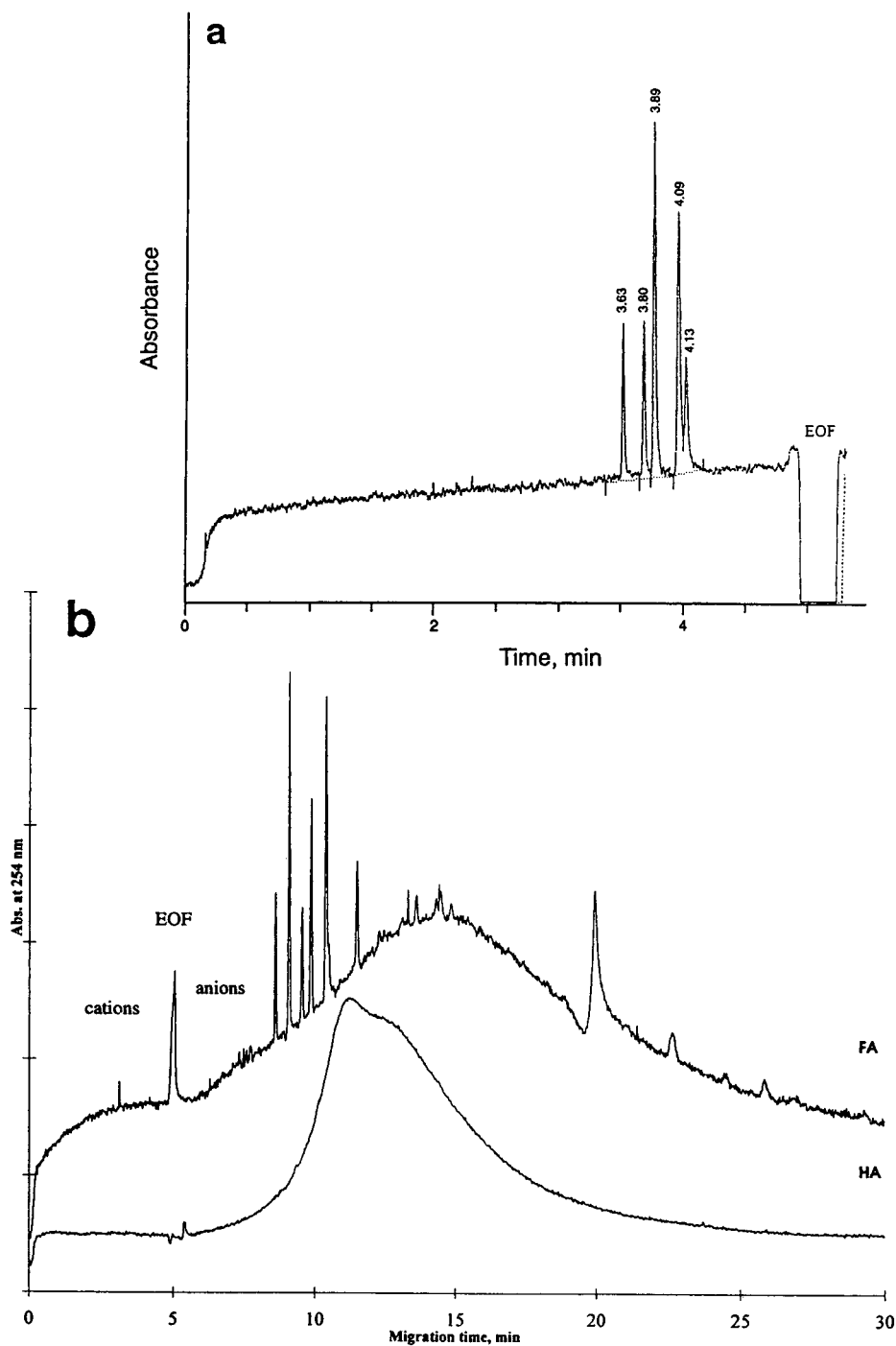
Fig. 4. Separation of five hydroxytriazines with acetate buffer (pH 4.65, 20 kV, 30°C). Peaks from left to right correspond to: hydroxyterbuthylazine,   hydroxydesisopropylatrazine,   hydroxyatrazine,   hydroxydesethylterbuthylazine   and   hydroxy-diaminoatrazine (ameline). (b) Separation of fulvic and humic acids used in this study with acetate buffer (pH 5.3, 20 kV, 30°C). EOF = Electroosmotic flow.

Table 2
Kinetic data on photodegradation of atrazine

Lamp	Atmosphere	Atrazine (5 ppm) solution	r_2	$K \times 10^{-3}$ (h^{-1})	$t_{1/2}$ (h)
Xenon	Air	Alone	99.2	10.49	66.08
		Fulvic acid (5 ppm)	99.4	13.97	49.62
HPK	Oxygen	Alone	99.8	22.21	31.21
		Humic acid (5 ppm)	98.4	34.35	20.18
	Nitrogen	Alone	99.7	18.32	37.84
		Humic acid (5 ppm)	99.5	25.39	27.30

First-order kinetics in all cases. K = Rate constant.

with the high-pressure mercury lamp (up to 70% of total photoproducts). The proportion of hydroxyatrazine compared to total photoproducts (obtained by difference between atrazine concentration and initial concentration) reaches a

maximum value in time before decreasing, probably due to further photodecomposition (dealkylation) (Fig. 6a and b).

Hydroxy metabolites have been found as photosolvolysis products of *s*-triazinic pesticides
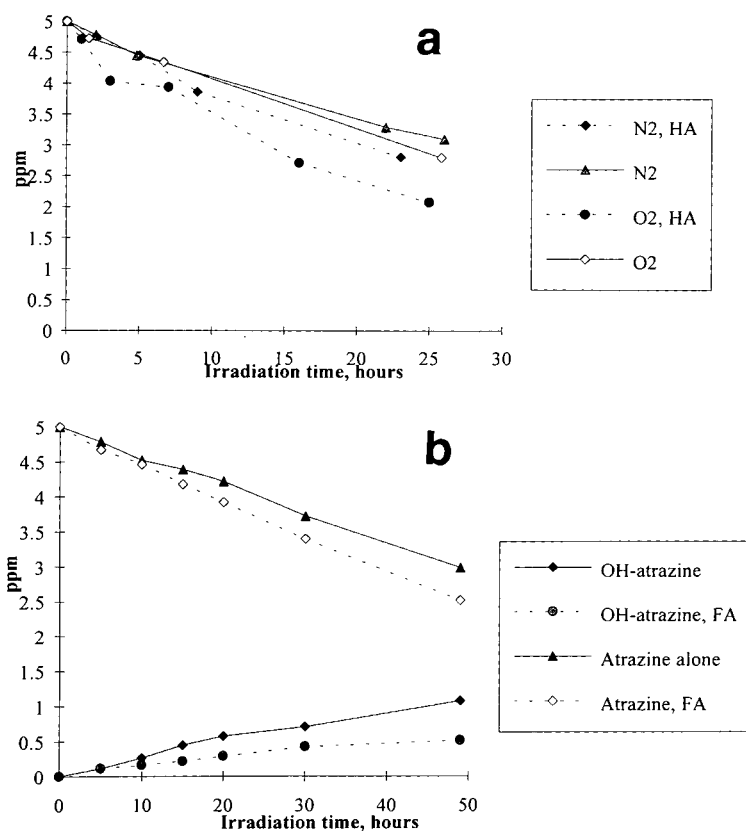
Fig. 5. (a) Atrazine photodecomposition under oxygen and nitrogen atmospheres with Philips HPK lamp; (b) atrazine photodecomposition with Heraeus Suntest apparatus.
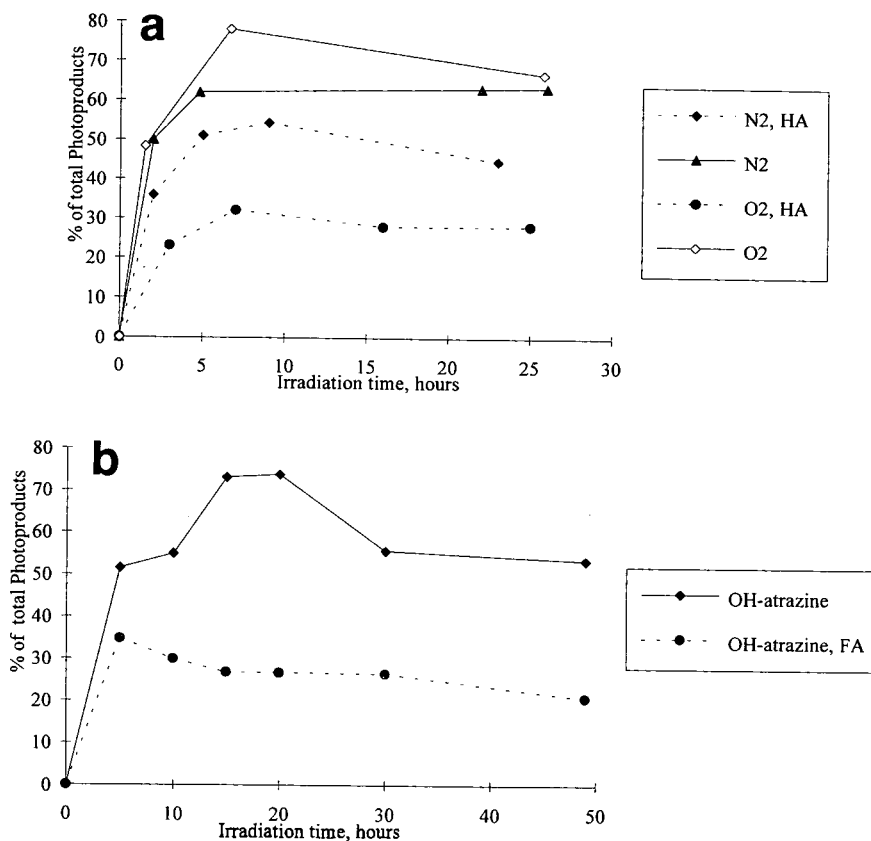
Fig. 6. (a) Variation of hydroxyatrazine produced by photodecomposition of atrazine under oxygen and nitrogen atmospheres with Philips HPK lamp; (b) variation of hydroxyatrazine produced by photodecomposition of atrazine in Heraeus Suntest apparatus.

in many other photochemical studies in aqueous media [37,38]. Low concentrations of desethylatrazine were found in the absence of humic substances. Deisopropylatrazine and ameline (2-hydroxy-4,6-diamino-s-triazine) were minor degradation products found in trace levels under those conditions.

The addition of dissolved humic material changed the photochemical degradation pathway of atrazine in aqueous solution. All quantitative results are given in Table 3. With humic acids and in the presence of oxygen, the absolute amount of hydroxyatrazine produced decreased 43% as shown in Fig. 6a. Under nitrogen con-

Table 3
Measured amount of products after irradiation (ppm)

	O_2	O_2, HA	N_2	N_2, HA
Atrazine	2.8	2.1	3.1	2.8
Hydroxyatrazine	1.47	0.83	1.21	0.98
Desethylatrazine	<0.08	0.37	<0.05	0.16
Ameline	Traces	0.2	Traces	0.15
Irradiation time (h)	26	25	26	23

ditions this decrease was only 20%. Rejto et al. [39] showed in a dye-sensitized photodegradation study, that riboflavine sensitizes *s*-triazine photodecomposition under sunlight and oxygen conditions by dealkylation without production of hydroxymetabolites. In this study desehylatrazine is the only dealkylated metabolite; its amount increases in the presence of humics and may occur by a sensitizing effect. Ameline is only quantified in the presence of humic substances; it is produced by the complete dealkylation of hydroxyatrazine. Khan and Schnitzer [4] also showed that the presence of fulvic acids enhances the dealkylation of photochemically formed hydroxyatrazine to ameline. The hydroxy intermediates (hydroxydesethylatrazine and hydroxydesisopropylatrazine) were not found in our experiments. Similar results were found by Khan and Gamble [40] with prometryn. Under the Heraeus Suntest apparatus, with milder simulated light conditions as shown by kinetics, only hydroxyatrazine (80%) is detected by HPCE. The amount of hydroxyatrazine is also lower in the presence of fulvic acids (30%), because as in previously described experiments, fulvic acids change the photochemical pathway

of atrazine. Desethylatrazine was found under traces in those photochemical conditions.

At the end of irradiation experiments all humic solutions were decolorized because of photooxidation affecting humic substances. The structural changes of the same humic acids as under these photochemical conditions have been studied by means of modern spectroscopic instrumentation (NMR, Fourier transform IR, FI–pyrolysis–MS) and will be reported elsewhere.

4. Conclusion: effect of humic substances on photodegradation of atrazine

We have shown that the presence of dissolved humic material alters the photochemical behavior of atrazine by accelerating its degradation. Changes in the degradation pathway of atrazine by addition of humic material are shown in Fig. 7. Dehalogenation was found to be the main degradation process to yield hydroxyatrazine (up to 70% of total photoproducts). Under oxygen-saturated conditions the relative amount of hydroxyatrazine is lower in the presence of dissolved humic material because
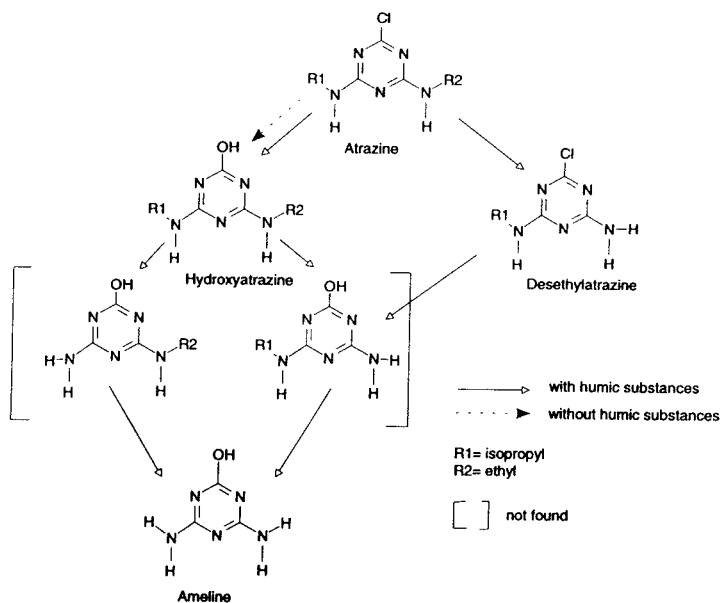
Fig. 7. Photochemical degradation pathways of atrazine with and without humic substances.

dealkylation of the side chain to produce desethylatrazine occurs (by sensitization). Under nitrogen the same photochemical pathway is observed. The production by the humics of reactive oxygen species (H_2O, OH, $^1O_2$, hydrated electrons) not only accelerates degradation of atrazine, but also effects photostability of the photoproducts.

HPCE in its free zone mode is a good tool for analysis of hydroxy-*s*-triazines in the presence of humic material. This analytical technique allows separation of the pesticides from the matrix without pretreatment of the samples.

Acknowledgments

References

[1] G.G. Choudhry, Humic substances–Photophysical and Free Radical Aspects and Interactions with Environmental Chemicals, in Current Topics in Environmental and Toxicological Chemistry, Vol. 17, Gordon and Breach Sci. Publ., New York, NY, 1984.

[2] K. Nick, H.F. Schöler, G. Mark, T. Söylemez, M.S. Akhlaq, H.P. Schuchmann and C. von Sontag, J. Water SRT-Aqua, 41(2) (1992) 82–87.

[3] C. Minero, E. Pramauro, E. Pelizzeti, M. Dolci and A. Marchesini, Chemosphere, 24 (1992) 1597–1606.

[4] S.U. Khan and M. Schnitzer, J. Environ. Sci. Health, B13 (1978) 299–310.

[5] M. Schiavon, Ecotoxicol. Environ. Saf., 15 (1988) 46–54.

[6] C.D. Adams and S.J. Randtke, Environ. Sci. Technol., 26 (1992) 2218–2227.

[7] D.W. Kolpin and S.J. Kalkhoff, Environ. Sci. Technol., 27 (1993) 134–139.

[8] D.C.G. Muir and B.E. Baker, J. Agric. Food Chem., 26 (1978) 420–424.

[9] Z. Wang, D. Gamble and C.H. Langford, Anal. Chim. Acta, 232 (1990) 181–188.

[10] K.A. Ramsteiner and W.D. Hörmann, J. Agric. Food Chem., 27 (1979) 934–938.

[11] N.M.J. Vermeulen, Z. Apostolides, D.J.J. Potgieter, P.C. Nel and S.H. Smit, J. Chromatogr., 240 (1982) 247–253.

[12] V. Pacakova, K. Stulik and M. Prihoda, J. Chromatogr., 442 (1988) 147–155.

[13] Q. Wenheng, N.A. Schultz, J.D. Stuart, J.C. Hogan, Jr. and A.S. Mason, J. Liq. Chromatogr., 14 (1991) 1367–1392.

[14] R.N. Lerch and W.W. Donald, J. Agric. Food Chem., 42 (1994) 922–927.

[15] D.S. Gamble and S.U. Khan, J. Agric. Food Chem., 38 (1990) 297–308.

[16] J.M. Schlaeppi, W. Föry and K. Ramsteiner, J. Agric. Food Chem., 37 (1989) 1532–1538.

[17] C. Wittmann and B. Hock, Food Agric. Immunol., 1 (1989) 211–224.

[18] H. Engelhardt, W. Beck, J. Kohr and T. Schmitt, Angew. Chem., 105 (1993) 659–680.

[19] A.W. Garrison, Ph. Schmitt, D. Martens and A. Kettrup, presented at the 24th International Symposium on Environmental Analytical Chemistry, Ottawa, 16–19 May 1994, poster.

[20] G. Dinelli, A. Vicari and P. Catizone, J. Agric. Food Chem., 41 (1993) 742–746.

[21] A.W. Garrison, Ph. Schmitt, D. Martens and A. Kettrup, J. Agric. Food Chem., (1995) submitted for publication.

[22] F. Foret, V. Sustacek and P. Boček, Electrophoresis, 11 (1990) 95–97.

[23] Ph. Schmitt, A.W. Garrison, D. Freitag and A. Kettrup, J. Chromatogr., (1994) submitted for publication.

[24] R.D. Voyksner, W.H. McFadden, S.A. Lammert, in J.D. Rosen (Editor), Applications of New Mass Spectrometry Techniques in Pesticide Chemistry, Wiley, New York, 1987, pp. 247–258.

[25] G. Durand, N. de Bertrand and D. Barceló, J. Chromatogr., 554 (1991) 233–250.

[26] D. Barceló, G. Durand, R.J. Vreeken, G.J. de Jong, H. Lingeman and U.A.Th. Brinkman, J. Chromatogr., 553 (1991) 311–328.

[27] G. Durand and D. Barceló, J. Chromatogr., 502 (1990) 275–286.

[28] G. Durand, N. de Bertrand and D. Barceló, J. Chromatogr., 562 (1991) 507–523.

[29] R.D. Voyksner, P. Pack, C. Smith, H. Swaisgood, D. Chen, in M.A. Brown (Editor), Applications in Agricultural, Pharmaceutical, and Environmental Chemistry (ACS Symposium Series, No. 420), American Chemical Society, Washington, DC, 1990, pp. 14–39.

[30] M.H.B. Hayes, in M.H.B. Aiken, D.M. McKnight, R.L. Wershaw and D.S. MacCarthy (Editors), Humic Substances in Soil Sediment and Water, Wiley-Interscience, New York, 1985, Ch. 13, pp. 329–362.

[31] J.W. Parson, in F. Frimmel and R.F. Christman (Editors), Humic Substances and their Role in the Environment, Wiley-Interscience, New York, 1988, pp. 3–14.

[32] J.B. Weber, Specktrochim. Acta, 23A (1967) 458–461.

[33] A.W. Garrison, Ph. Schmitt and A. Kettrup, Water Res., (1995) in press.

[34] R.G. Zepp, P.F. Scholtzhauer and R.M. Sink, Environ. Sci. Technol., 19 (1985) 74–81.

[35] R.G. Zepp, A.M. Braun, J. Hoigné and J.A. Leenheer, Environ. Sci. Technol., 21 (1987) 485–490.

[36] W.J. Cooper, Adv. Chem. Ser., 219 (1987) 333–362.

[37] D. Barceló, G. Durant, N. de Bertrand and J. Albaiges, Sci. Total Environ., 132 (1993) 283–296.

[38] P.E. Pape and M.J. Zabik, J. Agric. Food Chem., 18 (1970) 202–207.

[39] M. Rejto, S. Saltzmann, A.J. Acher and L. Muszkat, J. Agric. Food Chem., 31 (1983) 138–142.

[40] S.U. Khan and D.S. Gamble, J. Agric. Food Chem., 31 (1983) 1099–1104.

END OF SPECIAL ISSUE

Carbohydrate Analysis

High Performance Liquid Chromatography and Capillary Electrophoresis

Edited by **Z. El Rassi**

Journal of Chromatography Library, Volume 58

The objective of the present book is to provide a comprehensive review of carbohydrate analysis by HPLC and HPCE by covering analytical and preparative separation techniques for all classes of carbohydrates including mono- and disaccharides; linear and cyclic oligosaccharides; branched heterooligosaccharides (e.g., glycans, plant-derived oligosaccharides); glycoconjugates (e.g., glycolipids, glycoproteins); carbohydrates in food and beverage; compositional carbohydrates of polysaccharides; carbohydrates in biomass degradation; etc.

The book will be of interest to a wide audience, including analytical chemists and biochemists, carbohydrate, glycoprotein and glycolipid chemists, molecular biologists, biotechnologists, etc. It will also be a useful reference work for both the experienced analyst and the newcomer as well as for users of HPLC and HPCE, graduates and postdoctoral students.

Contents: Part I. The Solute.
1. Preparation of carbohydrates for analysis by HPLC and HPCE (A.J. Mort, M.L. Pierce).
Part II. Analytical and Preparative Separations.
2. Reversed-phase and hydrophobic interaction chromatography of carbohydrates and glycoconjugates (Z. El Rassi).
3. High performance hydrophilic interaction chromatography of carbohydrates with polar solvents (S.C. Churms).
4. HPLC of carbohydrates with cation- and anion-exchange silica and resin-based stationary phases (C.G. Huber, G.K. Bonn). 5. Analysis of glycoconjugates using high-pH anion-exchange chromatography (R.R. Townsend). 6. Basic studies on carbohydrate - protein interaction by high performance affinity chromatography and high performance capillary affinity electrophoresis using lectins as protein models (S. Honda). 7. Modern size exclusion chromatography of carbohydrates and glycoconjugates (S.C. Churms). 8. High performance capillary electrophoresis of carbohydrates and glycoconjugates (Z. El Rassi, W. Nashabeh). 9. Preparative HPLC of carbohydrates (K.B. Hicks).
Part III. The Detection.
10. Pulsed electrochemical detection of carbohydrates at gold electrodes following liquid chromatographic separation (D.C. Johnson, W.R. LaCourse). 11. On-column refractive index detection of carbohydrates separated by HPLC and CE (A.E. Bruno, B. Krattiger). 12. Mass spectrometry of carbohydrates and glycoconjugates (C.A. Settineri, A.L. Burlingame). 13. Evaporative light scattering detection of carbohydrates in HPLC (M. Dreux, M. Lafosse). 14. Chiroptical detectors for HPLC of carbohydrates (N. Purdie). 15. Pre- and post-column detection-oriented derivatization techniques in HPLC of carbohydrates (S. Hase). 16. Post-column enzyme reactors for the HPLC determination of carbohydrates (L.J. Nagels, P.C. Maes). 17. Other direct and indirect detection methods of carbohydrates in HPLC and HPCE (Z. El Rassi, J.T. Smith). Subject index.

©1995 692 pages Hardbound
Price: Dfl. 425.00 (US$250.00)
ISBN 0-444-89981-2

PUBLICATION SCHEDULE FOR THE 1995 SUBSCRIPTION

Journal of Chromatography A and *Journal of Chromatography B: Biomedical Applications*

MONTH	1994	J–M	A	M[a]	J	J	A	
Journal of Chromatography A	Vols. 683–688	689–695	696/1 696/2 697/1 + 2 698/1 + 2	699/1 + 2 700/1 + 2 702/1 + 2 703/1 + 2	704/1 704/2 705/1 705/2	706/1 + 2 707/1 707/2 708/1	708/2 709/1 709/2 710/1	The publication schedule for further issues will be published later.
Bibliography Section		713/1			713/2			
Journal of Chromatography B: Biomedical Applications		663–665	666/1 666/2	667/1 667/2	668/1 668/2	669/1 669/2	670/1 670/2	

[a] Vol. 701 (Cumulative Indexes Vols. 652–700) expected in October.

INFORMATION FOR AUTHORS

(Detailed *Instructions to Authors* were published in *J. Chromatogr. A*, Vol. 657, pp. 463–469. A free reprint can be obtained by application to the publisher, Elsevier Science B.V., P.O. Box 330, 1000 AH Amsterdam, Netherlands.)

Types of Contributions. The following types of papers are published: Regular research papers (full-length papers), Review articles, Short Communications and Discussions. Short Communications are usually descriptions of short investigations, or they can report minor technical improvements of previously published procedures; they reflect the same quality of research as full-length papers, but should preferably not exceed five printed pages. Discussions (one or two pages) should explain, amplify, correct or otherwise comment substantively upon an article recently published in the journal. For Review articles, see inside front cover under Submission of Papers.

Submission. Every paper must be accompanied by a letter from the senior author, stating that he/she is submitting the paper for publication in the *Journal of Chromatography A* or *B*.

Manuscripts. Manuscripts should be typed in **double spacing** on consecutively numbered pages of uniform size. The manuscript should be preceded by a sheet of manuscript paper carrying the title of the paper and the name and full postal address of the person to whom the proofs are to be sent. As a rule, papers should be divided into sections, headed by a caption (*e.g.*, Abstract, Introduction, Experimental, Results, Discussion, etc.). All illustrations, photographs, tables, etc., should be on separate sheets.

Abstract. All articles should have an abstract of 50–100 words which clearly and briefly indicates what is new, different and significant. No references should be given.

Introduction. Every paper must have a concise introduction mentioning what has been done before on the topic described, and stating clearly what is new in the paper now submitted.

Experimental conditions should preferably be given on a *separate* sheet, headed "Conditions". These conditions will, if appropriate, be printed in a block, directly following the heading "Experimental".

Illustrations. The figures should be submitted in a form suitable for reproduction, drawn in Indian ink on drawing or tracing paper. Each illustration should have a caption, all the *captions* being typed (with double spacing) together on a *separate sheet*. If structures are given in the text, the original drawings should be provided. Coloured illustrations are reproduced at the author's expense, the cost being determined by the number of pages and by the number of colours needed. The written permission of the author and publisher must be obtained for the use of any figure already published. Its source must be indicated in the legend.

References. References should be numbered in the order in which they are cited in the text, and listed in numerical sequence on a separate sheet at the end of the article. Please check a recent issue for the layout of the reference list. Abbreviations for the titles of journals should follow the system used by *Chemical Abstracts*. Articles not yet published should be given as "in press" (journal should be specified), "submitted for publication" (journal should be specified), "in preparation" or "personal communication".

Vols. 1–651 of the *Journal of Chromatography*; *Journal of Chromatography, Biomedical Applications* and *Journal of Chromatography, Symposium Volumes* should be cited as *J. Chromatogr.* From Vol. 652 on, *Journal of Chromatography A* (incl. Symposium Volumes) should be cited as *J. Chromatogr. A* and *Journal of Chromatography B: Biomedical Applications* as *J. Chromatogr. B*.

Dispatch. Before sending the manuscript to the Editor please check that the envelope contains four copies of the paper complete with references, captions and figures. One of the sets of figures must be the originals suitable for direct reproduction. Please also ensure that permission to publish has been obtained from your institute.

Proofs. One set of proofs will be sent to the author to be carefully checked for printer's errors. Corrections must be restricted to instances in which the proof is at variance with the manuscript.

Reprints. Fifty reprints will be supplied free of charge. Additional reprints can be ordered by the authors. An order form containing price quotations will be sent to the authors together with the proofs of their article.
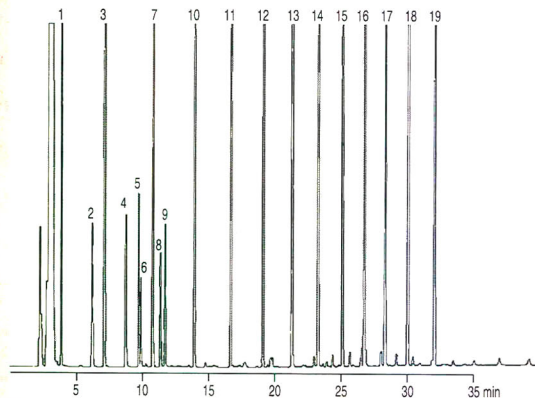
Advertisements. The Editors of the journal accept no responsibility for the contents of the advertisements. Advertisement rates are available on request. Advertising orders and enquiries can be sent to the Advertising Manager, Elsevier Science B.V., Advertising Department, P.O. Box 211, 1000 AE Amsterdam, Netherlands; Tel: 31 (20) 485 3796; Fax: 31 (20) 485 3810. Courier shipments to street address: Molenwerf 1, 1014 AG Amsterdam, Netherlands. *UK*: T.G. Scott & Son Ltd., Venessa Bird, Portland House, 21 Narborough Road, Cosby, Leics. LE9 5TA, UK; Tel: (0116) 2750 521/2753 333; Fax: (0116) 2750 522. *USA and Canada*: Weston Media Associates, Daniel S. Lipner, P.O. Box 1110, Greens Farms, CT 06436-1110, USA; Tel: (203) 261 2500; Fax: (203) 261 0101.